TOWARDS BIOMARKER DISCOVERY IN CONGENITAL URINARY TRACT OBSTRUCTION

by

Dennis J. Orton

Submitted in partial fulfilment of the requirements

for the degree of Doctor of Philosophy

at

Dalhousie University

Halifax, Nova Scotia

May 2014

For those who said I couldn't, and those who don't think they can.

TABLE OF CONTENTS

LIST OF TABLES

LIST OF FIGURES

ABSTRACT

Proteome analysis techonologies are commonly employed for discovery-based biomarker identification studies. This thesis aims to help bridge the gap between analytical technology development and clinical application by improving and appling a proteomics workflow for biomarker discovery in congenital urinary tract obstruction (UTO). By accentuating the importance of experimental design, and evaluating the biological relevance of quantitative proteome analyses, the results of this research provide confidence in a number of identified candidate biomarkers of UTO.

A sensitive method for quantification of proteome samples was developed using temperature controlled reversed-phase liquid chromatography (TPLC). The TPLC system provides high recovery (> 90 %), as well as high accuracy and precision in estimating the concentration across a number of protein sample types (CV < 10 %).

The need for extensive fractionation strategies coupled with LC-MS analysis challenges the throughput of the overall experiment. Development of a dual column LC-MS interface reduced the total analysis time by a factor of 2 over conventional single column LC-MS systems. The system was applied to a quantitative proteome analysis of proximal tubule cells exposed to mechanical stretch, mimicking the conditions they experience during UTO and a urinary exosomal proteome analysis for candidate biomarker identification of this disease.

A total of 1636 proteins were identified in the whole cell proteome analysis, of which 317 were found to be significantly altered in abundance. Analysis of the urinary exosomal proteome yielded 318 proteins, of which 189 were found to be altered in abundance due to obstruction. Western blot confirmation of a few select proteins provided backing to the quantitative proteome analysis, while gene ontology and KEGG pathway analysis yielded functional information.

The results from the quantitative analyses of the urinary exosomes and proximal tubule cells identified candidates for both diagnosis and prognosis of UTO. In addition, activation of a novel pathway was identified, presenting a potential drug target which could be exploited to improve recovery of children following relief of UTO. This thesis therefore contributes useful technological and methodological advancements towards routine proteome analysis, as well as providing candidate biomarker identification for the leading cause of renal functional loss in children.

LIST OF ABBREVIATIONS USED

HNE	4-hydroxy-2-nonenal
MAG-3	^{99m}Tc-mercapto-acetylglycyl-glycyl-glycine
A_{214}	Absorbance value at 214 nm
A_{280}	Absorbance value at 280 nm
ACN	Acetonitrile
ATP	Adenosine triphosphate
AR	Aldose reductase
ARI	Aldose reductase inhibitor
APN	Aminopeptidase N
ABC	Ammonium bicarbonate
BCA	Bicinchoninic acid
BSA	Bovine serum albumin
CP	Ceruloplasmin
CV	Coefficient of variation
CID	Collision induced dissociation
CUO	Complete ureteral obstruction
C	Cytoplasmic fraction of NRK-52E cell protein extract
Da	Dalton
DMEM	Dulbecco's modified eagle medium
DTT	Dithiothreitol
DR	Diuretic renography
ER	Endoplasmic reticulum
ECL	Enhanced chemiluminescence
ELISA	Enzyme-linked immunosorbent assay
EGF	Epidermal growth factor
EMT	Epithelial to mesenchymal transition
FDR	False discovery rate
FDA	Food and Drug Administration

FA	Formic acid
GO	Gene ontology
GFR	Glomerular filtration rate
GS	Glutathione
GSP	Glutathione peroxidase
HPLC	High performance liquid chromatography
GeLC-MS	In-gel digestion / liquid chromatography and mass spectrometry
ICAM-1	Intercellular adhesion molecule 1
IL	Interleukin
iTRAQ	isobaric tags for relative or absolute quantification
ICAT	Isotope coded affinity tag
KEGG	Kyoto encyclopedia of genes and genomes
LB	Luria-Bertani
LOQ	Limit of quantification
LTQ	Linear trap quadrupole
LC	Liquid chromatography
LC-MS	Liquid chromatography coupled to mass spectrometry
LC-UV	Liquid chromatography with detection in the ultraviolet range
Mac-1	Macrophage antigen 1
MS	Mass spectrometry
M	Membrane fraction of NRK-52E cell protein extract
MCP-1	Monocyte chemotactic protein 1
MVB	Multivesicular body
NSI	Nano-electrospray ionization
NIH	National Institute of Health
NSERC	Natural Sciences and Engineering Research Council of Canada
NCS	Newborn calf serum
NADP	Nicotinamide adenine dinucleotide phosphate
NSpH	Normalized spectral hit value
NSHRF	Nova Scotia Health Research Foundation
NFκB	Nuclear factor kappa-light-chain-enhancer of activated B cells B

OD_{600}	Optical density at 600 nm wavelength
PUO	Partial ureteral obstruction
% B	Percentage of solvent B
PBS	Phosphate buffered saline
PI3K	Phosphoinositol 3-kinase
PAGE	Polyacrylamide gel electrophoresis
PVDF	Polyvinyl-divinyl fluoride
ROS	Reactive oxygen species
RANTES	Regulated on activation, normal T cell expressed and secreted
RSD	Relative standard deviation
RAS	Renin-angiotensin system
RPLC	Reversed-phase liquid chromatography
SFU	Society of Fetal Urology
SDS	Sodium dodecyl sulfate
SpH	Spectral hit value
SILAC	Stable isotope labelling of amino acids in cell culture
SVM	Support vector machine
MS/MS	Tandem mass spectrometry
TPLC	Temperature programmed HPLC
TBMN	Thin-basement membrane nephropathy
TIC	Total ion chromatogram
TGF-β	Transforming growth factor β
TEM	Transmission electron microscopy
TFA	Trifluoroacetic acid
TBS	Tris buffered saline
TNF-α	Tumor necrosis factor α
UV	Ultraviolet
UTO	Urinary tract obstruction
VCAM-1	Vascular adhesion molecule 1
VUR	Vesicoureteral reflux

ACKNOWLEDGEMENTS

First and foremost, I would like to thank my supervisors Drs. Alan Doucette and Dawn MacLellan for their guidance and support over the last few years. At times when I felt all was lost, they managed to bring me back from the brink, helping me learn what it means to be a good scientist and generate high quality data. I would also like to thank my supervisory committee members, Drs. Bassam Nassar, David Byers, and Devanand Pinto for all the tips and tricks they provided along the way. I would especially like to thank Dr. Nassar, who pointed me towards the Clinical Biochemistry Fellowship program that will hopefully provide me an opportunity for a career path.

I also want to thank Dr. Daniel Figeys, who will make the trip to Halifax to act as my external examiner. His expertise in in the field is sure to leave a lasting impression.

Unfortunately, this section is not long enough for me to thank all the people who made enormous contributions to my success as a graduate student, but I will try. Courtney Stairs, who was an integral part of my life and from which I learned so much. Dr. Daniel Gaston for guidance on using statistical and bioinformatic tools for data analysis. Fellow graduate students, past and present, for troubleshooting protocols and repairing instruments: Andrew Crowell, Dr. Anna Greenshields, Carolyn Robinson, Christina Ridley, David Soutar, Dale Corkery, Douglas Veieria, Dr. Diane Matjia-Bothello and Dr. Mark Wall. In addition, a number of people who helped me remember that there is life outside the lab, Andrew Reid, Darren Cole, and of course the Halifax Pitbulls softball team, although I don't know how much The 48 contributed towards the thesis. I would also like to thank Nicole Rosin, who has been a stabilizing force on my life for the past year or so, and little Milo who has done the exact opposite.

I would also like to thank Paul Briggs and Heidi MacKinnon for tolerating my presence and helping with centrifuge issues.

I also extend special thanks to my family, especially my mom who provided me the means to go home for a visit every now and again and constantly kept me sane. Everything I am I owe to her.

Chapter 1: Introduction

Portions of this chapter have been published:

Orton, D.J.; Doucette, A.A. Proteomic Workflows for Biomarker Identification Using Mass Spectrometry - Technical and Statistical Considerations during Initial Discovery. *Proteomes* 2013, *1*, 109-127. *Reproduced with copyright permission.*

1.1. Preface

Having moved into an era of molecular medicine, high-throughput (omics) screening methods are being used to decipher informative, disease-specific markers. These markers show promise for effective treatment strategies by promoting individualized treatment regimens. Improved gene-based technologies are enabling rapid and cost-effective genome sequencing,[1] thus providing predictive strategies for disease classification and risk assessment.[2] Gene-based strategies are useful for evaluating familial disorders or predicting susceptibility to genetic diseases, although are of limited utility for evaluating the changing pathophysiological states occurring in response to external stimuli. To address this, researchers are now looking to the proteome for accurate and responsive predictors for disease progression and diagnosis.[3] Proteome workflows commonly aim to identify biological markers in the form of discrete proteins, or protein panels capable of diagnosis,[4] prognosis,[5] or classification of disease,[6] known as biomarkers. These biomarker discovery experiments primarily centre on high-throughput technologies involving mass spectrometry (MS) for protein identification and quantification. MS-based technologies are capable of profiling the abundance patterns of hundreds to thousands of proteins within a single experiment,[7,8] providing a snapshot in

time of the pathophysiological state of an individual. Unfortunately, current analysis methods and associated technologies make monitoring protein expression patterns less routine and thus more challenging than genetic profiling.

This thesis will focus on promoting technologies to aid in biomarker discovery research, with a goal of identifying novel effectors and candidate biomarkers of congenital urinary tract obstruction (UTO). Congenital UTO is a common anomaly in children that requires extensive evaluation by invasive procedures to determine if the patient will require surgical intervention to prevent loss of renal function.[9–11] The goal of biomarker discovery experimentation is therefore in line with improving the current diagnostic and prognostic techniques for UTO. A little over a decade ago, adaptation of proteomics technologies towards biomarker identification generated immediate excitement in the field.[12–14] Unfortunately, methodological limitations, experimental errors, and early failures in biomarker identification studies slowed progress towards reliable biomarker identification.[15–17] As the field of proteomics has matured, common methodological and technological challenges have been addressed and significant progress in the field of biomarker discovery has been made. The goal of this thesis is to address some challenges still faced today in proteomic research, and applies new technologies to conduct in-depth analyses of UTO, with the goal of identifying candidate biomarkers of the disease.

1.2. Proteomics

1.2.1. Overview

In essence, proteomics is the spatio-temporal study of the structure, function, or composition of the protein complement of a biological sample, defined as a proteome.[18] Arguably the most important contribution to the field of proteomics involved incorporation of MS for identification[19] and quantification[20] of proteins within a complex mixture. Application of MS to proteomics research was permitted through the development and adaptation of protein/peptide-friendly ionization methods in the late 1980's.[21,22] Though early identification strategies relied on the generation of peptide mass maps as 'fingerprints' for specific proteins,[23] the most popular methods today rely on tandem mass spectrometry (MS/MS) to provide sequence specific information for protein identification. Current protein identification methods employing MS/MS can be classified into two broad categories: bottom-up, and top-down.[24,25] Top-down proteomics is a term given to MS characterization beginning with the intact protein, with subsequent fragmentation and analysis that typically employs high resolution MS instrumentation. While this is perhaps the most logical approach to proteome analysis, the diverse physical and chemical nature of proteins negatively impact sample processing methods and generate complex fragmentation patterns for identification. These limitations make bottom-up strategies, based on peptide level fragmentation, more common. Bottom-up strategies employ chemical or enzymatic digestion of proteins prior to MS analysis. The most common digestion method for bottom-up proteome analysis employs the proteolytic enzyme trypsin. Trypsin selectively cleaves proteins at the C-terminal end of lysine and arginine, generating smaller peptide segments that can be more easily sequenced through

MS/MS. Although top-down proteomic strategies are making great strides in MS-based proteomics, the work presented in this thesis employs the more mature bottom-up approach to proteome analysis.

1.2.2. Mass spectrometry

A mass spectrometer functions by separating gas-phase ions according to their mass-to-charge ratio (*m/z*), and data are displayed as a mass spectrum showing the relative abundance of ions versus their *m/z* values. For proteomics applications, ionization is commonly conducted by nano-electrospray ionization (NSI).[26] The basis of NSI-MS is in-solution ionization, typically through protonation of the analyte under acidic conditions, followed by transition of peptides into the gas phase for MS detection. One limitation of this method is that peptide ions present in higher abundance in the solution can suppress the ionization efficiency of lower abundance components.[27] This effect, known as signal suppression, leads to an over-representation of high abundance peptides in the data. A secondary drawback of NSI is the innate susceptibility to interference by salts and other charged species commonly present in buffers and biological samples. These contaminants can lead to unstable spray during ionization, salt adduct formation, and ion suppression,[28–30] thus making removal of these interfering compounds an integral aspect of sample preparation prior to MS.[31] Techniques to purify protein samples capable of providing unbiased, quantitative analysis are therefore an important source of research in the proteomics community.[32–34]

Overcoming the effects of signal suppression from salts or abundant peptide components of a mixture can be partially accomplished by separating proteins or peptides

prior to MS detection. To this end, NSI normally employs reversed-phase high performance liquid chromatography (HPLC) separation in-line with MS detection.[35] Commonly referred to as LC-MS, reversed-phase HPLC solvent systems (*e.g.* acetonitrile, water) are compatible with NSI and promote high sensitivity for MS detection. The result of an LC-MS analysis is a chromatogram made up of a number of mass spectra taken at each time point. The data can be collectively displayed through what is known as a total ion chromatogram (TIC; Figure 1.1A), noting that at any point in time over the chromatogram, there is a complete mass spectrum recorded for those select components of the mixture with a particular retention time. In proteomics, owing to the complexity of the mixture, it is still common for multiple peptides to simultaneously elute from the HPLC column and be detected by MS.

1.2.3. Proteome analysis

The innate complexity of proteome samples generally requires more than a single dimension of separation (*i.e.* reversed-phase HPLC) to acquire good proteome coverage. Commonly used clinical samples such as serum and urine are known to contain several thousand proteins,[8,36,37] which exceeds the ability of a single dimension of separation to yield sensitive results. To this end, a range of proteome prefractionation methods have been developed and applied to increase the number of proteins identified, including gel electrophoresis,[38,39] immunodepletion,[40–42] and various forms of multidimensional chromatography.[43,44] Orthogonal separation methods are commonly combined to allow additional dimensions of separation and improve the number of protein identifications.[45–47] Extensive sample prefractionation strategies can significantly increase the number of protein identifications, however, the approach simultaneously increases the number of

LC-MS runs required. Re-equilibration of the HPLC column and lengthy sample loading times at the low flow rates employed for NSI contribute significant 'downtime' to sample analysis. This innate feature of LC-MS adds to the already lengthy multidimensional approach to proteome profiling (*e.g.* from hours to days). Changes in instrumental sensitivity over time, ambient temperature fluctuations, and error in sample injection are a few examples of problems that can be encountered when conducting such extensive experiments.[48] These issues cause irreparable harm for quantitative analysis of the data when undertaking biomarker discovery experiments. It is therefore important to temper the level of pre-fractionation in proteomic analyses depending on the desired application. To address limitations in throughput for proteomic analysis, Chapter 4 describes a system for improved throughput in LC-MS experiments.

Recent improvements in MS instrumentation and higher pressure chromatography (ultra high pressure liquid chromatography; UPLC) have allowed a single LC-MS analysis of yeast to identify over 4,000 proteins in just over one hour, without extensive prefractionation methods.[7] With such advances in instrumentation, the importance of 'front end' methods for sample preparation and time utilization cannot be understated. Common methods in MS workflows are thus the driving force behind the technology aspect of this thesis, as no matter the mass spectrometer employed, the fundamental principles of the proteomic MS workflow remain the same. To facilitate a better understanding of the methods employed in this thesis, a brief description of the function of the mass spectrometer as it pertains to protein identification and quantification is provided.

1.2.4. Peptide matching

Protein identification by bottom-up strategies are commonly accomplished by peptide matching. As a method for protein identification, peptide matching requires fragmentation of peptide ions in the mass spectrometer and matches the fragmentation pattern to theoretical peptide sequence from a database.[49] First, peptides are detected as their intact *m/z* value following elution from the HPLC column. These intact, precursor ions are subsequently fragmented and the resulting mixture of ions are recorded through generation of a tandem MS spectrum. For data acquisition in this thesis, the mass spectrometer is set to 'data-dependent mode' where the most abundant peptide ions eluting from the column are automatically isolated by the MS instrument and fragmented by collision-induced dissociation (CID) in an ion trap mass spectrometer (ThermoFisher LTQ XL). During CID, peptides are made to fragment through low energy collision (25-35 eV) with an inert gas (helium). CID results in cleavage of the peptide bonds between amino acid residues, yielding what is known as a b and y ion series, in a predictable fashion. Which particular peptide bond is broken is determined by the functional group of the amino acid resisudes within the peptide. The resulting mass spectrum is therefore compiled of a series of ions whose mass spacing corresponds to the mass of amino acid residues. The process of data-dependent acquisition is summarized in Figure 1.1. Depending on chromatographic peak width and instrumental resolving power, this method is able to identify thousands of peptides in a single LC-MS run.

Some limitations for the LC-MS experiment include inter-experimental variability in peak selection leading to variability in peptide identifications, and the time required for ion selection and fragmentation (*i.e.* scan speed) leading to missed ions that would

otherwise allow more protein identifications.[50] Overcoming the limitations of the variability in peptide identification in this manner can be accomplished through incorporation of technical replicate analyses, which promotes more complete proteome coverage and lends greater confidence in protein identification data. Improving throughput in LC-MS experimentation is thus an objective of this thesis, and the system described in Chapter 4 provides the means to increase technical replicate analyses in LC-MS experiments without adding significant analysis time.

This thesis employs the SEQUEST search algorithm[19] to identify proteins following LC-MS/MS (Figure 1.1). SEQUEST functions by a five step series of events ending in matching a theoretical peptide amino acid sequence to the experimental MS/MS fragmentation spectra. First, the experimental peptide mass obtained from the MS spectrum is used to calculate of the top 500 tryptic peptides with mass closest to what was observed. Second, from the MS/MS spectrum SEQUEST selects the 200 most abundant ions, and normalizes them to eliminate peak intensity from the calculation. Third, predicted b (N-terminal) and y (C-terminal) fragment ions from the database are calculated, with optional weighting on the associated a ions formed during fragmentation. Next, SEQUEST compares the theoretical spectra to the normalized experimental spectrum and assigns a score to the matching peptide based on how many ions match the theoretical fragment spectrum. Lastly, SEQUEST assignes a cross correlation score based on whether it was a b/y ion or neutral loss and is again compared to a normalized version of the spectrum to include intensity in the calculation. The data is resolved *via* a fourier transform deconvolution calculation which is used to define the confidence of a peptide identification and statistical cut-off filters are used to select the most likely peptide to fit

the MS/MS pattern. To control for false peptide assignments, a number of methods have been developed,[51–54] the simplest of which employs an attempt to match the experimental data to a decoy database to predict the peptide false discovery rate (FDR).[51] Decoy databases consist of nonsense amino acid sequences generated randomly or by reversing the protein database to be searched. Any seemingly matching peptides from the decoy database are therefore predictive of the peptide FDR using the applied filters (*e.g.* number of peptides identified in decoy database / number of peptides identified in actual database = FDR). The stringency of the filters can be adjusted to reduce the FDR, however a balance is required to provide good proteomic data by limiting false positives (type 1 error), and also false negatives (type 2 error). An illustration of this effect is provided in Figure 1.2. Incorporation of FDR calculations and adjustment of filters are included in newer software packages, such as Proteome Discoverer™ from ThermoFisher, providing high confidence peptide identifications from LC-MS/MS data.

1.2.5. Protein identification

Protein identification by SEQUEST is accomplished by matching the identified peptides to the protein sequences in the database. At this point, it is important to note the difference between peptide and protein level FDRs. Without proper evaluation of the data, redundancy in amino acid sequences of proteins in the database can make this process error prone. Therefore, to address the protein FDR, a number of methods can be employed depending on the desired application, a fact that is illustrated throughout this thesis. Proteome analyses geared towards confident protein identification commonly require matching two or more peptides to a protein sequence upon database searching. This prerequisite was employed in Chapter 4, where testing the system required stringent

protein identifications to insure the system design was applicable to high-throughput proteome analyses. Unfortunately, this method may exclude smaller or hydrophobic proteins which generate only a few peptides upon digestion, perhaps limiting the biological information obtained.

To maintain greater biological information in the proteome analysis in Chapter 5, a protein was accepted as being identified if it was observed on average at least once per biological replicate. In this case, redundancy in protein identifications from the same peptide were then removed by accepting only one protein per peptide sequence. This method helped maintain identification of low abundance or hydrophobic proteins in the data. Alternatively, redundancy in the protein identifications can be addressed by grouping proteins with redundant amino acid sequences in the resulting data. This method was employed in the exosomal protein analysis in Chapter 6, as proteins expressing similar amino acid sequences likely express similar physical properties and biological functions. Thus, grouping proteins in this manner can allow functional enrichment of the data. Grouping proteins by similar peptides is automatically incorporated in the Proteome Discoverer™ software package used in this thesis; however, when comparing datasets from different conditions (*e.g*. diseased *vs*. healthy) only the most likely match from the protein group is discussed.

1.2.6. Protein quantification

The driving force behind protein biomarker discovery by LC-MS is quantification of individual proteins within complex samples. This is the main advantage that proteomics holds over gene-based technologies, as quantifiable changes in protein

abundance are reflective of cellular responses to various stimuli. Biomarker discovery experimentation therefore can analyze samples from healthy and diseased groups, and the changes in protein abundance can be measured to characterize response to disease. A range of methods have been developed for protein quantification by LC-MS that can be divided into isotopic labelling, or label-free approaches.[55] The basis for isotopic labelling strategies requires chemical modification of protein or peptide samples from different sources (*e.g*. healthy *vs*. diseased) with isotopically-enriched 'tags', followed by combination into one sample for LC-MS analysis. The mass spectrometer is able to differentiate between the isotopically distinct peptide species and use their relative abundances to quantify them. A number of methods are available for this, including isotope-coded affinity tags (ICAT),[56] amine-specific dimethylation,[57] stable isotope labelling of amino acids in cell culture (SILAC),[58] and isobaric tags for relative or absolute quantification (iTRAQ),[59] among others.[60–63] These labelling strategies allow direct comparison of relative peptide abundances between samples within each LC-MS analysis. The relative abundance of each peptide from different sources thus corresponds to the relative abundance of the original protein in the sample.

Isotopic labelling strategies provide direct comparison of samples, however, the increase in sample complexity upon combination of two different states of the proteome, in addition to high reagent costs, can make label-free approaches more desirable. Label-free methods can be accomplished in either targeted or non-targeted (shotgun) fashions. Targeted methods provide excellent sensitivity and specificity for quantification by zeroing in on the mass range or fragment ion of interest, which significantly improves the signal-to-noise ratio in MS detection.[64] These methods, however, require prior knowledge

as to what *m/z* values or fragment ions are being analyzed. For this reason, targeted analyses are normally reserved for confirmation of quantitative results.[65,66] A popular non-targeted, label-free method developed by John Yates *et al.* for relative protein quantification by LC-MS, known as spectral counting, is employed throughout this thesis.[67] Spectral counting allows estimation of relative protein abundance by the number of unique and redundant peptides assigned to it in the LC-MS experiment.[50,67] As stated previously, the data-dependent method identifies peptides with higher abundance more often, thus proteins with higher abundance will be assigned a greater number of peptides. While a number of factors influence the number of times peptides are assigned to a protein, these variables are assumed to be identical for the same protein between samples, thus the number of spectral hits for the same protein can be compared between samples, providing relative quantification information.

The efficacy of spectral counting as a method for protein quantification from complex samples is limited by a number of factors. The relationship between protein abundance and spectral count is not linear, making it difficult to define the fold change in protein abundance. Additionally, the variability in peptide identifications discussed above can cause large baseline variability in the data which reduces the sensitivity of the method during statistical analysis.[50,68,69] Replication is therefore integral for overcoming baseline variability in spectral counting data. Unfortunately, technical replication during data acquisition is normally limited by extensive prefractionation and analysis time. Again the system design presented in Chapter 4 is meant to address this problem. In fact, all LC-MS analyses in this thesis were performed at least in duplicate by employing this system, providing greater statistical backing to quantitative results.

1.3. Biomarker discovery

1.3.1. Overview

Despite the maturing technologies for proteome analysis and quantification, clinically relevant biomarker identification remains elusive. A vast number of cell types, diseased tissues, and biological fluids on both clinical samples, as well as *in vitro* or *in vivo* disease models have been analyzed in an effort to bring biomarkers to the clinical setting. Problematically, despite numerous claims of success, no test derived from MS-based proteomic techniques is currently approved by the US Food and Drug Administration (FDA) for clinical application. Acknowledging the dynamic complexity of proteome samples, the lack of validated biomarkers is ultimately attributed to flaws in experimental design,[70,71] the use of biased or inconsistent methodology,[72,73] or inadequate statistical analysis.[74–76] Additionally, innate errors in biomarker discovery experimentation, coupled with irreproducible results in some high profile cases, have delayed progress and shaken confidence in the field of biomarker research.[16,77–79] Correction of these errors by education of researchers in the field has since become a commonly published subject.[71,80,81] To obtain highly confident results, proper consideration must be given to the number (*e.g.* multiple patient samples or multiple samples from one patient) and type (*e.g.* proximal fluid or tissue) of samples to be taken for analysis. Additionally, the method of sample collection (*e.g.* anesthetization of the patient or catheterization) and preservation (*e.g.* storage conditions or inclusion of protease inhibitors) must be given sufficient consideration prior to execution of the experiment. To this end, all protein samples used for LC-MS analysis in this thesis were extracted in the presence of protease inhibitors and stored at -80°C prior to analysis.

1.3.2. Phases of biomarker discovery

The process of biomarker discovery can be divided into discovery and validation phases. The discovery phase for biomarker identification requires a relatively small number of samples with few biological replicates to identify a large number of candidates in a shotgun format. While the exact number of samples to be analyzed in this phase are therefore dependent on factors such as the expected biological variability within the population, availability of resources, and the prevalence of the disease in question. Addressing these fundamental parameters prior to execution of a discovery phase biomarker experiment is important, however, incorporation of as many biological replicates as possible will yield the highest quality results possible.

The validation phase of biomarker discovery requires hundreds to thousands of samples to confirm quantitative results in a targeted fashion, and evaluate the applicability of the test to a large population.[82,83] Comparison of smaller numbers of samples in the discovery phase allows efficient time utilization, as well as limiting confounding factors by focussing the groups to investigate only those samples fitting specific criteria. Quantitative assessment of protein abundance between test groups can thus be accomplished by any number of means discussed above, where hundreds to thousands of proteins can be compared simultaneously. These tests commonly elucidate dozens to hundreds of proteins showing significant changes between the test groups.[6,84–88] At this point, significantly altered proteins can be considered ‘candidate biomarkers’, as they are able to distinguish between the groups, however, have not yet been assessed for use clinically.

Following the discovery phase, targeted analysis can be accomplished by multiple reaction monitoring (MRM)-LC-MS, or immunological techniques such as enzyme-linked immunosorbent assays (ELISA) and western blotting. MRM techniques make use of the peptide mass and fragmentation pattern for highly specific quantification of peptides in the sample.[65] The high specificity of MRM scans and immunological techniques therefore allow higher throughput for quantitative analysis of larger populations. Applying these analyses to larger populations provides an estimation of biological variability and direct assessment of the applicability of the identified proteins to characterize the disease. Methods for discovery and validation of biomarkers have been reviewed[82,83] and introduction of a pipeline geared towards bringing proteomic biomarkers into routine clinical use has been suggested.[89] This thesis aims to generate a list of candidate biomarkers for UTO.

1.3.3. Statistical implications for biomarker identification

As stated above, MS based techniques can identify thousands of proteins per sample. From a statistical standpoint, this means that each test sample generates thousands of data points to be compared between conditions. As the number of data points per sample approaches hundreds to thousands, the data become what is known as 'high dimensional'.[76] Traditional statistical methods such as t-tests are commonly used to compare the mean values of two samples to determine statistical significance between them. These methods are useful for determining differences between traditional, 'low dimensional' datasets, however break down during analysis of data in high dimensions.[76] As an example, the commonly employed confidence interval of a t-test of 95 % implies that 5 times out of 100 the reading is falsely identified as being significant. Following this

logic, conducting a t-test on expression profiles of 5,000 genes or proteins at 95 % confidence will potentially lead to 250 false positive identifications. Similar to the peptide identification process described in Figure 1.2, adjusting the confidence interval (statistical cut-off value) to decrease the number of false positive identifications can theoretically improve confidence in the data. However this in turn will lead to a significant increase in false negatives which reduces the overall sensitivity of the method. This confounding statistical problem is known as 'the curse of dimensionality'.[90]

Obviously, traditional statistical methods are not ideal for biomarker identification, thus a number of statistical packages have been developed that are better suited to high dimensional dataset analysis.[68,74,91] Additionally, a number of methods have been published in an attempt to circumvent or reduce the effects of the curse of dimensionality.[91–93] Such statistical algorithms take advantage of Bayesian statistics, hierarchical clustering, or quasi-Poisson distribution, and support vector machine methods to differentiate between data sets. A comparison of some of these statistical methods was conducted by Leitch *et al*.,[74] but no matter the statistical method employed, critical evaluation of the data is imperative. This thesis employs a statistical method known as QuasiTel for comparison of spectral counting data, which is shown to be one of the more stringent methods for quantitative analysis.[68] Additionally, confirmation of a select group of quantitative results at the discovery phase is accomplished by western blotting.

1.3.4. Characteristics of an ideal biomarker

The National Institute of Health (NIH) defines a biomarker as a "…*characteristic that is objectively measured and evaluated as an indicator of a normal biological*

process, pathogenic process, or pharmacologic responses to therapeutic intervention".[94] With respect to proteome analyses, the indicating characteristic may be one or more proteins expressing quantifiable changes in abundance in a clinically obtainable sample. What constitutes an ideal biomarker depends heavily on the disease in question, though the universal characteristics are summarized in Table 1.1. The stringent requirements of the ideal biomarker suggest a single gene or protein is not likely to be used as a biomarker for a given disease, thus combination of the significantly altered proteins may improve the efficacy of the biomarker test.

Existing FDA-approved biomarker tests such as MammaPrint and Ova1 employ panels of genes or proteins which together may promote clinical utility of the biomarker test.[95–98] The MammaPrint gene expression-based test for breast cancer recurrence employs a quantitative assessment of a panel of 70 genes for prediction.[96] The protein-based Ova1 test employs serum levels of the protein CA125 (an ovarian cancer tumor cell marker) and four other marker proteins (β2 microglobulin, transferrin, transthyretin and apolipoprotein A1) to assist in preoperative assessment of potential for ovarian cancer metastasis.[98] While these are examples of some commercially available diagnostic or prognostic tests based on a particular gene expression or protein abundance pattern, caution is required when increasing the number of components in a test.[99] With increasing numbers of components, there lies the potential for over-fitting data to test groups, which may limit the legitimacy of the biomarker test.

1.3.5. Sample sources for biomarker identification

In vitro disease models provide a simplified sample source for researchers to elucidate cell-specific physiological responses to disease or treatment. A model system has the benefit of limiting confounding variables which plague clinical samples by controlling test conditions. In effect, *in vitro* models provide the most simplistic, targeted method for evaluation of specific components of disease with limited biological variability. As an example, Chapter 5 of this thesis employs a well-established *in vitro* model of UTO on proximal tubule cells to investigate potential novel effector proteins in the disease. A mechanical stretch stimulus is applied to the cells, meant to mimic the physiological stresses experienced by proximal tubules as a result of UTO.[100,101] Previous work using this *in vitro* model has allowed characterization of a number of physiological processes occurring in UTO, demonstrating the applicability of the model to *in vivo* disease progression. By employing a high-throughput analysis of the cell culture system, a more complete view of the pathways affected can be elucidated. Identification of novel pathways and signalling proteins in the cell culture model can thus help to predict or explain the presence of candidate biomarkers in clinically relevant samples.

Tissue biopsies and core samples are a routine source for clinical diagnosis through microscopic evaluation following a number of staining techniques. Biopsies provide pathologists with direct access to diseased tissues, allowing characterization of the presence or progression of any number of diseases. Unfortunately, the fixation and staining processes required for pathological assessment make direct coupling to standard proteomic methodologies problematic.[102,103] This makes a direct comparison between proteomic analysis and pathological assessment difficult. Additionally, obtaining biopsy samples from a patient is not trivial, and has the potential to introduce complications such

as infection and bleeding that could lead to decreased quality of life for the patient. The characteristics of an ideal biomarker listed in Table 1.1 state that it should be present in a sample that is easily and non-invasively obtained, making biopsy a last resort for biomarker identification strategies. A better approach is to compile a list of candidate biomarkers from a non-invasively obtained sample source, and compare their efficacy for differentiating between disease groups to that of standard pathological assessment. Additionally, biopsy samples may be used to confirm the proteomic data by immunohistochemistry or other immunological means to provide backing to the results. This thesis employs pathological characterization of renal tissue sections as a method to confirm the presence of pathogenesis resulting from UTO in an *in vivo* model.

Serum and urine are by far the most commonly obtained biological samples in a clinical setting and therefore provide an optimal medium for biomarker research. These samples are generally employed for systemic measures, as opposed to tissue-specific indicators. A number of more specific proximal fluids have been investigated for biomarker discovery experiments, including cerebrospinal, bronchoalveolar lavage, cervicovaginal, cyst, ascites (abdominal fluid), nipple aspirate, amniotic, and blister, as well as bile, saliva, expressed prostatic secretion and seminal plasma, and pancreatic fluid (reviewed by Teng *et al*.).[104] While proximal fluids may provide enriched sources for biomarker identification from specific tissues, many require invasive collection procedures, making them undesirable for biomarker test development. As the focus of this thesis is on a congenital disorder of the urinary tract, urine as a non-invasive proximal fluid is employed for candidate biomarker discovery.

Urine provides an especially provocative sample for potential biomarker identification associated with diseases affecting tissues proximal to the urinary tract. The direct contact of cells lining the nephron results in a number of kidney-specific proteins being present in the sample.[8,37] Figure 1.3 provides a schematic of the nephron, highlighting the different segments therein. The non-invasive nature of urine collection makes urine an excellent source for employing biomarker tests in the clinic. Despite the simplicity of sample collection, biomarker identification from these samples has been especially lacking. Issues stemming from sample collection,[105–107] storage,[108,109] complexity, and protein concentration range[36,109,110] have been implicated in the lack of progress in the field. As discussed above, efforts to correct variables within each of these experimental parameters have begun to allow researchers to draw more informative conclusions from data obtained by these high-throughput technologies.[72,73,111] Contributing to the overall complexity of the urinary proteome are serum proteins that diffuse through the glomerular membrane and into the urine. While the majority of protein filtered through the glomerulus are reabsorbed by cells along the nephron, a large percentage of the urinary proteome is made up of proteins of serum origin.[8,37] Therefore, analyzing the entire urinary proteome for kidney-specific changes in protein abundance can be problematic. To overcome this effect, a subsample of the urinary proteome contained within exosomes can be isolated and independently analyzed. Methods for sample collection and storage within each experiment remain consistent, and include protease inhibitors to prevent sample degradation. Additionally, the methods chosen for urine sample collection and storage in this thesis have been shown to provide stable results over a period of several months.[112]

1.3.6. Urinary exosomes

Exosomes are small, extracellular membranous vesicles (30 – 100 nm in diameter) that are secreted by a number of cell types and were first described in cultured and circulating reticulocytes.[113,114] Since their initial discovery in 1983, exosomes have been found to be released by any number of cell types and are implicated in cell to cell communication,[115] regulation of the immune response,[116] cancer metastasis,[117] and most notably in this thesis, protein secretion into proximal fluids such as urine.[118–122] As shown in Figure 1.4, exosomes are formed by invagination of late endosomes into the limiting membrane of multivesicular bodies (MVBs) in the cytosol. The MVB then fuses with the plasma membrane, releasing exosomes into the extracellular space (*i.e*. urine). The innate properties of exosomes therefore suggest that they are enriched in proteins of the cell of origin, and that protein profile may be reflective of the pathophysiological state of the cell.[123] Proteomic analysis of exosomes from urine have resulted in identification of candidate biomarkers for diabetic nephropathy,[88] IgA nephropathy,[6] acute kidney injury,[124] and prostate cancer.[125] These studies have demonstrated the applicability of exosomes for candidate biomarker identification.

1.4. Congenital urinary tract obstruction

1.4.1. Prevalence

Congenital UTO presents clinically as hydronephrosis noted on prenatal ultrasound. Hydronephrosis is a common anomaly on prenatal ultrasound, present in 1 – 2 % of pregnancies.[9,126,127] Noted as a dilation of the renal pelvis or rounding of the calyces, the degree of hydronephrosis is graded on a scale developed by the Society of Fetal Urology (SFU 1 – 4).[128] The SFU grading scheme is based on the appearance of the renal pelvis, calyces and level of renal parenchymal thinning on prenatal ultrasound.[129] Hydronephrosis can be caused by transient dilation of the collecting system (41 – 88 % of cases), upper or lower urinary tract obstruction (UTO; 10 – 30 %), and non-obstructive processes such as vesicoureteral reflux (VUR; 10 – 20 %), among others.[130] Cases of transient hydronephrosis resolve spontaneously during fetal development or after birth, therefore, serial postnatal investigations are required to evaluate renal function and determine which cases will require corrective surgery.[131–133] Ultimately, approximately 19 – 25 % of UTO cases will require corrective surgery,[134,135] and structural anomalies stemming from congenital UTO remain a leading cause of chronic renal insufficiency in children.[136,137]

1.4.2. Pathophysiology

A hallmark of severe UTO includes infiltration of the renal interstitium by a number of inflammatory cell types.[138] A major contributor to tissue invasion by immune cells following UTO is activation of the renin-angiotensin system (RAS).[139,140] RAS activation leads to angiotensin II (angII) signaling, which promotes activation of the pro-

inflammatory protein nuclear factor kappa-light-chain-enhancer of activated B cells B (NFκB).[141,142] Activation of NFκB signaling results in transcription of cytokines (interleukin-6; IL-6),[140] chemokines (monocyte chemotactic protein 1; MCP-1, macrophage antigen 1; Mac-1),[143,144] adhesion molecules (inter-cellular adhesion molecule 1; ICAM-1, vascular adhesion molecule 1; VCAM-1)[139] and inflammatory response genes (tumor necrosis factor α; TNF-α, regulated on activation, normal T cell expressed and secreted; RANTES)[140,145,146] which facilitate invasion of immune cells into the tissue. NFκB activation is therefore a primary regulator of tissue infiltration by inflammatory cells.[140,147] Selective blockage of the RAS system almost completely blocks infiltration of inflammatory cells into the interstitium.[148] Unfortunately, normal kidney maturation requires selective activation of RAS, therefore inhibition has deleterious effects on the developing kidney.[149] Tissue infiltration and activation of the signalling molecules by NFκB subsequently leads to activation of interstitial fibrosis and apoptosis in the kidney, which negatively impacts renal development and function.

Progressive interstitial fibrosis is noted in a number of chronic renal diseases, including UTO.[150–152] Activation of fibrosis during UTO involves a complex series of events culminating in excessive deposition of extracellular fibronectin and collagen. A number of cell types in the kidney, including macrophages and cells lining the nephron exert pro-fibrotic and epithelial-mesenchymal transition (EMT) responses through release of transforming growth factor-β (TGF-β) as a result of UTO.[101,148,153,154] Initiation of EMT causes tubule cells to differentiate into fibroblasts that migrate into the tissue and promote extracellular protein deposition. AngII-mediated upregulation of TGF-β therefore plays a major role in initiation of pro-fibrotic signaling;[155] however, complete

reduction in fibrosis cannot be achieved by eliminating TGF-β *in vitro*, suggesting additional effectors in the fibrotic response. Endoplasmic reticulum (ER) stress,[156] reactive oxygen species (ROS) buildup,[157,158] as well as mechanical forces[101] have also been shown to activate fibrosis during UTO.

Tubular cell apoptosis resulting from UTO has been described extensively.[101,159–164] Apoptosis resulting from UTO is initiated by a number of pathways, including mitochondrial disruption and release of cytochrome C,[165] activation of Fas/FasL expression,[166] ER stress,[167,168] ROS buildup,[158,169] as well as p38[170] or p53[171] signalling pathway activation. In addition to these pathways initiating apoptosis, external factors such as TNF-α produced by infiltrating macrophages promote apoptosis of tubular cells.[172] Together, the three pathogenic processes of inflammation, fibrosis, and apoptosis can result in irreparable renal damage and functional loss if the obstruction is not relieved surgically. Unfortunately, the developing kidney exhibits a fine balance between each of these processes to allow normal renal maturation, thus making postnatal treatment strategies problematic.

1.4.3. Management of hydronephrosis

Following diagnosis of prenatal hydronephrosis (SFU grade 1 – 4), evaluation of persistence and severity of hydronephrosis is recommended by postnatal ultrasound.[131] If hydronephrosis is persistent but does not worsen, additional ultrasound examinations may be conducted every few months; however, children exhibiting moderate-to-severe hydronephrosis (SFU grade >2) at this point may require additional investigations to determine the extent of hydronephrosis and its effect on renal function.[10,130,131] In cases

where obstruction is suspected, diuretic renography (DR) is employed for estimation of differential renal function and drainage (*i.e.* contributions from left kidney 50 %, right kidney 50 %), which provides data on the severity of obstruction. Standardization of the procedure for DR has been attempted to promote inter-institutional comparison,[173] however, some centres employ variations of the protocol, making such comparisons problematic.

It is generally accepted that DR should be performed a minimum of 6 weeks after birth to allow renal maturation. The procedure measures the absorption and clearance of an intravenously injected radiotracer molecule (commonly ^{99m}Tc-mercapto-acetylglycyl-glycyl-glycine; MAG-3) from the kidneys. Introduction of a diuretic (furosemide) promotes clearance of the radiotracer and renal function can thus be determined by measuring time required for clearance. DR is thus capable of quantifying the relative ability of each kidney to clear the radiotracer, providing evidence for unilateral or bilateral obstruction, as well as drainage (post bladder obstruction).

The MAG-3 test provides a measure of renal function at the time of analysis, however, does not lend any prognostic capability towards predicting which children will require intervention.[174] To combat the lack of prognostic indicators for renal function, it is common to conduct serial investigations by ultrasound and MAG-3 tests to evaluate deterioration or recovery in each case. The invasive nature of these tests, coupled with the lengthy surveillance timeframe, makes current management methods undesirable. Therefore, identification of non-invasive clinically measurable markers capable of predicting which children will require surgery could improve patient care, avoid

unnecessary patient pain and anxiety, and limit the chances of renal functional impairment in children with UTO.[175]

1.5. Existing candidate biomarkers for UTO

Despite extensive studies into the pathophysiology of UTO, there remains an underlying lack of progress in identification of non-invasive biomarkers of UTO. In 2003, the NIH held a meeting in specifically geared towards fostering an understanding of the processes underway during UTO and declared a need to identify biomarkers of the disease to assist in prognosis.[175] Since then, a number of studies have been published attempting to identify proteins capable of being employed as biomarkers. Table 1.2 summarizes a list of proposed biomarker proteins that could be used as diagnostic or prognostic markers of UTO. While each of these proteins respond to UTO in either the kidney or urine, the lack of a clinically useful biomarker test suggests they may not be clinically applicable alone. The LC-MS studies listed in Table 1.2 point to the usefulness of MS for improving the lists of candidate biomarkers available in the urine.[85,86] Unfortunately, the LC-MS studies mentioned in Table 1.2 lack both confirmation of quantitative results and prefractionation prior to analysis. Therefore, the list of proteins presented are of limited utility moving forward into the validation phase of biomarker discovery. This thesis presents a complementary LC-MS analysis to those already published by using the exosomal sub-proteome of urine.

1.6. Disease models of UTO

Efforts to study the progression of disease in UTO have led to development of a number of *in vitro* and *in vivo* disease models. As discussed in above, the *in vitro*

model was developed to mimic the buildup of interstitial pressure and mechanical forces experienced by proximal tubule cells in the nephron as a result of obstruction.[176] To this end, the model applies a stretch stimulus to a monolayer of rat proximal tubule cells (NRK-52E).[100,101] Previous work has used this model to complement evidence from other sources showing the proximal tubule cells undergo apoptosis as a result of mechanical stretch, not only from cell signalling molecules or ischemia.[100,160,170] The mechanism of apoptosis has therefore been delineated,[170] as well as a number of other pathogenic signalling pathways.[100,101] Although these studies have demonstrated a number of pathways affected by stretch, the overall picture of disease progression resulting from stretch is incomplete. Therefore, this thesis aims to elucidate a more global response by proteome analysis to delineate previously undescribed effectors in progression of disease.

The simplest method for studying congenital UTO *in vivo* involves surgical introduction of obstruction by complete ureteral obstruction (CUO).[177] While this method provides information regarding severe obstruction, a more clinically relevant model of obstruction involves partial ureteral obstruction (PUO). A number of animal models have been used for evaluation of the effects of PUO and CUO on renal and urinary protein content, including pigs,[178] dogs,[179] sheep,[180] guinea pigs,[181] mice,[182] and rats.[183] Temporal and species-specific responses to UTO in the developing kidney makes the timing for introduction of obstruction in the model system critical. An example of a species specific response involves epidermal growth factor (EGF), which is generally noted to be decreased in abundance in kidneys and urine following UTO.[144,184,185] Disease models in rats and mice show similar decreases in EGF abundance, however, exogenous supplementation helps promote renal growth and

recovery in rats, but has a toxic effect in mice, exacerbating the negative effects of UTO.[186] This effect clearly demonstrates the importance of model system selection to allow clinically relevant data to be obtained.

The experimental model chosen to study congenital UTO should accurately reflect the developmental stage wherein the obstruction was noted. In humans, the majority of renal development is completed *in utero*, although nephron maturation continues through the first 6 months postnatally.[187] In contrast, the majority of renal development in the rat occurs postnatally, thus a 7-day old rat kidney is analogous to a third trimester human.[188] As the first signs of UTO are commonly noted on prenatal ultrasound, introduction of obstruction to a neonatal rat has similar effects to those noted in human fetuses.[150,188] This thesis employs unilateral PUO and CUO in a weanling rat model of UTO to simulate two degrees of increasing severity of obstruction. By analyzing increasing levels of severity of obstruction, changes in the protein profile can potentially elucidate specific markers of severe versus mild obstruction in a prognostic fashion. Furthermore, this thesis employs a partial obstruction method that has been suggested to be both mild and variable.[189] The rationale therein is to be able to detect alterations within the urinary proteome of rats with mild obstruction, potentially undetectable by other non-invasive means, and thus may be equivalent to asymptomatic or very mild obstruction that may not require surgery. Comparison of these rats to a severe form of obstruction can therefore improve on existing prognostic methods.

1.7. Research objectives

This chapter describes current proteome analysis methodology employed during LC-MS studies for biomarker discovery. Limitations of current methods and advances in MS instrumentation and associated methodology are therefore discussed. As the field of proteomics matures, the number of proteins identified in LC-MS experiments are increasing, and the confidence in quantitative results is improving. Despite this fact, a number of method-based limitations remain. When dealing in extremely low abundance sample sources such as exosomes, it is imperative that each component of the LC-MS experiment be optimized to produce high quality, reliable MS data. The work presented in this thesis aims to develop a number of tools for improving the LC-MS workflow, with application to *in vitro* and *in vivo* disease models of UTO for candidate biomarker identification.

The technology-development aspect of the thesis is presented in Chapters 3 and 4. Protein sample quantification prior to LC-MS analysis is commonly accomplished by colorimetric assays that require a portion of the sample to be sacrificed. The amount of protein sacrificed for reliable quantification (*e.g.* triplicate analysis) can become a significant portion of the sample when dealing in low abundance samples such as exosomes. Such sacrifice limits the number of technical replicate analyses that can be conducted. Chapter 3 describes an alternative method for protein sample quantification that allows high recovery using temperature-programmed HPLC. The sensitive and robust method provides an alternative for protein sample quantification prior to LC-MS analyses. With improved replication in mind, Chapter 4 presents a dual-column LC-MS interface that greatly improves throughput for proteome analysis. As noted above,

proteomic MS data is highly variable, making confident assessment of quantitative changes problematic. The dual-column system presented in Chapter 4 allows more replicate analyses to reduce technical variability and allow greater confidence in quantitative results. Additionally, improving throughput for proteome analysis by LC-MS gives advantages such as limiting time required for proteome analysis which reduces the effects of instrumental drift and other errors introduced by extensive LC-MS analyses.

Analyzing proteome samples from the *in vitro* and *in vivo* models of UTO are provided in Chapters 5 and 6, and the system presented in Chapter 4 was employed for all LC-MS analyses. Previous work on the *in vitro* model of UTO has delineated the role of a number of pathways affected by mechanical stretch on proximal tubules. In an effort to identify additional effector proteins responding to stretch, a whole proteome analysis was conducted and Chapter 5 presents the results. Bioinformatic analysis of the resulting data implicates a number of previously undescribed subcellular processes to be involved with stretch response. Evaluation of these subcellular responses could help in designing a biomarker test, or suggest drug targets to improve recovery following release of UTO. The final work presented in Chapter 6 consists of urinary exosomal proteomic analysis of an *in vivo* weanling rat model of UTO. A number of proteins not previously described in the literature are shown to express altered abundance, and a list of candidates capable of distinguishing between groups is generated. This study therefore presents a number of candidate biomarker proteins that could be incorporated into future studies of clinically-obtained children's samples. The advantage of this study over others includes isolation of the exosomal sub-proteome of urine with mild separation, allowing a more sensitive analysis than previous studies of the urinary proteome of children with UTO.

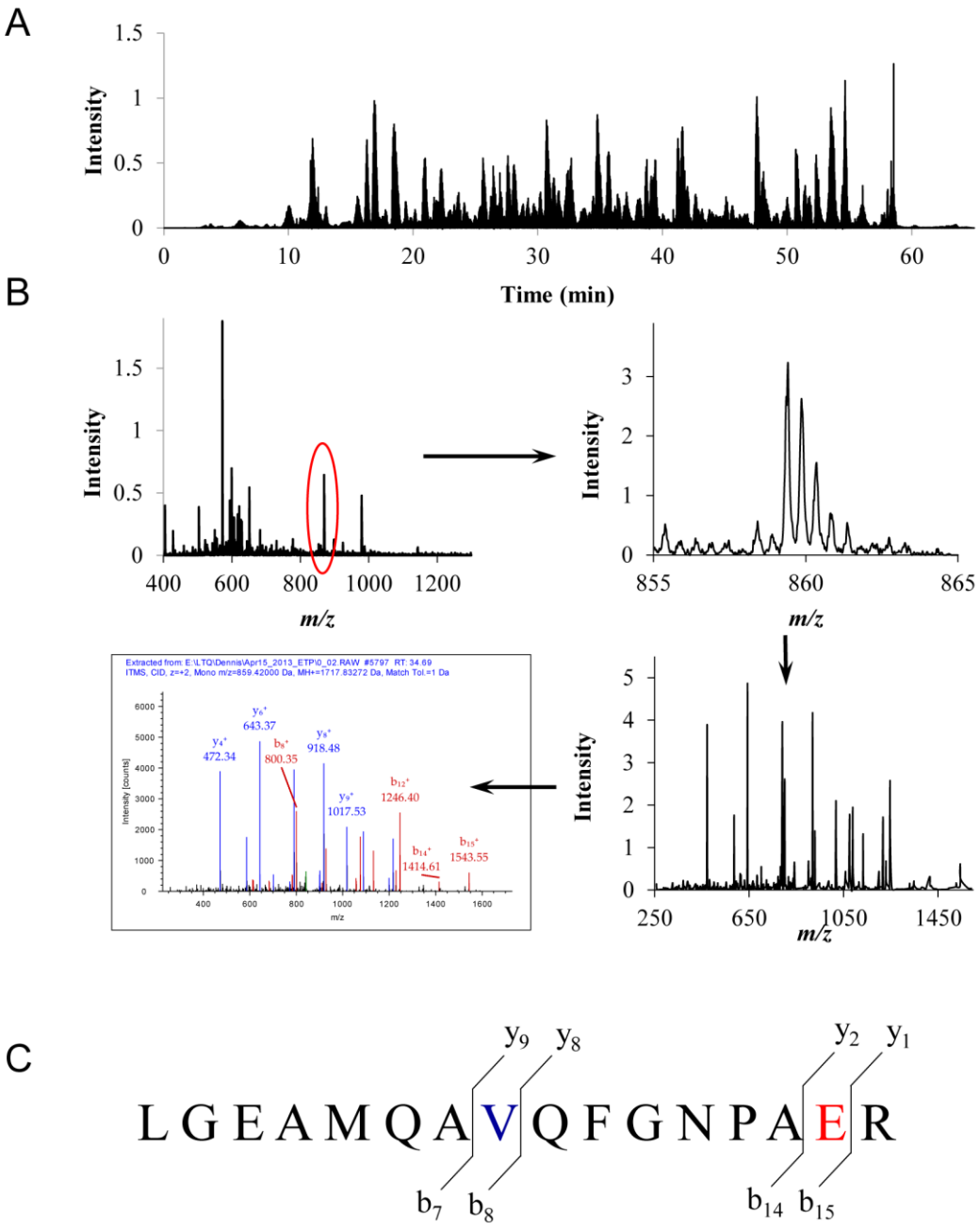

Figure 1.1: A representative schematic of an LC-MS analysis for peptide matching. (A) A TIC of a digested *E. coli* proteome sample. (B) The data-dependent analysis method functions by first conducting a wide range MS scan (*m/z* 400-1300), followed by a narrow range 'zoom scan' (*m/z* 855-865) of a peptide ion with an *m/z* of 859.4. The peptide is fragmented, and SEQUEST determines the b and y ion series to sequence the peptide. (C) A cartoon representation of the b and y fragments of the peptide mapped to the *E. coli* protein aldehyde dehydrogenase.

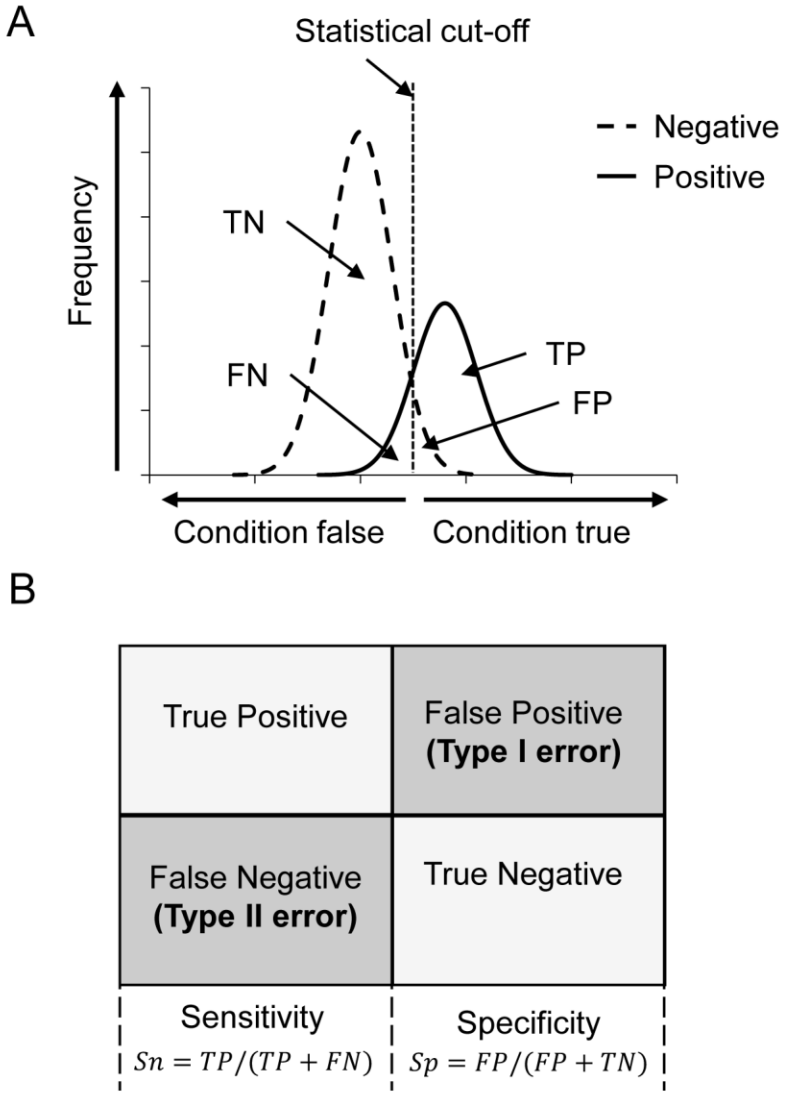

Figure 1.2: A representation of the effect of the statistical cut-off filters on the true and false positive rates.
(A) The two overlapping histograms represent the absolute frequency of condtion positive (solid line) and negative (dotted line) during statistical analysis. Decreasing the stringency of the filters to allow for more true positive (TP) assingments simultaneously increases the number of false positive (FP) assignments. Alternatively, increasing the stringency of the statistical cutoffs to reduce FP increases the number of false negative (FN) assignments. In any case, the number of true negative (TN) assignments should be higher frequency than TP. (B) The balance between true and false positive identifications is thus reflective of the sensitivity and specificity of the test for peptide identifications. Controlling these conditions is paramount for obtaining high quality data.

Table 1.1: Universal characteristics of an ideal biomarker.
Table is from Orton *et al*.[81]

Characteristic	Description
(1) Non-invasive collection	• Expression within a sample obtainable without discomfort to the patient
(2) Readily available	• Presentation in an easily obtainable sample that is commonly obtained clinically such as blood or urine
(3) High sensitivity	• Allows early detection of disease
(4) High specificity	• Present in the disease in question, with little or no overlap between comorbid conditions
(5) Rapid response	• Changes rapidly in response to treatment
(6) Risk stratification	• Provides prognostic information to the clinician, allowing classification of the disease along with diagnosis
(7) Insight to disease	• Provides insight into the underlying mechanism of the disease

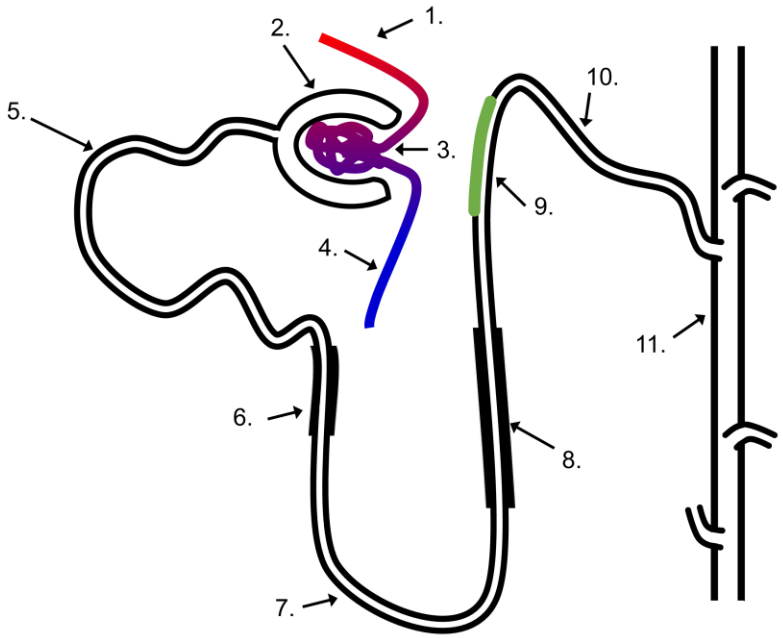

Figure 1.3: A schematic diagram of a nephron.
1) Afferent arteriole. 2) Bowman's capsule containing the 3) glomerular capillary. 4) Efferent arteriole. 5) Proximal tubule. 6) Thick descending limb of the loop of Henle. 7) Loop of Henle. 8) Thick ascending loop of Henle. 9) Juxtaglomerular apparatus. 10) Distal convoluted tubule. 11) Collecting duct.

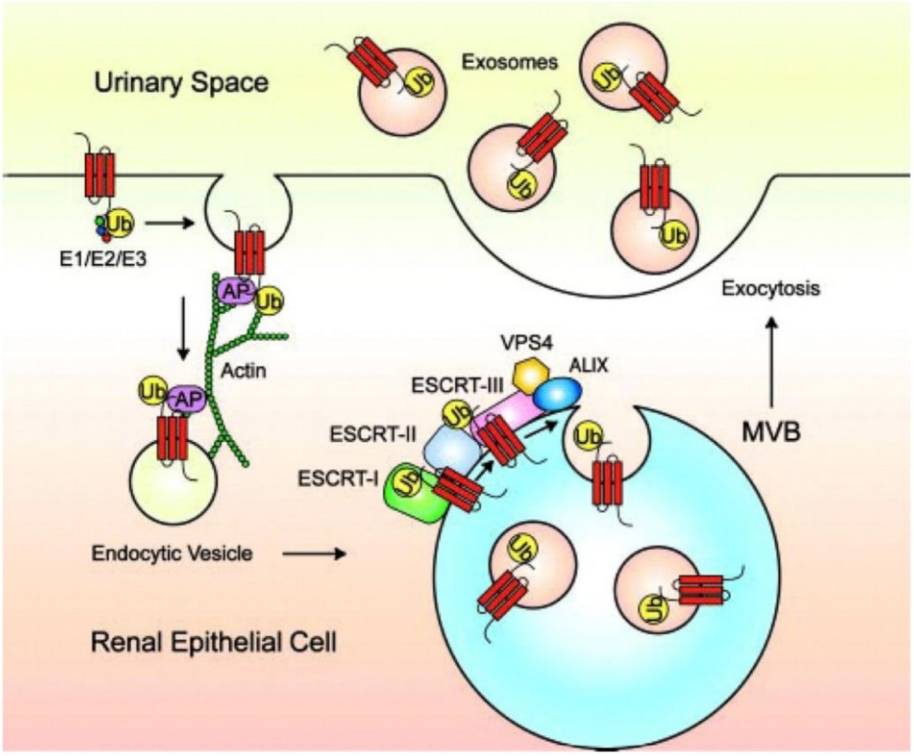

Figure 1.4: The process of exosome formation from renal epithelial cells.
The proposed mechanism for exosome formation and secretion in to the urine from renal epithelial cells. This figure is reproduced from from Pisitkun *et al*., 2004 with permission from PNAS.[119] Copyright (2004) National Academy of Sciences, U.S.A.

Table 1.2: Candidate biomarkers for UTO from the literature.

Protein ID	Source	Function	Reference
MCP-1	Monocytes	Chemotaxis	[185,190]
RANTES	Macrophages / lymphocytes	Chemokine, inflammation	[191]
TNF alpha	Macrophages	Inflammation, apoptosis	[192,193]
TGB beta	Tubules / macrophages	Fibrosis	[194]
NGAL	Neutrophils / tubules	Immune response, regulation of immune cell	[195,196]
Cystatin-C	Circulation	Marker of aberrant glomerular filtration	[195]
sFAS	Circulation	Inhibition of FASL	[191]
EGF	Kidney epithelium	Growth regulation	[185,190]
Osteopontin	Loop of Henle / Distal tubule	Antioxidant, CD44 interaction	[197]
β2-microglobulin	Circulation	MHC light chain	[193,195]
GGT	Brush border in proximal tubule	Amino acid transport and metabolism	[198]
Alkaline Phosphatase	Proximal tubules	Hydrolase	[198]
CE-MS signature	Urine	Various	[199]
LC-MS analysis	Urine	Various	[85,86]

Chapter 2: Materials and Methods

2.1. Materials

Bovine serum albumin (BSA; A9418), lysozyme (L6876), cytochrome C (C2506), ovalbumin (A5503), α-caseine (C6780), dephosphorylated α-caseine (C8032), trypsin (T802), phosphate buffered saline tablets (P4417), ammonium bicarbonate (ABC; A6141), protease inhibitor (P2714), acrylamide (A3699), Luria-Bertani (LB) media (L3022), agar (A5306), trifluoroacetic acid (TFA; T6508), and formic acid (FA; 94318) were obtained from Sigma (Oakville, ON, Canada). Materials for casting and running sodium dodecyl sulfate polyacrylamide gel electrophoresis (SDS-PAGE) and western blotting, including Tris (161-0719), SDS (161-0302) and blocking grade skim milk powder (170-6404), in addition to Quick Start™ Bradford (500-0201) and DC™ (500-0116) protein assay reagents, iodoacetamide (163-2109), and dithiothreitol (DTT; 161-0611) were purchased from Bio-Rad (Hercules, CA, USA). The bicinchoninic acid (BCA) protein assay was obtained from Pierce (Rockford, IL, USA). Methanol (A452), acetonitrile (ACN; A955) and acetone (BP2403) were of HPLC grade and were obtained from Fisher Scientific (Ottawa, ON, Canada). Sucrose (S7500) was from ACP Chemicals (Montreal, Canada). Non-sterile phosphate buffered saline (PBS), pH 7.4 (AM9625), tween-20 (BP337), sodium chloride (BP3581), and HEPES (845-1344) were also from Fisher. Cell culture reagents Dulbecco's Modified Eagle Medium (DMEM; 11965-092), newborn calf serum (NCS; 16010-159), sterile PBS (10010-023), sodium bicarbonate (25080-094), and EDTA-trypsin (25300-062) were obtained from Gibco (Carlsbad, CA, USA).

2.2. Cell culture and protein isolation

2.2.1. *Escherichia coli*

Escherichia coli (strain K12) was obtained as a gift from Dr. Andrew Roger (Department of Biochemistry and Molecular Biology, Dalhousie University, Halifax, Canada). *E. coli* culture was maintained on LB media containing agar plates. For protein isolation, a single colony was seeded into a large volume of LB broth media and grown at 37 °C with shaking to an optical density at 600 nm (OD_{600}) of ~1.2 using sterile LB broth media as a blank. Broth cultures were chilled in an ice water bath for ~10 min and *E. coli* cells were isolated from 15 mL aliquots by centrifugation at ~5,000 × *g* for 15 min. Cell pellets were washed once with ice-cold PBS (pH 7.4), and stored at -20°C. *E. coli* proteins were extracted by two rapid freeze-thaw cycles, with homogenization on ice using a PelletPestle™ (Fisher) and final suspension of the cell pellet in 1 % SDS. Insoluble material was removed by centrifugation at 21,000 × *g* for 20 min at 4 °C, and the protein concentration was estimated using the Pierce BCA assay.

2.2.2. NRK-52E cell culture and stretch

The rat proximal tubule cells, NRK-52E, were maintained at 37ºC (5 % CO_2) in 'growth media' (DMEM supplemented with 10 % NCS, 2 % sodium bicarbonate (*v*/*v*)). The stretch experiment was conducted similar to described previously.[100] A total of 10^6 NRK-52E cells were seeded onto six-well elastomer culture plates coated with collagen type I (Bioflex; Flexcell, Hillsborough, N.C., USA). Cells were grown to 75-80 % confluence and rendered quiescent by incubation for 12 hr in 'starvation media' (DMEM with 1 % NCS, 2 % sodium bicarbonate). Cells were then subjected to continuous cycles

of stretch-relaxation ('stretched cells') in a FX-4000 Flexercell Strain Unit (Flexcell), or alternatively incubated under identical atmospheric conditions without stretch ('control cells') for 24 hr. Each stretch/relaxation cycle consisted of 2 sec of stretch according to a sinusoidal half wave pattern and 2 sec of zero stretch relaxation. Stretch distribution and orientation on the membrane was 25 % maximal biaxial stretch in the membrane center region changing gradually to 25 % maximal radial stretch at the membrane periphery. Immediately following stretch, two wells from each test condition were sacrificed for cell death ELISA according to manufacturer's instructions (1 544 675; Roche, Indianapolis, Ind., USA). In this ELISA, the cell membranes are lysed gently without disrupting the nuclear membrane, and insoluble material is pelleted. The supernatant is analyzed for the presence of DNA histone complexes, whose formation is indicative of an apoptotic response. In each test, the relative levels of apoptosis were normalized to the basal level of apoptosis noted in the controls. Cells were visualized from random regions of the membrane with a Leica DMIRB inverted stage microscope.

2.2.3. NRK-52E protein isolation

For the experiment described in Chapter 5, cells were stretched as described in section 2.2.2. Wells were washed with PBS, the cells were collected by scraping, and pelleted by centrifugation at 300 × g for 5 min. Protein was isolated from the cell pellets in a two-step crude fractionation procedure. Cell pellets were suspended in 150 µL of modified RIPA buffer (150 mM NaCl, 50 mM Tris, 50 mM Na_2HPO_4 (EMD, SX0715), 0.1 % NP-40 (Biobasic, DB0385), 1 mM Na_3VO_4 (Fisher, S454), 1 mM NaF (Fisher, S299), pH 7.5, with protease inhibitor (Sigma) 1:10, *v*/*v*), homogenized with a PelletPestle™ (Fisher) for 30 seconds, and incubated on ice for 5 min. Insoluble material

was removed by ultracentrifugation at 100,000 × *g* for 1 hr at 4°C. The supernatant was collected and labeled as the cytoplasmic (C) protein fraction. Insoluble material was suspended in 150 µL detergent lysis buffer (0.5 % SDS, 1 % Triton X-100 (Fisher, BP151), PBS, 1:10 protease inhibitor) and incubated for 1 hour with gentle agitation at 4°C. Insoluble material was again removed by ultracentrifugation (100,000 × *g*, 1 hr at 4°C) and the isolated supernatant was labeled as the membrane (M) protein fraction. Fractions C and M were assayed for protein concentration and stored at -80°C prior to analysis. This process was completed over three consecutive passages of cells, simulating three biological replicate analyses. The total workflow is shown in Figure 5.1 (Chapter 5).

2.3. Animals

Sprague-Dawley male and female weanling rats were maintained on standard rat chow, and all experimental procedures were carried out in compliance with the Canadian Council on Animal Care (Dalhousie University protocol number 05-083). Anesthesia was applied with inhaled isoflurane and partial obstruction was introduced by burying the left ureter in the psoas muscle as described previously,[179] while complete obstruction was generated by complete ligation of the left ureter with a 6.0 proline suture (Ethicon, Skillman, NJ). The left ureter of control rats was similarly exposed but not manipulated. All animals were housed individually in metabolic cages (Thermo Fisher Scientific, Rochester, NY) during urine collection for approximately 16 hr at 7 and 14 days post-surgery, and 24 hr at 21 days post-surgery, at which point the animals were sacrificed. During urine collection, sample tubes were chilled and contained 0.1 % NaN_3 (Fisher, S227) to prevent bacterial growth. A 1 mL aliquot of each urine sample was taken for osmolality and creatinine testing, and protease inhibitor (1:10; *v*:*v*) was added to the

remainder, and samples were stored at -80°C prior to exosome isolation. Osmolality was determined at the core facility in the IWK Health Centre, while creatinine concentration was determined by QuantiChrome™ assay kit (Bioassay systems, DICT-500) by Ms. Fang Liu (Department of Pathology, Dalhousie University, Halifax, NS). Additionally, kidneys were harvested, split longitudinally and either fixed in 10 % formalin and embedded in paraffin, or split again horizontally and flash frozen in liquid nitrogen or suspended in RNAlater (GE Life Sciences) and stored at -80°C. Sections were taken from the formalin fixed paraffin embedded kidneys and analyzed by haematoxylin and eosin staining by Dr. Weei-Yuan Huang (IWK Health Centre, Halifax, NS).

2.4. Gel electrophoresis

All protein separations in this thesis by sodium dodecyl sulfate polyacrylamide gel electrophoresis (SDS PAGE) were conducted using the Mini-Protean® system (Bio-Rad). Gels contained either 12 or 15 % acrylamide (T), as specified in the experiment. Gels were cast according to the Laemmli protocol[200] into glass plates with a 1.0 mm spacer. All samples resolved on SDS PAGE gels were diluted with 1 × Laemmli sample buffer, which was prepared as a 5 × stock solution (0.1 g/L SDS, 125 mM tris, pH 6.8, 20 % glycerol, 5 g/L bromophenol blue, 10 % β-mercaptoethanol) and stored at -20 °C prior to dilution. Gel running buffer contained 25 mM tris, 191 mM glycine, and 0.1 % SDS, pH 8.3. For protein band visualization, gels were stained either by silver staining[45] or by Coomassie Brilliant Blue (6104-58-1, Fisher).

2.5. Temperature programmed HPLC

2.5.1. Calibration curves

Standard curves for the BCA, Bradford and Dc protein assays were generated using BSA as per the manufacturer's recommendations and recorded on an Agilent (8353) spectrophotometer (Mississauga, ON, Canada). For HPLC analysis, BSA and lysozyme were used to generate standard curves through triplicate injection of 0.1, 0.25, 0.5, 1.0, 2.5, 5.0, 10.0, 20.0, 40.0, 60.0, and 80.0 μg of protein, as determined by weighing of the standard protein on an analytical balance. Column blank runs were included following injections exceeding 5 μg of protein to assess carry-over and ensure accurate elution areas. For temperature programmed HPLC testing, the proteome mixtures were injected at approximately 10 μg, as determined through the BCA assay.

2.5.2. Calculation of theoretical protein extinction coefficients

The extinction coefficients were calculated for all proteins in the human Uniprot database (downloaded August, 2012) containing 70,101 entries (http://www.uniprot.org/) following the methods of Pace *et al*.[201] at 280 nm (Equation 2.1) and Kuipers and Gruppen[202] at 214 nm (Equation 2.2).

$$\varepsilon_{280nm} = n_W(5500\ M^{-1}cm^{-1}) + n_Y(1490\ M^{-1}cm^{-1}) + n_C(125\ M^{-1}cm^{-1})$$

(Eq. 2.1)

$$\varepsilon_{214nm} = 923\ M^{-1}cm^{-1} \times n_{peptidebonds} \sum_{i=1}^{20} (\varepsilon_{aminoacid(i)} \times n_{aminoacid(i)})$$

(Eq. 2.2)

Referring to Equation 2.1, ε_{280nm} is the extinction coefficient for a particular protein at 280 nm ($M^{-1}cm^{-1}$). The number of tryptophan, tyrosine, and cysteine residues in the protein are represented by n_W, n_Y, and n_C, respectively. The number of each amino acid residues in the protein are multiplied by their respective extinction coefficients and summed to equal the extinction coefficient at 280 nm for that protein.

Referring to Equation 2.2, ε_{214nm} is the extinction coefficient for a particular protein at 214 nm ($M^{-1}cm^{-1}$). The extinction coefficient for a peptide bond at 214 nm is 923 $M^{-1}cm^{-1}$ and is thus multiplied by the number of peptide bonds ($n_{peptidebonds}$) in the protein. The extinction coefficients for each amino acid ($\varepsilon_{aminoacid(i)}$) at 214 nm in the protein multiplied by the total number of residues in the protein ($n_{aminoacid(i)}$) can then be summed to equal the total contribution of the amino acid side chains to the total extinction coefficient of the protein. The extinction coefficients for individual amino acid residues are listed by Kuipers and Gruppen.[202] Individual extinction coefficients were normalized to the mean and displayed on a log2 scale.

2.5.3. Coefficient of variance for protein assays

Stock solutions of the protein standards were prepared by mass at an approximate concentration of 1.0 mg/mL and the 'true' concentration was determined using the extinction coefficient of the pure proteins at 280 nm (or 410 nm for cytochrome c), calculated using the ExPASy web-based tool for calculating the theoretical extinction coefficient of proteins (ProtParam) based on methods by Pace *et al*. (Equation 2.1).[201] The concentration of the complex proteome extracts was determined through ultraviolet (UV) absorbance measurements at 280 nm by dividing the absorbance (A_{280}) value by the path length (1 cm) as described previously.[203] For each assay tested, the protein stock was diluted to the center of the linear portion of the curve, taking five measurements of independent solutions, as well as reagent blanks. The coefficient of variation (CV) was determined from the average response factor of each protein standard, relative to the response of BSA.

2.5.4. Protein sample preparation

The SDS-containing *E. coli* protein extracts (described in section 2.2.1) were subject to detergent removal through protein precipitation in ice-cold acetone (4:1, acetone:sample, *v*:*v*) overnight at -20°C, with inclusion of a single acetone wash as described previously.[32] Prior to HPLC injection, the protein pellet was resuspended in a small volume (10–20 μL) of 70 % formic acid and diluted with water such that the protein concentration was within the linear range of the calibration curve. All remaining samples were directly acidified with 0.1 % TFA and diluted to an appropriate concentration prior to HPLC analysis. The rat proximal tubule cells, NRK-52E, were grown and maintained

as described in section 2.2.2. For this experiment, protein was isolated from control (non-stretched) NRK-52E cells by suspending them in pure water on ice to promote osmotic lysis, and homogenized for 30 sec using a Pelletpestle™ (Fisher).

A known mass of blocking grade milk powder (Bio-Rad) was suspended in pure water (18 MΩ • cm) at an estimated protein concentration of 10 mg/mL (assuming a protein content of 30 % by weight, as per manufacturers estimate). The sample was diluted to 0.1 mg/mL protein and subject to chloroform-methanol-water precipitation through addition of a 4 parts methanol, 1 part chloroform, and 3 parts water over the volume of the original sample, and centrifugation at 16,000 × *g*. The protein pellet formed at the interface between the methanol/water and chloroform was resolubilized to its original volume using 1 % SDS (for BCA) or 70 % formic acid (for temperature programmed HPLC) in preparation for quantitative analysis. A 15 %T SDS PAGE gel was loaded with approximately 10 μg protein per lane (based on 30 % protein content), noting that equal volumes of the sample were compared before versus after precipitation. Proteins in the gel were visualized through silver staining[45] and photographed with a digital camera.

2.5.5. Chromatographic instrumentation and data analysis

Chromatographic experiments were conducted on an Agilent 1100/1200 hybrid HPLC system (Mississauga, ON, Canada) constituted of an autosampler (G1313A) equipped with a 100 μL sample injection loop, diode array detector (G1315B) equipped with a 50 nL flow cell recording at 214 nm, and fraction collector (G1364D). Separations were on a 1 mm × 50 mm self-packed column containing 2000 Å pore size, 20 μm

diameter, POROS® R2 beads (Applied Biosystems, Carlsbad, CA). The flow was set to 100 μL/min and fractions were collected in 1.5 mL vials. The gradient between solvent A (0.1 % TFA/water) and solvent B (0.1 % TFA/ACN) was varied through injection of a constant mass (~10 μg) of SDS-extracted *E. coli* protein to optimize the protein elution window and peak shape. The final gradient includes an initial hold at 5 % B for 16 min, followed by a linear increase to 95 % B over 8 min (Figure 3.3). The temperature of the column was adjusted using the column heating compartment of the Agilent HPLC system. Samples were loaded at 4 °C, 25 °C, or 80 °C. Eluting temperatures of 25 °C and 80 °C were explored. In each case, the temperature of the column was allowed to equilibrate to a constant value for approximately 2 min prior to applying the solvent gradient.

Protein recoveries were obtained through injection of an equal volume of the corresponding protein sample through the complete HPLC system, but with omission of the column.[204] Fractions were collected over a 15 min time interval (from 26 to 41 min) to insure complete recovery of the eluting fraction. Samples were fully dried in a SpeedVac and re-suspended in water with 1 % SDS and diluted appropriately for recovery determination by the BCA assay. Peak areas were obtained by exporting the data from ChemStation software to Microsoft Excel for integration, obtained by summing all intensities measured in 0.4 s intervals over the fraction collection timeframe (see Figure 3.3). Peak areas are reported following subtraction of the average blank peak area (triplicate injection) of a solvent blank collected immediately prior to the sample injection.

2.6. Exosome isolation and confirmation

Urine was thawed to room temperature, vigorously vortexed, and insoluble material was removed by centrifugation at 17,000 × *g* for 10 min at 4 °C. Exosomes were then isolated from the clarified urine as described previously.[205] Each clarified urine sample was overlaid onto a 30 % sucrose/D_2O cushion with 20 mM HEPES buffer at pH 7.4 and centrifuged at 200,000 × *g* for 1 hr at 4 °C with a Beckman SW41 Ti rotor in a Beckman L-90 ultracentrifuge (Beckman Coulter, Mississauga, ON). The sucrose cushion was collected and diluted in cold PBS with 1:10 (*v*:*v*) protease inhibitor (Sigma) and centrifuged again at 200,000 × *g* for 1 hr at 4 °C. A small volume of wash buffer was left at the bottom of the ultracentrifuge tube so to not disturb the invisible pellet. Exosomes were collected within the small volume of buffer, assayed for protein concentration by the Pierce BCA assay (Rockford, IL, USA) and stored at -80 °C prior to analysis.

For confirmation of the presence of exosomes, samples were subject to transmission electron microscopy (TEM) following a negative staining procedure conducted by Mary Ann Trevors (Department of Microbiology and Immunology, Dalhousie University, Halifax, NS). First a drop of sample was placed onto a Formvar/Carbon coated grid and allowed to sit for ~10 min. The sample was then rinsed with distilled water and a droplet of 2 % uranyl acetate was added for approximately 30 sec. The uranyl acetate was removed and the samples obtained from the 7 day post-surgery exosome pellets from control, complete, and partially obstructed rat groups were analyzed by TEM at the specified magnifications.

2.7. Mass spectrometry analysis workflow

2.7.1. Preface

The workflow employed for LC-MS analysis is similar throughout the thesis, although slight modifications were applied in each study, depending on the desired application. To clarify the specifics of each experiment, Figure 2.1 highlights the sample source, number of biological replicate analyses, gel slices, and replicate analyses conducted in each chapter. The specifics the experimental protocols are listed below.

2.7.2. In-gel digestion procedure

Following SDS PAGE, gels were stained with Coomassie Brilliant Blue (Bio-Rad, 161-0400) to visualize protein bands. Subsequent to destaining, each lane was sectioned horizontally into the specified number of gel slices and diced into ~ 1 mm^3 pieces. In Chapter 4, gels were sectioned into 5 or 10 slices per lane, depending on the desired application. In Chapter 5, gels were sectioned into 15 slices per lane, containing cytoplasmic (C) or membrane (M) fractions, totaling 30 slices per biological replicate. In Chapter 6, protein samples were only partially resolved into the gel, and thus were sectioned into only three slices per lane.

The in-gel digestion procedure is described in detail by Shevchenko *et al*.[39] Diced gel slices were first dehydrated with ACN for 10 min at room temperature. ACN was removed, and disulfide bonds were reduced for 30 min by adding enough 10 mM DTT in 100 mM ABC to cover the gel pieces and incubating the gel slices in a hot water bath (56 °C). Gel slices were again dehydrated with ACN for 10 min. Following removal of ACN,

reduced cysteine residues were alkylated by covering the gel pieces with 55 mM iodoacetamide in 100 mM ABC and incubating at room temperature in the dark for 25 min. Gel slices were dehydrated with ACN again, and following solvent removal were covered with a solution of 13 ng/µL trypsin in 10 mM ABC with 10 % ACN (*v*:*v*). To promote longevity of trypsin activity during gel slice rehydration and trypsin diffusion into the gel matrix, gel pieces were incubated in the refrigerator at 4 °C for 90 min, adding additional trypsin buffer to maintain gel coverage during rehydration. In-gel digestion was then conducted overnight (~16 hours) in a 37 °C water bath.

Following digestion, peptides were extracted in a solution of 1:2 (*v*:*v*) 5 % FA/water : ACN for 15 min at 37°C. The gel slices were spun down and the supernatant was collected. A second extraction was then conducted by re-hydrating gel slices with 10 mM ABC for 20 min, followed by incubation in the extraction buffer for another 15 min at 37 °C. Both extraction solutions were combined, dried completely in a SpeedVac, and stored at -20 °C prior to use.

2.7.3. Peptide sample preparation for LC-MS

Prior to LC-MS analysis, all peptide samples were de-salted and quantified offline by reversed-phase HPLC. Peptide cleanups were conducted on the Agilent 1100/1200 hybrid HPLC system described in section 2.5.5. Separations were on a 1 mm × 50 mm self-packed column containing 5 µm diameter, 300 Å pore size, Waters Spherisorb S5 OD52 C_{18} beads (Milford, MA, USA). The flow was set to 100 µL/min and fractions were collected in 1.5 mL vials.

For cleanup, dried peptide extract samples were resuspended in a solution containing 5 % ACN/0.1 % TFA/water by brief sonication in a sonicating water bath and vortexing. Peptide samples were loaded onto the column by the autosampler and eluted with an instantaneous gradient from 5 to 85 % B over 0.1 min. This gradient eluted peptides eluted in a single peak which was collected, dried in a SpeedVac, and stored at -20 °C prior to analysis.

2.7.4. LC-MS instrumentation

All LC-MS analyses were conducted on a hybrid Agilent 1050/1200 nanoflow reversed-phase liquid chromatography system (Oakville, ON, Canada), coupled to a ThermoFisher LTQ linear ion trap mass spectrometer (San Jose, CA, USA) through a modified dual column nanospray ionization source (spray voltage 2.5 kV). Validation of the system is presented in Chapter 4 and a schematic is presented in Figure 4.1. The solvents employed were 0.1 % FA/water (solvent A), and 0.1 % FA/ACN (solvent B). An Agilent 1200 Nanoflow pump (G2226A) was used for gradient elution of peptides from the capillary columns, while an Agilent 1050 quaternary pump flowing through a flow splitting T ahead of the autosampler (G1313A) to reduce the initial 100 μL/min flow from the pump to a rate of 300 nL/min using a solvent comprising 5 % B in solvent A was used for sample loading. A combination of PEEKsil (Upchurch) and silica capillary tubing (PolyMicro Technologies, Phoenix, AZ) was employed, all having inner diameters of 50 μm. A two-position six-port valve equipped with external relay contact control (Rheodyne MXP7980 high-pressure nano switch valve; Idex Health and Science, Oak Harbor, WA, USA) was used to direct flow.

The power supply from the LTQ nanospray source was routed through a custom designed high voltage switch, which directs voltage to one of the two capillary columns, connected *via* a liquid junction through a 360 μm OD Upchurch MicroTee (Idex Health and Science). Capillary columns (30 cm × 75 μm i.d.) were packed in-house with reversed-phase Phenomenex (Torrance, CA) Jupiter beads (C12, 4 μm, 90 Å pore size) into silica PicoFrit Emitters (New Objectives, Woburn, MA), and connected to the MicroTee. The emitters were mounted to a piece of plastic affixed to the existing *xyz* stage of the LTQ nanospray interface.

2.7.5. LC-MS analysis

Desalted peptide samples were analyzed using one of two gradients between solvent A (0.1 % FA/water) and solvent B (0.1 % FA/ACN) totaling 65 or 125 min elution gradients. Samples (10 μL volume) were sequentially loaded onto each column with the load pump while eluting from the opposing column with the Agilent 1200 Nanoflow pump at a flow rate of 250 nL/min. The 65 min gradient was as follows: 0 min, 5 % B; 0.1 min, 7.5 % B; 45 min, 20.0 % B; 57.5 min, 25 % B; 60 min, 35 % B; 61 min, 80 % B; 64.9 min, 80 % B; 65 min, 5 % B. The 125 min gradient was as follows: 0 min, 5 % B; 0.1 min, 7.5 % B; 90 min, 20 % B; 115 min, 25 % B; 120 min, 35 % B; 121 min, 80 % B; 125 min, 80 % B; 125.1 min, 5 % B. The LTQ was set to data-dependent mode (MS followed by MS/MS of top three peaks) as described in the introduction. The timing of sample injection and column selection on the dual spray system is described in detail in Appendix A1.

2.7.6. Data Analysis

Database searching used the SEQUEST algorithm within the Thermo Proteome Discoverer (v. 1.3) software package. MS spectra were searched against the species-specific database. Peptide tolerances were set to 2.0 Da for precursor and 1.0 Da fragment ions. Allowable modifications included static carbamidomethylation (+57.0215 Da) of cysteine residues, dynamic phosphorylation (+79.9663 Da) of serine, tyrosine, and threonine residues (dynamic phosphorylation was omitted for rat urine exosome analysis in Chapter 6), and dynamic oxidation (+15.9949 Da) of methionine, with up to two missed trypsin cleavages allowed. Peptide filters were adjusted to provide a false discovery rate of 1 % or less by decoy database searching, and proteins required a minimum of two unique peptides for positive identification. The spectral count value (SpH) per protein is defined as the total number of assigned peptide identifications per protein.

2.7.7. Spectral counting and statistical analysis

Label-free quantitative analysis of relative protein abundance was accomplished by spectral counting with appropriate normalization.[67,206] Each spectral hit value (the number of peptides mapped to that protein by SEQUEST) was divided by the total number of spectral hits in their respective sample (gel lane), and then multiplied by the largest number of spectral hits per replicate in the comparison. This normalization technique corrects for errors in protein concentration between samples and variations in gel extraction efficiency (annotated NSpH). In Chapter 5, peptide spectral matches were pooled from membrane (M) and cytoplasmic (C) subcellular fractions within each

biological replicate prior to normalization. Technical replicate data (*e.g*. the separate MS analyses of each gel slice) were included for statistical analysis. Each biological replicate in Chapter 5 was analyzed in duplicate, while those in Chapter 6 were conducted in quadruplicate. Normalized spectral count data were then analyzed using a previously published method for analyzing spectral counting data known as QuasiTel available freely online as an R script,[68] modified slightly to accommodate the input format for this experiment. The modified R script is provided in the supplementary information in Orton, *et al*.[207] All proteins with a quasi-Poisson p-value < 0.05 were considered to be significantly altered in abundance.

2.7.8. Protein annotation (GO and KEGG)

Functional enrichment of gene ontology (GO) terms of significantly altered proteins was accomplished using the online functional enrichment database tool DAVID.[208,209] Significantly altered protein lists were uploaded and the *Rattus Norvegicus* proteome background was employed. KEGG (Kyoto Encyclopedia of Genes and Genomes) pathway functional enrichment was determined by searching using the KOBAS 2.0 online tool,[210] again using the *Rattus Norvegicus* background. Default filters and settings were used in each case.

2.8. Western blotting

Confirmation of quantitative proteomic results in Chapters 5 and 6 was conducted by western blotting. Protein samples were isolated by suspending the respective samples in 1 % SDS lysis solution and resolved on 12 % T SDS PAGE gels. Protein was transferred to polyvinyl-divinyl fluoride (PVDF) membranes in a Mini Trans-Blot cell®

(Bio-Rad), blocked in 5 % milk for variable lengths of time, and probed for a number of different proteins. An appropriate secondary antibody conjugated to horseradish peroxidase was applied and detected on X-films by application of Amersham ECL Prime Western Blotting Detection Reagent (GE Healthcare Life Sciences, Baie d'Urfe, Quebec). Table 2.2 displays information for all antibodies employed in this study.

Table 2.1: Molar extinction coefficients at 214 nm of amino acids.
Values taken from Kuipers and Gruppen, 2007.[202]

Amino Acid	ε_{214nm}	Amino Acid	ε_{214nm}
Alanine (A)	32	Leucine (L)	45
Arginine (R)	102	Lysine (K)	41
Asparagine (N)	136	Methionine (M)	980
Aspartate (D)	58	Phenylalanine (F)	5200
Cysteine (C)	225	Proline (P)	30
Glutamine (Q)	142	Serine (S)	34
Glutamate (E)	78	Threonine (T)	41
Glycine (G)	21	Tryptophan (W)	29050
Histidine (H)	5125	Tyrosine (Y)	5375
Isoleucine (I)	45	Valine (V)	43

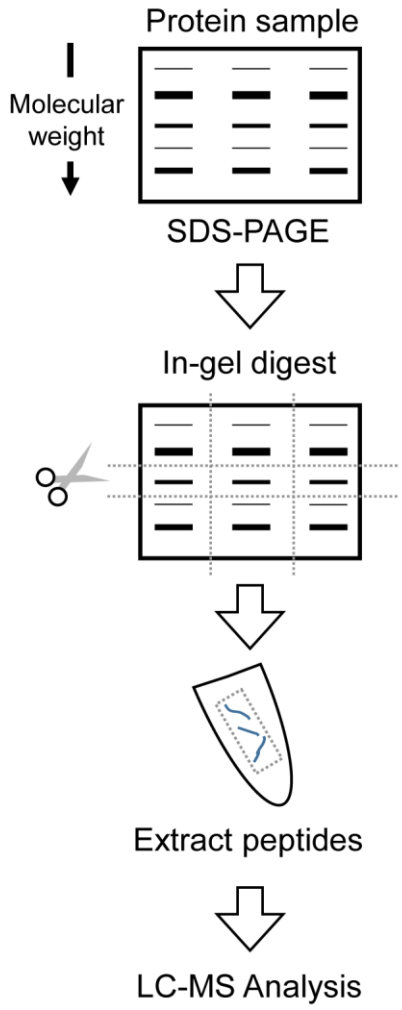

	Chapter 4	Chapter 5	Chapter 6
Protein sample:	• *E. coli* • Standard sample	• NRK-52E • *In vitro* UTO model	• Urinary exosomes • *In vivo* UTO model
Gel Lanes:	• 6 lane × 50 µg *E. coli*	• 3 passages • Stretched / control cells	• Pool: 3 sham, 3 PUO, 3 CUO • N = 22 rats
# Gel Slices:	• 5 or 10	• 15 Cytoplasm • 15 Membrane	• 3 per pooled biological replicate
Technical replicates:	• One to six	• Two	• Four

Figure 2.1: A summary MS workflow for the chapters described in this thesis. All MS analyses in this thesis employed in-gel digestion prior to LC-MS analysis. Chapter 3 did not involve LC-MS, thus it is excluded from this figure. Chapter 4 presents a dual-column interface for LC-MS analyses. The system was used to justify various amounts of protein-level fractionation versus technical replication. Chapter 5 conducts a whole-cell proteome analysis requiring extensive sample prefractionation, but only limited technical replication. Chapter 6 conducts an exosomal proteomic analysis for candidate biomarker discovery that requires only slight fractionation, but extensive replication.

Table 2.2: Antibody information.

Target protein	Host	Source	Product #
Aldose Reductase	Rabbit	Novus Biologicals	NBP1-00709
CD44	Mouse	Novus Biologicals	NBP1-47386
Annexin A1	Rabbit	Cell Signalling	3299
Vimentin	Mouse	Santa Cruz	SC-32322
Alpha-catenin	Rabbit	Novus Biologicals	NB110-55563
Ceruloplasmin	Rabbit	Abcam	AB131220
Aminopeptidase N (CD13)	Rabbit	Abcam	AB108310
Rabbit IgG – HRP	Goat	Acris	R1364HRP
Mouse IgG - HRP	Rabbit	Acris	R1253HRP

Chapter 3:

Universal, high recovery assay for protein quantitation through temperature programmed liquid chromatography (TPLC)

3.1. Preface

Preliminary work into isolation and proteome analysis of exosomes revealed the extremely low abundance of these protein samples (~1 μg/10 mL urine). To reduce excessive sample sacrifice for estimation of protein concentration, this chapter introduces a method employing temperature controlled HPLC to provide quantitative assessment of protein concentration while allowing high sample recovery (>95 %). In addition to the high sample recovery, this method also demonstrates a more robust method for quantification exhibiting less variability between protein samples compared to other quantitative methods (RSD ~9 %). Unfortunately, the time required for validation of this method prevented its application to subsequent chapters in this thesis. This work is published in the manuscript: Orton, D.J.; Doucette, A.A. Universal, high recovery assay for protein quantitation through temperature programmed liquid chromatography (TPLC). *J. Chromatogr. B*. **2013**, *15*, 975-980.

*Writing and experiments were completed by Dennis Orton. Dr. Alan Doucette contributed to experimental design and revisions to the manuscript.

3.2. Introduction

Accurate estimation of total protein concentration is integral to the proteome analysis workflow. Direct UV absorbance measurement at 280 nm (A_{280}) is the classic approach to quantify single proteins in a sample.[203] The protein's extinction coefficient at 280 nm is primarily dependent on the tyrosine and tryptophan content and can be determined computationally,[201,211] or empirically.[212] Given the extinction coefficient, A_{280} measurements afford high accuracy and sensitivity for determination of protein concentration, while circumventing the need for standard calibration. However, when the protein sequence is unknown, or when estimating total protein in a mixture, A_{280} measurements will only approximate the protein concentration (absorbance of 1.0 = 1.0 mg/mL).[203] The direct absorbance assay is also highly susceptible to interference by non-protein substances, making it unavailable for numerous proteome applications.[213] Consequently, a direct UV absorbance assay is not the favored tool for total protein quantitation.

Colorimetric reagent assays (*e.g.* BCA,[214] Bradford,[215] or D_C/Lowry[216]) provide an alternative to direct absorbance measurements. Such assays provide improved selectivity toward proteins which minimizes the concerns of interfering substances. Nonetheless, with a differing response toward various protein types, colorimetric assays require calibration with an appropriate standard. Of particular concern, however, is the use of a colorimetric assay in protein limited applications. Given the sensitivity of colorimetric assays (μg/mL), and depending on the volume requirements of the spectrometer, these assays may consume a significant portion of the available sample.

Therefore, the development of a sensitive and selective quantitative assay with high protein recovery would provide a desirable alternative for sample limited proteome applications.

Coupling UV absorbance with reversed-phase liquid chromatography (RPLC) is a ubiquitous tool for quantitative analysis. Chromatographic separation affords improved detection selectivity as analytes are separated from interfering compounds. Although most interferences are removed, protein quantitation by RPLC with UV detection (LC-UV) at A_{280} continues to impart high response variability between proteins. For this reason, LC-UV at 280 nm is most commonly used to quantify single proteins relative to a calibrated response curve of the purified standard. Alternatively, the concentration can be determined relative to a calculated response factor based on the amino acid sequence,[217] or can be referenced to an internal standard.[218] With emphasis on proteins lacking absorbance at 280 nm (*i.e.* without aromatic residues), Kuipers and Gruppen estimated the molar extinction coefficient of proteins and peptides at 214 nm based on the amino acid composition.[202] They demonstrate that protein absorbance measurements at 214 nm provide increased sensitivity, and by incorporating the peptide bond into the response, allow a more universal protein detection strategy. Following a similar strategy, LC-UV at 214 nm has been used to quantify the total peptide concentration in a complex mixture.[34] This method used a standard curve constructed from a set of four digested proteins to calibration the response of a complex peptide sample and conveniently provides a form of automated sample cleanup.[34] To date, the strategy has not been applied to quantify intact proteins from a proteome mixture.

One of the limiting factors of an LC-UV approach to quantify total protein in a mixture is the variable recovery of intact proteins from reversed phase separation. Choosing the correct solvent system and stationary phase are of utmost importance for improving quantitative results.[219] Along with optimization of column and solvent conditions, the use of elevated temperatures has been shown to improve separation efficiency and recovery of proteins, approaching 100 % recovery.[204,220–222] The objective of this Chapter is to incorporate a reversed phase approach involving temperature-programmed liquid chromatography (TPLC) to recover intact proteins in high yield and allow protein quantitation. Eluting proteins are recovered over a narrow time window, and are observed as a sharp quantifiable peak. Through calibration with a single protein standard, TPLC demonstrates high recovery and accurate quantitation of complex protein mixtures in sample limited proteome applications (<1 μg).

3.3. Experimental in brief

Determination of the experimental parameters yielding the best sample recovery and quantitative results was conducted by testing various temperature and solvent gradient conditions. The optimal wavelength was determined by applying the formulas proposed by Kuipers and Gruppen,[202] and Pace *et al*.[201] to the human Uniprot proteome (downloaded August, 2012; containing 70,101 entries). These values were normalized to the molecular mass of each protein to correct for protein size and allow comparison. Testing of the quantitative ability of this method was then conducted by comparing the responses of a number of protein samples to that of BSA, and interferences were investigated by quantitative analysis of skim milk as an example of a protein sample containing interfering substances.

3.4. Results and discussion

Quantitation of total protein by RPLC is herein accomplished by eluting all components over a narrow window. This facilitates integration of the sample peak, further enabling high protein recovery within a single collection vial. Figure 3.1 displays the resulting chromatograms of ~10 μg injected protein using a rapid solvent gradient from 5 to 95 % over 8 min. The combination of temperature and solvent gradients consistently elutes protein as a single peak over an approximate 2 min window. Shifting retention times of the eluting proteins do not affect the quantitative assay, as the chromatogram is integrated over a broader interval (15 min). An instantaneous solvent gradient from 5 to 95 % B also yielded a single eluting peak, although higher background variability generated by the solvent front increased the limit of quantitation. Therefore the 8 min gradient was selected to assess total protein concentration.

3.4.1. Effect of temperature on protein recovery

Conducting RPLC separations at constant elevated temperature has previously been shown to provide high protein recovery, approaching 100 %.[204,220] However, as applied here, separations conducted at a constant 80 °C led to a gradual degradation of column performance. Specifically, protein recovery dropped from a high of 90 to 95 % and ended below 60 % after 10 replicate injections. Although the polymeric stationary phase employed in this study was selected for its heat stability and favourability for intact protein separation, the performance of the column could not be restored through simple washes. Given the reduced recovery, an alternative heating strategy was investigated.

Previous studies have shown that varying the column temperature can have a profound effect on analyte retention. In fact, a 4-5 °C change in temperature is shown to correspond to an approximate 1 % change in solvent composition.[223] Figure 3.2 shows that at a constant 25 °C, the solvent gradient alone yielded approximately 65 % recovery. The resulting protein loss corresponds to components which retain on the column, as evident by the absence of protein in the non-retained fraction (injection peak). Application of a temperature change from 4 °C during loading to 25 °C for elution provides an increase in protein recovery to 82 %, clearly demonstrating the influence of temperature on protein retention. Extending the temperature program from 4 to 80 °C (load-elute) further improved recovery to 93 %. However, given the added time requirements to cool the column below room temperature (~100 min total run time), a temperature program from 25 to 80 °C was selected, and found to provide similar protein recovery (94 %). It is further noted that no degradation of column performance was observed when employing the temperature program. The reversed phase column remained stable over the entire course of the experiments (>100 sample injections). Thus, the 25-80 °C temperature program is the preferred method for maintaining high protein recovery across a complex proteome mixture.

The efficacy of the 25-80 °C method was tested at lower protein loading by injecting a 1 µg sample of *E. coli* total proteome extract. As shown in Figure 3.2, recovery remains high (99 %), illustrating the potential for TPLC to permit quantitative analysis of proteins without sacrificing the sample. A sample chromatogram displaying the final TPLC method is provided in Figure 3.3. Column temperature is allowed to equilibrate at maximum temperature for a minimum of 2 min prior to analyte elution. The

collection window is also noted in Figure 3.3 where, at a flow rate of 100 μL min^{-1}, a 15 min fraction can be collected in a single 1.5 mL vial.

3.4.2. Wavelength selection

Accurate assessment of total protein concentration by response curve generation assumes the sensitivity of the calibrant is similar to that of the unknown. A_{280} measurements are known to display high signal variability, given that the extinction coefficient depends primarily on the aromatic amino acid content of the protein.[201,211] At 214 nm, the sensitivity is reported as approximately 15-20 fold higher than at 280 nm.[202] Furthermore, in probing the peptide bond, all proteins will show appreciable absorbance at this wavelength. Figure 3.4 summarizes the protein-to-protein variation of computationally derived molar extinction coefficients at 280 and 214 nm, as calculated across the entire human proteome. The average extinction at 214 nm (calculated at 673,043 M^{-1} cm^{-1}) was approximately 16.5 fold higher than at 280 nm (40,771 M^{-1} cm^{-1}). For ease of comparison, the individual extinction coefficients were therefore normalized with respect to their average values at each wavelength.

As seen in Figure 3.4A, on a molar basis, significant variation in signal response exists for individual proteins across the human proteome at both wavelengths. This is to be expected, as low molecular weight proteins will generally exhibit a lower molar extinction coefficient. The coefficient of variance in the extinction coefficient was similar at these wavelengths, equating to 133 % at 214 nm versus 126 % at 280 nm. The box and whisker plots demonstrate the skew from a normal distribution, as the median (line at center of box) is significantly lower than the normalized average. Translating these values

for measuring protein concentration, it can be concluded that absorbance measurements at 214 and at 280 nm would provide significant differences in sensitivity on a per mole basis (*e*.*g*. mol/L). However, total protein quantitation is more typically assessed on a mass basis (*e*.g. g/L). Thus, comparison of extinction coefficients requires consideration of the protein molecular mass.

Figure 3.4B demonstrates the spread between extinction coefficients normalized according to the molecular mass of the protein. The units of these extinction coefficients are L cm^{-1} g^{-1}, meaning that the absorbance readings provide a measure of the protein concentration in g/L. Following normalization, the spread in the extinction coefficient is significantly reduced at both wavelengths. However, the distribution at 214 nm shows lower inter-protein variability, as measured by a CV of 21 % (versus 42 % at 280 nm). At 214 nm, peptide bonds were calculated to account for approximately 51 % of the total protein absorbance across the proteome. Thus, accounting for the molecular mass, absorbance measures at this wavelength show tight agreement across the proteome. As seen in Figure 3.4B, while both distributions (214 and 280 nm) are approximately normal, the spread at is significantly reduced at 214 nm. These calculations justify the use of 214 nm to probe total protein concentration with minimal variation in signal response across individual proteins. Thus, a representative protein standard can be selected to calibrate the response of all proteins in a LC-UV quantitation assay.

3.4.3. Protein response curves

Figure 3.5 illustrates the response curves of BSA and lysozyme over the range 0.1-80 μg at 214 nm (Figure 3.5A) and 280 nm (Figure 3.5B). At 280 nm, the sensitivity

of lysozyme is significantly greater than that of BSA, being a consequence of the variable extinction coefficients at this wavelength. However, as seen in Figure 3.5B, at 214 nm these two proteins show nearly overlapping signal response across the range 0.1-80 μg. Thus, if BSA is used as a calibrating standard, estimation of the lysozyme concentration would be more accurate at 214 nm than at 280 nm.

The inset in Figure 3.5A displays the non-linear signal response of BSA and lysozyme at 214 nm beyond 10 μg injections. This is a consequence of the higher sensitivity at 214 nm which leads to absorbance signal saturation in the sharply eluting peak (peak maximum exceeds an absorbance of 2). The linear range at 214 nm extends to 5 μg, but can be fit to a second order polynomial up to 10 μg injected. Subsequent blank run peak areas showed undetectable protein carry-over with injections over the linear range, extending up to 20 μg injected. Based on the linear regression, a lower limit of quantification (LOQ) of 0.74 μg and 0.71 μg are calculated for BSA and lysozyme, respectively. It is further noted that the response curves at 280 nm are linear up to 80 μg, suggesting that protein recovery remains consistent up to this higher loading amount. Thus, the capacity of the column is not exceeded up to 80 μg. However, higher mass (40-80 μg) injections display carry-over nearing 2.5–5 % of total mass injected (by peak area), and therefore require a blank run prior to subsequent sample analysis (data not shown).

3.4.4. Assay comparison

The accuracy of a protein assay will be influenced by the variation in response between the unknown and the calibrant. The choice of calibrant is therefore an important

variable when calculating concentration based on response curves. Here BSA was chosen as the calibrant and used to assess the variation in response for five distinct single protein standards and two proteome mixtures. Direct comparison between the TPLC-UV assay and three commonly employed colorimetric assays (BCA, Bradford, and DC) is provided in Table 3.1.

The observed CV of the conventional colorimetric assays ranged from 19 % (BCA) to 23 % (Bradford), which is in agreement with the advertised values as reported by the manufacturer. By comparison, the TPLC method displays a CV of 9.6 %, with the most variation found in the protein α-casein. This protein is highly phosphorylated, contributing to an increase in detector response relative to a non-phosphorylated standard. As shown in Table 3.1, dephosphorylated α-casein shows greater agreement to the response of BSA by TPLC, suggesting highly phosphorylated proteins provide higher response TPLC. Application of TPLC for total protein quantitation reveals close agreement to the 'true' protein concentration (determined by $A_{260/280}$), with an error below 14 %. These response values are in closer agreement with the response of BSA (as calibrant), compared to the reagent assays. It is further noted that the *E. coli* proteome extract was obtained in solution containing 1 % SDS. However, detergent removal and subsequent protein resolubilization in 70 % formic acid enables accurate assessment of protein concentration of a sample originally prepared in SDS. A gel image showing the recovery from each process is provided in Figure 3.6. When employing a single calibration standard, TPLC is shown to be a reliable assay for total protein quantitation.

3.4.5. Application of TPLC for quantitative analysis

The TPLC method was applied to quantify a sample of milk protein. The total protein content of skim milk powder (Bio-Rad) is reported to be approximately 30% by weight. However, as shown in Figure 3.7 the protein content as determined by BCA was 55%. It is proposed that the presence of lactose in the milk sample overestimates the protein concentration through the BCA assay. Protein precipitation removes this interference, and allows a more accurate estimation of protein concentration (25 %). The gel image in Figure 3.7 shows the high recovery of the precipitation step, suggesting the difference in protein concentration before and after precipitation is a primary consequence of the interference being removed, as opposed to limited protein recovery. TPLC removes lactose and other non-protein contaminants, including buffer additives such as salts, reducing agents and urea prior to quantitation, allowing a more accurate assessment of protein concentration. The protein content in the milk sample as determined by TPLC (before and after precipitation) was similar to the BCA assay following removal of the interference. The TPLC method is compatible with many buffer additives and interfering compounds, however, detergents must be removed prior to quantitative analysis, as they retain on reversed-phase columns and interfere with quantitation. Here, either acetone or chloroform/methanol/water precipitation methods were used to remove SDS and other interfereing compounds. Following precipitation, concentrated formic acid is used for RPLC-friendly protein resolubilization to yield good quantitative results.

3.5. Concluding remarks

A method for total protein quantitation with high analyte recovery has been developed using a single standard protein to calibrate the LC/UV response at 214 nm. Incorporation of temperature programming increases recovery to greater than 90 %. This method was validated over a period of several months, with little to no change in sensitivity. This implies that construction of the calibration curve need only be conducted once over the lifetime of the UV lamp. The method is applicable to quantify low quantities of protein, and as a non-destructive technique, is particularly valuable in sample limited applications.

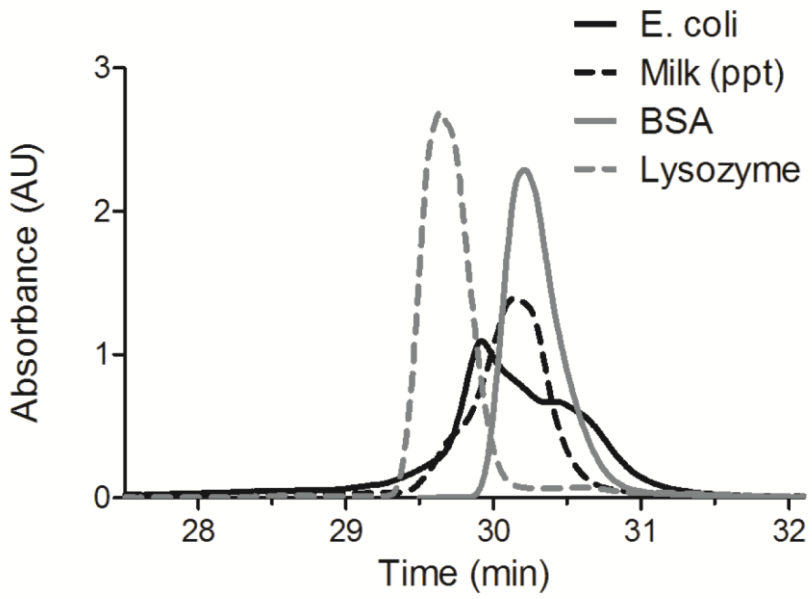

Figure 3.1: Example chromatograms following TPLC of various proteins and proteome mixtures.
The final gradient for eluting protein from a reversed phase column (1 mm × 50 mm) was an 8 min solvent gradient (5-95 % ACN) and following application of a temperature program from 25◦C to 80◦C (load-elute). The absorbance was recorded at 214 nm, with a single fraction collected over the time interval 26-41 min.

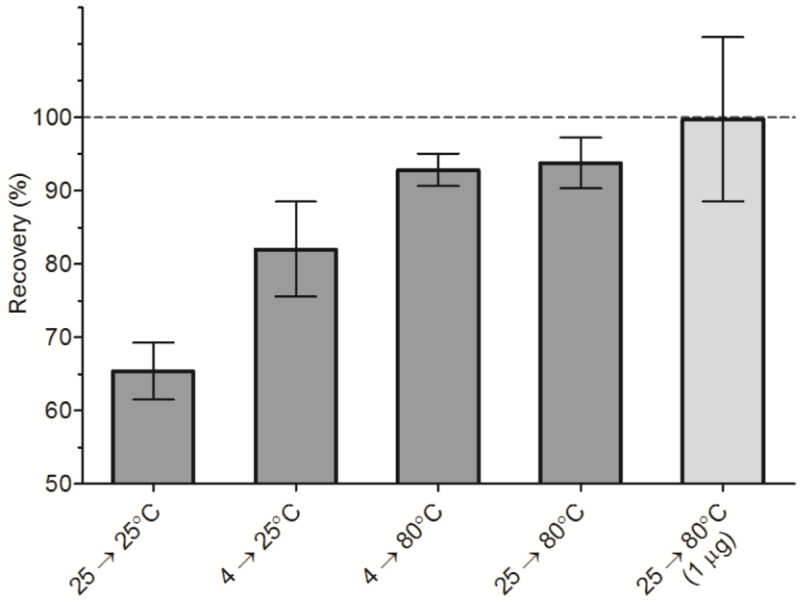

Figure 3.2: Assessment of protein recovery with temperature programming. Total protein injected was 10 µg (gray bars) or 1 µg (white bar) *E. coli* total proteome extract. The temperature of the column is listed below the bars as (load temperature) → (elution temperature). Error bars represent the standard deviation from 5 replicate injections.

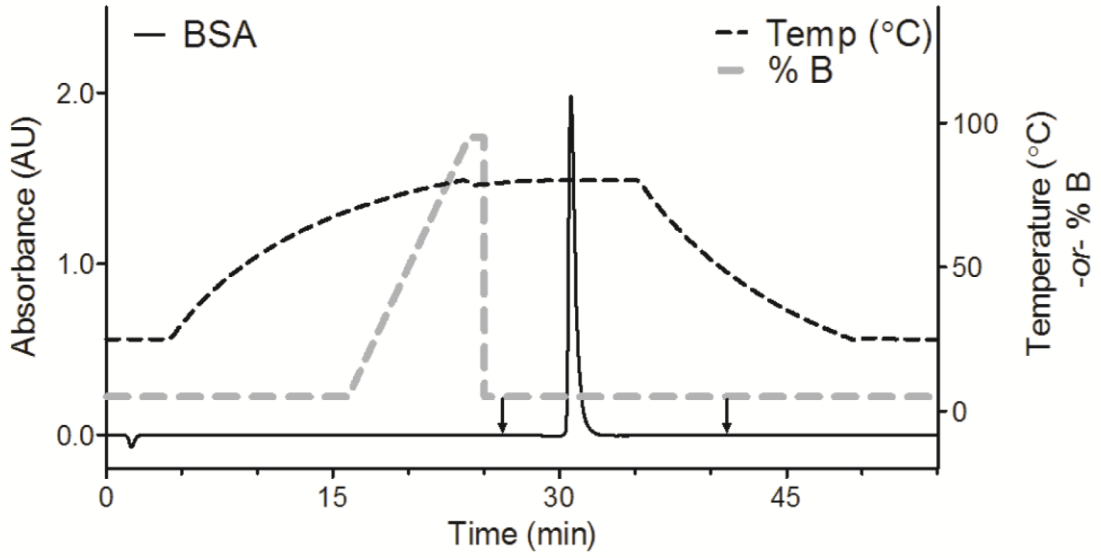

Figure 3.3: A representative TPLC run showing the A_{214}, temperature, and solvent gradient.
The TPLC method employs a solvent gradient from 5 to 95 % acetonitrile, over an 8 min period, following elevation of the column temperature to 80 °C. The protein fraction elutes as a sharp peak and is collected in a single vial (arrows indicate time over which fraction is collected).

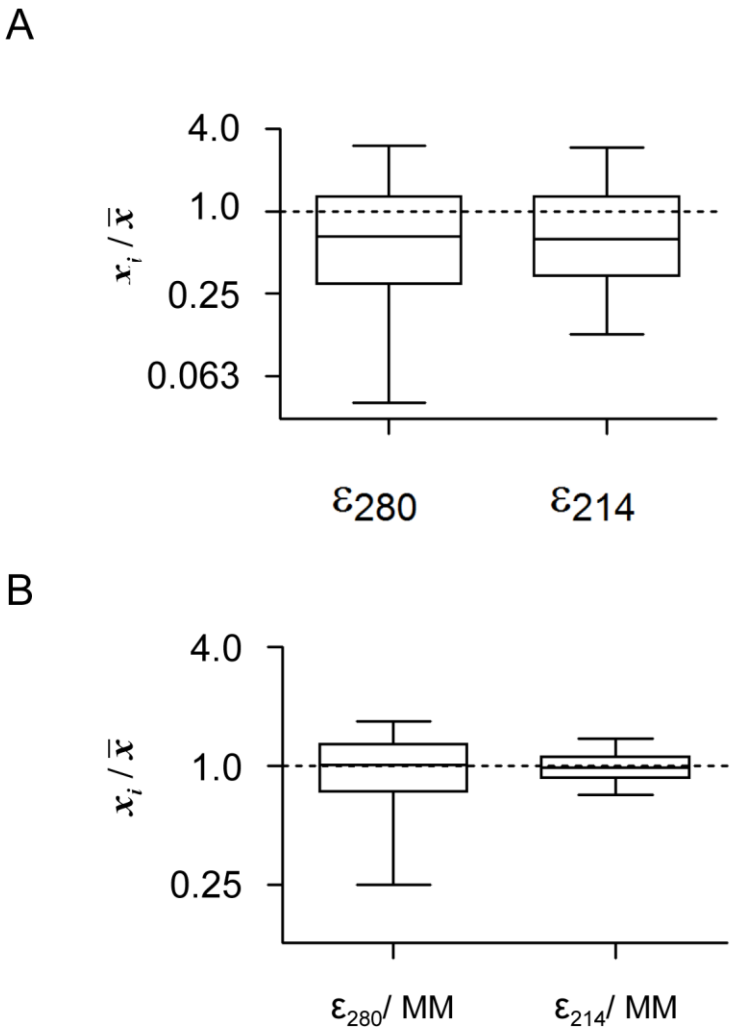

Figure 3.4: Box and whisker plots displaying the variation in calculated protein extinction coefficients across the human proteome at 214 and 280 nm.
(A) Plots represent the 1st and 3rd quartiles (box) together with median (solid line in box) and the 5th and 95th percentile (bars) for the molar extinction coefficient ($cm^{-1}M^{-1}$), following normalization to the average at each wavelength. (B) Shows an equivalent plot of the extinction coefficient accounting for the molecular mass ($cm^{-1}g^{-1}L$) of the protein.

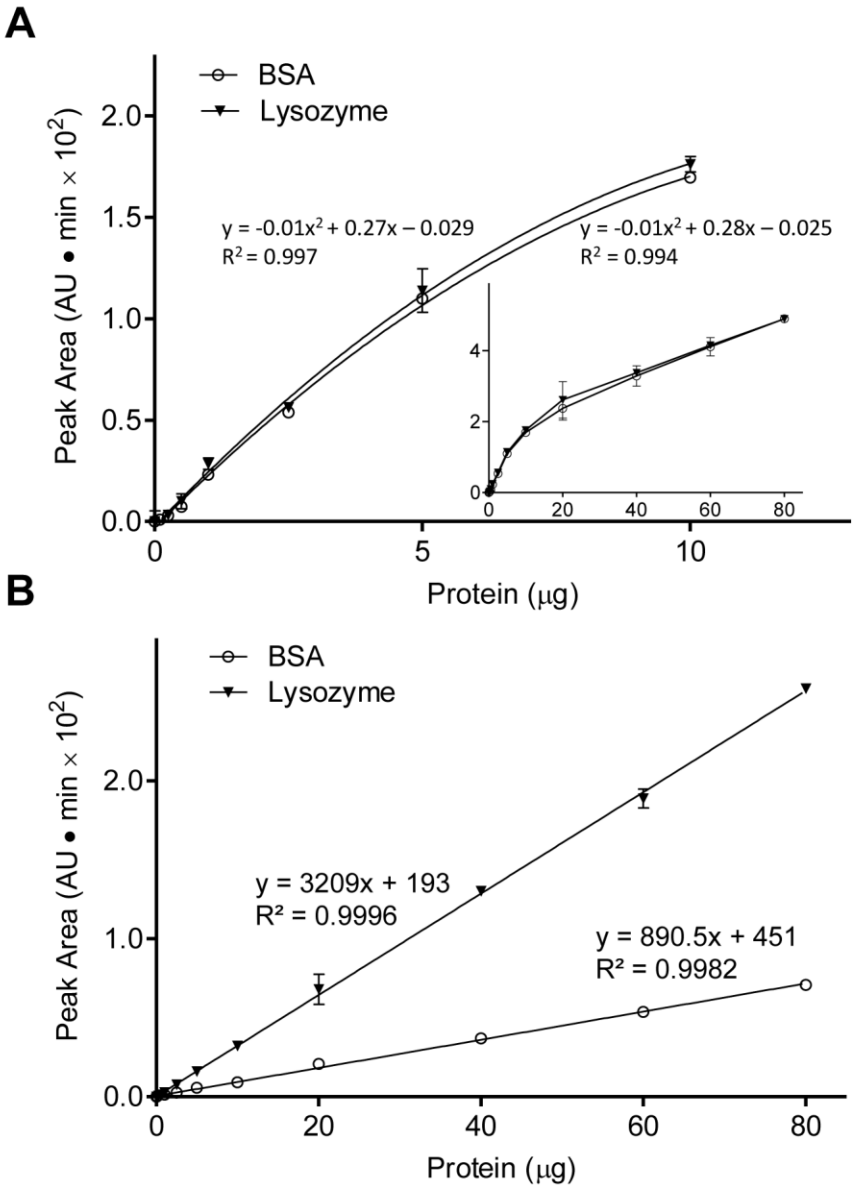

Figure 3.5: TPLC response curves of BSA and of lysozyme.
Curves are shown at (A) 214 nm and (B) 280 nm. The inset of (A) plots the response of BSA and lysozyme over a broader range of 0.1–80 μg. The error bars represent the standard deviation in peak area from triplicate injections (some being too small to observe on the scale). Formula for the regression curves are listed, together with the R^2 values.

Table 3.1: Coefficient of variation determined from the relative response of a common set of proteins for various quantitative assays to BSA.

Sample	LC-UV (214nm)	Bradford	Dc	BCA
BSA	1.00 ± 0.04	1.00 ± 0.03	1.00 ± 0.02	1.00 ± 0.03
Lysozyme	1.00 ± 0.10	0.83 ± 0.01	1.36 ± 0.03	1.18 ± 0.02
Cytochrome C	1.13 ± 0.02	1.25 ± 0.02	1.27 ± 0.02	1.08 ± 0.04
Ovalbumin	1.04 ± 0.03	0.77 ± 0.06	1.20 ± 0.04	0.98 ± 0.04
α-Casein	1.19 ± 0.01	0.64 ± 0.02	1.34 ± 0.48	0.86 ± 0.10
Dephosphorylated α-Casein	1.03 ± 0.02	0.68 ± 0.01	0.74 ± 0.02	0.58 ± 0.03
E. coli	1.01 ± 0.04	0.83 ± 0.01	1.46 ± 0.04	1.20 ± 0.07
NRK-52E	[a] 0.86 ± n/a	0.73 ± 0.04	1.13 ± 0.08	0.99 ± 0.10
Coefficient of Variation	9.6	23.6	19.3	20.1

[a] Single injection

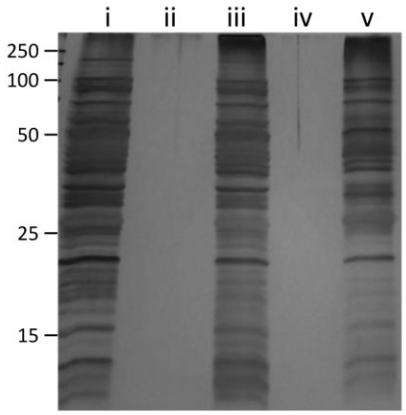

Figure 3.6: Gel image showing the recovery of the *E. coli* protein extract following the TPLC workflow.
(i) Pre-precipitated *E. coli* protein extract in 1 % SDS showing the normal banding pattern of the SDS-extracted *E. coli* proteome. (ii) Following precipitation, acetone supernatant was dried and resolved in parallel to protein extract. (iii) *E. coli* protein pellet following acetone precipitation. (iv) Injection peak (first 5 min) of the TPLC run. (v) The collected fraction following TPLC showing good recovery of the original SDS-extracted *E. coli* proteome sample.

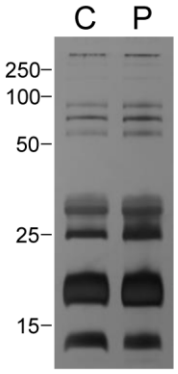

	Protein content (% w/w)	
Assay	**Control (P)**	**Precipitated (P)**
BCA	55.0 ± 0.79	25.1 ± 1.92
TPLC	24.4 ± 1.73	21.6 ± 0.51

Figure 3.7: Assessment of protein content in a sample of milk before or after protein precipitation.
Milk protein concentration was determined before and after precipitation by chloroform/methanol/water to remove contaminants. The SDS PAGE image demonstrates the high protein recovery between the unprecipitated control (C) and the pellet (P). The true protein content in the milk sample, as estimated by Kjeldahl nitrogen content, is reported at approximately 30 %. Error bars represent the standard deviation of triplicate injections.

Chapter 4:

Dual LC-MS platform for high throughput proteome analysis

4.1. Preface

Despite the ability to identify thousands of proteins in an experiment, proteomics workflows employing NSI suffer from limited throughput due to excessive sample loading times and column re-equilibration. Pertaining to biomarker discovery, limited throughput can reduce technical replication, which reduces the sensitivity of the experiment upon statistical analysis. To improve throughput in LC-MS experimentation, this chapter introduces a two-column, dual spray interface for the mass spectrometer capable of nearly doubling throughput for LC-MS applications. This work is published in the manuscript: Orton, D.J.; Wall, M.J.; Doucette, A.A. Dual LC-MS platform for high throughput proteome analysis. *J. Proteome Res.* **2013**, *12*, 5963-5970.

*All experiments and manuscript preparation were conducted by Dennis Orton. Dr. Alan Doucette contributed to experimental design and assisted with manuscript revisions. Dr. Mark Wall, in concert with Dr. Doucette designed and constructed the system presented in this chapter.

4.2. Introduction

Advances in instrumentation and associated methodology have expanded the capacity of LC-MS for in-depth proteome characterization. Together with improvements in MS resolution, scan speed, and sensitivity,[224] the adoption of low flow capillary chromatography with online nanospray[225,226] has provided researchers with a high-throughput tool for proteome analysis.[20,227] Nevertheless, with RPLC, an extensive fraction of time must still be devoted to sample loading and column re-equilibration; this issue is further exaggerated under low-flow conditions. Given that extensive (multidimensional) fractionation of the proteome is often required for improved characterization, it follows that methods that improve proteomic throughput are an important objective for large-scale proteome analysis.

The duty cycle of the LC–MS experiment can be defined as the fraction of time the MS instrument acquires useful data relative to the total analysis time. Duty cycle can therefore be improved by decreasing any 'down time' experienced, for example, during column regeneration and sample loading. In the capillary LC-MS experiment, researchers have adopted various strategies to permit a higher rate of sample loading. The simplest perhaps is to inject the smallest possible volume of sample. However, this strategy necessitates reconstitution of the peptide mixture in a very low volume of solvent, which challenges the precision of solvent delivery as well as the complete resolubilization of the sample. Increasing the injection volume implies that a greater proportion of the sample can be injected, although longer injection times will be required. At 250 nL/min, a 10 μL injection would take a minimum 40 min to load the sample. Trap column configurations can be employed, as they can accommodate higher flow rates, thereby dramatically

decreasing the required loading time. If two pumps are employed (a high-flow pump for loading and a low-flow gradient pump to run samples), a trap column configuration offers the advantage of sequential sample loading and column regeneration while operating the analytical column. Unfortunately, elution of analytes through a trap column and onto the analytical column will cause peaks to broaden, thereby reducing separation efficiency and impacting proteome characterization.[228] To preserve the advantage of the trap column in terms of sample cleanup (desalting), it is common to employ an offline column configuration.[34,229] This also has the distinct advantage of being able to quantify the concentration of analyte in the sample to optimize the amount of sample injection for LC-MS.

Trap column configurations are perhaps the most commonly adopted form of multiplexed chromatography for proteome analysis. Various instrument platforms, including commercial configurations, have been described to distribute MS acquisition among multiple column configurations.[230–237] The MUX interface couples multiple columns having independent electrospray nozzles to a single MS detector by rapid sampling from each column as the remaining emitters are blocked.[235,238] Adaptation of this technology into a nanospray configuration has not been reported, making MUX technology of limited use for proteome analysis. In 2001, Smith *et al*. described the first true multiplexed configuration of capillary chromatography coupled to mass spectrometry,[239] which was automated in 2004.[240] This system demonstrated the potential for sequential regeneration of one column with sample loading and elution from another. Smith *et al*. later adapted the system into an automated LC-MS platform approaching 100 % duty cycle.[241] The later system employed four columns operating through two

independent gradient pumps, along with four nanospray emitters, being coupled to MS on a moving stage. The actively moving stage enables the selection of a given spray emitter for MS data acquisition by positioning it in front of the MS orifice. Thibault *et al*. described a multiplex platform for high-throughput proteomics that coupled two trap columns to two capillary columns, each within independent emitters also on a moving stage.[242] Thibault's strategy involved rapid cycling of data acquisition across the two simultaneous eluting columns with the moving stage. Characterization of complex proteome mixtures in this fashion may suffer as reduced acquisition time per column lowers the overall sensitivity. In another approach, Hanash *et al*. coupled four columns (two traps, two capillary columns) to a single nanospray emitter for sequential regeneration and loading on one column and analysis from the second.[243] This was the first demonstration of a multiplexed nanoflow platform, wherein flow rates of 250 nL/min were employed. By eliminating the moving nanospray stage, this system provides a more robust approach for high-throughput analysis. However, coupling a single emitter to multiple columns through a switching valve introduced post-column dead volume, causing peak broadening and reducing sensitivity.

In this work, we describe a fully automated, simple and robust dual column LC-MS system which nearly doubles the duty cycle over a conventional (single column) format for proteome analysis. The system eliminates the use of trap columns, packing two capillary columns that are integrated to two nanospray emitters which are fixed in position during operation. Voltage is applied to one of the two columns, while the second column is sequentially equilibrated and loaded for a subsequent run. The system is evaluated in terms of column-to-column reproducibility and validated for high throughput

GeLC-MS analysis of an *E. coli* proteome extract. The system is a readily adaptable technology for improving throughput in proteome analyses.

4.3. Experimental in brief

Six consecutive lanes of a 12 % T SDS PAGE gel were loaded with 50 µg of *E. coli* protein extract as described in Figure 2.1. Following Coomassie staining, each lane was processed into five (sample A) or ten (sample B) gel slices as shown in Figure 4.1 and subjected to in-gel trypsin digestion and LC-MS analysis. Peptides extracted from each gel slice were analyzed using either the 65 or 125 min solvent gradients and MS data were searched against an *E. coli* Uniprot database (4,584 entries, downloaded February 14, 2013) as described in section 2.7. A spreadsheet of all identified proteins, with their number of peptide spectral matches (PSM), is provided in the Appendix.

4.4. Results and Discussion

4.4.1. System Design

This Chapter presents a robust, low-cost, fully automated dual capillary LC-nanospray MS platform for high-throughput proteome analysis. The system maximizes the utility of the mass spectrometer through sequential loading of sample onto one of two analytical columns while acquiring data using the other column, thereby improving LC-MS duty cycle relative to a single column platform.

Figure 4.2 provides a schematic of the dual column platform. An Agilent 1200 Nano flow binary pump (annotated ‘run pump’ in Figure 4.2) provides a stable flow of

250 nL/min for analyte elution from the capillary column (*e.g.* 'column 1' in Figure 4.2A). Simultaneously, sample loading to the alternate column is provided through an Agilent 1050 isocratic pump (annotated as 'load pump' in Figure 4.2), connected to an Agilent 1100 autosampler. The load pump need not directly possess low-flow capabilities, as a simple splitting T will maintain a flow near 300 nL/min. At this flow rate, 65 min is sufficient to re-equilibrate the column and load up to 10 μL of sample prior to column switching. A single two-position six-port switching valve (<30 nL port-to-port) directs the flow from each pump to the respective column. A high voltage switch is used to alternately apply current for nanospray operation of one of the two columns. While voltage is applied to one column, the second is in a standby mode, wherein solvent continues to flow from the load pump and accumulates at the end of the spray tip (Figure 4.2C). The two nanospray emitters are affixed at the entrance orifice of the LTQ (Figure 4.2C), positioned at an approximate 11° offset angle and spaced by a distance of 0.5 cm at the tips. Positioning two emitter tips in this fashion demonstrates negligible signal variance relative to the conventional single nanospray emitter of the LTQ.

The basic operation of the dual column system follows a well-known strategy of regenerating and loading sample onto one column while eluting sample through gradient HPLC from the second (preloaded) column. The solvent flow path as well as the spray voltage is controlled via relay contacts connected to the HPLC system. The timing of events (voltage application, diverting flow paths, injection of sample, application of LC gradient, and triggering the mass spectrometer to record data) is fully automated and programmed through Chemstation software (Appendix).

4.4.2. Performance Evaluation

The dual-column platform for high-throughput proteomics employs two distinct capillary columns packed within two distinct nanospray emitters. Integrated emitters eliminate the potential for postcolumn peak broadening, maximizing chromatographic resolution and analyte sensitivity. Sample is directly loaded onto the analytical column, avoiding the need for trap columns. This further simplifies the fluidic design of our dual column platform. Carryover between the two columns was assessed and found to be negligible (Figure 4.3). Evaluation of the reproducibility of the system is shown in Figure 4.4 through duplicate analysis of *E. coli* peptides extracted from SDS-PAGE gel slice B3 (see Figure 4.1) following fractionation and in gel digestion. The base peak chromatograms (Figure 4.4A) demonstrate consistent separation of analytes on each of the two columns, while the ion maps show identification of numerous peptides with varying *m*/*z* values observed over the elution gradient (Figure 4.4B). The extracted ion chromatograms obtained for four distinct peptides (Figure 4.4C) depict the strong agreement in peak intensities as well as retention times across the two columns. These performance characteristics suggest the system to be capable of delivering consistent separation and detection of peptides for high-throughput proteome analysis.

Evaluation of system reproducibility is further shown in Figure 4.5. Figure 4.5A and B plot the retention times and the peak areas obtained for the four distinct peptides shown in Figure 4.5C. Each sample was analyzed through six replicate injections on each column. Figure 4.5A demonstrates the high agreement in retention times for the four peptides across columns. The retention time variability between columns was within that observed on a single column (<1 % relative standard deviation, RSD). In terms of peak

area (Figure 4.5B), the run-to-run variation for peptides detected on a single nanospray emitter was approximately 12 % RSD. Averaging the data from the four select peptides, their detection on column 2 appears to provide slightly higher peak areas than column 1. This difference becomes inconsequential in the context of the inherent variability of detection by capillary LC-NSI-MS.

The consistency of peptide separation and detection on the two columns is extended to proteome profiling of the *E. coli* digest (gel slice B3). Figure 4.5C plots the average retention time of 347 peptides observed in at least 3 of the 6 replicate injections on column 2 versus column 1. The data are highly correlated, with slope near one and intercept equalling that of the solvent delay between columns (0.44). These results demonstrate the consistent separation of the peptide mixture on each column over the entire elution gradient. Figure 4.5D uses SpH data as an indication of detection reproducibility for a proteome mixture on the two columns. The number of SpH on each column is near constant (slope 1.04); the slight increase in spectral counts on column 2 versus column 1 is consistent with the higher peak areas observed in Figure 4.5B. Despite these minor differences, the dual-column platform achieves reproducible separations with similar sensitivity across the two independent nanospray emitter capillary columns. The reduced number of fluidic connections between the pump and column decreases the possibility of dead volume and solvent mixing, thereby providing a consistent delivery of the solvent gradient from a common nanoflow pump with minimal variation in solvent delay to each column.

Next, evaluation of the extent of proteome coverage was conducted between column 1 and column 2. The same *E. coli* proteome extract (gel slice B3) was subject to

12 replicate injections (six per column). Table 4.1 summarizes the results of the experiment, listing the number of unique peptides and proteins identified per column, together with the degree of overlap observed between the runs. The total number of unique peptide and protein identifications showed high agreement across the two columns. For example, an average of 479 peptides was identified per run on column 1, with 481 peptides per run on column 2. This difference is well within the 2 % intracolumn variance for replicate injections. Pooling 3 replicate runs on a given column increased the number of unique identifications, again showing high agreement between the columns (702 vs 693 peptides on columns 1 and 2, respectively). Similar results are seen through the number of unique protein identifications, wherein no differences were observed between the two columns.

Despite the consistent total number of identified peptides and proteins, it was found that a different subset of peptides was identified for each replicate injection on a given column. From Table 4.1, the intracolumn overlap from replicate injections was 55 and 81 % for peptides and proteins, respectively. Such an observation is to be expected for a proteomics experiment.[67] Pooling the number of replicates into a multiconsensus data set increases the intra-column overlap, with 68 % agreement in peptides from three merged runs and 94 % agreement in protein identifications. It is noted that complete overlap, even on a single column, would require an impractical number of replicates. The number of unique peptides identified was found to continue to increase up to the 12th replicate injection (total of 1006 peptides), while the number of unique proteins identified reached a plateau (123 proteins) after seven replicate injections (Figure 4.6).[67] Thus, when comparing the proteome data across columns with a limited number of replicates, a

slightly different subset of peptides was identified on each column, as seen through a marginal drop in inter-column overlap (51 %) relative to the intra-column overlap (55 %). This drop in inter-column overlap continues with the merged peptide data sets. Protein identifications showed greater consistency across the columns. Given the high degree of variability in proteome characterization by LC-MS and noting the relatively small drop in inter-column overlap, the difference between columns is negligible. The reproducibility of our dual-column platform for proteome characterization is comparable to that of a conventional single column LC-MS platform.

4.4.3. Application to High-Throughput Proteomics

Comprehensive proteome analysis will benefit from a higher throughput platform. A routine application of in-depth proteome characterization by LC-MS employs a high degree of fractionation, with 2-D or even 3-D separations required for comprehensive proteome coverage.[32,36,43,45,244] However, increasing the level of fractionation necessitates more MS analyses. The time devoted to column regeneration and sample loading limits the throughput of the experiment. Application of a dual-column platform for sequential loading and running of samples reduces the down time of the mass spectrometer (increases the LC-MS duty cycle), thereby increasing the number of samples that can be processed in a given time. As shown in Figure 4.7A, a conventional (single column) system provides a duty cycle near 50 %. This value is based on a 65 min gradient, during which peptides elute from the column and are detected, alternating with a 60 min period for column regeneration and sample loading (10 μL) and an additional 10 min delay between the pump and the detector. The dual LC–MS platform offers the potential to improve throughput using one of three strategies: perform more technical replicates of

any given sample of the proteome mixture (Figure 4.7B), improve separation by employing longer (shallow) LC gradients during online LC–MS analysis (Figure 4.7C), or increase the level of fractionation of the proteome prior to LC–MS analysis, as seen through application of a 2-D separation platform (Figure 4.7D). An *E. coli* proteome extract was employed to test the throughput of the system, with SDS-PAGE for protein fractionation in the first dimension ahead of online reversed-phase peptide separation with LC-MS.

Table 4.2 summarizes the proteomic data obtained through characterization of the sample using the 4 analysis methods depicted in Figure 4.7. Figure 4.8 provides Venn diagrams that summarize the protein and peptide identifications in each of the four analysis methods. The total run time of the LC-MS experiments with the dual-column platform increased over that of the single-column platform (Method A). However, the dual platform enabled the analysis of twice as many samples (Methods B and D) or allowed application of longer LC gradients, which ultimately improves the characterization of the proteome. The duty cycle of the method is a function of the LC gradient length, relative to column regeneration, sample loading, and solvent delays between pump and column. Employing 125 min gradients on the dual column platform provides the highest duty cycle (85 %), although 65 min gradients also showed a significant increase in duty cycle over the single-column format. Proteomic data obtained from each of the four analysis methods demonstrates the improved characterization of the sample on a dual-column platform. As seen in Table 4.2, the addition of a second replicate injection for each of the five gel slices on the dual column platform (Method B) identified 720 more peptides and 95 more proteins compared with Method A (single

injections on a single-column platform). However, given an increase in total analysis time, the rate of peptide and protein identification showed only marginal improvements on the dual platform relative to the single column platform (7 % increase in peptides identified per hour, 3 % increase in proteins per hour). Increasing the number of replicate injections per sample to improve proteome coverage can be further aided by integrating data exclusion strategies to minimize overlap in the identified peptides.[245,246] Considering the marginal gains in throughput experienced when applying replicate runs in the dual-column platform, the analysis methods which increased the level of fractionation for the *E. coli* proteome (*i.e*. Methods C and D) resulted in more significant improvements in proteome coverage and identification throughput. As shown in Table 4.2, doubling the LC gradient time (Method C) increased the number of unique peptide identifications to 3506, while doubling the number of SDS PAGE fractions (Method D) yielded a total of 3837 unique peptides. Similar increases were seen for the total number of proteins identified through these methods. These numbers translate into a 50 % improvement in the number of peptides/proteins identified with Method D over Method A. Noting the different total analysis times, the rate of identification was in fact quite similar between Method C and D. Nonetheless, they offered a 24-27 % increase in the number of peptides or proteins identified per hour compared with a conventional single-column platform. Applying a higher degree of peptide level or protein level separation using the dual-column platform enables improved characterization of the sample without undue increase in total run time for the experiment. Additional dimensions of separation (*e.g*. ion exchange, isoelectric focusing) may further simplify the mixture resulting in improved proteome coverage for more complex organisms. In summary, the dual-column platform

enables an improved duty cycle that increases the potential to characterize multiple fractions in a given period of time.

4.5. Concluding Remarks

This Chapter demonstrates the development of a robust dual-column platform that increases throughput for proteome characterization by maximizing the duty cycle of the system. This platform involves minimal reconfiguration over a conventional single-column platform. A single-gradient HPLC pump is required to elute peptides from one of two analytical capillary columns with integrated nanospray emitters. The second pump, used for sample loading, need not possess gradient capabilities, and the low-loading flow rate can be achieved with a simple splitting T. Sequential LC-MS runs can be obtained in fully automated fashion without additional software, as the column switching valve and high voltage switch are controlled with simple relay contacts. The data presented here demonstrate the high column-to-column reproducibility, in terms of both LC retention as well as MS signal intensity. As is inherent to nanoflow applications, improper fluidic connections can introduce significant time delays. Column conditioning with standardized samples (BSA digest) is therefore a critical aspect of the dual-column platform and is used to validate system performance across multiple columns. The system avoids the use of trap columns by directly injecting sample onto one of the two analytical columns. Prior to online analysis, all peptide samples are subject to offline sample cleanup, which is necessary to avoid buildup of contaminants on the nanospray emitter tip. With this system, we observed an improvement in proteome coverage and identification throughput by analyzing more replicates or increasing the level of fractionation. Our dual-column platform therefore represents a valuable tool for high-throughput proteome analysis,

which is easily configured to operate on most any LC-MS platform. Other applications of the system may include increased replicate analysis for statistical validation of biomarkers or high-throughput pharmaceutical analysis where multiple samples are processed.

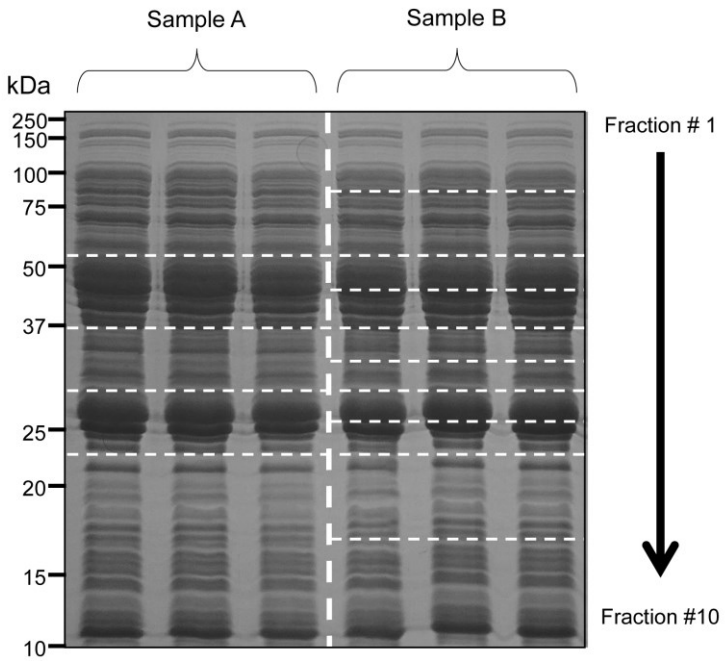

Figure 4.1: Image of the SDS PAGE gel used to validate the system.
Each lane contains 50 µg of *E. coli* protein extracts. Lanes were sectioned into either 5 (sample A) or 10 (sample B) slices for their respective analyses.

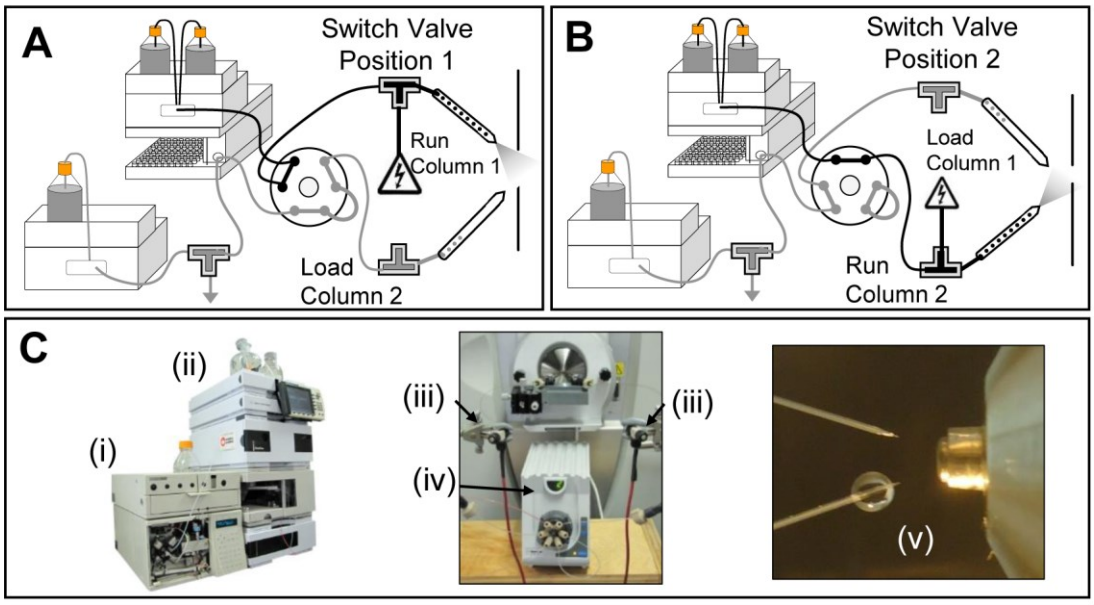

Figure 4.2: Schematic of the dual column LC/MS system.
The system is composed of two independent pumps: the 'load pump' delivers solvent through the autosampler to the column, while the nanoflow 'run pump' delivers a solvent gradient to the opposing column. (A) With switch valve in position 1, and voltage to column 1, the run pump operates column 1 while column 2 is equilibrated then loaded with the load pump. (B) In position 2, both the solvent switching valve and the high voltage source are diverted, operating column 2 with the run pump while sample is loaded on column 1. (C) Photos of the system show: (i) the Agilent 1050 'load pump', (ii) Agilent 1200 nano-flow 'run pump' atop the autosampler, (iii) dual nano-flow capillary columns, (iv) voltage application through the MicroTee, (v) the dual nanospray emitter tips in front of the MS source, wherein the upper column is in run mode while solvent builds on the end of the second tip during column equilibration and sample loading.

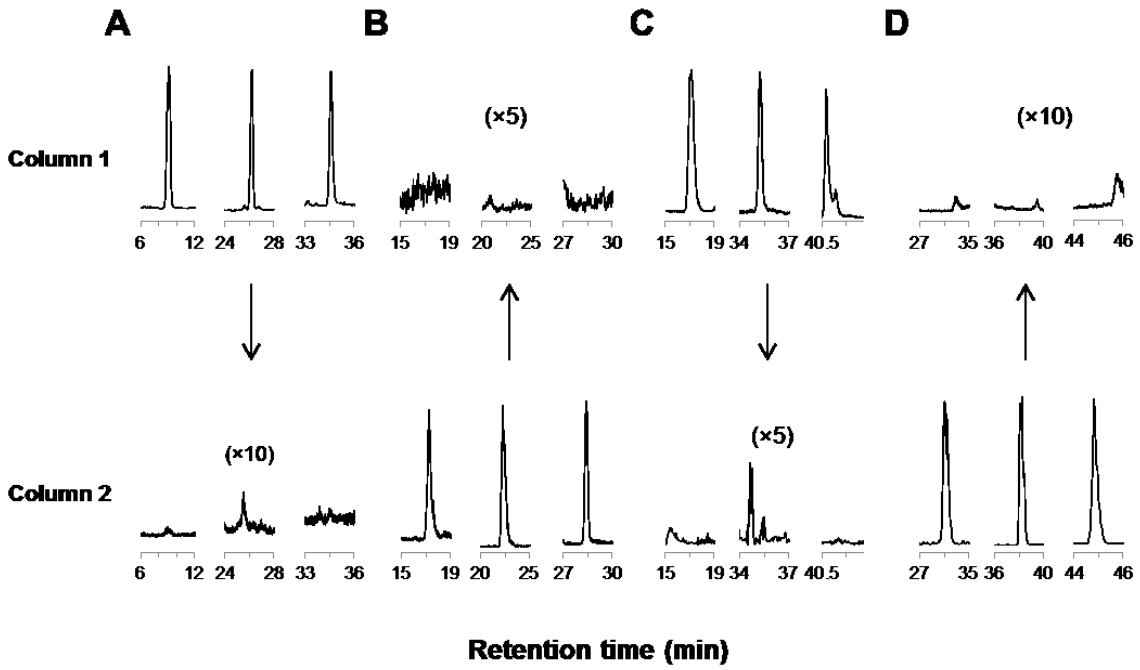

Figure 4.3: A demonstration of the lack of carryover between columns.
(A/B) Column 1 is loaded with 1 pmol of ovalbumin digest. During elution of ovalbumin, 100 fmol of carbonic anhydrase digest is loaded onto column 2. (A) Shows extracted ion chromatograms for three eluting ovalbumin peptides (*m/z* 592.0, 519.3, 791.3) on column 1 (top) which show no carryover into the subsequent carbonic anhydrase run on column 2 (bottom). (B) Extracted ion chromatograms for three carbonic anhydrase peptides (*m/z* 706.0, 509.8, 673.8) on columns 1 (top) and 2 (bottom). There are no detectable carbonic anhydrase peptides during the ovalbumin run on column 1 while the sample is loaded on column 2. (C) Similarly, 100 fmol of lysozyme digest is injected onto column 1 (extraction ion chromatograms for *m/z* 714.7, 523.2, 877.4), which are not detected in the following run on column 1 (1 pmol BSA digest). (D) 1 pmol of BSA is loaded onto column 2 (extracted ion chromatograms for *m/z* 526.2, 473.8, 507.8), which show no detectable peptides on column 1.

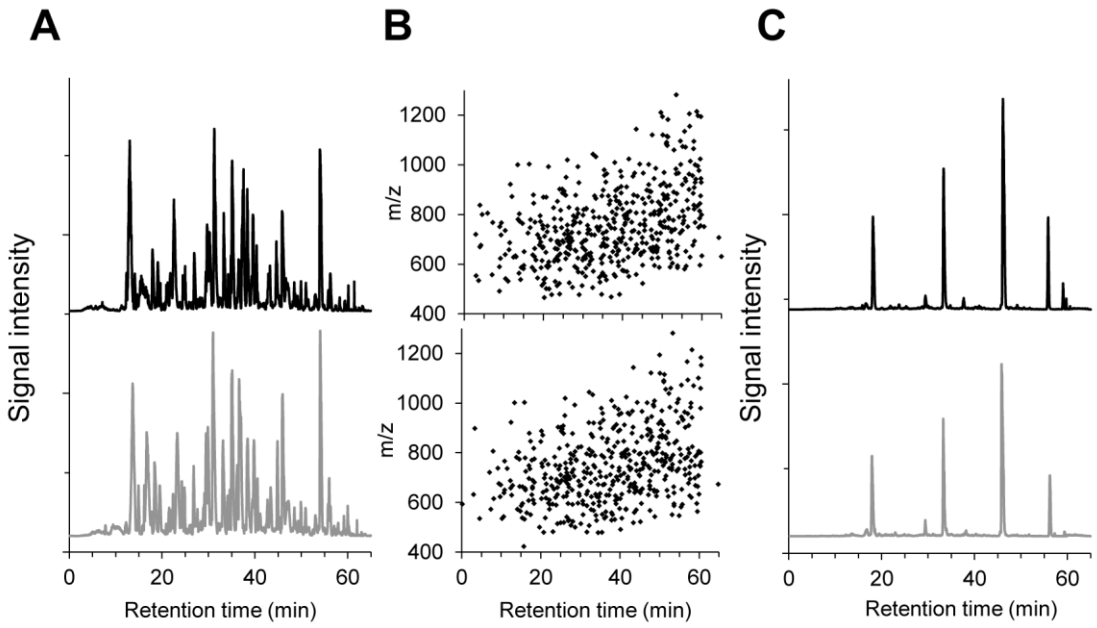

Figure 4.4: Representative LC-MS analysis of an in-gel digested sample of *E. coli* on the dual spray system.
(A) Base peak chromatograms show similar separation of peptides across column 1 (top) and column 2 (bottom). (B) Total ion map of peptides detected from each column demonstrate an even distribution of ions eluting from each column over the entire elution period. (C) Extracted ion chromatograms of four select peptides from the *E. coli* digest on each column show the reproducibility in signal intensity and retention time between columns.

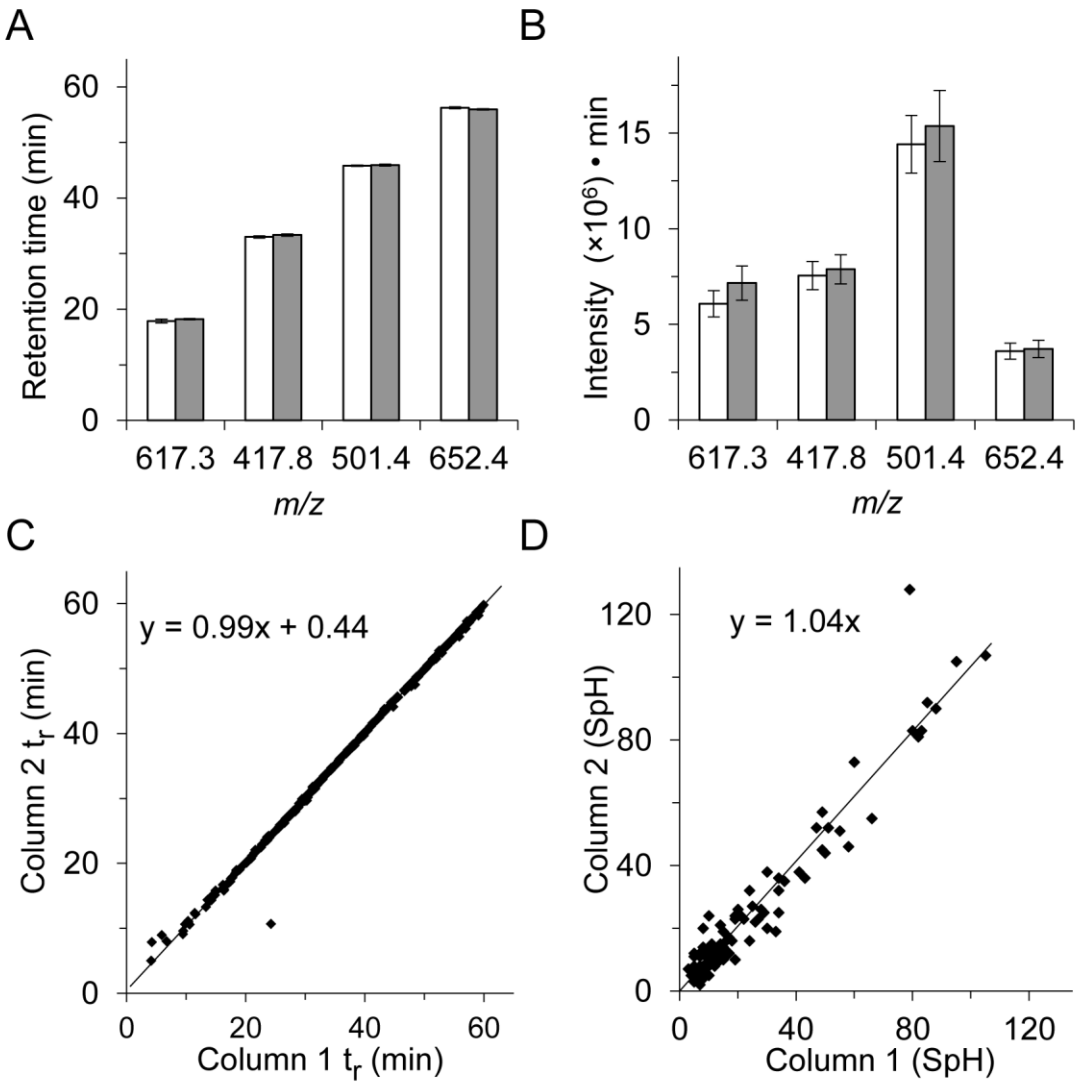

Figure 4.5: Evaluation of column-to-column performance characteristics for separation and analysis of digested *E. coli* peptides.
(A) The retention times for four representative peptides are compared on column 1 (white bars) vs. column 2 (grey bars). Error bars depict the standard deviation from 6 replicate injections per column. (B) The peak areas for the four select peptides detected on column 1 (white bars) vs. column 2 (grey bars) are compared (n=6). (C) Retention time consistency between columns is compared for 347 peptides, demonstrating high correlation across the separation window. (D) Raw spectral hits (SpH) for all proteins identified following analysis on each column.

Table 4.1: Dual column consistency for proteome analysis using 6 replicate injections per column.
Pooling 1, 2, or 3 of the runs into a multiconsensus dataset of identified peptides or proteins.

	# Injections	Avg. # Identified		Intra-column Overlap (%)	Inter-column Overlap (%)
		Column 1	Column 2		
Peptides	1	479 ± 10	481 ± 12	55 ± 2	51 ± 3
	2	617 ± 12	615 ± 13	63 ± 2	58 ± 1
	3	702 ± 16	693 ± 13	68 ± 1	61 ± 1
Proteins	1	102 ± 5	101 ± 3	81 ± 3	79 ± 3
	2	112 ± 3	112 ± 4	89 ± 2	87 ± 3
	3	116 ± 2	117 ± 3	94 ± 2	91 ± 2

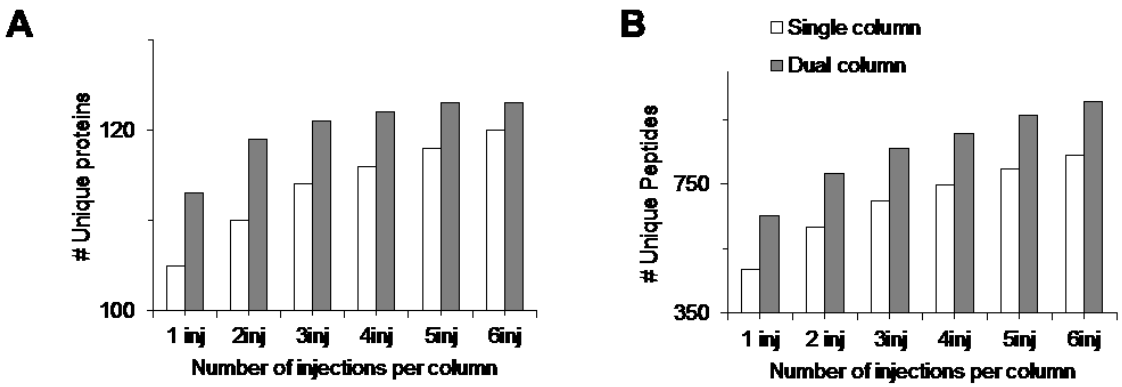

Figure 4.6. Increasing the number of injections increases the number of proteins and peptides identified.
The number of proteins (A) and peptides (B) identified through increasing replicate LC-MS analyses of *E. coli* peptides extracted from gel slice B3. The 6 injections on the dual column system represents 12 actual injections. The number of unique proteins identified in a single experiment reaches maximum at 7 consecutive LC-MS runs. The number of unique peptides has yet to plateau even after the 12th replicate injection. The dual spray system is able to reach this maximum number in less run time by eliminating the need for re-equilibration times.

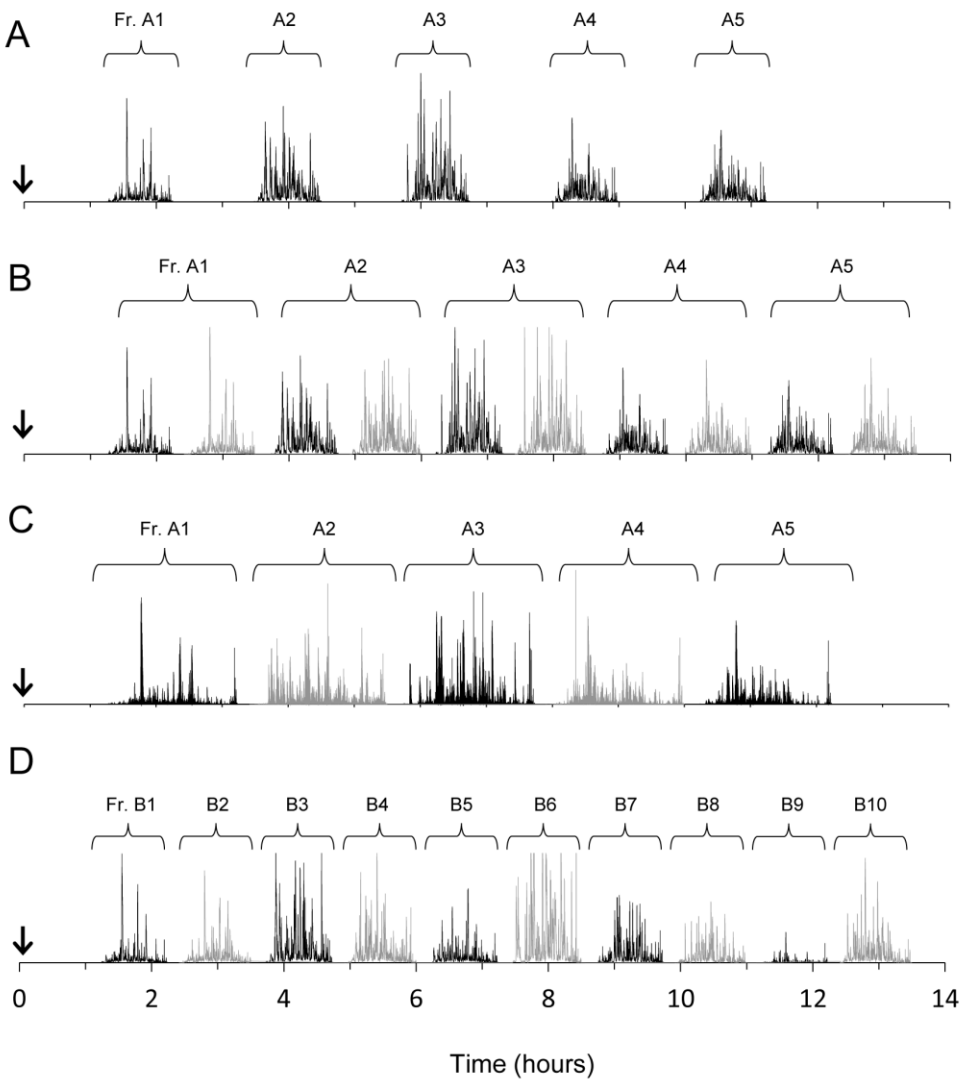

Figure 4.7: Schematic representation of LC/MS analysis using the dual spray system as compared to a single column setup.
With a single column employing a 65 min gradient, peptides are detected 70 min into the experiment, allowing 60 min for column equilibration & sample loading, and an additional 10 min solvent delay between pump and MS. (A) Analysis of five gel slices from an *E. coli* proteome extract requires 675 min. (B-D) Sequential analysis from the dual column platform (black trace for column 1, grey for column 2). Again, 70 min are required for initial sample loading and column equilibration. However, only a 10 min delay remains between each subsequent chromatogram (solvent delay between pump and MS). (B) The five gel slices are analyzed twice (once on each column) using a 65 min gradient, totalling 810 min of analysis time. (C) Five gel slices are analyzed using an extended (125 min) LC gradient, totalling 735 min of run time. (D) Ten gel slices are analyzed without replication using 65 min gradients, totalling 810 min of analysis time. The chromatograms shown are the base peak chromatograms observed for the respective fractions. Table 4.2 provides additional information on the detected peptides and proteins.

Table 4.2: Throughput of the dual column platform for proteome analysis, using one of four methods described in Figure 4.7.

Method	Inj/ Gel Slice	# Gel Slices	Platform	Gradient (min)	Run Time (hr)	Duty Cycle	# Pep's (Total)	# Pep's / hour	# Prot's (Total)	# Prot's / hour
A	1	5	Single	65	11.25	48 %	2529	225	405	36
B	2	5	Dual	65	13.5	80 %	3249	241	500	37
C	1	5	Dual	125	12.25	85 %	3506	286	554	45
D	1	10	Dual	65	13.5	80 %	3837	284	601	45

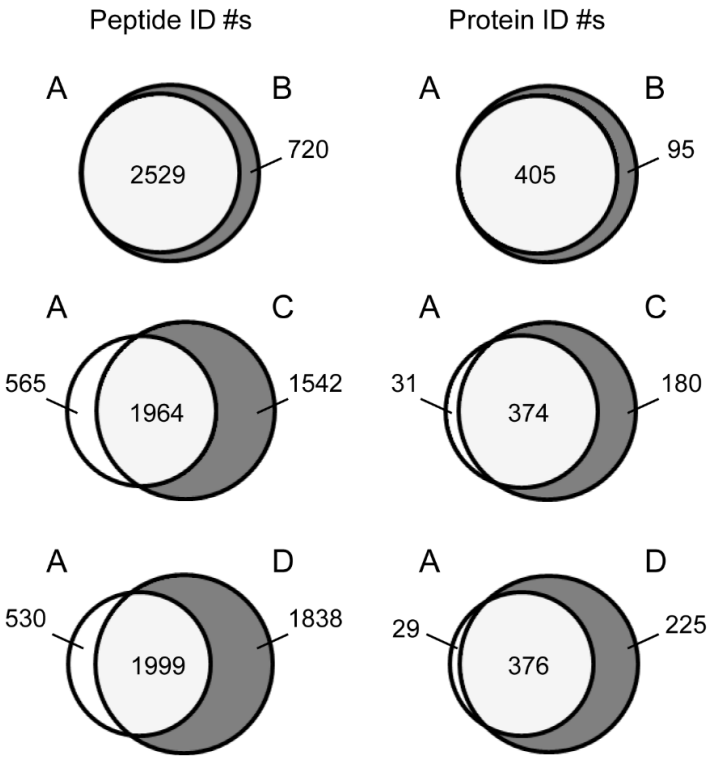

Figure 4.8: Venn diagrams comparing the peptide and protein identifications using each of the four analysis methods described in Table 4.2.

Chapter 5:

Proteome analysis of rat proximal tubule cells following stretch-induced apoptosis in an *in vitro* model of kidney obstruction

5.1. Preface

The previously developed *in vitro* model of UTO applying a stretch stimulus to a monolayer of primary proximal tubule cells has previously been used to evaluate specific effectors following UTO, demonstrating its applicability for studying the disease. Here, the model is employed to investigate potential novel pathways and effector proteins activated following mechanical stretch by whole-cell proteome analysis. A number of novel effector proteins are identified, and their potential role in disease progression is discussed. This work is published as: Orton, D.J.; Doucette, A.A.; Maksym, G.N.; MacLellan, D.M. Proteome analysis of rat proximal tubule cells following stretch-induced apoptosis in an *in vitro* model of kidney obstruction. *J. Proteomics* **2013**, [*epub ahead of print*].

* All experiments, data analysis, and manuscript preparation were conducted by Dennis Orton. Dr. Dawn MacLellan contributed to experimental design and assisted with editing of the manuscript. Dr. Alan Doucette contributed to execution of MS experimentation as well as some revisions to the manuscript. Dr. Geoffrey Maksym provided the cell culture facilities and instrumentation required for the experiment and assisted in setup of the experiment.

5.2. Introduction

Urinary tract obstruction (UTO) is a common congenital anomaly that leads to morphological changes within the kidney including dilation, hydronephrosis, renal tissue fibrosis, and tubular cell apoptosis.[247] Noted in up to 1 % of pregnancies on prenatal ultrasound, many cases may resolve spontaneously, however some children with UTO require surgical intervention to prevent permanent loss of kidney function.[9] Postnatal management therefore requires lengthy surveillance of renal function with invasive testing to determine which children will require surgical intervention.[248] To improve care of children experiencing UTO, a more complete understanding of the molecular processes is required.

Previous studies have demonstrated the role of oxidative stress,[169,249,250] renal metabolism,[251,252] and tissue fibrosis[101,142] in UTO. These studies suggest renal interstitial fibrosis and tubular cell apoptosis to be the major effectors leading to loss of kidney function. To study the pathophysiology of UTO, an *in vitro* model of UTO was developed.[100] The model employs a mechanical stretch stimulus applied to proximal tubule cells grown on a flexible membrane which mimics the physiological characteristics experienced by these cells during UTO.[100,101,160,170] Application of this model has demonstrated many effectors in tubular cell damage and fibrosis on proximal tubule cells, including TGF-β,[101] NO,[160] and apoptosis.[170] While these studies characterize specific effectors in disease progression during UTO, this Chapter applies a quantitative proteomic analysis of the rat proximal tubule cell line NRK-52E to elucidate global changes in protein abundance as a result of UTO simulation. We used a gel-based method

coupled to spectral counting as a label-free method to quantify changes in protein abundance as a result of UTO simulation.

Proteins altered in abundance were assessed by GO and KEGG classifications to demonstrate specific pathways and subcellular processes that are affected by simulation of UTO. Furthermore, we discuss the specific protein alterations resulting from stretch that have been described to play critical roles in the pathophysiology of other models of renal injury. The aim of this study is therefore to characterize the effects that mechanical stretch have on proximal tubule cells and to identify novel effector pathways that are important in UTO.

5.3. Experimental in brief

The experimental workflow for Chapter 5 is summarized in Figure 5.1. Briefly, NRK-52E cells were grown on flexible, 6-well BioFlex^{TM} plates and subjected to the stretch protocol described in section 2.2.2. Protein was extracted from the cytoplasmic (C) and membrane (M) fractions and 50 µg of each fraction were resolved on a 12 % T SDS PAGE gel and stained with Coomassie Brilliant Blue. Each lane was processed into 15 gel slices, subjected to in-gel digestion and analyzed in duplicate by LC-MS with the 125 minute gradient described in section 2.7. Data were searched against a rat Uniprot database (27,353 entries, downloaded August 1, 2013) and proteins identified with greater than six spectral counts across all analyses were accepted. The method QuasiTel[68] was employed for statistical analysis of the spectral counting data and significantly altered proteins were classified by GO and KEGG terms for functional enrichment.

5.4. Results

5.4.1. NRK-52E cells experience morphological and subcellular changes in response to stretch

Figure 5.2 displays the morphological differences between cells undergoing mechanical stretch relative to control cells. Displayed in Figure 5.2A, NRK-52E cells normally exhibit an epithelial-like morphology, whereas stretched cells adopt a rounded, shrunken appearance (Figure 5.2B), consistent with cells undergoing apoptosis. Further confirmation that stretch induces apoptosis is provided by cell death ELISA, which detects cytoplasmic DNA histone complexes, as described in the methods section. As seen in Figure 5.2C, ELISA confirms an approximate 5 fold increase in apoptosis for cells which have undergone mechanical stretch. These results demonstrate NRK-52E cells subjected to stretch undergo apoptosis, simulating the effects of obstruction on proximal tubule cells *in vivo*.

5.4.2. SDS PAGE shows similar protein banding patterns between stretched and control cells and effective proteome fractionation prior to GeLC-MS

Following the 24 hour stretch period, proteins from the cytosolic (C) and membrane (M) fractions were resolved by SDS PAGE and stained with Coomassie Brilliant Blue (Figure 5.3). The resulting banding patterns reveal differences in the protein content of C and M fractions, suggesting effective protein fractionation, which will improve sensitivity during LC-MS analysis. Prominent bands in the low mass region of the membrane fractions are notable, suggesting the presence of histone proteins, which are solubilized with membrane proteins during the detergent lysis. Additionally, the

banding patterns between stretched (Figure 5.3A) and control (Figure 5.3B) cells appear very similar overall, suggesting most of the proteins expressed by these cells are unaffected by stretch. A basal level of biological variation is demonstrated by differences in banding patterns within biological replicates. This difference appears much more prominent in stretched cells, noting specifically the absence of a band in the M lane of replicate P1 that appears prominent in P2 and P3. This result is not unexpected, as the proteome of cells experiencing the experimental condition is expected to express a higher degree of flux as a result of stretch. These results therefore show similarity in protein expression patterns between cell states, and confirm subcellular fractionation.

5.4.3. GeLC-MS/MS data is highly reproducible between cell states

Analysis of stretched and control cell protein fractions reveals a high degree of overlap among each biological replicate from each test condition. After processing the gels and analyzing them by GeLC-MS, proteomic data for each subcellular fraction (*i.e.* cytoplasmic and membrane fractions) were combined within each biological replicate, and the number of proteins identified in each is displayed in Figure 5.4. These data demonstrate the highly reproducible nature of the experimental procedure within each test condition. Of the 1601 and 1570 proteins identified in control and stretched cells (Figure 5.4A and B, respectively), only 59 and 77 are identified in a single biological replicate from each test condition, respectively. The reproducibility of protein identifications within each test condition lends a high degree of confidence in the statistical interpretation of the proteomic data. These results appear to be in agreement with the Coomassie-stained SDS PAGE gels seen above, where the majority of proteins appear to remain unchanged between stretched and control cells. Figure 5.4C further

demonstrates agreement between the gel images and the proteomic data, as 1541 proteins were identified in both test conditions, with only 60 and 29 exclusively identified in control and stretched cells, respectively.

5.4.4. Spectral counting reveals differences in protein abundance between cell states

Statistical analysis of the normalized spectral hit values for all identified proteins was accomplished using the quasi-Poisson *p*-value from the QuasiTel package.[68] Protein abundance was said to be significantly altered when comparison of the spectral hit values yielded a *p*-value of less than 0.05. In total, 317 of the 1630 proteins identified with greater than 6 spectral hits were found to be significantly altered in abundance. Complete protein identification lists for control and stretched cells, with their associated quasi-Poisson *p*-value are provided in Table A2 in the Appendix. Table 5.1 summarizes the results of the proteomic data analysis and displays the number of significantly altered proteins in each cell state. Specifically, 182 proteins are decreased in abundance in stretched cells (*i.e.* are significantly altered in control cells) while 135 are increased in abundance in stretched cells (*i.e.* significantly altered in stretched cells). Figure 5.5 displays results of western blot confirming the quantitative changes in abundance of aldose reductase (up), annexin 1 (up), alpha catenin (down), and CD44 (up). Relative densitometry was conducted on each protein using vimentin as a standard to determine the relative quantity of each protein in each sample. Vimentin shows no significant change in abundance according to spectral counting (quasi-Poisson *p*-value 0.706; Appendix Table A2).

5.4.5. Characterization of proteomic changes by Gene Ontology (GO)

Characterization of the proteins altered as a result of stretch was conducted using GO annotation of molecular function and biological process according to the DAVID online annotation tool. A complete list of GO annotations for all the significantly altered proteins with their associated *p*-values for functional enrichment is provided in the supplemental material of Orton *et al*.[207] Highlights from the list of GO annotations of altered abundance proteins with respect to their molecular function (Figure 5.6A) shows that proteins expressing calcium and phospholipid binding as well as unfolded protein binding properties were significantly increased in abundance in stretched cells. Conversely, proteins expressing cytoskeletal, identical protein and ribonucleotide binding and hydrolase activity are decreased in abundance in stretched cells. These results suggest a disruption in cytoskeletal organization and phospholipid organization as a result of stretch.

A similar analysis of the biological process (Figure 5.6B) of proteins with altered abundance shows a higher proportion of proteins associated with carbohydrate metabolism activity are increased in stretched cells. Conversely, proteins shown to be decreased in abundance in stretched cells include cytoskeletal organization proteins and normal cell growth (mitotic) proteins. These results agree with the molecular function annotations, where cells are undergoing reorganization and experiencing a loss of homeostatic mechanisms resulting from stretch.

5.4.6. Changes in protein abundance are characterized by KEGG Ontology

Further characterization of the significantly altered proteins was conducted by KEGG ontology using the KOBAS online search tool (v. 2.0).[210] A complete list of KEGG annotations, with their assigned proteins from each respective cell condition also with their associated *p*-values is provided in supplemental material in Orton *et al*.[207] Highlights are presented in Table 5.2 and Table 5.3, showing pathways associated with proteins identified as significant in control and stretched cells, respectively. As expected, there is a degree of redundancy between the pathways identified in each cell state, emphasizing the complexity of regulation of the pathways affected by stretch.

Table 5.2 shows highlights from the list of KEGG pathways that are significantly (Fisher's Exact test *p*-value <0.1) decreased in stretched cells. These pathways include a number of cell interaction pathways such as gap, adherens, and tight junction proteins, but also a number of metabolic pathways such as amino acid and fatty acid metabolic proteins. In addition, DNA replication and cytoskeletal proteins are also decreased, which is in agreement with GO annotations and microscopic findings suggesting these cells are undergoing a number of morphological changes as a result of stretch. Table 5.3 similarly shows KEGG pathways that are significantly enriched in stretched cells. Most notable of these include a number of metabolic changes in carbohydrate usage, protein recycling and protein processing in the ER which suggest a shift in metabolic function and protein synthesis as a result of stretch.

5.5. Discussion

This study demonstrates changes in protein abundance in rat proximal tubule cells following stretch-induced apoptosis as an *in vitro* model of UTO. Three consecutive passages of NRK-52E cells were used in the experiment to more closely resemble relevant biological replication. Mechanically stretching these cells mimics the physiological stress experienced by proximal tubule cells subject to obstruction, which eventually leads to proximal tubule cell apoptosis and tissue fibrosis.[100,101,170] In an effort to boost protein identification numbers and promote greater confidence in quantitative results, protein was isolated from each replicate in a stepwise manner following a proteome fractionation procedure. A total of 1630 proteins were identified in the experiment, with 1601 non-redundant proteins from the control and 1570 from stretched cells. Of these, 135 proteins are noted to be increased and 182 decreased in abundance in response to stretch following statistical analysis using the QuasiTel statistical analysis package. The cellular processes affected by stretch were determined by analyzing significantly altered proteins by GO and KEGG annotations, and the change in abundance noted by spectral counting was confirmed for a number of proteins by western blot (Figure 5.5). Figure 5.7 summarizes the results of the experiment and highlights a number of the proteins and pathways found to play possible roles in the pathophysiology resulting from mechanical stretch.

5.5.1. Activation of apoptosis and fibrosis

A major contributor to renal failure that results from UTO involves proximal tubular cell apoptosis.[247] Previous work has demonstrated that renal tubular cells

experience apoptosis as a result of stretch,[100,101,182] and that apoptosis occurs *via* caspase-3 and -9 mediated pathways.[170] We demonstrate a number of proteins with GO annotations that show significant enrichment for cellular response to stress and cytoskeletal organization in control cells, while calcium dependent protein binding and phospholipid binding show enrichment in stretched cells. Such enrichment of these processes suggests that these cells are actively undergoing cellular reorganization and cell membrane recycling, two indicators of induction of apoptosis. Specifically, α-catenin and RhoA, which interact to strengthen adhesive association between cells are decreased in abundance, suggesting a loss in inter-cellular interaction.[253] In addition, the number of apoptosis marker proteins from the annexin family are increased in abundance in stretched cells. These proteins bind negatively charged phospholipids in a calcium dependent manner and are commonly used as cell surface markers of apoptosis,[254] and also play a major role in cytoskeletal arrangement, which is disrupted during stretch.[255] While these results could be expected as a result of the experiment, the specific involvement of α-catenin and Rho in this model have not been previously described in the literature.

In addition to apoptosis, UTO results in tissue fibrosis, which contributes to decreased renal function.[101,142] Activation of the fibrotic response is caused by signaling through the profibrotic cytokine TGF-β. CD44 is a known effector of TGF-β signaling in a variety of renal diseases leading to fibrosis,[256–258] and it was increased in abundance in stretched cells. Although TGF-β signaling is commonly noted in this stretch model, and CD44 is known to play a role in fibrosis in the kidney, it has not been described previously in the stretch model, suggesting it may be a novel effector of fibrosis in UTO. Another protein significantly altered by stretch that is regulated by TGF-β signaling is

prohibitin, a downstream effector regulating inner mitochondrial permeability[259] shown here to be increased in abundance as a result of stretch. Interestingly, prohibitin has not been described previously as a result of stretch or UTO, making it a potential novel effector of the pathophysiology of UTO.

Another effector that has been demonstrated to lead to both oxidative stress and cell death is chronic stress to the ER. ER stress and its role in apoptosis have been extensively reviewed by Xu *et al*.[260] As noted in Table 5.2 and Table 5.3, a number of proteins involved in protein processing in the ER show altered abundance in stretched cells. Specifically, the proteins calnexin and endoplasmin, proteins known to be oxidized and degraded as a result of oxidative stress, are decreased in abundance. It has been hypothesized that these proteins are highly susceptible to oxidative stress due to their function in promoting protein folding in the ER. The decrease in abundance of these proteins suggests that a loss in normal cellular processes and induction of a stress response result from stretch. Involvement of ER stress during UTO has been previously described, however the role of calnexin and endoplasmin have yet to be noted, demonstrating the efficacy of this proteomic investigation for unearthing novel effector proteins in UTO.

5.5.2. The role of oxidative stress in proximal tubule cells and UTO

It is well established that proximal tubule cells experience oxidative stress as a result of stretch *in vitro* as well as UTO *in vivo*.[160,249,250] Oxidative stress can result from a number of subcellular processes and can lead to cell apoptosis through a variety of mechanisms such as ER stress, or mitochondrial damage. Although excess ROS can result from a number of intracellular processes, they are mainly generated in the mitochondria

through the electron transport chain and β-oxidation of fatty acids. Three major effector proteins involved in oxidative stress response are shown here to be significantly altered in abundance as a result of stretch. Glutathione peroxidase (GSP; down) and glutathione S-transferase-α (up), two regulators of detoxification of ROS, are shown to be altered in abundance. An additional antioxidant enzyme, catalase, is also decreased in abundance. Glutathione (GS) is a potent intracellular antioxidant, therefore regulation of intracellular GS levels have major impacts on the oxidative state of proximal tubular cells. Glutathione S-transferase-α is involved in detoxification of cytotoxic lipid peroxidation products such as 4-hydroxy-2-nonenal (HNE) through conjugation of GS to HNE, and subsequently GS-HNE has been used as a biomarker of oxidative stress-induced lipid peroxidation.[261–263] GSP directly detoxifies hydrogen peroxide, protecting the cell. However, GSP activity is dependent on the presence of the essential cofactor nicotinamide adenine dinucleotide phosphate (NADP), which is required for a variety of other processes. Additionally, KEGG ontology suggests a reduction in fatty acid synthesis proteins in stretched cells, which agrees with previous work that utilization of fatty acids by beta-oxidation is decreased during UTO.[264]

Another regulator of intracellular oxidative state involves the two-enzyme polyol pathway. The rate limiting enzyme of the polyol pathway, aldose reductase (AR), is noted here to be increased in abundance. While the polyol pathway has been implicated in a number of chronic renal diseases, it has not been described in UTO. AR is a well-known effector in ischemic injury of the heart by disrupting the intracellular balance of $NADPH/NADP^+$ and promoting a so-called 'pseudo-hypoxic' state. Activation of the polyol pathway has a downstream effect on the expression of several genes *via* NFκB, as well as the PI3K/Akt cell signaling pathways, all of which are known effectors in UTO.

Mechanical stretch activation of this pathway may occur as a result of the metabolic shift described above, therefore promoting oxidative stress by disrupting intracellular $NADPH/NADP^+$ levels. These results therefore implicate AR to be a novel effector in progression of oxidative stress during UTO.

5.5.3. Metabolic changes as a result of mechanical stretch

Previous literature has shown a number of metabolic processes are affected by UTO.[251,265,266] Our data agree with these studies, as noted by KEGG ontology (Table 5.2 and Table 5.3). According to KEGG and GO annotations, the most affected metabolic processes are glycolysis and gluconeogenesis, amino acid, and fatty acid metabolism. Previous work shows changes in urinary concentration of metabolic intermediates in UTO,[267] while other studies show changes in metabolic processes in response to various forms of UTO *in vivo*.[266] A well characterized effect of UTO involves a shift in metabolic activity from aerobic glycolysis to anaerobic gluconeogenesis.[266,268,269] We demonstrate a shift in the number of glycolytic proteins, however the complexity of regulation of the pathway makes it difficult to speculate on the specific processes that occur as a result of stretch. Notably, one enzyme in the pyruvate dehydrogenase complex is identified as increased in abundance (dihydrolipoyllysine-residue acetyltransferase). This enzyme complex is important for metabolism of pyruvate to acetyl-coA for progression to the Kreb's cycle. Two proteins from the Kreb's cycle, 2-oxoglutarate dehydrogenase, which is responsible for the sixth step in the cycle, and ATP citrate lyase, which is important for synthesis of acetyl-coA in the cytoplasm from citrate, are shown to be decreased in abundance. These data agree with previous studies that show a disruption of the Kreb's cycle in UTO.[267]

5.6. Conclusions

Characterization of the changes in protein expression in these cells provides greater insight into the molecular pathophysiology of proximal tubule cells as a result of obstruction. Analysis of proteomic data shows a number of processes known to be altered by stretch using GO and KEGG annotations, suggesting good compliance with previous work using the model. Additionally, a number of proteins significantly altered in abundance are identified as a result of stretch that have not been previously characterized in the pathophysiology of UTO. Specifically, evidence for involvement of AR as a novel effector in UTO is presented, as well as a number of fibrotic and apoptotic effectors not previously identified. These findings contribute to a more thorough understanding of the cellular processes occurring during stretch of proximal tubule cells. Application of orthogonal proteomic technologies such as western blotting, ELISAs, immunostaining, or targeted MS will allow more in depth analysis of the identified pathways, however specific characterization of effectors in UTO was not the goal of this study. Expansion on the findings here will allow a greater understanding of the disease, potentially leading to improved care for children with urinary tract obstruction in the future.

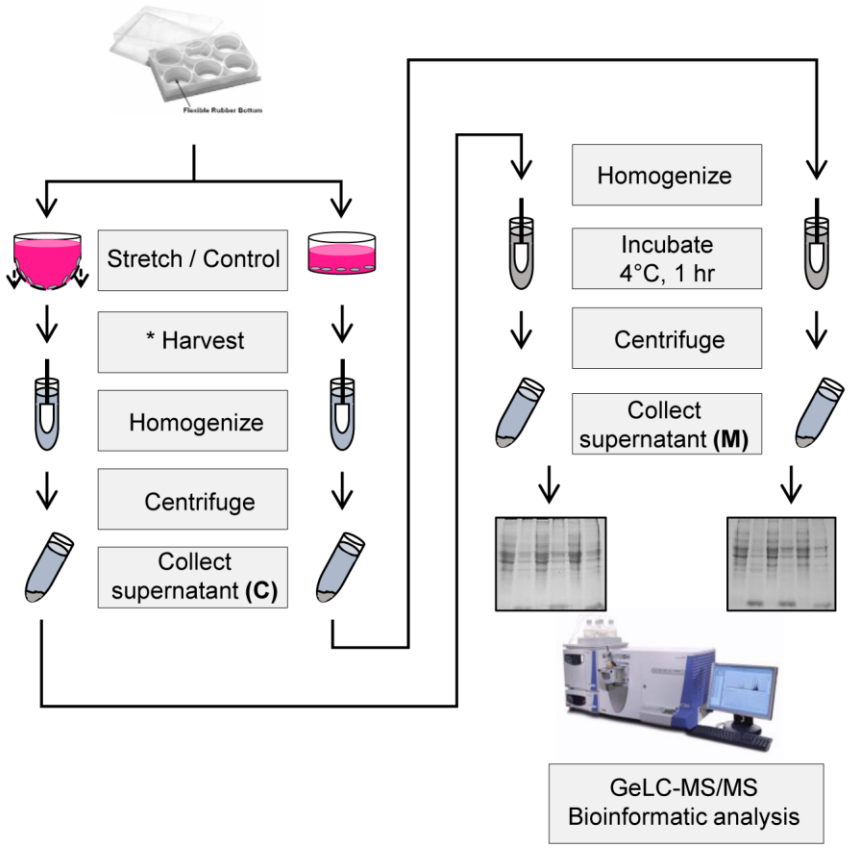

Figure 5.1: Experimental workflow diagram.
Cells were grown on Bioflex™ plates, stretched or incubated under identical conditions for 24 h. Cells were collected and homogenized in RIPA buffer. The homogenate was subject to centrifugation at 100,000 × *g* for 1 hr. The supernatant was collected (cytoplasmic fraction; C) and pellet resuspended in lysis buffer. Insoluble material was incubated in lysis buffer for 1 hr at 4 °C with gentle agitation and ultracentrifuged again. The supernatant was collected (membrane fraction; M) and C and M were subjected to GeLC-MS/MS analysis and spectral counting.

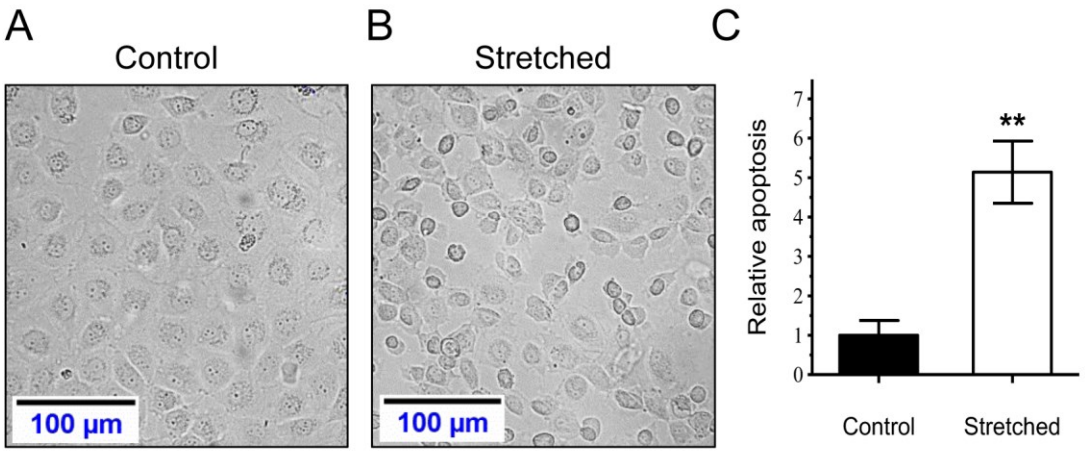

Figure 5.2: Assessment of NRK-52E cells for morphological and biochemical changes following stretch.
Microscopic evaluation of (A) control and (B) stretched cells following 24 hour stretch period. (C) Results of the cell death ELISA across three biological replicate analyses, normalized to control. ** Indicates a significant increase in cell death in stretched cells over controls (p-value = 0.009) by students' t-test.

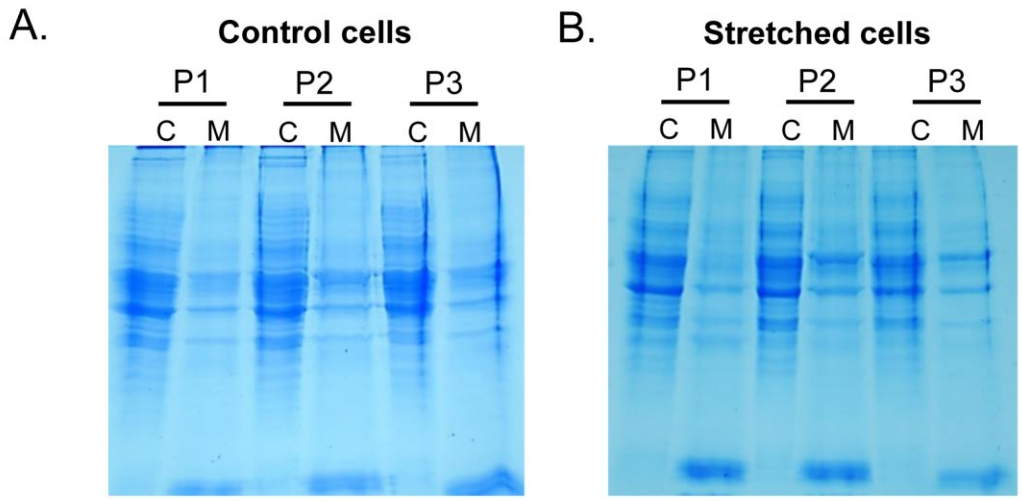

Figure 5.3: Coomassie-stained SDS-PAGE gels of cytoplasmic and membrane protein extracts.
Similar banding patterns are noted between control (A) and stretched (B) cell protein extracts. Cytoplasmic (C) and membrane (M) fractions were resolved in parallel in each biological replicate, annotated P1, P2, or P3. These gels were subsequently sectioned into 15 slices per lane and analyzed by GeLC-MS/MS.

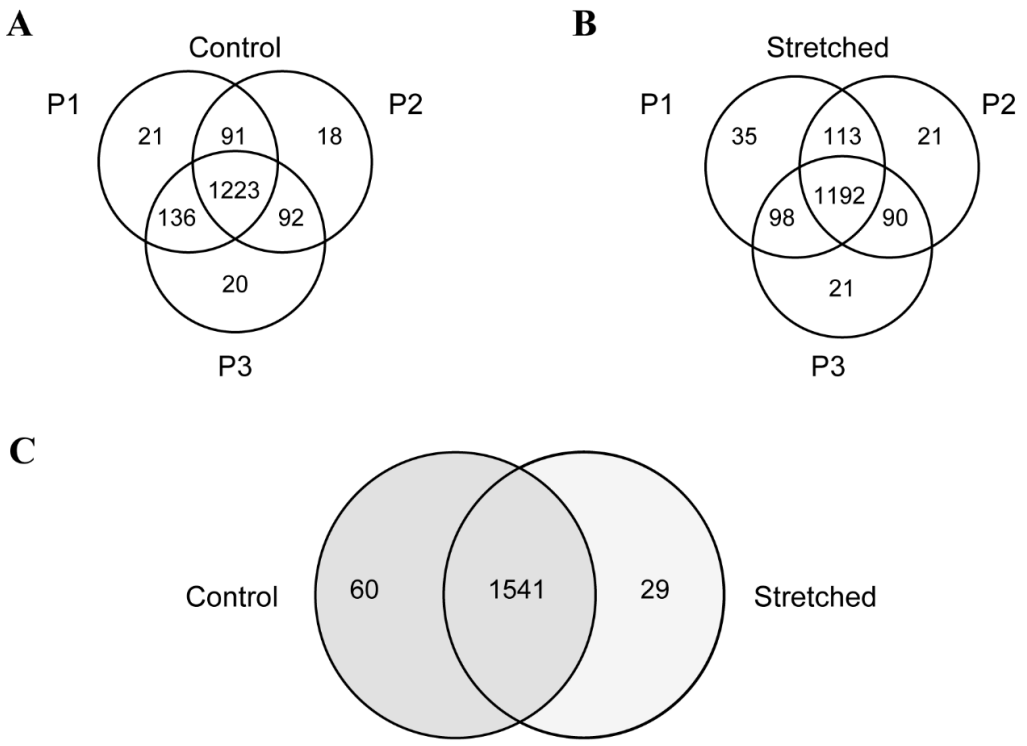

Figure 5.4: Venn diagrams showing the overlap of identified proteins from stretched and control cells.
Proteins identified in each biological replicate in (A) control and (B) stretched cells. (C) Shows the overlap of the non-redundant proteins identified between each cell condition, showing proteins identified as unique to stretched (29) and control (60) cells.

Table 5.1: Summary of proteomic data across the three biological replicate analyses.

Condition	Replicate	# Proteins identified	Nonredundant proteins	Proteins with significant change in abundance
Control	P1	1471	1601	182
	P2	1424		
	P3	1471		
Stretched	P1	1438	1570	135
	P2	1416		
	P3	1401		

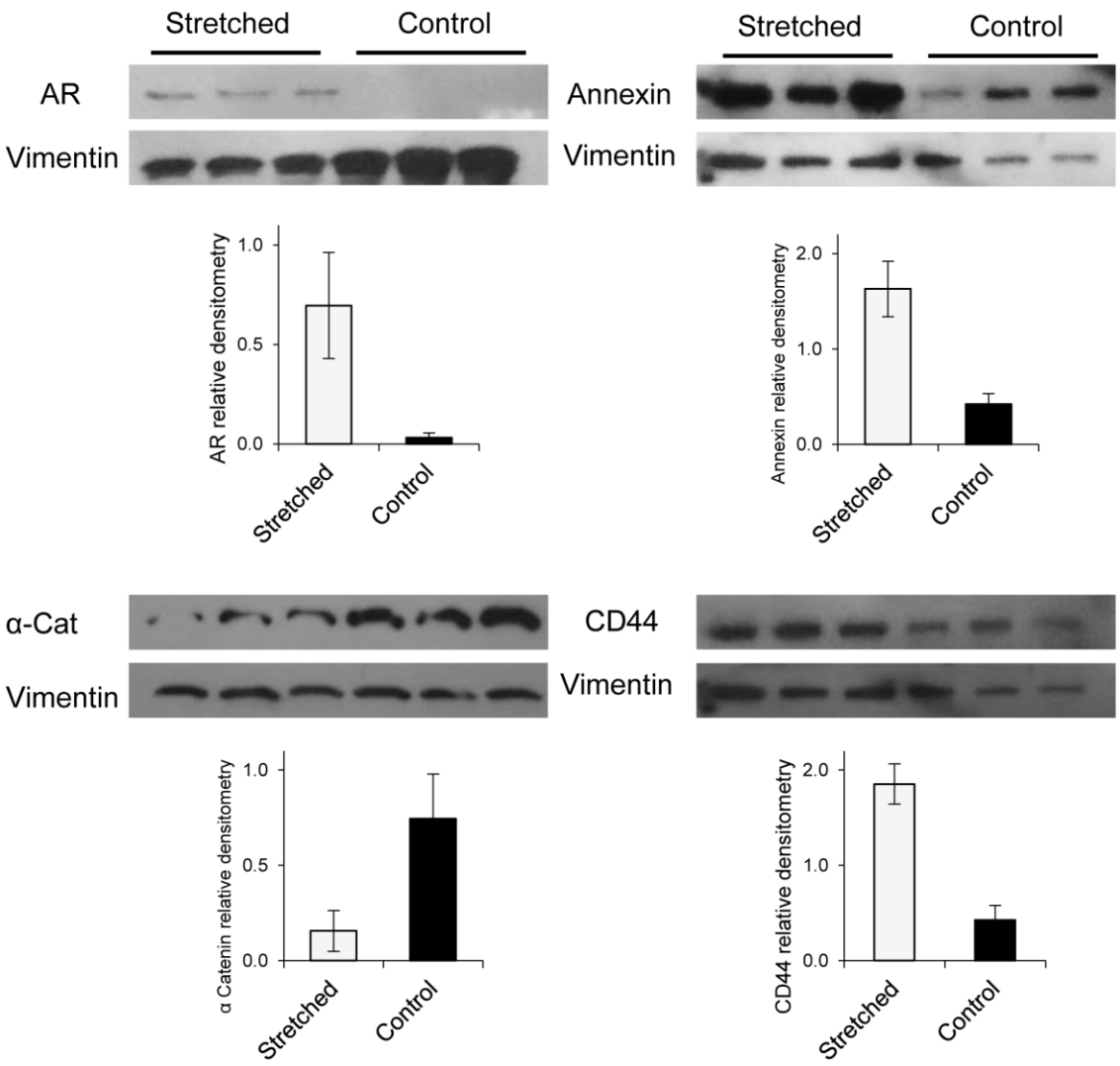

Figure 5.5: Western blot confirmation of quantitative LC-MS results.
Aldose reductase (AR), annexin 1 (Anx), alpha catenin (α-Cat), and CD44. Bar graphs represent the relative densitometry of each protein to vimentin as the standard ± the standard deviation (n = 3). AR, Anx, and CD44 are shown to be significantly increased in abundance (*p*-values 0.048, 0.012, and 0.0012, respectively), while α-Cat is shown to be decreased in abundance (*p*-value 0.033), by student's t-test.

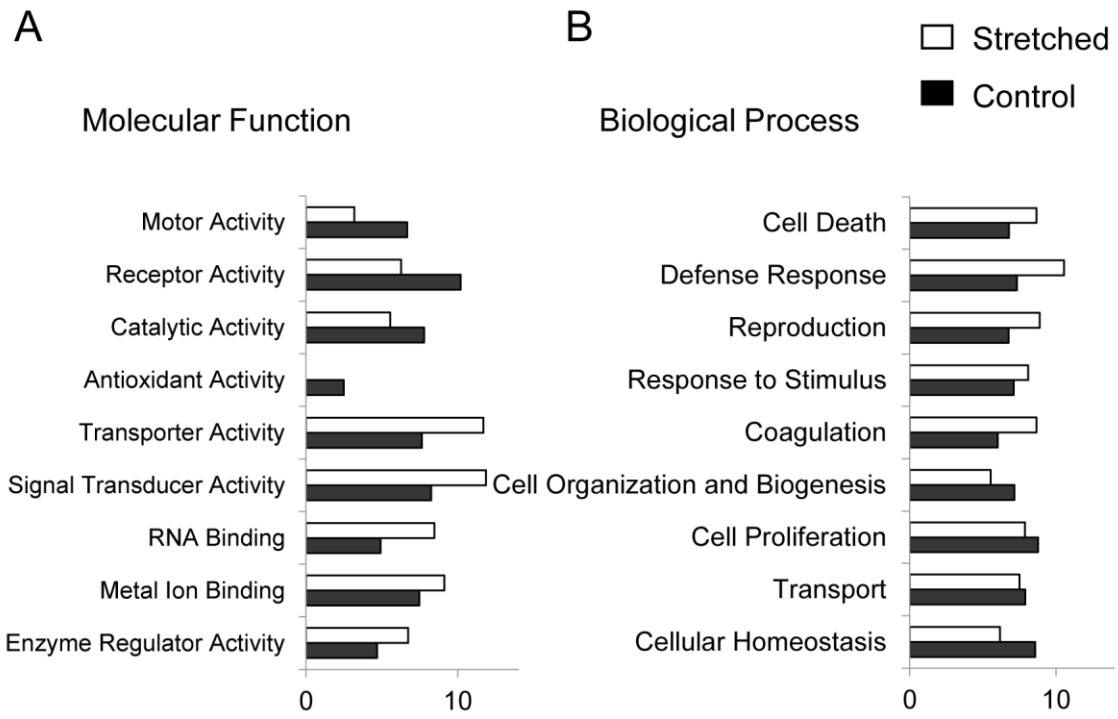

Figure 5.6: Gene ontology (GO) annotations following mechanical stretch of NRK-52E cells.
Molecular function (A) and biological process (B) of proteins increased (white bars) and decreased (black bars) in abundance as a result of stretch. The relative number of proteins are shown as a percentage of the total number of altered proteins in each state normalized to the total number of proteins with each annotation identified in the experiment.

Table 5.2: KEGG pathways significantly enriched in control cells.
Pathways express a Fisher Exact p-value <0.1, and are listed with the number of proteins identified in each pathway.

Pathway	# Proteins	*p*-value
Gap junction	5	3.89E-03
Adherens junction	4	1.05E-02
DNA replication	3	1.11E-02
Tight junction	5	1.92E-02
Phagosome	6	2.24E-02
Arginine and proline metabolism	3	2.75E-02
Protein processing in ER	5	4.07E-02
D-Glutamine and D-glutamate metabolism	1	4.35E-02
Citrate cycle (TCA cycle)	2	4.85E-02
Regulation of actin cytoskeleton	5	9.19E-02
Fatty acid metabolism	2	1.02E-01

Table 5.3: KEGG pathways significantly enriched in stretched cells.
Pathways express a Fisher Exact p-value <0.1, and are listed with the number of proteins identified in each pathway.

Pathway	# Proteins	*p*-value
Protein digestion and absorption	4	2.16E-03
Ribosome biogenesis in eukaryotes	4	3.16E-03
Proximal tubule bicarbonate reclamation	2	9.23E-03
Lysosome	4	1.05E-02
Peroxisome	3	1.72E-02
Glycolysis / Gluconeogenesis	3	1.72E-02
Fructose and mannose metabolism	2	2.75E-02
Carbohydrate digestion and absorption	2	2.89E-02
Pyruvate metabolism	2	3.30E-02
Protein processing in endoplasmic reticulum	3	1.01E-01

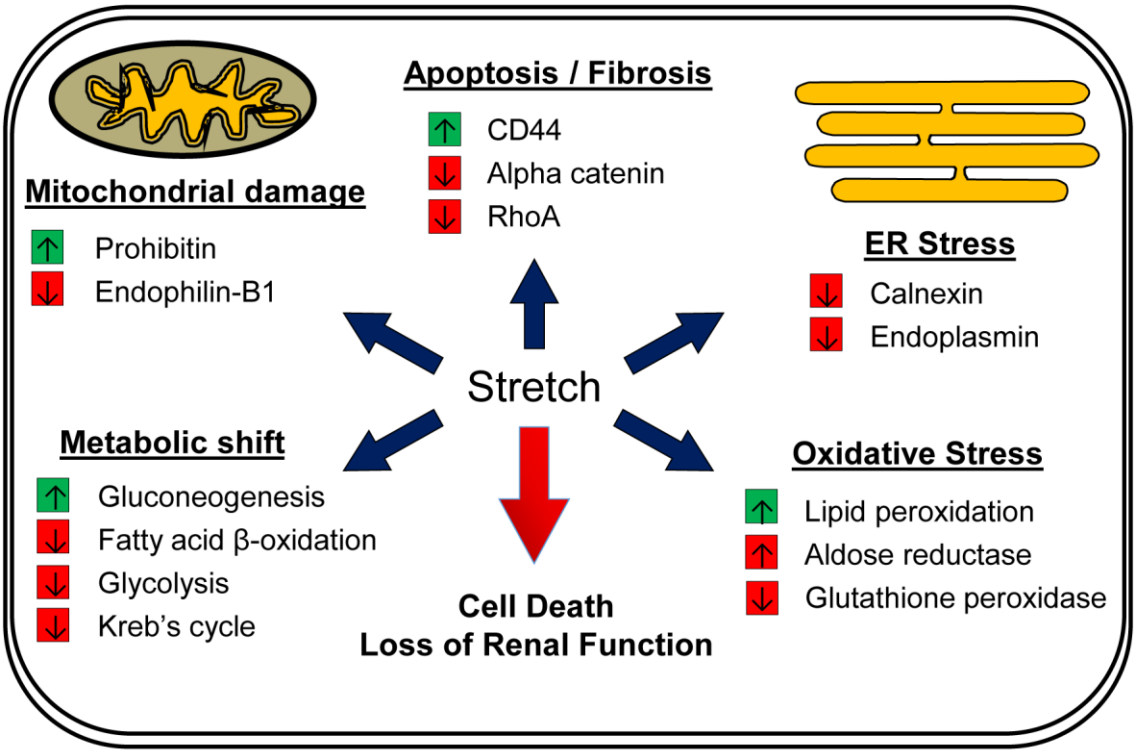

Figure 5.7: A proposed diagram for the effects of mechanical stretch on the rat proximal tubule cells.
Major effectors in cell response to mechanical stretch proposed here include oxidative stress, mitochondrial damage, ER stress, initiation of apoptosis/fibrosis, and altered metabolism. Specific proteins and pathways associated with each process are noted. Together these processes lead to initiation of cell death.

Chapter 6:

Quantifiable changes in the proteome of urinary exosomes following urinary tract obstruction are severity-dependent

6.1. Preface

This Chapter presents a proteomic analysis of urinary exosomes obtained from rats with surgically-introduced UTO with comparison to controls. The goal of this study was to identify candidate biomarker proteins capable of distinguishing between healthy and diseased rats, but also between mild and severe forms of UTO. Quantitative evaluation of the proteins identified can therefore allow identification of prognostic and diagnostic markers of UTO. Mild obstruction was introduced by PUO, while severe obstruction was introduced by CUO. This work is being prepared for publication with the Authors: Orton, D.J.; Doucette, A.A.; Huang, W.F.; MacLellan, D.L.

* All experiments, data analysis, manuscript preparation, and exosome isolation were conducted by Dennis Orton. Surgeries and manuscript revisions were conducted by Dr. Dawn MacLellan Dr. Alan Doucette contributed to execution of MS. Pathology assessment and tissue imaging was conducted by Dr. Weei Huang.

6.2. Introduction

Congenital urinary tract obstruction (UTO) is a common cause of prenatally diagnosed hydronephrosis,[9,126,136] and remains the leading cause of renal functional loss in children.[136,137] Hydronephrosis often resolves spontaneously, however, it has the potential to deleteriously affect renal function and require surgical intervention to avoid further renal functional loss. Current management strategies may require years of invasive renal function investigations before clinical manifestation of renal functional damage.[175,270,271] The invasive nature of these tests, coupled with the lengthy surveillance required to measure renal functional impairment, makes current management methods undesirable. Therefore, identification of non-invasive clinically measurable markers capable of predicting which children will require surgery could improve patient care, avoid unnecessary patient anxiety, and limit the chances of renal functional impairment in children with UTO.[175]

High throughput proteome analyses are becoming popular for biomarker identification in a variety of diseases. The proximity of urine to the kidney, and the non-invasive nature of sample collection makes it an excellent medium for identifying biomarkers of UTO. Unfortunately, studies of the human urinary proteome require extensive prefractionation strategies ahead of liquid chromatography (LC) and mass spectrometry (MS) for sensitive analysis. Studies have identified as many as 2,362 proteins from urine,[8] with many more suspected to be present. The highly dynamic concentration range and diverse physical and chemical properties expressed by these proteins clearly elucidates complexity of the urinary proteome.

Recently, Mesrobian *et al.* conducted two quantitative analyses of the urinary proteome of children exhibiting high-grade hydronephrosis caused by UTO.[85,86] These studies contribute a list of proteins with significant changes in the urine of children with severe UTO. A drawback in the analyses is the lack of sample fractionation prior to LC-MS analysis. With no separation, only the most abundant proteins are identified by LC-MS, thus reducing the sensitivity of the results. Additionally, while Mesrobian *et al.* identified a number of interesting proteins with diagnostic potential, the prognostic ability of the proteins was not addressed.[85,86] A more sensitive analysis of the urinary proteome will therefore provide additional information to improve the efficacy of any future biomarker tests resulting from these high throughput analyses.

This study employs an LC-MS analysis of urinary exosomal protein obtained from rats with surgically introduced UTO in an effort to investigate the diagnostic and prognostic applicability of quantifiable changes in protein abundance. Exosomes are small extracellular vesicles secreted by a number of cell types, including those lining the urinary tract.[119] Exosomes in urine therefore present a unique protein profile that reflects the protein composition of their parent cells. Selective isolation and analysis of exosomal proteins from the urine can therefore provide kidney-specific functional information.[272] This study aims to use the changing proteome profile of urinary exosomes to identify sensitive and kidney-specific markers of UTO to aid in development of biomarkers for the disease. To this end, two degrees of severity of obstruction are introduced (partial and complete), urinary exosomes are isolated and analyzed by quantitative LC-MS analysis in comparison to a sham-operated control group. Evaluation of proteomic changes resulting from partial (mild) and complete (severe) UTO can thus distinguish between disease groups with varying degrees of obstruction.

6.3. Experimental in brief

Surgery was conducted on weanling rats wherein the left ureter was exposed but not manipulated (control), partially, or completely obstructed. A total of 22 rats were used for exosomal proteome analysis. There were 9 control rats, 7 partially obstructed rats, and 7 completely obstructed rats. Urinary exosomes were isolated from each individual rat, as noted in section 2.6. Protein concentration was assessed by BCA assay, and pooled into three replicates per test group. Approximately 25 μg of protein from each pooled sample were loaded into a 12 % T SDS PAGE gel and partially resolved (~3 cm) on the gel. Each lane was processed into 3 gel slices, subjected to in-gel digestion, and analyzed by LC-MS in quadruplicate with the 65 minute gradient described in section 2.7. Data were searched against a rat Uniprot database (27,353 entries, downloaded August 1, 2013) and proteins identified with greater than six spectral counts across all analyses were accepted. The method QuasiTel was employed for statistical analysis of the spectral counting data and significantly altered proteins were assessed as described below.

6.4. Results

6.4.1. Physical and histopathological assessment of animals

At 21 days post-surgery, urine was collected for 24 hours, serum and kidneys were harvested, and rats were sacrificed. To evaluate a number of potential physiological measures that proposed to be able to distinguish between healthy and obstructed groups, a number of physiological characteristics were evaluated (Table 6.1). Creatinine concentration and clearance, often used as a measure of glomerular filtration rate and kidney function, showed no significant changes between healthy and obstructed rat groups, suggesting no detectable renal functional loss. The concentrating ability of the

kidneys, assessed by urine osmolality also showed no difference between groups. In fact, only the kidney weight and volume were capable of differentiating between healthy and obstructed groups. Interestingly, both the weight and volume of the contralateral (unobstructed) kidney were increased in the complete obstruction model, demonstrating compensatory growth not noted in the partially obstructed rat group. These results support the hypothesis that a more sensitive biomarker is needed to assess the pathogenesis of UUO on renal function.

Representative histological sections of control, partial, and completely obstructed rat kidneys following 21 days of obstruction are presented in Figure 6.1. These sections clearly demonstrate the effects of obstruction on renal parenchymal thickness, as well as fibrosis and inflammation. Normal kidney morphology with well-defined cortex and medullary regions, with normal tubule and glomerular distribution in control rats are shown in Figure 6.1A, D, G. In contrast, localized parenchymal tissue loss, tubular atrophy, immune cell infiltration and fibrosis can be noted in partially obstructed kidneys (arrowhead, Figure 6.1B, E, H). Completely obstructed kidneys portray severe loss of the interstitium, a distorted renal pelvis, widespread lymphocyte invasion and tubular atrophy, as well as extensive collagen deposition resulting from fibrosis (Figure 6.1C, F, I). Taken together, these results show the pathology associated with an obstructed kidney,[273,274] and suggest that the methods presented in Table 6.1 are incapable of diagnosing extensive kidney damage.

6.4.2. Proteomic analysis of urinary exosomes

The presence of urinary exosomes is confirmed by electron microscopy in Figure 6.2. Small, extracellular vesicles (30-100 nm in diameter) are present in the pellet

obtained from the 200,000 × *g* sucrose layer from the urine of rats from all three groups. A pooled proteomic analysis of the urinary exosome samples identified a total of 318 proteins with greater than 6 peptide assignments across all LC-MS analyses in the experiment. Figure 6.3 shows a Venn diagram of the overlapping identities of the proteins identified from each test group. In total, 310 proteins were identified from control group exosomes, 300 proteins from the completely obstructed group, and 289 proteins from the partially obstructed group. As expected, the vast majority of proteins identified in this study were commonly found in all three study groups, suggesting a similar protein profile between rat groups.

6.4.3. Statistical analysis of changes in protein abundance

Quantitative analysis of urinary exosomal proteins in each group was conducted in a pairwise manner, comparing control to partial and complete obstruction groups, as well as partial to complete. Table 6.2 summarizes the results of the analysis, showing approximately half of the proteins identified from proteomic analysis from each group are significantly altered when compared to the other two groups. The relative changes in abundance of these proteins were increased or decreased in one or more of the other test groups. Specifically, comparing control and partial obstruction showed 133 significantly altered proteins, while 99 proteins were significantly altered between control and complete obstruction. There was a large amount of overlap in the significantly altered proteins between these groups, and when comparing complete and partial obstruction groups, 83 proteins were significantly different. Analysis of the data in this manner provides stratification of the protein abundance in models of increasingly severe obstruction. In addition, a number of these proteins are increased in abundance in one

form of obstruction as well as decreased in the other. The intricate balance between protein abundance in each could therefore be exploited to distinguish between mild and severe obstruction. Confirmation of the quantitative results is provided in Figure 6.4, and the implications of these results are discussed below.

6.5. Discussion

Previous studies of the urinary proteome by LC-MS have elucidated a number of candidate biomarker proteins for UTO. Problematically, these studies do not address the prognostic implications of the proteins, and do not discuss whether the protein abundance is increased or decreased.[85,86] The goal of this study was to quantify changing protein abundance in response to UTO, but also assess the ability of these proteins to differentiate between groups with varied degrees of severity. To this end, proteome analysis of urinary exosomes shows a number of proteins that are capable of differentiating between control and obstructed (control versus partial or complete), as well as stratifying the severity of UTO (partial versus complete). A major finding of this study is the ability to identify significant changes in protein abundance resulting from mild obstruction not measurable by other non-invasive means.

6.5.1. Quantitative analysis identifies a number of proteins previously implicated in renal disease

Previous work on a number of renal diseases has elucidated the roles of many proteins with respect to disease progression and pathogenesis. Many of these studies are carried out at the tissue or serum level, with a number looking into the effects of the disease on protein abundance in the urine. Table 6.3 provides a list of proteins identified in this study to express altered abundance as a result of UTO (up or down) that have been

described in other renal diseases or in UTO. As was expected, there is some overlapping proteins identified in this study of urinary exosomes with the Mesrobian study of the whole urinary proteome on children with severe UTO.[86] This study has the advantage of isolating exosomes from the urine for analysis, therefore, providing a large number proteins that have not been previously linked to obstruction are identified in this experiment and contributing to our understanding of the disease itself. In addition, each protein in the table was searched against a database compiled from a number of previous urinary exosome studies known as Exocarta. This allows confirmation that the proteins identified here are of exosomal origin.

6.5.2. Functional assessment of altered proteins have implications on renal functional assessment

Functional assessment of the protein groups resulting from obstruction (partial or complete) shows a number of ion transport proteins are altered in abundance (Table 6.3). These proteins are involved in regulation of the urine osmolite and metabolite concentration, acidity, and control the concentrating ability of the kidneys. A subgroup of solute carrier proteins, known as aquaporins, are known to be decreased in abundance in human studies of UTO.[275,276] Additionally, surface expression of aquaporins may be regulated by exosomal secretion.[119] In addition, a number of studies have been conducted to evaluate the changes in urinary metabolite concentration following UTO.[252,267] Interestingly, a number of the ion transport proteins noted here are increased in abundance, while others are decreased. These results reflect the changes in urine composition occurring as a result of UTO. In addition, voltage-dependent anion-selective channel proteins 1 and 2 (VDAC1/2) are decreased in abundance in both partial and

complete obstruction. These proteins are also involved in Cl^- ion transport across membranes and have been suggested to play a role in apoptosis of renal epithelial cells.[277] While it has been suggested that the urinary osmolite balance and glomerular filtration rate may be used as an indicators of renal function, they appear to be of limited use in this study (Table 6.1). This is attributed to the compensatory response by the contralateral, unobstructed kidney shielding these effects. These results suggest protein level analysis is able to distinguish changes in ion transporter abundance and thus delineate changes in renal concentrating ability due to mild and severe obstruction.

6.5.3. Urinary enzymes are indicators of tubular cell damage

Another group of proteins shown here to be altered in abundance resulting from obstruction are tubular cell enzymes. Enzymuria resulting from tubular cell damage is well established, and current methods to measure the extent of enzymuria commonly employ spectrophotometric analyses.[278] Interestingly, a number of enzymes known to be rapid responders to tubule stress are shown here to be altered in abundance in UTO. Established markers of tubule stress in UTO and a number of other renal diseases identified here include alkaline phosphatase, γ-glutamyl transferase, lactate dehydrogenase, and aminopeptidase N (APN).[198,279,280] While these proteins show quantitative changes here, their usefulness for predicting significant renal damage in UTO has been questioned due to their low threshold for release, occurring as a result of mild insult to the kidney.[278] Despite this, these proteins could easily be adapted into biomarker panels as early markers of tubular cell damage in UTO. In addition, a number of enzymes exhibiting exo- and amino-peptidase activity were identified here (Table 6.4). Dipeptidyl peptidase-4 and -7, serpin-1 (α1-antitrypsin), meprin A, and neprilysin are all identified as

having altered abundance following UTO. The peptidase results back the results found in the Mesrobian study of UTO,[85,86] however meprin-A and neprilysin, although noted to change in expression following UTO, have not had those changes noted in urine.[281,282] The importance of these proteins are well established in the progression and regulation of fibrosis and angiotensin signaling, as well as being candidate biomarkers for a number of other renal diseases.[6,281,283–285]

6.5.4. Prognostic ability of changes in protein abundance

It is interesting to note that while these proteins all demonstrate changes in abundance resulting from obstruction, that change is not always consistent with increasing severity. Figure 6.4 shows western blot confirmations of the abundance pattern of two proteins (ceruloplasmin and APN) with inverted abundance patterns. Spectral counting data shows ceruloplasmin to be significantly decreased in partial and increased in complete obstruction. These results are confirmed by western blot in Figure 6.4, showing a lack of signal in the partially obstructed group corresponds to the zero spectral counts by LC-MS. Conversely, spectral counting data shows a significant increase of APN in the partially obstructed group versus a significant decrease in the completely obstructed group, also confirmed by western blot in Figure 6.4. Of particular interest here is the variation in APN abundance in the partially obstructed group. Histopathological assessment of the rat kidneys corresponding to the urine samples employed for western blot shows that the weaker band in the partial group in Figure 6.4 corresponds to a more severe response to obstruction than the bolder band. These results, in concert with the weaker bands in the complete obstruction group, suggest that APN abundance in the urine decreases following more severe obstruction.

Ceruloplasmin, a serum protein suggested to play a role in oxidative stress response[286] and fibrogenesis,[287] is shown to have an opposing abundance pattern to APN where it is decreased in abundance in partially obstructed rat urine and increased in the complete group. While this pattern may be counterintuitive, it has been noted previously in a proteome analysis of urinary exosomes from groups experiencing IgA nephropathy (IgAN) and thin-basement membrane nephropathy (TBMN).[6] A point to consider is that IgAN, the more severe of the two pathologies, expresses a pattern the same as that noted here in the complete obstruction group. These results can therefore be used to suggest an increase in abundance of APN is a marker of mild tubular cell damage, while the increase in ceruloplasmin is a marker of severe renal damage.

A large number of proteins identified in this study can be adapted to provide insight into the severity of obstruction on changes in the urinary proteome. Haptoglobin, increased only in complete obstruction, is a marker of fibrosis in the kidney and acute phase responder.[288] Cubilin, a protein localized to the proximal tubule that regulates protein reabsorption, noted to be decreased in obstruction (partial or complete) is similarly decreased in abundance in a study on oxidative stress of the kidney.[289] Epidermal growth factor (EGF), identified here as "Uncharacterized Protein M0RAK7," is well known to be decreased in abundance in both urine and renal tissue during obstruction.[144,185] Targeted analyses of a select number of the proteins presented here will allow better estimation of the role they play in disease progression, as well as determine how well they can differentiate between cases of mild and severe obstruction.

6.6. Concluding remarks

This study presents a number of proteins noted to express altered abundance in urine following introduction of UTO in weanling rats. Studies aiming to uncover biomarkers for this disease have primarily centered on elucidating the abundance of previously identified proteins in the urine of children with this disease. While these studies tend to offer good correlation between protein abundance and disease progression, there still exists a lack of validation of these candidate biomarkers for clinical application. It is hypothesized that the inability to design effective biomarker tests using these well-known proteins is due to the lack of specificity to the disease and inability to stratify progression of the disease so to act as prognostic indicators of UTO. A recently published series of papers have expanded the list of known protein effectors in order to provide additional data for biomarker test development.[85,86] These studies contribute a number of additional candidate biomarkers to existing knowledge. Unfortunately, the data published in these studies do not specify if the proteins identified are increased or decreased in abundance, and there is no validation of quantitative MS results, nor does the study specify the prognostic ability of these proteins for UTO. This study therefore aimed to simultaneously derive both diagnostic and prognostic information in a kidney-specific panel of proteins from exosomes in urine. The proteins identified here are to provide additional markers to those previously described in urine following congenital UTO as well as some backing to the data obtained in the Mesrobian study. Researchers are encouraged to use the data provided in this study to build a list of candidate biomarkers for clinical testing. Protein markers for metabolite imbalance, oxidative stress, tubule cell

damage, apoptosis, and fibrosis can be used in combination to develop effective tests for the progression of UTO in children.

Table 6.1: Summary of the physiological characteristics measured from each rat at 21 days post-surgery.

Parameter	Control	Partial	Complete
n	9	7	7
Surgery Weight (g)	80.8 ± 18.0	82.7 ± 18.6	83.7 ± 20.6
Day 21 Post Surge Weight (g)	171.1 ± 10.5	176.0 ± 5.2	172.3 ± 12.9
Urine Volume (mL)	14.2 ± 5.3	20.0 ± 12.8	14.3 ± 6.7
Right Kidney Weight (g)	0.83 ± 0.06	0.87 ± 0.11	1.22 ± 0.19 †
Right Kidney Volume (mm^3)	1126 ± 197	1260 ± 290	1733 ± 288 †
[a] Left Kidney Weight (g)	0.78 ± 0.08	0.87 ± 0.08	1.54 ± 1.27
[a] Left Kidney Volume (mm^3)	1162 ± 265	2054 ± 499 †	17318 ± 7722 †
Serum Creatinine (mg/dL)	1.04 ± 0.40	1.08 ± 0.38	1.22 ± 0.27
Urine Creatinine (mg/dL)	68.8 ± 20.3	62.8 ± 25.7	65.6 ± 19.6
Creatinine Clearance (mg/min/kg)	3.65 ± 1.04	4.37 ± 1.99	2.91 ± 0.85
Osmolality (mOsm/kg H_2O)	880 ± 247	925 ± 403	846 ± 325

[a] Obstructed kidney

† p-value < 0.05 compared to control

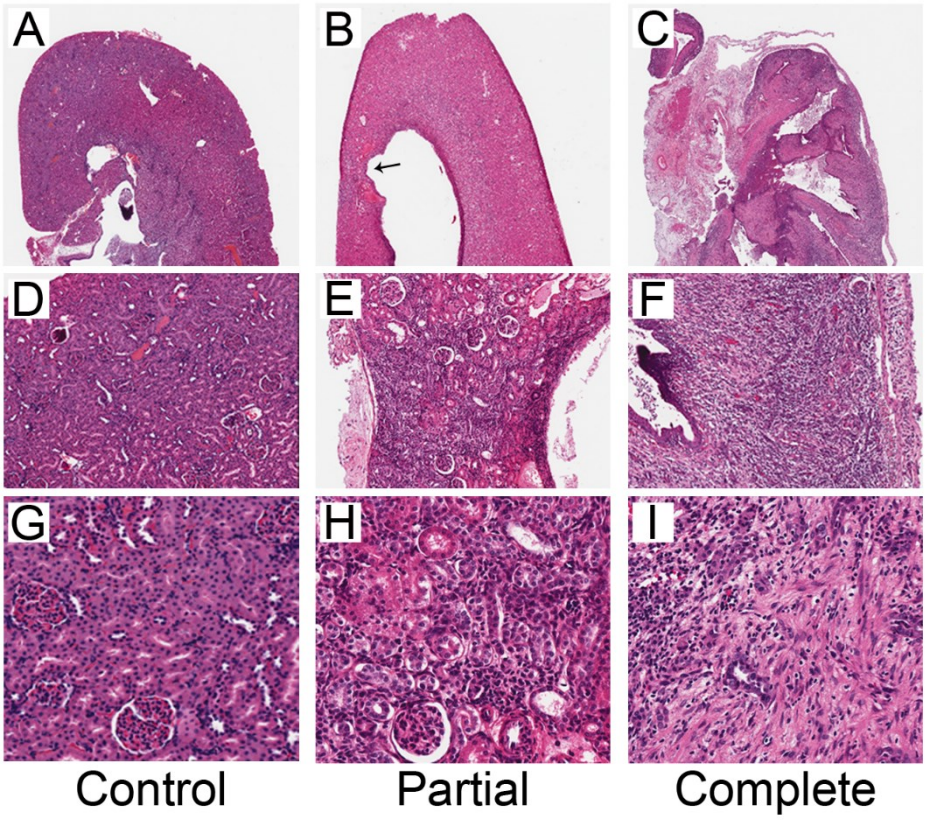

Figure 6.1: Representative photomicrographs of obstructed rat kidneys at 21 days post surgery.
Sham operated (A,D,G), mild (partial) obstruction (B,E,H), and severe (complete) obstruction (C,F,I). Low magnification (2X) analysis shows the morphological changes occurring as a result of increasing severity of obstruction (A-C). Control (A) kidneys exhibit well defined cortical and medullary regions. Mild obstruction (B) has the effect of localized thinning of the parenchyma (arrowhead) and rounding of the calyces, although maintains the majority of normal structure. Severe obstruction (C) shows massive changes in renal structure, loss of parenchyma and ill-defined medullary and cortical regions. Higher power magnification (10X) allows visualization of normal (D) tubular and glomerular distribution throughout the cortex. Mild obstruction (E) leads to regional lymphocyte invasion, with mild tubular atrophy and loss of interstitial tissue. Severe (complete) obstruction (F) shows extensive tissue fibrosis and lymphocyte infiltration. High power (20X) magnification allows further evaluation of the effects of obstruction. Control kidneys show healthy interstitium with a large number of tubule cells. Partial obstruction (H) demonstrates a large amount of infiltration of lymphocytes with some tubular atrophy and some loss in interstitium, while complete (severe) obstruction shows extensive fibrosis and a complete loss of tubular cells.

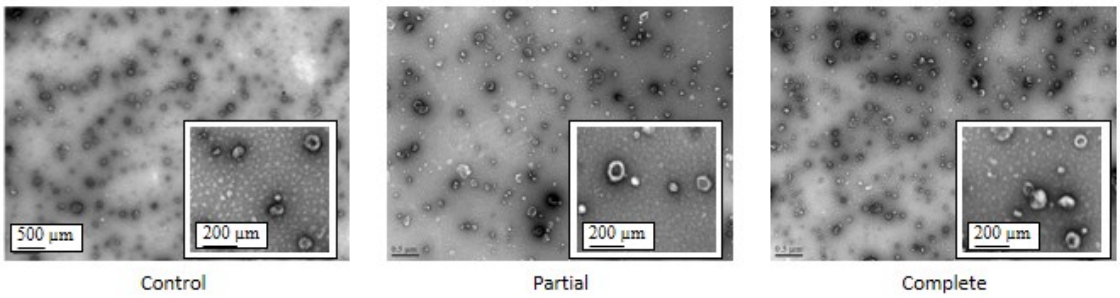

Figure 6.2: Electron microscopy confirmation of the presence of exosomes in each test group.
The 200,000 × *g* sucrose cushion was collected, washed, and directly analyzed by negative staining and electron microscopy.

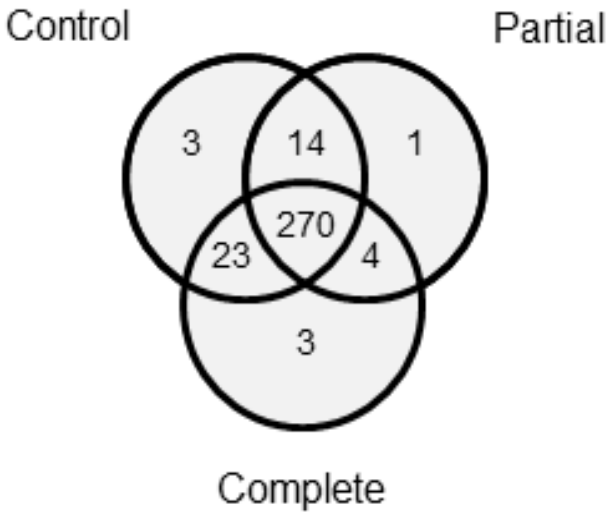

Figure 6.3: Venn diagram showing the number of proteins identified in each test group.
In total, 310 proteins were identified in control group exosomes, 289 proteins from the partially obstructed group and 300 from the completely obstructed group. The protein identities show an overlap of 270 proteins found in all test groups.

Table 6.2: A summary of the quantitative results of the exosomal proteomic analysis. Each test group is listed with their number of proteins idenfied in each biological replicate. The number of proteins noted to be significantly altered in each test group encompasses comparison to the other two groups.

Condition	Replicate	# Proteins ID'd	Nonredundant proteins	Proteins with significant change in abundance
Control	P1	290	310	170
	P2	289		
	P3	273		
Partial	P1	171	289	144
	P2	275		
	P3	160		
Complete	P1	239	300	124
	P2	288		
	P3	126		

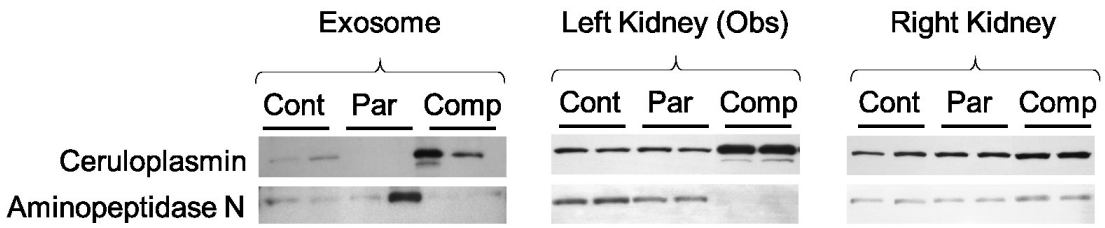

Figure 6.4: Western blot confirmation of spectral counting results.
Ceruloplasmin (CP), expressed in control rat urine, is decreased in abundance in the partially obstructed group, and increased in abundance in the completely obstructed group by LC-MS. This result is similarly seen in the kidney tissue. Similar to CP, aminopeptidase N (APN) is normally expressed in control urine, however is increased in abundance in partially obstructed rats and decreased in abundance in the completely obstructed group.

Table 6.3: A number of proteins with altered abundance in this study and their association with known kidney diseases.
*Indicates the protein was present in the Mesrobian *et al.* LC-MS study.[86]

Protein Accession	Protein Description	Disease	Comments	In Exocarta?	Ref.
P10111*	Cyclophilin A	UTO	Initiates fibrogenesis in UUO	Yes	290
O70244*	Cubilin	AKI/ Ischemia	Protein reuptake in the proximal tubule	Yes	291
Q9JI92	Syntenin-1	Ischemia	Regulates exosome formation	Yes	292,293
M0RAK7*	EGF	UTO	Regulates renal maturation	Yes	144,184,185
Q5I0E1*	Leucine-rich α-2-glycoprotein 1	IgAN, UTO	Up-regulated in kidney transplant	Yes	294
P12346	Serotransferrin	UTO	Decreased in urine in BUO	No	295
P17475*	α-1-antitrypsin	AKI/ IgAN	Candidate biomarker in IgAN	Yes	6,296
P15684	Aminopeptidase N	AKI/ IgAN	Candidate biomarker in IgAN	Yes	6,283
G3V7K3	Ceruloplasmin	AKI/ IgAN	Candidate biomarker in IgAN	Yes	6,294
F1M7X5*	Dipeptidyl peptidase 4	DN/ CKD	Marker of tubule dysfunction	Yes	283
D3ZZ76	Uroplakin	VUR	VUR as a gene mutation	Yes	297
P70490	Lactadherin	Prostate cancer	Candidate biomarker for prostate cancer	Yes	125
Q4KLZ0	Vannin-1	AKI/ DN	Candidate biomarker for DN	No	298,299
P62963*	Profilin-1	UTO	Overexpressed in renal carcinoma	Yes	300
P08289*	Alkaline phosphatase	UTO	Marker of renal damage	Yes	301,302
O88989*	Malate dehydrogenase	UTO	Metabolic protein with altered abundance in UTO	Yes	303
G3V8H1*	Kallikrein-1	UTO	RAS associated vasodilator	Yes	149,304
P01048*	T-kininogen 1	Type 1 Diabetes	Candidate biomarker of renal decline in type 1 diabetes	Yes?	305
O70247	Solute carrier family 5 member 6	BUO	One of many, leads to concentration defect	Yes	306,307
Q9Z0M0/ P27274	CD55/CD59	PCKD	Membrane glycoproteins	No/Yes	308
P50123*	Glutamyl aminopeptidase	Renal dysfunction	Predictive of renal damage	Yes	309
Q64240*	α-1 microglobulin	Transplant	Increased kidney graft rejection	Yes	310
P07314*	Γ-glutamyl transpeptidase 1	Ox. Stress	Marker of oxidative stress	Yes	311
P07861	Neprilysin	BUO	Regulates water channels	No	312
P19468	Glutamate cysteine ligase	TIN/ CKD	Nrf2 regulated protein	No	313
Q64230	Meprin A subunit α	UUO/ KD	Down-regulated in UUO	No	281
G3V9W9	Protein Fat1	DN	Candidate biomarker of DN	Yes	314
Q99MA2	Aminopeptidase P	UUO	Peptidase affecting NO levels	Yes	315
P06866	Haptoglobin	UTO/ others	Associated with renal damage	Yes	303,310,316

Chapter 7: Discussion

7.1. Thesis Summary

Biomarker discovery through proteome analysis is a rapidly expanding field, with emerging methodologies and advanced instrumentation helping improve our ability to analyze complex biological samples. Learning from early setbacks in failed biomarker discovery experiments has led to a better understanding of the intricacies of analyzing such complex datasets.[15,48] Furthermore, as our understanding of protein interactions expands, so does our ability to comprehend complex changes in the proteome resulting from disease.[317,318] Chapter 1 of this thesis outlined some of the challenges in proteomic analyses as well as some methods commonly employed in biomarker discovery experimentation. Introduction of these topics highlighted the innate difficulties in MS-based biomarker discovery workflows. Chapter 1 also introduced congenital urinary tract obstruction (UTO) as an interesting case for biomarker discovery, as it occurs in the pediatric population and current management strategies may be insufficient for prevention of renal functional loss. A brief review of the pathological processes and current management strategies were therefore discussed in Chapter 1.

The LC-MS experimental workflow is compiled of a number of components which are littered with examples of error-prone or variable methods which represent potential sources of error.[48] Following sample isolation, the first step towards proteome analysis requires estimation of protein concentration. The importance of this stage of proteome analyses is commonly overlooked, and the methods used are not normally assessed for accuracy and precision prior to experimentation. Unfortunately, this can be

problematic when accurate estimation of concentration is important for quantitative proteomic studies. Additionally, pertaining to biomarker discovery experiments with low sample concentration and abundance such as exosomes, sacrificing 1-5 μg of protein for estimation of the protein concentration can be a significant portion of the total sample. Chapter 3 therefore presented researchers with a tool to accurately quantify, purify, and recovery protein samples. Common buffer additives such as urea and salts could interfere with subsequent digestion or intact LC-MS analyses, making this method applicable for both top down and bottom up experimentation. This method was not ultimately employed for proteome analyses in this thesis, as the protein level separation by SDS PAGE does not require precise protein concentration estimation. A good utilization of the method would be adaptation to intact (top down) proteome analyses, or proteome analysis of extremely low abundant exosomes from cell culture media. The method is amenable to intact proteome analyses, or removal of buffer contaminants which could affect downstream LC-MS analyses.

Throughput in NSI-based proteome analyses is a major limiting factor for biomarker discovery or extensive proteome characterization experiments.[239,242] Of particular relevance in this thesis, spectral counting for quantitative analysis is negatively affected by noisy data collection stemming from peptide ionization and detection.[50] Specialized statistical analysis methods help to compensate for the noisy data,[68,91] but the lack of technical replication presents a secondary challenge that cannot be addressed. No matter the method chosen for quantitative LC-MS analysis, replication will aid in data analysis, thus improved throughput is of great benefit. Chapter 4 presented a system that improves throughput in a simple, reliable, reproducible manner, without requiring any specialized software or difficult to obtain parts. Application to a simplistic model

proteome of *E. coli* demonstrated the effect of improved throughput over a typical proteome analysis. It should be noted that this system was employed for all subsequent proteome analyses conducted in this thesis.

Current understanding of pathogenesis in the *in vitro* model of UTO with proximal tubule cells has been limited to specific investigations of a number of physiological processes. Chapter 5 employed a more holistic evaluation of subcellular changes in protein abundance in order to develop a more well-rounded understanding of the pathogenesis leading to cell death in proximal tubule cells. A number of proteins and pathways were identified in the study that are well established in pathogenesis of UTO, confirming the efficacy of the model; however, also identified a number of novel effectors not previously shown. The shift in metabolic processes were the most notable, with activation of the polyol pathway (aldose reductase; AR) being the most intriguing. Activation of AR is an Nrf2-dependent response, a mediator of antioxidant response elements (ARE).[249]

Inhibitors of AR (ARI) can be extracted as natural products from a number of sources including spinach, cumin seeds, fennel seeds, basil leaves, lemon, black pepper, orange, curry leaves, and cinnamon.[319] Additionally, ARI have been shown to have anti-tumor, anti-fibrotic, and anti-apoptotic effects in a number of different diseases *via* a number of pathways.[320–322] The major role of AR during oxidative stress is detoxification of lipid peroxidation products, such as 4-hydroxy-2-nonenol (HNE). Interestingly, the presence of AR-mediated derivatives of HNE in urine have been proposed as biomarkers of oxidative stress in the kidney.[261] Additionally, because of the associated shift in metabolism away from normal beta oxidation of fatty acids to membrane recycling, it is hypothesized that lipid peroxidation could be a major effector in UTO.[323] Some

preliminary data have shown a similar increase in AR expression in obstructed kidneys, and suggested that treating stretched cells with ARI may reduce apoptosis and oxidative stress following stretch (Appendix Figure 1). The results found in this study therefore helped in understanding of the progression disease in UTO, as well as elucidated a potential treatment for children with UTO that may improve recovery post-surgery by limiting tubule cell apoptosis during pathogenesis.

Current methods for diagnosis and prognosis in UTO are undesirable, as described in detail in the Chapter 1. Better methods for diagnosis and prognosis are therefore required to improve quality of life and reduce the anxiety associated with the current approach for postnatal management of UTO. Exosomes in the urine were first described a decade ago,[119] and have since been suggested to express a number of proteins that could act as biomarkers and aide in postnatal management of a variety of urinary tract diseases.[118] Previous work using the CUO and PUO models of obstruction have aimed to primarily assess UTO pathogenesis or investigate the effects of treatment on recovery following relief.[150,183,264,324] Chapter 6 provided a study that applied the model towards identification of a number of candidate biomarker proteins of mild and severe UTO. A number of the proteins identified are corroborated by a recent study by Mesrobian *et al*.[86] Unfortunately, the Mesrobian study does not indicate which proteins were increased or decreased in the urine, and does not confirm the LC-MS results by any secondary means. The study presented in Chapter 6 therefore provides a useful addition to the existing literature with some confirmation in the form of western blotting and literature searching. A notable achievement in Chapter 6 is therefore the ability to use protein abundance as indicators of the severity of obstruction, an effect that has never been described in the literature for UTO. Specifically, the abundance of urinary enzymes appears to be

increased in PUO, and decreased in CUO, whereas acute phase proteins such as haptoglobin are unaffected in PUO and increased in CUO. Other proteins, such as ceruloplasmin and α-1-antitrypsin have been described in the literature to show similar abundance patterns (down in PUO, up in CUO) to that of other renal disorders. Thus the absence of these proteins, coupled with the increase in enzymes could be predictive of mild UTO, whereas the increase in haptoglobin, ceruloplasmin, and α-1-antitrypsin could be indicative of severe obstruction. This study therefore provides evidence for a number of candidate biomarkers that potentially have applicability in the clinic.

7.2. Future directions

The future directions of the work presented here include validation of the biomarker data on clinically-relevant samples or other, higher throughput models of obstruction. Additionally, further evaluation of AR expression and inhibition could allow elucidation of a novel treatment strategy of UTO. Validation of the candidate biomarkers must be conducted to evaluate their clinical utility. It should be noted that there are many potentially important and novel findings in this thesis, thus other researchers are encouraged to use the lists of proteins identified to formulate testable hypotheses for further evaluation of disease progression in UTO.

It should be noted that the exosomal protein samples from Chapter 6 were pooled prior to LC-MS analysis, thus estimation of normal biological variability is lost. To assess the expected level of variation that could be expressed within each population, the obstruction experiment should be repeated on more rats, but employing targeted proteome analysis strategies. By drawing from the current study, targeted LC-MS experiments can be developed towards specific evaluation of the relative protein abundances found here.

Additionally, of interest is the association in protein abundance with pathophysiology of the rat. With a targeted analysis, quantitative proteomic data can be obtained at specific time points over the course of obstruction and sacrifice of animals followed by histopathological analyses could allow comparison of the protein abundance with disease severity. Also of interest would be to conduct a similar imaging experiment to the clinically-employed diuretic renography on the rats for a direct comparison of the efficacy of the current diagnostic method to that of the quantitative changes in protein abundance.

It should be noted that mouse models of obstruction[182] may be of better use for confirmation of the data found in this thesis. The rat model was employed to produce sufficient urine volume for exosomal protein isolation and subsequent proteome analysis. Now that the candidate list is generated, it could be a simple matter to use smaller volumes of urine from mice, with the added benefit of more biological replication for less cost. Additionally, a temporal evaluation (*i.e.* hours, days and weeks) of the changes in abundance of the candidate biomarkers could result in greater evaluation of the diagnostic potential of these proteins.

7.3. Conclusions

This thesis has provided researchers with a few tools that will assist in analyzing proteome samples for candidate biomarker, or simply to improve sensitivity and throughput for current experiments. In addition, a number of candidate biomarkers are identified and a more complete picture of pathogenesis of UTO are delineated. Together, these results will provide future researchers with the ability to develop sensitive and specific biomarker tests for UTO that may be used to improve the quality of life for children experiencing this disease.

BIBLIOGRAPHY

(1) Sheridan, C. Illumina Claims $1,000 Genome Win. *Nat. Biotechnol.* **2014**, *32*, 115–115.

(2) Shattuck-Eidens, D.; Oliphant, A.; McClure, M.; McBride, C.; Gupte, J.; Rubano, T.; Pruss, D.; Tavtigian, S.V.; Teng, D.H.; Adey, N.; Staebell, M.; Gumpper, K.; Lundstrom, R.; Hulick, M.; Kelly, M.; Holmen, J.; Lingenfelter, B.; Manley, S.; Fujimura, F.; Luce, M.; Ward, B.; Cannon-Albright, L.; Steele, L.; Offit, K.; Thomas, A. BRCA1 Sequence Analysis in Women at High Risk for Susceptibility Mutations. Risk Factor Analysis and Implications for Genetic Testing. *JAMA* **1997**, *278*, 1242–1250.

(3) McDonald, W.H.; Yates, J.R. Shotgun Proteomics and Biomarker Discovery. *Dis. Markers* **2002**, *18*, 99–105.

(4) Buhimschi, I.A.; Zambrano, E.; Pettker, C.M.; Bahtiyar, M.O.; Paidas, M.; Rosenberg, V.A.; Thung, S.; Salafia, C.M.; Buhimschi, C.S. Using Proteomic Analysis of the Human Amniotic Fluid to Identify Histologic Chorioamnionitis. *Obstet. Gynecol.* **2008**, *111*, 403–412.

(5) Leung, F.; Diamandis, E.P.; Kulasingam, V. From Bench to Bedside: Discovery of Ovarian Cancer Biomarkers Using High-Throughput Technologies in the Past Decade. *Biomark. Med.* **2012**, *6*, 613–625.

(6) Moon, P.G.; Lee, J.E.; You, S.; Kim, T.K.; Cho, J.H.; Kim, I.S.; Kwon, T.H.; Kim, C.D.; Park, S.H.; Hwang, D.; Kim, Y.L.; Baek, M.C. Proteomic Analysis of Urinary Exosomes from Patients of Early IgA Nephropathy and Thin Basement Membrane Nephropathy. *Proteomics* **2011**, *11*, 2459–2475.

(7) Hebert, A.S.; Richards, A.L.; Bailey, D.J.; Ulbrich, A.; Coughlin, E.E.; Westphall, M.S.; Coon, J.J. The One Hour Yeast Proteome. *Mol. Cell. Proteomics* **2014**, *13*, 339–347.

(8) Kentsis, A.; Monigatti, F.; Dorff, K.; Campagne, F.; Bachur, R.; Steen, H. Urine Proteomics for Profiling of Human Disease Using High Accuracy Mass Spectrometry. *Proteomics. Clin. Appl.* **2009**, *3*, 1052–1061.

(9) Belarmino, J.M.; Kogan, B.A. Management of Neonatal Hydronephrosis. *Early Hum. Dev.* **2006**, *82*, 9–14.

(10) Sinha, A.; Bagga, A.; Krishna, A.; Bajpai, M.; Srinivas, M.; Uppal, R.; Agarwal, I. Revised Guidelines on Management of Antenatal Hydronephrosis. *Indian J. Nephrol.* **2013**, *23*, 83–97.

(11) Yiee, J.; Wilcox, D. Management of Fetal Hydronephrosis. *Pediatr. Nephrol.* **2008**, *23*, 347–353.

(12) Srinivas, P.R.; Verma, M.; Zhao, Y.; Srivastava, S. Proteomics for Cancer Biomarker Discovery. *Clin. Chem.* **2002**, *48*, 1160–1169.

(13) Pang, J.X.; Ginanni, N.; Dongre, A.R.; Hefta, S.A.; Opiteck, G.J. Biomarker Discovery in Urine by Proteomics. *J. Proteome Res.* **2002**, *1*, 161 – 169.

(14) Rai, A.J.; Zhang, Z.; Rosenzweig, J.; Shih, I.M.; Pham, T.; Fung, E.T.; Sokoll, L.J.; Chan, D.W. Proteomic Approaches to Tumor Marker Discovery. *Arch. Pathol. Lab. Med.* **2002**, *126*, 1518–1526.

(15) Lim, M.D.; Dickherber, A.; Compton, C.C. Before You Analyze a Human Specimen, Think Quality, Variability, and Bias. *Anal. Chem.* **2011**, *83*, 8–13.

(16) Petricoin, E.F.I.; Ardekani, A.M.; Hitt, B.A.; Levine, P.J.; Fusaro, V.A.; Steinberg, S.M.; Mills, G.B.; Simone, C.; Fishman, D.A.; Kohn, E.C.; Liotta, L.A. Mechanisms of Disease Use of Proteomic Patterns in Serum to Identify Ovarian Cancer *Lancet* **2002**, *360*, 572–577.

(17) Petricoin, E.F.; Ornstein, D.K.; Paweletz, C.P.; Ardekani, A.; Hackett, P.S.; Hitt, B.A.; Velassco, A.; Trucco, C.; Wiegand, L.; Wood, K.; Simone, C. B.; Levine, P.J.; Linehan, W.M.; Emmert-Buck, M.R.; Steinberg, S.M.; Kohn, E.C.; Liotta, L.A. Serum Proteomic Patterns for Detection of Prostate Cancer. *J. Natl. Cancer Inst.* **2002**, *94*, 1576–1578.

(18) Wilkins, M.R.; Pasquali, C.; Appel, R.D.; Ou, K.; Golaz, O.; Sanchez, J.C.; Yan, J.X.; Gooley, A.A.; Hughes, G.; Humphery-Smith, I.; Williams, K.L.; Hochstrasser, D.F. From Proteins to Proteomes: Large Scale Protein Identification by Two-Dimensional Electrophoresis and Amino Acid Analysis. *Biotechnology (N. Y)* **1996**, *14*, 61–65.

(19) Eng, J.K.; McCormack, A.L.; Yates, J.R. An Approach to Correlate Tandem Mass Spectral Data of Peptides with Amino Acid Sequences in a Protein Database. *J. Am. Soc. Mass Spectrom.* **1994**, *5*, 976–989.

(20) DeSouza, L.V; Siu, K.W.M. Mass Spectrometry-Based Quantification. *Clin. Biochem.* **2013**, *46*, 421–431.

(21) Fenn, J.B.; Mann, M.; Meng, C.K.; Wong, S.F.; Craig, M.; Meng, C.K.A.I.; Mann, M.; Whitehouse, C.M. Electrospray Ionization of Large for Mass Spectrometry Biomolecules. **2013**, *246*, 64–71.

(22) Tanaka, K.; Waki, H.; Ido, Y.; Akita, S.; Yoshida, Y.; Yoshida, T.; Matsuo, T. Protein and Polymer Analyses up To *m/z* 100 000 by Laser Ionization Time-of-Flight Mass Spectrometry. *Rapid Commun. Mass Spectrom.* **1988**, *2*, 151–153.

(23) Pappin, D.J.; Hojrup, P.; Bleasby, A.J. Rapid Identification of Proteins by Peptide-Mass Fingerprinting. *Curr. Biol.* **1993**, *3*, 327–332.

(24) Chait, B.T.; Kent, S.B. Weighing Naked Proteins: Practical, High-Accuracy Mass Measurement of Peptides and Proteins. *Science* **1992**, *257*, 1885–1894.

(25) Aebersold, R.; Mann, M. Mass Spectrometry-Based Proteomics. *Nature* **2003**, *422*, 198–207.

(26) Wilm, M.; Mann, M. Analytical Properties of the Nanoelectrospray Ion Source. *Anal. Chem.* **1996**, *68*, 1–8.

(27) Righetti, P.G.; Castagna, A.; Antonioli, P.; Boschetti, E. Prefractionation Techniques in Proteome Analysis: The Mining Tools of the Third Millennium. *Electrophoresis* **2005**, *26*, 297–319.

(28) Ducret, A.; Van Oostveen, I.; Eng, J.K.; Yates, J.R.; Aebersold, R. High Throughput Protein Characterization by Automated Reverse-Phase Chromatography/electrospray Tandem Mass Spectrometry. *Protein Sci.* **1998**, *7*, 706–719.

(29) Beaudry, F.; Vachon, P. Electrospray Ionization Suppression, a Physical or a Chemical Phenomenon? *Biomed. Chromatogr.* **2006**, *20*, 200–205.

(30) Mallet, C.R.; Lu, Z.; Mazzeo, J.R. A Study of Ion Suppression Effects in Electrospray Ionization from Mobile Phase Additives and Solid-Phase Extracts. *Rapid Commun. Mass Spectrom.* **2004**, *18*, 49–58.

(31) Iavarone, A.T.; Udekwu, O.A.; Williams, E.R. Buffer Loading for Counteracting Metal Salt-Induced Signal Suppression in Electrospray Ionization. *Anal. Chem.* **2004**, *76*, 3944–3950.

(32) Gilar, M.; Bouvier, E.S.P.; Compton, B.J. Advances in Sample Preparation in Electromigration, Chromatographic and Mass Spectrometric Separation Methods. *J. Chromatogr. A* **2001**, *909*, 111–135.

(33) Botelho, D.; Wall, M.J.; Vieira, D.B.; Fitzsimmons, S.; Liu, F.; Doucette, A. Top-down and Bottom-up Proteomics of SDS-Containing Solutions Following Mass-Based Separation. *J. Proteome Res.* **2010**, *9*, 2863–2870.

(34) Crowell, A.M.J.; Wall, M.J.; Doucette, A.A. Maximizing Recovery of Water-Soluble Proteins through Acetone Precipitation. *Anal. Chim. Acta* **2013**, *796*, 48–54.

(35) Wang, N.; Xie, C.; Young, J.B.; Li, L. Off-Line Two-Dimensional Liquid Chromatography with Maximized Sample Loading to Reversed-Phase Liquid Chromatography-Electrospray Ionization Tandem Mass Spectrometry for Shotgun Proteome Analysis. *Anal. Chem.* **2009**, *81*, 1049–1060.

(36) Anderson, N.L. The Human Plasma Proteome: History, Character, and Diagnostic Prospects. *Mol. Cell. Proteomics* **2002**, *1*, 845–867.

(37) Adachi, J.; Kumar, C.; Zhang, Y.; Olsen, J.V; Mann, M. The Human Urinary Proteome Contains More than 1500 Proteins, Including a Large Proportion of Membrane Proteins. *Genome Biol.* **2006**, *7*, R80.

(38) O'Farrell, P.H. High Resolution Two-Dimensional Electrophoresis of Proteins. *J. Biol. Chem.* **1975**, *250*, 4007–4021.

(39) Shevchenko, A.; Tomas, H.; Havlis, J.; Olsen, J.V; Mann, M. In-Gel Digestion for Mass Spectrometric Characterization of Proteins and Proteomes. *Nat. Protoc.* **2006**, *1*, 2856–2860.

(40) Martosella, J.; Zolotarjova, N.; Liu, H.; Nicol, G.; Boyes, B. Reversed-Phase High-Performance Liquid Chromatographic Prefractionation of Immunodepleted Human Serum Proteins to Enhance Mass Spectrometry Identification of Lower-Abundant Proteins. *J. Protome Res.* **2005**, *4*, 1522-1537.

(41) Pieper, R.; Gatlin, C.L.; McGrath, A.M.; Makusky, A.J.; Mondal, M.; Seonarain, M.; Field, E.; Schatz, C.R.; Estock, M.A.; Ahmed, N.; Anderson, N. G.; Steiner, S. Characterization of the Human Urinary Proteome: A Method for High-Resolution Display of Urinary Proteins on Two-Dimensional Electrophoresis Gels with a Yield of Nearly 1400 Distinct Protein Spots. *Proteomics* **2004**, *4*, 1159–1174.

(42) Smith, M.P.W.; Wood, S.L.; Zougman, A.; Ho, J.T.C.; Peng, J.; Jackson, D.; Cairns, D.A.; Lewington, A.J.P.; Selby, P.J.; Banks, R.E. A Systematic Analysis of the Effects of Increasing Degrees of Serum Immunodepletion in Terms of Depth of Coverage and Other Key Aspects in Top-down and Bottom-up Proteomic Analyses. *Proteomics* **2011**, *11*, 2222–2235.

(43) Washburn, M.P.; Wolters, D.; Yates, J.R. Large-Scale Analysis of the Yeast Proteome by Multidimensional Protein Identification Technology. *Nat. Biotechnol.* **2001**, *19*, 242–247.

(44) Chen, E.I.; Hewel, J.; Felding-Habermann, B.; Yates, J. Large Scale Protein Profiling by Combination of Protein Fractionation and Multidimensional Protein Identification Technology (MudPIT). *Mol. Cell. Proteomics* **2006**, *5*, 53–56.

(45) Shevchenko, A.; Wilm, M.; Vorm, O.; Mann, M. Mass Spectrometric Sequencing of Proteins Silver-Stained Polyacrylamide Gels. *Anal. Chem.* **1996**, *68*, 850–858.

(46) Atanassov, I.; Urlaub, H. Increased Proteome Coverage by Combining PAGE and Peptide Isoelectric Focusing : Comparative Study of Gel-Based Separation Approaches. *Proteomics* **2013**, 2947–2955.

(47) Boichenko, A.P.; Govorukhina, N.; van der Zee, A.G.J.; Bischoff, R. Multidimensional Separation of Tryptic Peptides from Human Serum Proteins Using Reversed-Phase, Strong Cation Exchange, Weak Anion Exchange, and Fused-Core Fluorinated Stationary Phases. *J. Sep. Sci.* **2013**, *36*, 3463–3470.

(48) Cairns, D.A. Statistical Issues in Quality Control of Proteomic Analyses: Good Experimental Design and Planning. *Proteomics* **2011**, *11*, 1037–1048.

(49) Hunt, D.F.; Yates, J.R.; Shabanowitz, J.; Winston, S.; Hauer, C.R. Protein Sequencing by Tandem Mass Spectrometry. *Proc. Natl. Acad. Sci.* **1986**, *83*, 6233–6237.

(50) Lundgren, D.H.; Hwang, S.I.; Wu, L.; Han, D.K. Role of Spectral Counting in Quantitative Proteomics. *Expert Rev. Proteomics* **2010**, *7*, 39–53.

(51) Peng, J.; Elias, J.E.; Thoreen, C.C.; Licklider, L. J; Gygi, S.P. Evaluation of Multidimensional Chromatography Coupled with Tandem Mass Spectrometry (LC/LC-MS/MS) for Large-Scale Protein Analysis: The Yeast Proteome. *J. Proteome Res. 2*, 43–50.

(52) Weatherly, D.B.; Atwood, J.A.; Minning, T.A.; Cavola, C.; Tarleton, R.L.; Orlando, R.A Heuristic Method for Assigning a False-Discovery Rate for Protein Identifications from Mascot Database Search Results. *Mol. Cell. Proteomics* **2005**, *4*, 762–772.

(53) Elias, J.E.; Gygi, S.P. Target-Decoy Search Strategy for Increased Confidence in Large-Scale Protein Identifications by Mass Spectrometry. *Nat. Methods* **2007**, *4*, 207–214.

(54) Keller, A.; Nesvizhskii, A.I.; Kolker, E.; Aebersold, R. Empirical Statistical Model to Estimate the Accuracy of Peptide Identifications Made by MS/MS and Database Search. *Anal. Chem.* **2002**, *74*, 5383–5392.

(55) Vaudel, M.; Sickmann, A.; Martens, L. Peptide and Protein Quantification: A Map of the Minefield. *Proteomics* **2010**, *10*, 650–670.

(56) Gygi, S.P.; Rist, B.; Gerber, S.A.; Turecek, F.; Gelb, M.H.; Aebersold, R. Quantitative Analysis of Complex Protein Mixtures Using Isotope-Coded Affinity Tags. *Nat. Biotechnol.* **1999**, *17*, 994–999.

(57) Melanson, J.E.; Avery, S.L.; Pinto, D.M. High-Coverage Quantitative Proteomics Using Amine-Specific Isotopic Labeling. *Proteomics* **2006**, *6*, 4466–4474.

(58) Ong, S.E. Stable Isotope Labeling by Amino Acids in Cell Culture, SILAC, as a Simple and Accurate Approach to Expression Proteomics. *Mol. Cell. Proteomics* **2002**, *1*, 376–386.

(59) Wiese, S.; Reidegeld, K.A.; Meyer, H.E.; Warscheid, B. Protein Labeling by iTRAQ: A New Tool for Quantitative Mass Spectrometry in Proteome Research. *Proteomics* **2007**, *7*, 340–350.

(60) Stewart, I.I.; Thomson, T.; Figeys, D. ^{18}O Labeling: A Tool for Proteomics. *Rapid Commun. Mass Spectrom.* **2001**, *15*, 2456–2465.

(61) Ji, C.; Guo, N.; Li, L. Differential Dimethyl Labeling of N-Termini of Peptides after Guanidination for Proteome Analysis Research Articles. *J. Proteome Res.* **2005**, 2099– 2108.

(62) Cagney, G.; Emili, A. De Novo Peptide Sequencing and Quantitative Profiling of Complex Protein Mixtures Using Mass-Coded Abundance Tagging. *Nat. Biotechnol.* **2002**, *20*, 163–170.

(63) Rauniyar, N.; McClatchy, D.B.; Yates, J.R. Stable Isotope Labeling of Mammals (SILAM) for in Vivo Quantitative Proteomic Analysis. *Methods* **2013**, *61*, 260–268.

(64) Melanson, J.E.; Chisholm, K.A.; Pinto, D. M. Targeted Comparative Proteomics by Liquid Chromatography/matrix-Assisted Laser Desorption/ionization Triple-Quadrupole Mass Spectrometry. *Rapid Commun. Mass Spectrom.* **2006**, *20*, 904–910.

(65) DeSouza, L.V; Romaschin, A.D.; Colgan, T.J.; Siu, K.W.M. Absolute Quantification of Potential Cancer Markers in Clinical Tissue Homogenates Using Multiple Reaction Monitoring on a Hybrid Triple Quadrupole/linear Ion Trap Tandem Mass Spectrometer. *Anal. Chem.* **2009**, *81*, 3462–3470.

(66) Anderson, N.L.; Anderson, N.G.; Haines, L.R.; Hardie, D.B.; Olafson, R.W.; Pearson, T.W. Mass Spectrometric Quantitation of Peptides and Proteins Using Stable Isotope Standards and Capture by Anti-Peptide Antibodies (SISCAPA). *J. Proteome Res.* **2004**, 235–244.

(67) Liu, H.; Sadygov, R.G.; Yates, J.R. A Model for Random Sampling and Estimation of Relative Protein Abundance in Shotgun Proteomics. *Anal. Chem.* **2004**, *76*, 4193–4201.

(68) Li, M.; Gray, W.; Zhang, H.; Chung, C.H.; Billheimer, D.; Yarbrough, W.G.; Liebler, D.C.; Shyr, Y.; Slebos, R.J.C. Comparative Shotgun Proteomics Using Spectral Count Data and Quasi-Likelihood Modeling. *J. Proteome Res.* **2010**, *9*, 4295–4305.

(69) Old, W.M.; Meyer-Arendt, K.; Aveline-Wolf, L.; Pierce, K.G.; Mendoza, A.; Sevinsky, J.R.; Resing, K.A.; Ahn, N.G. Comparison of Label-Free Methods for Quantifying Human Proteins by Shotgun Proteomics. *Mol. Cell. Proteomics* **2005**, *4*, 1487–1502.

(70) Reddy, M.M.; Wilson, R.; Wilson, J.; Connell, S.; Gocke, A.; Hynan, L.; German, D.; Kodadek, T. Identification of Candidate IgG Biomarkers for Alzheimer's Disease via Combinatorial Library Screening. *Cell* **2011**, *144*, 132–142.

(71) Pepe, M.S.; Feng, Z. Improving Biomarker Identification with Better Designs and Reporting. *Clin. Chem.* **2011**, *57*, 1093–1095.

(72) Hu, J.; Coombes, K.R.; Morris, J.S.; Baggerly, K.A. The Importance of Experimental Design in Proteomic Mass Spectrometry Experiments: Some Cautionary Tales. *Brief. Funct. Genomic. Proteomic.* **2005**, *3*, 322–331.

(73) Banks, R.E.; Stanley, A.J.; Cairns, D.A.; Barrett, J.H.; Clarke, P.; Thompson, D.; Selby, P.J. Influences of Blood Sample Processing on Low-Molecular-Weight Proteome Identified by Surface-Enhanced Laser Desorption/ionization Mass Spectrometry. *Clin. Chem.* **2005**, *51*, 1637–1649.

(74) Leitch, M.C.; Mitra, I.; Sadygov, R.G. Generalized Linear and Mixed Models for Label-Free Shotgun Proteomics. *Stat. Interface* **2012**, *5*, 89–98.

(75) Johnstone, I.M.; Titterington, D.M. Statistical Challenges of High-Dimensional Data. *Philos. Trans. A. Math. Phys. Eng. Sci.* **2009**, *367*, 4237–4253.

(76) Clarke, R.; Ressom, H.W.; Wang, A.; Xuan, J.; Liu, M.C.; Gehan, E.A.; Wang, Y. The Properties of High-Dimensional Data Spaces: Implications for Exploring Gene and Protein Expression Data. *Nat. Rev. Cancer* **2008**, *8*, 37–49.

(77) Adam, B.; Qu, Y.; Davis, J.W.; Ward, M.D.; Clements, M.A.; Cazares, L.H.; Semmes, O.J.; Schellhammer, P.F.; Yasui, Y.; Feng, Z.; Wright, G.L. Serum Protein Fingerprinting Coupled with a Pattern-Matching Algorithm Distinguishes Prostate Cancer from Benign Prostate Hyperplasia and Healthy Men. *Cancer Res.* **2002**, *62*, 3609–3614.

(78) McLerran, D.; Grizzle, W.E.; Feng, Z.; Bigbee, W.L.; Banez, L.L.; Cazares, L.H.; Chan, D.W.; Diaz, J.; Izbicka, E.; Kagan, J.; Malehorn, D.E.; Malik, G.; Oelschlager, D.; Partin, A.; Randolph, T.; Rosenzweig, N.; Srivastava, S.; Srivastava, S.; Thompson, I.M.; Thornquist, M.; Troyer, D.; Yasui, Y.; Zhang, Z.; Zhu, L.; Semmes, O.J. Analytical Validation of Serum Proteomic Profiling for Diagnosis of Prostate Cancer: Sources of Sample Bias. *Clin. Chem.* **2008**, *54*, 44–52.

(79) McLerran, D.; Grizzle, W.E.; Feng, Z.; Thompson, I.M.; Bigbee, W.L.; Cazares, L.H.; Chan, D.W.; Dahlgren, J.; Diaz, J.; Kagan, J.; Lin, D.W.; Malik, G.; Oelschlager, D.; Partin, A.; Randolph, T.W.; Sokoll, L.; Srivastava, S.; Srivastava, S.; Thornquist, M.; Troyer, D.; Wright, G.L.; Zhang, Z.; Zhu, L.; Semmes, O.J. SELDI-TOF MS Whole Serum Proteomic Profiling with IMAC Surface Does Not Reliably Detect Prostate Cancer. *Clin. Chem.* **2008**, *54*, 53–60.

(80) Rundle, A.; Ahsan, H.; Vineis, P. Better Cancer Biomarker Discovery through Better Study Design. *Eur. J. Clin. Invest.* **2012**, *42*, 1350–1359.

(81) Orton, D.; Doucette, A. Proteomic Workflows for Biomarker Identification Using Mass Spectrometry — Technical and Statistical Considerations during Initial Discovery. *Proteomes* **2013**, *1*, 109–127.

(82) Rifai, N.; Gillette, M.A.; Carr, S.A. Protein Biomarker Discovery and Validation: The Long and Uncertain Path to Clinical Utility. *Nat. Biotechnol.* **2006**, *24*, 971–983.

(83) Ransohoff, D.F. Rules of Evidence for Cancer Molecular-Marker Discovery and Validation. *Nat. Rev. Cancer* **2004**, *4*, 309–314.

(84) Paulo, J.A.; Kadiyala, V.; Lee, L.S.; Banks, P.A.; Conwell, D.L.; Steen, H. Proteomic Analysis (GeLC-MS/MS) of ePFT-Collected Pancreatic Fluid in Chronic Pancreatitis. *J. Proteome Res.* **2012**, *11*, 1897–1912.

(85) Mesrobian, H.G.O.; Mitchell, M.E.; See, W.A.; Halligan, B.D.; Carlson, B.E.; Greene, A.S.; Wakim, B.T. Candidate Urinary Biomarker Discovery in Ureteropelvic Junction Obstruction: A Proteomic Approach. *J. Urol.* **2010**, *184*, 709–714.

(86) Mesrobian, H.G.O.; Kryger, J.V; Groth, T.W.; Fiscus, G.E.; Mirza, S.P. Urinary Proteome Analysis in Patients with Stable SFU Grade 4 Ureteropelvic Junction Obstruction Differs from Normal. *Urology* **2013**, *82*, 745.e1–10.

(87) Paulo, J.A.; Urrutia, R.; Banks, P.A.; Conwell, D.L.; Steen, H. Proteomic Analysis of an Immortalized Mouse Pancreatic Stellate Cell Line Identifies Differentially-Expressed Proteins in Activated vs Nonproliferating Cell States. *J. Proteome Res.* **2011**, *10*, 4835–4844.

(88) Raimondo, F.; Corbetta, S.; Morosi, L.; Chinello, C.; Gianazza, E.; Castoldi, G.; Di Gioia, C.; Bombardi, C.; Stella, A.; Battaglia, C.; Bianchi, C.; Magni, F.; Pitto, M. Urinary Exosomes and Diabetic Nephropathy: A Proteomic Approach. *Mol. Biosyst.* **2013**, *9*, 1139–1146.

(89) Mischak, H.; Ioannidis, J.P.A.; Argiles, A.; Attwood, T.K.; Bongcam-Rudloff, E.; Broenstrup, M.; Charonis, A.; Chrousos, G.P.; Delles, C.; Dominiczak, A.; Dylag, T.; Ehrich, J.; Egido, J.; Findeisen, P.; Jankowski, J.; Johnson, R.W.; Julien, B.A.; Lankisch, T.; Leung, H.Y.; Maahs, D.; Magni, F.; Manns, M.P.; Manolis, E.; Mayer, G.; Navis, G.; Novak, J.; Ortiz, A.; Persson, F.; Peter, K.; Riese, H.H.; Rossing, P.; Sattar, N.; Spasovski, G.; Thongboonkerd, V.; Vanholder, R.; Schanstra, J.P.; Vlahou, A. Implementation of Proteomic Biomarkers: Making It Work. *Eur. J. Clin. Invest.* **2012**, *42*, 1027–1036.

(90) Bellman, R. *Adaptive Control Processes—A Guided Tour*; Princeton University Press: Princeton, NJ, USA, 1961.

(91) Choi, H.; Fermin, D.; Nesvizhskii, A.I. Significance Analysis of Spectral Count Data in Label-Free Shotgun Proteomics. *Mol. Cell. Proteomics* **2008**, *7*, 2373–2385.

(92) Pavelka, N.; Pelizzola, M.; Vizzardelli, C.; Capozzoli, M.; Splendiani, A.; Granucci, F.; Ricciardi-Castagnoli, P. A Power Law Global Error Model for the Identification of Differentially Expressed Genes in Microarray Data. *BMC Bioinformatics* **2004**, *5*, 203.

(93) Suykens, J.A.K.; Vandewalle, J. Least Squares Support Vector Machine Classifiers. *Neural Process. Lett.* **1999**, *9*, 293–300.

(94) Atkinson, A.J.; Colburn, W.A.; DeGruttola, V.G.; DeMets, D.L.; Downing, G.J.; Hoth, D.F.; Oates, J.A.; Peck, C.C.; Schooley, R.T.; Spilker, B.A.; Woodcock, J.; Zeger, S.L. Biomarkers and Surrogate Endpoints: Preferred Definitions and Conceptual Framework. *Clin. Pharmacol. Ther.* **2001**, *69*, 89–95.

(95) Paik, S.; Shak, S.; Tang, G.; Kim, C.; Baker, J.; Cronin, M.; Baehner, F.L.; Walker, M.G.; Watson, D.; Park, T.; Hiller, W.; Fisher, E.R.; Wickerham, D.L.; Bryant, J.; Wolmark, N. A Multigene Assay to Predict Recurrence of Tamoxifen-Treated, Node-Negative Breast Cancer. *N. Engl. J. Med.* **2004**, *351*, 2817–2826.

(96) Bedard, P.L.; Mook, S.; Piccart-Gebhard, M.J.; Rutgers, E.T.; van't Veer, L.J.; Cardoso, F. MammaPrint 70-Gene Profile Quantifies the Likelihood of Recurrence for Early Breast Cancer. *Expert Opin. Med. Diagn.* **2009**, *3*, 193–205.

(97) Deng, M.C.; Eisen, H.J.; Mehra, M.R.; Billingham, M.; Marboe, C.C.; Berry, G.; Kobashigawa, J.; Johnson, F.L.; Starling, R.C.; Murali, S.; Pauly, D.F.; Baron, H.; Wohlgemuth, J.G.; Woodward, R.N.; Klingler, T.M.; Walther, D.; Lal, P.G.; Rosenberg, S.; Hunt, S. Noninvasive Discrimination of Rejection in Cardiac Allograft Recipients Using Gene Expression Profiling. *Am. J. Transplant* **2006**, *6*, 150–160.

(98) Ueland, F.R.; Desimone, C.P.; Seamon, L.G.; Miller, R.A.; Goodrich, S.; Podzielinski, I.; Sokoll, L.; Smith, A.; van Nagell, J.R.; Zhang, Z. Effectiveness of a Multivariate Index Assay in the Preoperative Assessment of Ovarian Tumors. *Obstet. Gynecol.* **2011**, *117*, 1289–1297.

(99) Ambroise, C.; McLachlan, G.J. Selection Bias in Gene Extraction on the Basis of Microarray Gene-Expression Data. *Proc. Natl. Acad. Sci. U. S. A.* **2002**, *99*, 6562–6566.

(100) Nguyen, H.T.; Bride, S.H.; Badawy, A.B.; Adam, R.M.; Lin, J.; Orsola, A.; Guthrie, P.D.; Freeman, M.R.; Peters, C.A. Heparin-Binding EGF-like Growth Factor Is up-Regulated in the Obstructed Kidney in a Cell- and Region-Specific Manner and Acts to Inhibit Apoptosis. *Am. J. Pathol.* **2000**, *156*, 889–898.

(101) Miyajima, A.; Chen, J.; Lawrence, C.; Ledbetter, S.; Soslow, R.A.; Stern, J.; Jha, S.; Pigato, J.; Lemer, M.L.; Poppas, D.P.; Vaughan, E.D.; Felsen, D. Antibody to Transforming Growth Factor-Beta Ameliorates Tubular Apoptosis in Unilateral Ureteral Obstruction. *Kidney Int.* **2000**, *58*, 2301–2313.

(102) Vincenti, D.C.; Murray, G.I. The Proteomics of Formalin-Fixed Wax-Embedded Tissue. *Clin. Biochem.* **2012**.

(103) Wiśniewski, J.R.; Duś, K.; Mann, M. Proteomic Workflow for Analysis of Archival Formalin Fixed and Paraffin Embedded Clinical Samples to a Depth of 10,000 Proteins. *Proteomics. Clin. Appl.* **2012**.

(104) Teng, P.; Bateman, N.W.; Hood, B.L.; Conrads, T.P. Advances in Proximal Fluid Proteomics for Disease Biomarker Discovery. *J. Proteome Res.* **2010**, *9*, 6091–6100.

(105) Traum, A.Z.; Wells, M.P.; Aivado, M.; Libermann, T.A.; Ramoni, M.F.; Schachter, A.D. SELDI-TOF MS of Quadruplicate Urine and Serum Samples to Evaluate Changes Related to Storage Conditions. *Proteomics* **2006**, *6*, 1676–1680.

(106) Drake, S.K.; Bowen, R.A.R.; Remaley, A.T.; Hortin, G.L. Potential Interferences from Blood Collection Tubes in Mass Spectrometric Analyses of Serum Polypeptides. *Clin. Chem.* **2004**, *50*, 2398–2401.

(107) Hsieh, S.Y.; Chen, R.K.; Pan, Y.H.; Lee, H.L. Systematical Evaluation of the Effects of Sample Collection Procedures on Low-Molecular-Weight Serum/plasma Proteome Profiling. *Proteomics* **2006**, *6*, 3189–3198.

(108) Thomas, C.E.; Sexton, W.; Benson, K.; Sutphen, R.; Koomen, J. Urine Collection and Processing for Protein Biomarker Discovery and Quantification. *Cancer Epidemiol. Biomarkers Prev.* **2010**, *19*, 953–959.

(109) Timms, J.F.; Arslan-Low, E.; Gentry-Maharaj, A.; Luo, Z.; T'Jampens, D.; Podust, V.N.; Ford, J.; Fung, E.T.; Gammerman, A.; Jacobs, I.; Menon, U. Preanalytic Influence of Sample Handling on SELDI-TOF Serum Protein Profiles. *Clin. Chem.* **2007**, *53*, 645–656.

(110) Griffin, T.J.; Bandhakavi, S. Dynamic Range Compression: A Solution for Proteomic Biomarker Discovery? *Bioanalysis* **2011**, *3*, 2053–2056.

(111) Rai, A.J.; Gelfand, C.A.; Haywood, B.C.; Warunek, D.J.; Yi, J.; Schuchard, M.D.; Mehigh, R.J.; Cockrill, S.L.; Scott, G.B.I.; Tammen, H.; Schulz-Knappe, P.; Speicher, D.W.; Vitzthum, F.; Haab, B.B.; Siest, G.; Chan, D.W. HUPO Plasma Proteome Project Specimen Collection and Handling: Towards the Standardization of Parameters for Plasma Proteome Samples. *Proteomics* **2005**, *5*, 3262–3277.

(112) Zhou, H.; Yuen, P.S.T.; Pisitkun, T.; Gonzales, P.A.; Yasuda, H.; Dear, J.W.; Gross, P.; Knepper, M.A.; Star, R.A. Collection, Storage, Preservation, and Normalization of Human Urinary Exosomes for Biomarker Discovery. *Kidney Int.* **2006**, *69*, 1471–1476.

(113) Harding, C.; Heuser, J.; Stahl, P. Receptor-Mediated Endocytosis of Transferrin and Recycling of the Transferrin Receptor in Rat Reticulocytes Biochemical Approaches to Transferrin. *J. Cell Biol.* **1983**, *97*, 329-339.

(114) Johnstone, R.M.; Adam, M.; Hammond, J.R.; Orr, L.; Turbide, C. Vesicle Formation during Reticulocyte Maturation. Association of Plasma Membrane Activities with Released Vesicles (exosomes). *J. Biol. Chem.* **1987**, *262*, 9412–9420.

(115) Camussi, G.; Deregibus, M.C.; Bruno, S.; Cantaluppi, V.; Biancone, L. Exosomes/microvesicles as a Mechanism of Cell-to-Cell Communication. *Kidney Int.* **2010**, *78*, 838–848.

(116) Zitvogel, L.; Regnault, A.; Lozier, A.; Wolfers, J.; Flament, C.; Tenza, D.; Ricciardi-Castagnoli, P.; Raposo, G.; Amigorena, S. Eradication of Established Murine Tumors Using a Novel Cell-Free Vaccine: Dendritic Cell-Derived Exosomes. *Nat. Med.* **1998**, *4*, 594–600.

(117) Anderson, H.C.; Mulhall, D.; Garimella, R. Role of Extracellular Membrane Vesicles in the Pathogenesis of Various Diseases, Including Cancer, Renal Diseases, Atherosclerosis, and Arthritis. *Lab. Invest.* **2010**, *90*, 1549–1557.

(118) Hoorn, E.J.; Pisitkun, T.; Zietse, R.; Gross, P.; Frokiaer, J.; Wang, N.S.; Gonzales, P.A.; Star, R.A.; Knepper, M.A. Prospects for Urinary Proteomics: Exosomes as a Source of Urinary Biomarkers. *Nephrology (Carlton).* **2005**, *10*, 283–290.

(119) Pisitkun, T.; Shen, R.F.; Knepper, M.A. Identification and Proteomic Profiling of Exosomes in Human Urine. *Proc. Natl. Acad. Sci. U. S. A.* **2004**, *101*, 13368–13373.

(120) Runz, S.; Keller, S.; Rupp, C.; Stoeck, A.; Issa, Y.; Koensgen, D.; Mustea, A.; Sehouli, J.; Kristiansen, G.; Altevogt, P. Malignant Ascites-Derived Exosomes of Ovarian Carcinoma Patients Contain CD24 and EpCAM. *Gynecol. Oncol.* **2007**, *107*, 563–571.

(121) Keller, S.; Rupp, C.; Stoeck, A.; Runz, S.; Fogel, M.; Lugert, S.; Hager, H.D.; Abdel-Bakky, M.S.; Gutwein, P.; Altevogt, P. CD24 Is a Marker of Exosomes Secreted into Urine and Amniotic Fluid. *Kidney Int.* **2007**, *72*, 1095–1102.

(122) Lässer, C.; Alikhani, V.S.; Ekström, K.; Eldh, M.; Paredes, P.T.; Bossios, A.; Sjöstrand, M.; Gabrielsson, S.; Lötvall, J.; Valadi, H. Human Saliva, Plasma and Breast Milk Exosomes Contain RNA: Uptake by Macrophages. *J. Transl. Med.* **2011**, *9*, 9.

(123) Knepper, M.A.; Pisitkun, T. Exosomes in Urine: Who Would Have Thought...? *Kidney Int.* **2007**, *72*, 1043–1045.

(124) Zhou, H.; Pisitkun, T.; Aponte, A.; Yuen, P.S.T.; Hoffert, J.D.; Yasuda, H.; Hu, X.; Chawla, L.; Shen, R.F.; Knepper, M.A.; Star, R.A. Exosomal Fetuin-A Identified by Proteomics: A Novel Urinary Biomarker for Detecting Acute Kidney Injury. *Kidney Int.* **2006**, *70*, 1847–1857.

(125) Duijvesz, D.; Burnum-Johnson, K.E.; Gritsenko, M.A.; Hoogland, M.A.; Vredenbregt-van den Berg, M. S.; Willemsen, R.; Luider, T.; Paša-Tolić, L.; Jenster, G. Proteomic Profiling of Exosomes Leads to the Identification of Novel Biomarkers for Prostate Cancer. *PLoS One* **2013**, *8*, e82589.

(126) Tan, P.H.; Chiang, G.S.; Tay, A.H. Pathology of Urinary Tract Malformations in a Paediatric Autopsy Series. *Ann. Acad. Med. Singapore* **1994**, *23*, 838–843.

(127) Mallik, M.; Watson, A.R. Antenatally Detected Urinary Tract Abnormalities: More Detection but Less Action. *Pediatr. Nephrol.* **2008**, *23*, 897–904.

(128) Fernbach, S.K.; Maizels, M.; Conway, J.J. Pediatric Radiology Ultrasound Grading of Hydronephrosis : Introduction to the System Used by the Society for Fetal Urology. *J. Pediatr. Surg.* **1993**, 478–480.

(129) Fernbach, S.K.; Maizels, M.; Conway, J.J. Ultrasound Grading of Hydronephrosis: Introduction to the System Used by the Society for Fetal Urology. *Pediatr. Radiol.* **1993**, *23*, 478–480.

(130) Nguyen, H.T.; Herndon, C.D.A.; Cooper, C.; Gatti, J.; Kirsch, A.; Kokorowski, P.; Lee, R.; Perez-Brayfield, M.; Metcalfe, P.; Yerkes, E.; Cendron, M.; Campbell, J.B. The Society for Fetal Urology Consensus Statement on the Evaluation and Management of Antenatal Hydronephrosis. *J. Pediatr. Urol.* **2010**, *6*, 212–231.

(131) Woodward, M.; Frank, D. Postnatal Management of Antenatal Hydronephrosis. *BJU Int.* **2002**, *89*, 149–156.

(132) Feldman, D.M.; DeCambre, M.; Kong, E.; Borgida, A.; Jamil, M.; McKenna, P.; Egan, J.F. Evaluation and Follow-up of Fetal Hydronephrosis. *J. Ultrasound Med.* **2001**, *20*, 1065–1069.

(133) Broadley, P.; McHugo, J.; Morgan, I.; Whittle, M.J.; Kilby, M.D. The 4 Year Outcome Following the Demonstration of Bilateral Renal Pelvic Dilatation on Pre-Natal Renal Ultrasound. *Br. J. Radiol.* **1999**, *72*, 265–270.

(134) Palmer, L.S.; Maizels, M.; Cartwright, P.C.; Fernbach, S.K.; Conway, J.J. Surgery versus Observation for Managing Obstructive Grade 3 to 4 Unilateral Hydronephrosis: A Report from the Society for Fetal Urology. *J. Urol.* **1998**, *159*, 222–228.

(135) Dhillon, H.K. Prenatally Diagnosed Hydronephrosis: The Great Ormond Street Experience. *Br. J. Urol.* **1998**, *81*, 39–44.

(136) Seikaly, M.G.; Ho, P.L.; Emmett, L.; Fine, R.N.; Tejani, A. Chronic Renal Insufficiency in Children: The 2001 Annual Report of the NAPRTCS. *Pediatr. Nephrol.* **2003**, *18*, 796–804.

(137) Smith, J.M.; Stablein, D.M.; Munoz, R.; Hebert, D.; McDonald, R.A. Contributions of the Transplant Registry: The 2006 Annual Report of the North American Pediatric Renal Trials and Collaborative Studies (NAPRTCS). *Pediatr. Transplant.* **2007**, *11*, 366–373.

(138) Schreiner, G.F.; Harris, K.P.; Purkerson, M.L.; Klahr, S. Immunological Aspects of Acute Ureteral Obstruction: Immune Cell Infiltrate in the Kidney. *Kidney Int.* **1988**, *34*, 487–493.

(139) Ruiz-Ortega, M.; Rupérez, M.; Esteban, V.; Rodríguez-Vita, J.; Sánchez-López, E.; Carvajal, G.; Egido, J. Angiotensin II: A Key Factor in the Inflammatory and Fibrotic Response in Kidney Diseases. *Nephrol. Dial. Transplant* **2006**, *21*, 16–20.

(140) Esteban, V. Angiotensin II, via AT1 and AT2 Receptors and NF- B Pathway, Regulates the Inflammatory Response in Unilateral Ureteral Obstruction. *J. Am. Soc. Nephrol.* **2004**, *15*, 1514–1529.

(141) Morrissey, J.J.; Klahr, S. Rapid Communication. Enalapril Decreases Nuclear Factor Kappa B Activation in the Kidney with Ureteral Obstruction. *Kidney Int.* **1997**, *52*, 926–933.

(142) Morrissey, J.; Klahr, S. Transcription Factor NF-kappaB Regulation of Renal Fibrosis during Ureteral Obstruction. *Semin. Nephrol.* **1998**, *18*, 603–611.

(143) Takeda, A.; Fukuzaki, A.; Kaneto, H.; Ishidoya, S.; Ogata, Y.; Sasaki, T.; Konda, R.; Sakai, K.; Orikasa, S. Role of Leukocyte Adhesion Molecules in Monocyte/ Macrophage Infiltration in Weanling Rats with Unilateral Ureteral Obstruction. *Int. J. Urol.* **2000**, *7*, 415–420.

(144) Grandaliano, G.; Gesualdo, L.; Bartoli, F.; Ranieri, E.; Monno, R.; Leggio, A.; Paradies, G.; Caldarulo, E.; Infante, B.; Schena, F.P. MCP-1 and EGF Renal Expression and Urine Excretion in Human Congenital Obstructive Nephropathy. *Kidney Int.* **2000**, *58*, 182–192.

(145) Wolf, G.; Ziyadeh, F.N.; Thaiss, F.; Tomaszewski, J.; Caron, R.J.; Wenzel, U.; Zahner, G.; Helmchen, U.; Stahl, R.A. Angiotensin II Stimulates Expression of the Chemokine RANTES in Rat Glomerular Endothelial Cells. Role of the Angiotensin Type 2 Receptor. *J. Clin. Invest.* **1997**, *100*, 1047–1058.

(146) Kaneto, H.;Morrissey, J.J.; Mccracken, R.; Ishidoya, S.; Reyes, A.; Klahr, S. The Expression of mRNA for Tumour Necrosis Factor alpha Increases in the Obstructed Kidney of Rats Soon after Unilateral Ureteral Ligation. *Nephrology* **1996**, 161–166.

(147) Miyajima, A.; Kosaka, T.; Seta, K.; Asano, T.; Umezawa, K.; Hayakawa, M. Novel Nuclear Factor Kappa B Activation Inhibitor Prevents Inflammatory Injury in Unilateral Ureteral Obstruction. *J. Urol.* **2003**, *169*, 1559–1563.

(148) Pimentel, J.L.; Sundell, C.L.; Wang, S.; Kopp, J.B.; Montero, A.; Martínez-Maldonado, M. Role of Angiotensin II in the Expression and Regulation of Transforming Growth Factor-Beta in Obstructive Nephropathy. *Kidney Int.* **1995**, *48*, 1233–1246.

(149) Chen, C.O.; Park, M.H.; Forbes, M.S.; Thornhill, B.A.; Kiley, S.C.; Yoo, K.H.; Chevalier, R.L. Angiotensin-Converting Enzyme Inhibition Aggravates Renal Interstitial Injury Resulting from Partial Unilateral Ureteral Obstruction in the Neonatal Rat. *Am. J. Physiol. Renal Physiol.* **2007**, *292*, F946–55.

(150) Chevalier, R.L.; Forbes, M.S.; Thornhill, B.A. Ureteral Obstruction as a Model of Renal Interstitial Fibrosis and Obstructive Nephropathy. *Kidney Int.* **2009**, *75*, 1145–1152.

(151) Sharma, K.A.; Mauer, S.M.; Kim, Y.; Michael, F.A. Interstitial Fibrosis in Obstructive Nephropathy. *Kidney Int.* **1993**, *44*, 774–788.

(152) Klahr, S.; Morrissey, J.; Ii, A.N.G. Obstructive Nephropathy and Renal Fibrosis. *Am. J. Physiol. Renal Physiol.* **2002**, *283*, F861-875.

(153) García-Sánchez, O.; López-Hernández, F.J.; López-Novoa, J.M. An Integrative View on the Role of TGF-Beta in the Progressive Tubular Deletion Associated with Chronic Kidney Disease. *Kidney Int.* **2010**, *77*, 950–955.

(154) Liu, Y. Epithelial to Mesenchymal Transition in Renal Fibrogenesis: Pathologic Significance, Molecular Mechanism, and Therapeutic Intervention. *J. Am. Soc. Nephrol.* **2004**, *15*, 1–12.

(155) Fern, R.J.; Yesko, C.M.; Thornhill, B.A.; Kim, H.S.; Smithies, O.; Chevalier, R.L. Reduced Angiotensinogen Expression Attenuates Renal Interstitial Fibrosis in Obstructive Nephropathy in Mice. *J. Clin. Invest.* **1999**, *103*, 39–46.

(156) Chiang, C.K.; Hsu, S.P.; Wu, C.T.; Huang, J.W.; Cheng, H.T.; Chang, Y.W.; Hung, K.Y.; Wu, K.D.; Liu, S.H. Endoplasmic Reticulum Stress Implicated in the Development of Renal Fibrosis. *Mol. Med.* **2011**.

(157) Tashiro, K.; Tamada, S.; Kuwabara, N.; Komiya, T.; Takekida, K.; Asai, T.; Iwao, H.; Sugimura, K.; Matsumura, Y.; Takaoka, M.; Nakatani, T.; Miura, K. Attenuation of Renal Fibrosis by Proteasome Inhibition in Rat Obstructive Nephropathy: Possible Role of Nuclear Factor kappa B. *Int. J. Mol. Med.* **2003**, *12*, 587–592.

(158) Ricardo, S.D.; Ding, G.; Eufemio, M.; Diamond, J.R.; Hershey, M.S. Antioxidant Expression in Experimental Hydronephrosis: Role of Mechanical Stretch and Growth Factors. *Am. J. Physiol.* **1997**, *272*, F789-798.

(159) Chevalier, R.L.; Chung, K.H.; Smith, C.D.; Ficenec, M.; Gomez, R.A. Renal Apoptosis and Clusterin Following Ureteral Obstruction: The Role of Maturation. *J. Urol.* **1996**, *156*, 1474–1479.

(160) Miyajima, A.; Chen, J.; Poppas, D.P.; Vaughan, E.D.; Felsen, D. Role of Nitric Oxide in Renal Tubular Apoptosis of Unilateral Ureteral Obstruction. *Kidney Int.* **2001**, *59*, 1290–1303.

(161) Power, R.E.; Doyle, B.T.; Higgins, D.; Brady, H.R.; Fitzpatrick, J.M.; Watson, R.W.G. Mechanical Deformation Induced Apoptosis in Human Proximal Renal Tubular Epithelial Cells Is Caspase Dependent. *J. Urol.* **2004**, *171*, 457–461.

(162) Chevalier, R.L.; Smith, C.D.; Wolstenholme, J.; Krajewski, S.; Reed, J.C. Chronic Ureteral Obstruction in the Rat Suppresses Renal Tubular Bcl-2 and Stimulates Apoptosis. *Exp. Nephrol.* **2000**, *8*, 115–122.

(163) Kennedy, W.A.; Stenberg, A.; Lackgren, G.; Hensle, T.W.; Sawczuk, I.S. Renal Tubular Apoptosis after Partial Ureteral Obstruction. *J. Urol.* **1994**, *152*, 658–664.

(164) Gobe, G.C.; Axelsen, R.A. Genesis of Renal Tubular Atrophy in Experimental Hydronephrosis in the Rat. Role of Apoptosis. *Lab. Invest.* **1987**, *56*, 273–281.

(165) Kiley, S.C.; Thornhill, B.A; Tang, S.S.; Ingelfinger, J.R.; Chevalier, R.L. Growth Factor-Mediated Phosphorylation of Proapoptotic BAD Reduces Tubule Cell Death *in vitro* and *in vivo*. *Kidney Int.* **2003**, *63*, 33–42.

(166) Bhaskaran, M.; Reddy, K.; Radhakrishanan, N.; Franki, N.; Ding, G.; Singhal, P.C. Angiotensin II Induces Apoptosis in Renal Proximal Tubular Cells. *Am. J. Physiol. Renal Physiol.* **2003**, *284*, F955–65.

(167) Yeh, C.; Chiang, H.; Lai, T.; Chien, C. Unilateral Ureteral Obstruction Evokes Renal Tubular Apoptosis via the Enhanced Oxidative Stress and Endoplasmic Reticulum Stress in the Rat. *Neurourol. Urodyn.* **2011**, *479*, 472–479.

(168) Groenendyk, J.; Michalak, M. Endoplasmic Reticulum Quality Control and Apoptosis. *Acta Biochim. Pol.* **2005**, *52*, 381–395.

(169) Kinter, M.; Wolstenholme, J.T.; Thornhill, B.A; Newton, E.A.; McCormick, M.L.; Chevalier, R.L. Unilateral Ureteral Obstruction Impairs Renal Antioxidant Enzyme Activation during Sodium Depletion. *Kidney Int.* **1999**, *55*, 1327–1334.

(170) Nguyen, H.T.; Hsieh, M.H.; Gaborro, A.; Tinloy, B.; Phillips, C.; Adam, R.M. JNK/SAPK and p38 SAPK-2 Mediate Mechanical Stretch-Induced Apoptosis via Caspase-3 and -9 in NRK-52E Renal Epithelial Cells. *Nephron. Exp. Nephrol.* **2006**, *102*, e49–61.

(171) Morrissey, J.J.; Ishidoya, S.; McCracken, R.; Klahr, S. Control of p53 and p21 (WAF1) Expression during Unilateral Ureteral Obstruction. *Kidney Int. Suppl.* **1996**, *57*, S84–92.

(172) Vallés, P.G.; Pascual, L.; Manucha, W.; Carrizo, L.; Rüttler, M. Role of Endogenous Nitric Oxide in Unilateral Ureteropelvic Junction Obstruction in Children. *Kidney Int.* **2003**, *63*, 1104–1115.

(173) Conway, J.J.; Maizels, M. The "Well Tempered" Diuretic Renogram: A Standard Method to Examine the Asymptomatic Neonate with Hydronephrosis or Hydroureteronephrosis. A Report from Combined Meetings of The Society for Fetal Urology and Members of The Pediatric Nuclear Medicine Council – The Society of Nuclear Medicine. *J. Nucl. Med.* **1992**, *33*, 2047–2051.

(174) Amarante, J.; Anderson, P.J.; Gordon, I. Impaired Drainage on Diuretic Renography Using Half-Time or Pelvic Excretion Efficiency Is Not a Sign of Obstruction in Children with a Prenatal Diagnosis of Unilateral Renal Pelvic Dilatation. *J. Urol.* **2003**, *169*, 1828–1831.

(175) Chevalier, R.L.; Peters, C.A. Congenital Urinary Tract Obstruction: Proceedings of the State-Of-The-Art Strategic Planning Workshop-National Institutes of Health, Bethesda, Maryland, USA, 11-12 March 2002. *Pediatr. Nephrol.* **2003**, *18*, 576–606.

(176) Harris, K.P.; Klahr, S.; Schreiner, G. Obstructive Nephropathy: From Mechanical Disturbance to Immune Activation? *Exp. Nephrol. 1*, 198–204.

(177) Radović, N.; Cuzić, S.; Knotek, M. Effect of Unilateral Ureteral Obstruction and Anti-Angiotensin II Treatment on Renal Tubule and Interstitial Cell Apoptosis in Rats. *Croat. Med. J.* **2008**, *49*, 600–607.

(178) Eskild-Jensen, A.; Frøkiaer, J.; Djurhuus, J. C.; Jørgensen, T. M.; Nyengaard, J. R. Reduced Number of Glomeruli in Kidneys with Neonatally Induced Partial Ureteropelvic Obstruction in Pigs. *J. Urol.* **2002**, *167*, 1435–1439.

(179) Ulm, A.H.; Miller, F. An Operation to Produce Experimental Reversible Hydronephrosis in Dogs. *J. Urol.* **1962**, *88*, 337–341.

(180) Gobet, R.; Park, J.M.; Nguyen, H.T.; Chang, B.; Cisek, L.J.; Peters, C.A. Renal Renin-Angiotensin System Dysregulation Caused by Partial Bladder Outlet Obstruction in Fetal Sheep. *Kidney Int.* **1999**, *56*, 1654–1661.

(181) Chevalier, R.L.; Peach, M.J. Hemodynamic Effects of Enalapril on Neonatal Chronic Partial Ureteral Obstruction. *Kidney Int.* **1985**, *28*, 891–898.

(182) Cachat, F.; Lange-Sperandio, B.; Chang, A.Y.; Kiley, S.C.; Thornhill, B.A.; Forbes, M.S.; Chevalier, R.L. Ureteral Obstruction in Neonatal Mice Elicits Segment-Specific Tubular Cell Responses Leading to Nephron Loss. *Kidney Int.* **2003**, *63*, 564–575.

(183) Thornhill, B.A.; Burt, L.E.; Chen, C.; Forbes, M.S.; Chevalier, R.L. Variable Chronic Partial Ureteral Obstruction in the Neonatal Rat: A New Model of Ureteropelvic Junction Obstruction. *Kidney Int.* **2005**, *67*, 42–52.

(184) Bartoli, F.; Penza, R.; Aceto, G.; Niglio, F.; D'Addato, O.; Pastore, V.; Campanella, V.; Magaldi, S.; Lasalandra, C.; Di Bitonto, G.; Gesualdo, L. Urinary Epidermal Growth Factor, Monocyte Chemotactic Protein-1, and β2-Microglobulin in Children with Ureteropelvic Junction Obstruction. *J. Pediatr. Surg.* **2011**, *46*, 530–536.

(185) Madsen, M.G.; Nørregaard, R.; Palmfeldt, J.; Olsen, L.H.; Frøkiær, J.; Jørgensen, T.M. Epidermal Growth Factor and Monocyte Chemotactic Peptide-1: Potential Biomarkers of Urinary Tract Obstruction in Children with Hydronephrosis. *J. Pediatr. Urol.* **2013**, *9*, 838–845.

(186) Kiley, S.C.; Thornhill, B.A.; Belyea, B.C.; Neale, K.; Forbes, M.S.; Luetteke, N.C.; Lee, D.C.; Chevalier, R.L. Epidermal Growth Factor Potentiates Renal Cell Death in Hydronephrotic Neonatal Mice, but Cell Survival in Rats. *Kidney Int.* **2005**, *68*, 504–514.

(187) Macdonald, M.S.; Emery, J.L. The Late Intrauterine and Postnatal Development of Human Renal Glomeruli. *J. Anat.* **1959**, *93*, 331–340.

(188) Merlet-Bénichou, C.; Gilbert, T.; Muffat-Joly, M.; Lelièvre-Pégorier, M.; Leroy, B. Intrauterine Growth Retardation Leads to a Permanent Nephron Deficit in the Rat. *Pediatr. Nephrol.* **1994**, *8*, 175–180.

(189) Josephson, S.; Robertson, B.; Claesson, G.; Wikstad, I. Experimental Obstructive Hydronephrosis in Newborn Rats. I. Surgical Technique and Long-Term Morphologic Effects. *Invest. Urol.* **1980**, *17*, 478–483.

(190) Diamond, J.R.; Kees-Folts, D.; Ding, G.; Frye, J.E.; Restrepo, N.C. Macrophages, Monocyte Chemoattractant Peptide-1, and TGF-Beta 1 in Experimental Hydronephrosis. *Am. J. Physiol.* **1994**, *266*, F926–33.

(191) Gawłowska-Marciniak, A.; Niedzielski, J.K. Evaluation of TGF-β1, CCL5/RANTES and sFas/Apo-1 Urine Concentration in Children with Ureteropelvic Junction Obstruction. *Arch. Med. Sci.* **2013**, *9*, 888–894.

(192) Madsen, M.G.; Nørregaard, R.; Stødkilde, L.; Christensen, J.H.; Jørgensen, T.M.; Frøkiær, J. Urine and Kidney Cytokine Profiles in Experimental Unilateral Acute and Chronic Hydronephrosis. *Scand. J. Urol. Nephrol.* **2012**, *46*, 91–96.

(193) Chevalier, R.L. Obstructive Nephropathy: Towards Biomarker Discovery and Gene Therapy. *Nat. Clin. Pract. Nephrol.* **2006**, *2*, 157–168.

(194) Furness, P.D.; Maizels, M.; Han, S.W.; Cohn, R.A.; Cheng, E.Y. Elevated Bladder Urine Concentration of Transforming Growth Factor-beta1 Correlates with Upper Urinary Tract Obstruction in Children. *J. Urol.* **1999**, *162*, 1033–1036.

(195) Madsen, M.G.; Nørregaard, R.; Palmfeldt, J.; Olsen, L.H.; Frøkiær, J.; Jørgensen, T.M. Urinary NGAL, Cystatin C, β2-Microglobulin, and Osteopontin Significance in Hydronephrotic Children. *Pediatr. Nephrol.* **2012**, *27*, 2099–2106.

(196) Kuwabara, T.; Mori, K.; Mukoyama, M.; Kasahara, M.; Yokoi, H.; Saito, Y.; Yoshioka, T.; Ogawa, Y.; Imamaki, H.; Kusakabe, T.; Ebihara, K.; Omata, M.; Satoh, N.; Sugawara, A.; Barasch, J.; Nakao, K. Urinary Neutrophil Gelatinase-Associated Lipocalin Levels Reflect Damage to Glomeruli, Proximal Tubules, and Distal Nephrons. *Kidney Int.* **2009**, *75*, 285–294.

(197) Yoo, K.H.; Thornhill, B.A.; Forbes, M.S.; Coleman, C.M.; Marcinko, E.S.; Liaw, L.; Chevalier, R.L. Osteopontin Regulates Renal Apoptosis and Interstitial Fibrosis in Neonatal Chronic Unilateral Ureteral Obstruction. *Kidney Int.* **2006**, *70*, 1735–1741.

(198) Schäffer, P.; Molnár, L.; Lukász, P.; Máttyus, I.; Verebély, T.; Szabó, A. Urinary Enzyme Excretion in Childhood Uropathy. *Orv. Hetil.* **2002**, *143*, 2135–2139.

(199) Decramer, S.; Wittke, S.; Mischak, H.; Zürbig, P.; Walden, M.; Bouissou, F.; Bascands, J.L.; Schanstra, J.P. Predicting the Clinical Outcome of Congenital Unilateral Ureteropelvic Junction Obstruction in Newborn by Urinary Proteome Analysis. *Nat. Med.* **2006**, *12*, 398–400.

(200) Laemmli, U.K. Cleavage of Structural Proteins during the Assembly of the Head of Bacteriophage T4. *Nature* **1970**, *227*, 680–685.

(201) Pace, C.N.; Vajdos, F.; Fee, L.; Grimsley, G.; Gray, T. How to Measure and Predict the Molar Absorption Coefficient of a Protein. *Protein Sci.* **1995**, *4*, 2411–2423.

(202) Kuipers, B.J.H.; Gruppen, H. Prediction of Molar Extinction Coefficients of Proteins and Peptides Using UV Absorption of the Constituent Amino Acids at 214 nm to Enable Quantitative Reverse Phase High-Performance Liquid Chromatography-Mass Spectrometry Analysis. *J. Agric. Food Chem.* **2007**, *55*, 5445–5451.

(203) Layne, E. *Methods Enzymol.* **1957,** *3*,447.

(204) Martosella, J.; Zolotarjova, N.; Liu, H.H.; Nicol, G.; Boyes, B.E.B. Reversed-Phase High-Performance Liquid Chromatographic Prefractionation of Immunodepleted Human Serum Proteins to Enhance Mass Spectrometry Identification of Lower-Abundant Proteins. *J. Proteome Res. 4*, 1522–1537.

(205) Lamparski, H.G.; Metha-Damani, A.; Yao, J.Y.; Patel, S.; Hsu, D.H.; Ruegg, C.; LePecq, J.B. Production and characterization of clinical grade exosomes derived from dendritic cells. *J. Immunol. Methods* **2002**, *270*, 211–26.

(206) Dong, M.Q.; Venable, J.D.; Au, N.; Xu, T.; Park, S.K.; Cociorva, D.; Johnson, J.R.; Dillin, A.; Yates, J.R. Quantitative Mass Spectrometry Identifies Insulin Signaling Targets in *C. Elegans*. *Science* **2007**, *317*, 660–663.

(207) Orton, D.J.; Doucette, A.A.; Maksym, G.N.; Maclellan, D.L. Proteomic Analysis of Rat Proximal Tubule Cells Following Stretch-Induced Apoptosis in an *in vitro* Model of Kidney Obstruction. *J. Proteomics* **2013**, 1–11.

(208) Huang, D.W.; Sherman, B.T.; Lempicki, R.A. Bioinformatics Enrichment Tools: Paths toward the Comprehensive Functional Analysis of Large Gene Lists. *Nucleic Acids Res.* **2009**, *37*, 1–13.

(209) Huang, D.W.; Sherman, B.T.; Lempicki, R.A. Systematic and Integrative Analysis of Large Gene Lists Using DAVID Bioinformatics Resources. *Nat. Protoc.* **2009**, *4*, 44–57.

(210) Xie, C.; Mao, X.; Huang, J.; Ding, Y.; Wu, J.; Dong, S.; Kong, L.; Gao, G.; Li, C.Y.; Wei, L. KOBAS 2.0: A Web Server for Annotation and Identification of Enriched Pathways and Diseases. *Nucleic Acids Res.* **2011**, *39*, W316–22.

(211) Gill, S.C.; von Hippel, P.H. Calculation of Protein Extinction Coefficients from Amino Acid Sequence Data. *Anal. Biochem.* **1989**, *182*, 319–326.

(212) Edelhoch, H. Spectroscopic Determination of Tryptophan and Tyrosine in Proteins. *Biochemistry* **1967**, *6*, 1948–1954.

(213) Murphy, J.B.; Kies, M.W. Note on Spectrophotometric Determination of Proteins in Dilute Solutions. *Biochim. Biophys. Acta* **1960**, *45*, 382–384.

(214) Smith, P.K.; Krohn, R.I.; Hermanson, G.T.; Mallia, A.K.; Gartner, F.H.; Provenzano, M.D.; Fujimoto, E.K.; Goeke, N.M.; Olson, B.J.; Klenk, D.C. Measurement of Protein Using Bicinchoninic Acid. *Anal. Biochem.* **1985**, *150*, 76–85.

(215) Bradford, M. A Rapid and Sensitive Method for the Quantitation of Microgram Quantities of Protein Utilizing the Principle of Protein-Dye Binding. *Anal. Biochem.* **1976**, *72*, 248–254.

(216) Lowry, O.H.; Rosenbrough, N.J.; Farr, A.L.; Randall, R.J. Protein Measurement with the Folin Phenol Reagent. *J. Biol. Chem.* **1951**, *193*, 265–275.

(217) Eberlein, G.A. Quantitation of Proteins Using HPLC-Detector Response rather than Standard Curve Comparison. *J. Pharm. Biomed. Anal.* **1995**, *13*, 1263–1271.

(218) Moffatt, F.; Senkans, P.; Ricketts, D. Approaches towards the Quantitative Analysis of Peptides and Proteins by Reversed-Phase High-Performance Liquid Chromatography in the Absence of a Pure Reference Sample. *J. Chromatogr. A* **2000**, *891*, 235–242.

(219) Engelhardt, H.; Müller, H. Optimal Conditions for the Reversed-Phase Chromatography of Proteins. *Chromatographia* **1984**, *19*, 77–84.

(220) Martosella, J.; Zolotarjova, N.; Liu, H.; Moyer, S.C.; Perkins, P.D.; Boyes, B.E. High Recovery HPLC Separation of Lipid Rafts for Membrane Proteome Analysis. *J. Proteome Res.* **2006**, *5*, 1301–1312.

(221) Speers, A.E.; Blackler, A.R.; Wu, C.C. Shotgun Analysis of Integral Membrane Proteins Facilitated by Elevated Temperature. *Anal. Chem.* **2007**, *79*, 4613–4620.

(222) Blackler, A.R.; Speers, A.E.; Wu, C.C. Chromatographic Benefits of Elevated Temperature for the Proteomic Analysis of Membrane Proteins. *Proteomics* **2008**, *8*, 3956–3964.

(223) Tran, J.V; Molander, P.; Greibrokk, T.; Lundanes, E. Temperature Effects on Retention in Reversed Phase Liquid Chromatography. *J. Sep. Sci.* **2001**, *24,* 930–940.

(224) Olsen, J.V.; de Godoy, L.M.F.; Li, G.; Macek, B.; Mortensen, P.; Pesch, R.; Makarov, A.; Lange, O.; Horning, S.; Mann, M. Parts per Million Mass Accuracy on an Orbitrap Mass Spectrometer via Lock Mass Injection into a C-Trap. *Mol. Cell. Proteomics* **2005**, *4*, 2010–2021.

(225) Gatlin, C.L.; Kleemann, G.R.; Hays, L.G.; Link, J.A.; Yates, J.R. Protein Identification at the Low Femtomole Level from Silver-Stained Gels Using a New Fritless Electrospray Interface for Liquid Chromatography-Microspray and Nanospray Mass Spectrometry. *Anal. Biochem.* **1998**, *263*, 93–101.

(226) Davis, M.T.; Stahl, D.C.; Hefta, S.A.; Lee, T.D. A Microscale Electrospray Interface for on-Line, Capillary Liquid Chromatography/tandem Mass Spectrometry of Complex Peptide Mixtures. *Anal. Chem.* **1995**, *67*, 4549–4556.

(227) De Godoy, L.M.F.; Olsen, J.V; Cox, J.; Nielsen, M.L.; Hubner, N.C.; Fröhlich, F.; Walther, T.C.; Mann, M. Comprehensive Mass-Spectrometry-Based Proteome Quantification of Haploid versus Diploid Yeast. *Nature* **2008**, *455*, 1251–1254.

(228) Noga, M.; Sucharski, F.; Suder, P.; Silberring, J. A Practical Guide to Nano-LC Troubleshooting. *J. Sep. Sci.* **2007**, *30*, 2179–2189.

(229) Orton, D.J.; Doucette, A.A. A Universal, High Recovery Assay for Protein Quantitation through Temperature Programmed Liquid Chromatography (TPLC). *J. Chromatogr. B. Analyt. Technol. Biomed. Life Sci.* **2013**, *921-922*, 75–80.

(230) Karsten, M.; Maio, G.; Steiner, F.; Franz, H.; Arnold, F.; Swart, R. Increasing Throughput in LC and LC-MS with a Parallel HPLC System LC Method. *Proceedings of the 57th annual PITTCON,* Orlando, FL. March 12, **2006**.

(231) Li, S.; Hao, Q.; Gounarides, J.; Wang, Y.K. Full Utilization of a Mass Spectrometer Using on-Demand Sharing with Multiple LC Units. *J. Mass Spectrom.* **2012**, *47*, 1074–1082.

(232) Ngo, B.; Svobodova, H.; Berg, A.; Valaskovic, G. Robust Dual-Column Nanospray Source for Improving Nano-LCMS Duty Cycle. *Proceedings of the 60th annual meeting of the American Society for Mass Spectrometry.* Vancouver, BC, May 20-24, **2012**.

(233) Korfmacher, W.A.; Veals, J.; Dunn-Meynell, K.; Zhang, X.; Tucker, G.; Cox, K.A.; Lin, C.C. Demonstration of the Capabilities of a Parallel High Performance Liquid Chromatography Tandem Mass Spectrometry System for Use in the Analysis of Drug Discovery Plasma Samples. *Rapid Commun. Mass Spectrom.* **1999**, *13*, 1991–1998.

(234) Zweigenbaum, J.; Heinig, K.; Steinborner, S.; Wachs, T.; Henion, J. High-Throughput Bioanalytical LC/MS/MS Determination of Benzodiazepines in Human Urine: 1000 Samples per 12 Hours. *Anal. Chem.* **1999**, *71*, 2294–2300.

(235) Roddy, T.P.; Horvath, C.R.; Stout, S.J.; Kenney, K.L.; Ho, P.I.; Zhang, J.H.; Vickers, C.; Kaushik, V.; Hubbard, B.; Wang, Y.K. Mass Spectrometric Techniques for Label-Free High-Throughput Screening in Drug Discovery. *Anal. Chem.* **2007**, *79*, 8207–8213.

(236) Waanders, L.F.; Almeida, R.; Prosser, S.; Cox, J.; Eikel, D.; Allen, M.H.; Schultz, G.A.; Mann, M. A Novel Chromatographic Method Allows on-Line Reanalysis of the Proteome. *Mol. Cell. Proteomics* **2008**, *7*, 1452–1459.

(237) Wu, J.T. The Development of a Staggered Parallel Separation Liquid Chromatography/tandem Mass Spectrometry System with on-Line Extraction for High-throughout Screening of Drug Candidates in Biological Fluids. *Rapid Commun. Mass Spectrom.* **2001**, *15*, 73–81.

(238) De Biasi V; Haskins, N.; Organ, A.; Bateman, R.; Giles, K.; Jarvis, S. High Throughput Liquid Chromatography/mass Spectrometric Analyses Using a Novel Multiplexed Electrospray Interface. *Rapid Commun. Mass Spectrom.* **1999**, *13*, 1165–1168.

(239) Shen, Y.; Tolić, N.; Zhao, R.; Pasa-Tolić, L.; Li, L.; Berger, S.J.; Harkewicz, R.; Anderson, G.A.; Belov, M.E.; Smith, R.D. High-Throughput Proteomics Using High-Efficiency Multiple-Capillary Liquid Chromatography with on-Line High-Performance ESI FTICR Mass Spectrometry. *Anal. Chem.* **2001**, *73*, 3011–3021.

(240) Belov, M.E.; Anderson, G.A.; Wingerd, M.A.; Udseth, H.R.; Tang, K.; Prior, D.C.; Swanson, K.R.; Buschbach, M.A.; Strittmatter, E.F.; Moore, R.J.; Smith, R.D. An Automated High Performance Capillary Liquid Chromatography-Fourier Transform Ion Cyclotron Resonance Mass Spectrometer for High-Throughput Proteomics. *J. Am. Soc. Mass Spectrom.* **2004**, *15*, 212–232.

(241) Livesay, E.A.; Tang, K.; Taylor, B.K.; Buschbach, M.A.; Hopkins, D.F.; LaMarche, B.L.; Zhao, R.; Shen, Y.; Orton, D.J.; Moore, R.J.; Kelly, R.T.; Udseth, H.R.; Smith, R.D. Fully Automated Four-Column Capillary LC-MS System for Maximizing Throughput in Proteomic Analyses. *Anal. Chem.* **2008**, *80*, 294–302.

(242) Bonneil, E.; Tessier, S.; Carrier, A.; Thibault, P. Multiplex Multidimensional nanoLC-MS System for Targeted Proteomic Analyses. *Electrophoresis* **2005**, *26*, 4575–4589.

(243) Wang, H.; Hanash, S.M. Increased Throughput and Reduced Carryover of Mass Spectrometry-Based Proteomics Using a High-Efficiency Nonsplit Nanoflow Parallel Dual-Column Capillary HPLC system. *J. Protome Res.* **2008**, *7*, 2743–2755.

(244) Tran, J.C.; Wall, M.J.; Doucette, A.A. Evaluation of a Solution Isoelectric Focusing Protocol as an Alternative to Ion Exchange Chromatography for Charge-Based Proteome Prefractionation. *J. Chromatogr. B. Analyt. Technol. Biomed. Life Sci.* **2009**, *877*, 807–813.

(245) Wang, N.; Li, L. Exploring the Precursor Ion Exclusion Feature of Liquid Chromatography-Electrospray Ionization Quadrupole Time-of-Flight Mass Spectrometry for Improving Protein Identification in Shotgun Proteome Analysis. *Anal. Chem.* **2008**, *80*, 4696–4710.

(246) Bendall, S.C.; Hughes, C.; Campbell, J.L.; Stewart, M.H.; Pittock, P.; Liu, S.; Bonneil, E.; Thibault, P.; Bhatia, M.; Lajoie, G.A. An Enhanced Mass Spectrometry Approach Reveals Human Embryonic Stem Cell Growth Factors in Culture. *Mol. Cell. Proteomics* **2009**, *8*, 421–432.

(247) Walsh, P.C.; Retik, A.B.; Vaughan, E.D.; Wein, A.J.; Campbell, M.F. *Campbell's Urology*; 8th Edition; Saunders, **2002**.

(248) Coplen, D.E. Hydronephrosis: Prenatal and Postnatal. *Current Clinical Urology; Pediatric Urology*; Humana Press, **2011**.

(249) Kawada, N.; Moriyama, T.; Ando, A.; Fukunaga, M.; Miyata, T.; Kurokawa, K.; Imai, E.; Hori, M. Increased Oxidative Stress in Mouse Kidneys with Unilateral Ureteral Obstruction. *Kidney Int.* **1999**, *56*, 1004–1013.

(250) Haugen, E.; Nath, K.A. The Involvement of Oxidative Stress in the Progression of Renal Injury. *Blood Purif.* **1999**, *17*, 58–65.

(251) Tannenbaum, J.; Purkerson, M.L.; Klahr, S. Effect of Unilateral Ureteral Obstruction on Metabolism of Renal Lipids in the Rat. *Am. J. Physiol.* **1983**, *245*, F254-262.

(252) Krarup, P.M.; Stolle, L.B.; Rawashdeh, Y.F.; Skott, O.; Djurhuus, J.C.; Froekiaer, J. Regional Changes in Renal Cortical Glucose, Lactate and Urea during Acute Unilateral Ureteral Obstruction. *Scand. J. Urol. Nephrol.* **2007**, *41*, 47–53.

(253) Fukata, M.; Kaibuchi, K. Rho-Family GTPases in Cadherin-Mediated Cell-Cell Adhesion. *Nat. Rev. Mol. Cell Biol.* **2001**, *2*, 887–897.

(254) Vermes, I.; Haanen, C.; Steffens-Nakken, H.; Reutelingsperger, C. A Novel Assay for Apoptosis. Flow Cytometric Detection of Phosphatidylserine Expression on Early Apoptotic Cells Using Fluorescein Labelled Annexin V. *J. Immunol. Methods* **1995**, *184*, 39–51.

(255) Gerke, V.; Moss, S.E. Annexins: From Structure to Function. *Physiol. Rev.* **2002**, *82*, 331–371.

(256) Rouschop, K.M.A. CD44 Deficiency Increases Tubular Damage But Reduces Renal Fibrosis in Obstructive Nephropathy. *J. Am. Soc. Nephrol.* **2004**, *15*, 674–686.

(257) Lewington, A.J.; Padanilam, B.J.; Martin, D.R.; Hammerman, M.R. Expression of CD44 in Kidney after Acute Ischemic Injury in Rats Expression of CD44 in Kidney after Acute Ischemic Injury in Rats. *Am. J. Physiol. Regul. Integr. Comp. Phsysiol.* **2013**, *278*, R247-254.

(258) Rouschop, K.M.A.; Roelofs, J.J.T.H.; Claessen, N.; da Costa Martins, P.; Zwaginga, J.J.; Pals, S.T.; Weening, J.J.; Florquin, S. Protection against Renal Ischemia Reperfusion Injury by CD44 Disruption. *J. Am. Soc. Nephrol.* **2005**, *16*, 2034–2043.

(259) Zhu, B.; Zhai, J.; Zhu, H.; Kyprianou, N. Prohibitin Regulates TGF-Beta Induced Apoptosis as a Downstream Effector of Smad-Dependent and -Independent Signaling. *Prostate* **2010**, *70*, 17–26.

(260) Xu, C.; Bailly-maitre, B.; Reed, J.C. Endoplasmic Reticulum Stress: Cell Life and Death Decisions. *J. Clin. Invest.* **2005**, *115*, 2656-2664.

(261) Völkel, W.; Alvarez-Sánchez, R.; Weick, I.; Mally, A.; Dekant, W.; Pähler, A. Glutathione Conjugates of 4-Hydroxy-2(E)-Nonenal as Biomarkers of Hepatic Oxidative Stress-Induced Lipid Peroxidation in Rats. *Free Radic. Biol. Med.* **2005**, *38*, 1526–1536.

(262) Il'yasova, D.; Scarbrough, P.; Spasojevic, I. Urinary Biomarkers of Oxidative Status. *Clin. Chim. Acta.* **2012**, *413*, 1446–1453.

(263) Eckl, P.M.; Ortner, A.; Esterbauer, H. Genotoxic Properties of 4-Hydroxyalkenals and Analogous Aldehydes. *Mutat. Res.* **1993**, *290*, 183–192.

(264) Moosavi, S.M.S.; Ashtiyani, S.C.; Hosseinkhani, S.; Shirazi, M. Comparison of the Effects of L: -Carnitine and Alpha-Tocopherol on Acute Ureteral Obstruction-Induced Renal Oxidative Imbalance and Altered Energy Metabolism in Rats. *Urol. Res.* **2010**, *38*, 187–194.

(265) Blondin, J.; Purkerson, M.L.; Rolf, D.; Schoolwerth, A.C.; Klahr, S. Renal Function and Metabolism after Relief of Unilateral Ureteral Obstruction. *Proc. Soc. Exp. Biol. Med.* **1975**, *150*, 71–76.

(266) Klahr, S.; Schwab, S.J.; Stokes, T.J. Metabolic Adaptations of the Nephron in Renal Disease. *Kidney Int.* **1986**, *29*, 80–89.

(267) MacLellan, D.L.; Mataija, D.; Doucette, A.; Huang, W.; Langlois, C.; Trottier, G.; Burton, I.W.; Walter, J.A.; Karakach, T.K. Alterations in Urinary Metabolites due to Unilateral Ureteral Obstruction in a Rodent Model. *Mol. Biosyst.* **2011**, *7*, 2181–2188.

(268) Middleton, G.W.; Beamon, C.R.; Panko, W.B.; Gillenwater, J.Y. Effects of Ureteral Obstruction on the Renal Metabolism of Alpha-Ketoglutarate and Other Substrates *in vivo*. *Invest. Urol.* **1977**, *14*, 255–262.

(269) Stecker, J.F.; Vaughan, E.D.; Gillenwater, J.Y. Alteration in Renal Metabolism Occurring in Ureteral Obstruction *in vivo*. *Surg. Gynecol. Obstet.* **1971**, *133*, 846–848.

(270) Trnka, P.; Hiatt, M.J.; Tarantal, A.F.; Matsell, D.G. Congenital Urinary Tract Obstruction: Defining Markers of Developmental Kidney Injury. *Pediatr. Res.* **2012**, *72*, 446–454.

(271) Takla, N.V; Hamilton, B.D.; Cartwright, P.C.; Snow, B.W. Apparent Unilateral Ureteropelvic Junction Obstruction in the Newborn: Expectations for Resolution. *J. Urol.* **1998**, *160*, 2175–2178.

(272) Pisitkun, T.; Johnstone, R.; Knepper, M.A. Discovery of Urinary Biomarkers. *Mol. Cell. Proteomics* **2006**, *5*, 1760–1771.

(273) Chevalier, R.L.; Thornhill, B.A.; Forbes, M.S.; Kiley, S.C. Mechanisms of Renal Injury and Progression of Renal Disease in Congenital Obstructive Nephropathy. *Pediatr. Nephrol.* **2010**, *25*, 687–697.

(274) Huang, W.Y.; Peters, C.A.; Zurakowski, D.; Borer, J.G.; Diamond, D.A.; Bauer, S.B.; McLellan, D.L.; Rosen, S. Renal Biopsy in Congenital Ureteropelvic Junction Obstruction: Evidence for Parenchymal Maldevelopment. *Kidney Int.* **2006**, *69*, 137–143.

(275) Li, Z.Z.; Xing, L.; Zhao, Z.Z.; Li, J.S.; Xue, R.; Chandra, A.; Nørregaard, R.; Wen, J.G. Decrease of Renal Aquaporins 1-4 Is Associated with Renal Function Impairment in Pediatric Congenital Hydronephrosis. *World J. Pediatr.* **2012**, *8*, 335–341.

(276) Wen, J.G.; Li, Z.Z.; Zhang, H.; Wang, Y.; Wang, G.; Wang, Q.; Nielsen, S.; Djurhuus, J.C.; Frøkiaer, J. Expression of Renal Aquaporins Is down-Regulated in Children with Congenital Hydronephrosis. *Scand. J. Urol. Nephrol.* **2009**, *43*, 486–493.

(277) Jeong, J.J.; Park, N.; Kwon, Y.J.; Ye, D.J.; Moon, A.; Chun, Y.J. Role of Annexin A5 in Cisplatin-Induced Toxicity in Renal Cells: Molecular Mechanism of Apoptosis. *J. Biol. Chem.* **2014**, *289*, 2469–2481.

(278) Trof, R.J.; Di Maggio, F.; Leemreis, J.; Groeneveld, A.B.J. Biomarkers of Acute Renal Injury and Renal Failure. *Shock* **2006**, *26*, 245–253.

(279) Scherberich, J.E. Urinary Proteins of Tubular Origin: Basic Immunochemical and Clinical Aspects. *Am. J. Nephrol.* **1990**, *10 Suppl 1*, 43–51.

(280) Westhuyzen, J.; Endre, Z.H.; Reece, G.; Reith, D.M.; Saltissi, D.; Morgan, T.J. Measurement of Tubular Enzymuria Facilitates Early Detection of Acute Renal Impairment in the Intensive Care Unit. *Nephrol. Dial. Transplant* **2003**, *18*, 543–551.

(281) Ricardo, S.D.; Bond, J.S.; Johnson, G.D.; Kaspar, J.; Diamond, J.R. Expression of Subunits of the Metalloendopeptidase Meprin in Renal Cortex in Experimental Hydronephrosis. *Am. J. Physiol.* **1996**, *270*, F669–76.

(282) Ma, M.C.; Huang, H.S.; Chen, C.F. Impaired Renal Sensory Responses after Unilateral Ureteral Obstruction in the Rat. *J. Am. Soc. Nephrol.* **2002**, *13*, 1008–1016.

(283) Mitic, B.; Lazarevic, G.; Vlahovic, P.; Rajic, M.; Stefanovic, V. Diagnostic Value of the Aminopeptidase N, N-Acetyl-Beta-D-Glucosaminidase and Dipeptidylpeptidase IV in Evaluating Tubular Dysfunction in Patients with Glomerulopathies. *Ren. Fail.* **2008**, *30*, 896–903.

(284) Kodera, R.; Shikata, K.; Takatsuka, T.; Oda, K.; Miyamoto, S.; Kajitani, N.; Hirota, D.; Ono, T.; Usui, H.K.; Makino, H. Dipeptidyl Peptidase-4 Inhibitor Ameliorates Early Renal Injury through Its Anti-Inflammatory Action in a Rat Model of Type 1 Diabetes. *Biochem. Biophys. Res. Commun.* **2014**, *443*, 828–833.

(285) Kaushal, G.P.; Haun, R.S.; Herzog, C.; Shah, S.V. Meprin A Metalloproteinase and Its Role in Acute Kidney Injury. *Am. J. Physiol. Renal Physiol.* **2013**, *304*, F1150–8.

(286) Ece, A.; Kelekçi, S.; Hekimoğlu, A.; Kocamaz, H.; Balik, H.; Yolbaş, I.; Erel, O. Neutrophil Activation, Protein Oxidation and Ceruloplasmin Levels in Children with Henoch-Schönlein Purpura. *Pediatr. Nephrol.* **2007**, *22*, 1151–1157.

(287) Novo, E.; Parola, M. Redox Mechanisms in Hepatic Chronic Wound Healing and Fibrogenesis. *Fibrogenesis Tissue Repair* **2008**, *1*, 5.

(288) Tolosano, E. Enhanced Splenomegaly and Severe Liver Inflammation in Haptoglobin/hemopexin Double-Null Mice after Acute Hemolysis. *Blood* **2002**, *100*, 4201–4208.

(289) Santoyo-Sánchez, M.P.; Pedraza-Chaverri, J.; Molina-Jijón, E.; Arreola-Mendoza, L.; Rodríguez-Muñoz, R.; Barbier, O.C. Impaired Endocytosis in Proximal Tubule from Subchronic Exposure to Cadmium Involves Angiotensin II Type 1 and Cubilin Receptors. *BMC Nephrol.* **2013**, *14*, 211.

(290) Reese, S.; Vidyasagar, A.; Jacobson, L.; Acun, Z.; Esnault, S.; Hullett, D.; Malter, J.S.; Djamali, A. The Pin 1 Inhibitor Juglone Attenuates Kidney Fibrogenesis via Pin 1-Independent Mechanisms in the Unilateral Ureteral Occlusion Model. *Fibrogenesis Tissue Repair* **2010**, *3*, 1.

(291) Christensen, E.I.; Nielsen, R.; Birn, H. From Bowel to Kidneys: The Role of Cubilin in Physiology and Disease. *Nephrol. Dial. Transplant* **2013**, *28*, 274–281.

(292) Hurley, J.H.; Odorizzi, G. Get on the Exosome Bus with ALIX. *Nat. Cell Biol.* **2012**, *14*, 654–655.

(293) Kong, H.J.; Kim, J.M.; Moon, J.H.; Kim, Y.O.; Nam, B.H.; Kim, W.J.; Lee, J.H.; Lee, S.J.; Kim, K.K.; Yeo, S.Y.; Lee, C.H. Hypoxia Induces the PDZ Domain-Containing Syntenin in the Marine Teleost Paralichthys Olivaceus. *Comp. Biochem. Physiol. C. Toxicol. Pharmacol.* **2010**, *152*, 195–201.

(294) Kalantari, S.; Rutishauser, D.; Samavat, S.; Nafar, M.; Mahmudieh, L.; Rezaei-Tavirani, M.; Zubarev, R.A. Urinary Prognostic Biomarkers and Classification of IgA Nephropathy by High Resolution Mass Spectrometry Coupled with Liquid Chromatography. *PLoS One* **2013**, *8*, e80830.

(295) Stødkilde, L.; Madsen, M.G.; Palmfeldt, J.; Topcu, S.O.; Nørregaard, R.; Olsen, L.H.; Jørgensen, T.M.; Frøkiær, J. Urinary Proteome Analysis in Congenital Bilateral Hydronephrosis. *Scand. J. Urol.* **2013**, *47*, 43–51.

(296) Aregger, F.; Uehlinger, D.E.; Witowski, J.; Brunisholz, R.A.; Hunziker, P.; Frey, F.J.; Jörres, A. Identification of IGFBP-7 by Urinary Proteomics as a Novel Prognostic Marker in Early Acute Kidney Injury. *Kidney Int.* **2013**, 1–11.

(297) Van Eerde, A.M.; Duran, K.; van Riel, E.; de Kovel, C.G.F.; Koeleman, B.P.C.; Knoers, N.V.A.M.; Renkema, K.Y.; van der Horst, H.J.R.; Bökenkamp, A.; van Hagen, J.M.; van den Berg, L.H.; Wolffenbuttel, K.P.; van den Hoek, J.; Feitz, W.F.; de Jong, T.P.V.M.; Giltay, J.C.; Wijmenga, C. Genes in the Ureteric Budding Pathway: Association Study on Vesico-Ureteral Reflux Patients. *PLoS One* **2012**, *7*, e31327.

(298) Hosohata, K.; Ando, H.; Fujimura, A. Urinary Vanin-1 as a Novel Biomarker for Early Detection of Drug-Induced Acute Kidney Injury. *J. Pharmacol. Exp. Ther.* **2012**, *341*, 656–662.

(299) Fugmann, T.; Borgia, B.; Révész, C.; Godó, M.; Forsblom, C.; Hamar, P.; Holthöfer, H.; Neri, D.; Roesli, C. Proteomic Identification of Vanin-1 as a Marker of Kidney Damage in a Rat Model of Type 1 Diabetic Nephropathy. *Kidney Int.* **2011**, *80*, 272–281.

(300) Minamida, S.; Iwamura, M.; Kodera, Y.; Kawashima, Y.; Ikeda, M.; Okusa, H.; Fujita, T.; Maeda, T.; Baba, S. Profilin 1 Overexpression in Renal Cell Carcinoma. *Int. J. Urol.* **2011**, *18*, 63–71.

(301) Shokeir, A. A. Role of Urinary Biomarkers in the Diagnosis of Congenital Upper Urinary Tract Obstruction. *Indian J. Urol.* **2008**, *24*, 313–319.

(302) Taha, M.A; Shokeir, A.A.; Osman, H.G.; Abd El-Aziz, A.E.A.F.; Farahat, S.E. Obstructed versus Dilated Nonobstructed Kidneys in Children with Congenital Ureteropelvic Junction Narrowing: Role of Urinary Tubular Enzymes. *J. Urol.* **2007**, *178*, 640–646.

(303) Giannakis, E.; Samuel, C.S.; Hewitson, T.D.; Boon, W.M.; Macris, M.; Reeve, S.; Lawrence, J.; Ian Smith, A.; Tregear, G.W.; Wade, J.D. Aberrant Protein Expression in Plasma and Kidney Tissue during Experimental Obstructive Nephropathy. *Proteomics. Clin. Appl.* **2009**, *3*, 1211–1224.

(304) el-Dahr, S.S.; Gee, J.; Dipp, S.; Hanss, B.G.; Vari, R.C.; Chao, J. Upregulation of Renin-Angiotensin System and Downregulation of Kallikrein in Obstructive Nephropathy. *Am. J. Physiol.* **1993**, *264*, F874–81.

(305) Merchant, M.L.; Niewczas, M.A.; Ficociello, L.H.; Lukenbill, J.A.; Wilkey, D.W.; Li, M.; Khundmiri, S.J.; Warram, J.H.; Krolewski, A.S.; Klein, J.B. Plasma Kininogen and Kininogen Fragments Are Biomarkers of Progressive Renal Decline in Type 1 Diabetes. *Kidney Int.* **2013**, *83*, 1177–1184.

(306) Li, C.; Wang, W.; Kwon, T.H.; Knepper, M.A.; Nielsen, S.; Frøkiaer, J. Altered Expression of Major Renal Na Transporters in Rats with Bilateral Ureteral Obstruction and Release of Obstruction. *Am. J. Physiol. Renal Physiol.* **2003**, *285*, F889–901.

(307) Li, C.; Wang, W.; Knepper, M.A.; Nielsen, S.; Frøkiaer, J. Downregulation of Renal Aquaporins in Response to Unilateral Ureteral Obstruction. *Am. J. Physiol. Renal Physiol.* **2003**, *284*, F1066–79.

(308) Su, Z.; Wang, X.; Gao, X.; Liu, Y.; Pan, C.; Hu, H.; Beyer, R.P.; Shi, M.; Zhou, J.; Zhang, J.; Serra, A.L.; Wüthrich, R.P.; Mei, C. Excessive Activation of the Alternative Complement Pathway in Autosomal Dominant Polycystic Kidney Disease. *J. Intern. Med.* **2014**, [*epub ahead of print*].

(309) Quesada, A.; Vargas, F.; Montoro-Molina, S.; O'Valle, F.; Rodríguez-Martínez, M.D.; Osuna, A.; Prieto, I.; Ramírez, M.; Wangensteen, R. Urinary Aminopeptidase Activities as Early and Predictive Biomarkers of Renal Dysfunction in Cisplatin-Treated Rats. *PLoS One* **2012**, *7*, e40402.

(310) Stubendorff, B.; Finke, S.; Walter, M.; Kniemeyer, O.; von Eggeling, F.; Gruschwitz, T.; Steiner, T.; Ott, U.; Wolf, G.; Wunderlich, H.; Junker, K. Urine Protein Profiling Identified Alpha-1-Microglobulin and Haptoglobin as Biomarkers for Early Diagnosis of Acute Allograft Rejection Following Kidney Transplantation. *World J. Urol.* **2014**.

(311) Scibior, A.; Gołębiowska, D.; Adamczyk, A.; Niedźwiecka, I.; Fornal, E. The Renal Effects of Vanadate Exposure: Potential Biomarkers and Oxidative Stress as a Mechanism of Functional Renal Disorders-Preliminary Studies. *Biomed Res. Int.* **2014**, *2014*, [*epub ahead of print*].

(312) Ryndin, I.; Gulmi, F.A.; Chou, S.Y.; Mooppan, U.M.M.; Kim, H. Renal Responses to Atrial Natriuretic Peptide Are Preserved in Bilateral Ureteral Obstruction and Augmented by Neutral Endopeptidase Inhibition. *J. Urol.* **2005**, *173*, 651–656.

(313) Aminzadeh, M.A.; Nicholas, S.B.; Norris, K.C.; Vaziri, N.D. Role of Impaired Nrf2 Activation in the Pathogenesis of Oxidative Stress and Inflammation in Chronic Tubulo-Interstitial Nephropathy. *Nephrol. Dial. Transplant* **2013**, *28*, 2038–2045.

(314) Zheng, M.; Lv, L.L.; Cao, Y.H.; Liu, H.; Ni, J.; Dai, H.Y.; Liu, D.; Lei, X.D.; Liu, B.C. A Pilot Trial Assessing Urinary Gene Expression Profiling with an mRNA Array for Diabetic Nephropathy. *PLoS One* **2012**, *7*, e34824.

(315) Sun, D.; Wang, Y.; Liu, C.; Zhou, X.; Li, X.; Xiao, A. Effects of Nitric Oxide on Renal Interstitial Fibrosis in Rats with Unilateral Ureteral Obstruction. *Life Sci.* **2012**, *90*, 900–909.

(316) D'Armiento, J.; Dalal, S.S.; Chada, K. Tissue, Temporal and Inducible Expression Pattern of Haptoglobin in Mice. *Gene* **1997**, *195*, 19–27.

(317) Venkatesan, K.; Rual, J.F.; Vazquez, A.; Stelzl, U.; Lemmens, I.; Hirozane-Kishikawa, T.; Hao, T.; Zenkner, M.; Xin, X.; Goh, K.I.; Yildirim, M.A.; Simonis, N.; Heinzmann, K.; Gebreab, F.; Sahalie, J.M.; Cevik, S.; Simon, C.; de Smet, A.S.; Dann, E.; Smolyar, A.; Vinayagam, A.; Yu, H.; Szeto, D.; Borick, H.; Dricot, A.; Klitgord, N.; Murray, R.R.; Lin, C.; Lalowski, M.; Timm, J.; Rau, K.; Boone, C.; Braun, P.; Cusick, M.E.; Roth, F.P.; Hill, D.E.; Tavernier, J.; Wanker, E.E.; Barabási, A.L.; Vidal, M. An Empirical Framework for Binary Interactome Mapping. *Nat. Methods* **2009**, *6*, 83–90.

(318) Rual, J.F.; Venkatesan, K.; Hao, T.; Hirozane-Kishikawa, T.; Dricot, A.; Li, N.; Berriz, G.F.; Gibbons, F.D.; Dreze, M.; Ayivi-Guedehoussou, N.; Klitgord, N.; Simon, C.; Boxem, M.; Milstein, S.; Rosenberg, J.; Goldberg, D.S.; Zhang, L.V; Wong, S.L.; Franklin, G.; Li, S.; Albala, J.S.; Lim, J.; Fraughton, C.; Llamosas, E.; Cevik, S.; Bex, C.; Lamesch, P.; Sikorski, R.S.; Vandenhaute, J.; Zoghbi, H.Y.; Smolyar, A.; Bosak, S.; Sequerra, R.; Doucette-Stamm, L.; Cusick, M.E.; Hill, D.E.; Roth, F.P.; Vidal, M. Towards a Proteome-Scale Map of the Human Protein-Protein Interaction Network. *Nature* **2005**, *437*, 1173–1178.

(319) Saraswat, M.; Muthenna, P.; Suryanarayana, P.; Petrash, J.M.; Reddy, G.B. Dietary Sources of Aldose Reductase Inhibitors: Prospects for Alleviating Diabetic Complications. *Asia Pac. J. Clin. Nutr.* **2008**, *17*, 558–565.

(320) Dunlop, M. Aldose Reductase and the Role of the Polyol Pathway in Diabetic Nephropathy. *Kidney Int. Suppl.* **2000**, *77*, S3–12.

(321) Tammali, R.; Saxena, A.; Srivastava, S.K.; Ramana, K.V. Aldose Reductase Inhibition Prevents Hypoxia-Induced Increase in Hypoxia-Inducible Factor-1alpha (HIF-1alpha) and Vascular Endothelial Growth Factor (VEGF) by Regulating 26 S Proteasome-Mediated Protein Degradation in Human Colon Cancer Cells. *J. Biol. Chem.* **2011**, *286*, 24089–24100.

(322) Shoeb, M.; Ramana, K.V; Srivastava, S.K. Aldose Reductase Inhibition Enhances TRAIL-Induced Human Colon Cancer Cell Apoptosis through AKT/FOXO3a-Dependent Upregulation of Death Receptors. *Free Radic. Biol. Med.* **2013**, *63*, 280–290.

(323) Yadav, U.C.S.; Ramana, K.V. Regulation of NF-κB-Induced Inflammatory Signaling by Lipid Peroxidation-Derived Aldehydes. *Oxid. Med. Cell. Longev.* **2013**, [*epub ahead of print*].

(324) Thornhill, B.A.; Forbes, M.S.; Marcinko, E.S.; Chevalier, R.L. Glomerulotubular Disconnection in Neonatal Mice after Relief of Partial Ureteral Obstruction. *Kidney Int.* **2007**, *72*, 1103–1112.

Appendix A: Supplemental data

A1.1 Evidence for AR activation in *in vivo* UTO

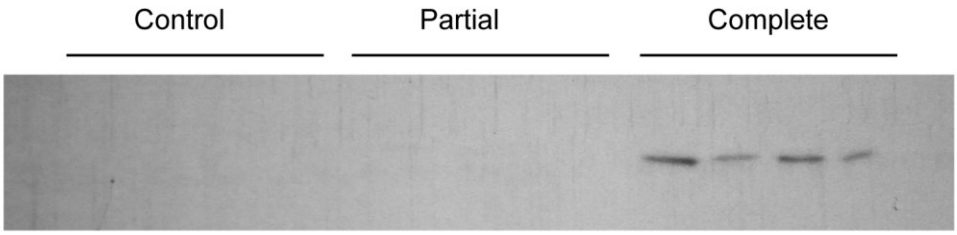

Figure A1: Western blot for Aldose reductase in the left (obstructed) kidney of rats. Aldose reductase is not present in either control or PUO, however appears to be increased in the CUO rats.

A1.2 Contact control timing for the dual spray system

Table A1: Timing for the column selection, sample injection, and gradient execution in the Dual-column LC-MS system.

Time	Action	Method file entry
0 min	Divert solvent flow (gradient to column 1)	Contact 2 Open
	Apply Voltage (to column 1)	Contact 3 Open
	Inject Sample (to column 2)	10 µL sample volume
	Apply Gradient (65 or 125 minute)	See Materials and Methods Section
10 min	Activate MS acquisition	Contact 1 Closed / Open
End of gradient (65 or 125 min)	Return solvent composition to 5 % B	End of gradient; takes ~ 10 min to reach MS
End + 10 min	Stop MS acquisition	End of data file
***** Load new method *****		
0 min	Divert solvent flow (gradient to column 2)	Contact 2 Closed
	Apply Voltage (to column 2)	Contact 3 Closed
	Inject Sample (to column 1)	10 µL sample volume
	Apply Gradient (65 or 125 minute)	See Materials and Methods Section
10 min	Activate MS acquisition	Contact 1 Closed / Open
End of gradient (65 or 125 min)	Return solvent composition to 5 % B	End of gradient; takes ~ 10 min to reach MS
End + 10 min	Stop MS acquisition	End of data file
***** Load new method *****		

Notes:
Contact 1 controls MS acquisition
Contact 2 controls solvent switch
Contact 3 controls voltage application

A1.3 Supplemental tables for proteins identified

Table A2: The list of proteins identified in Chapter 4. Each protein is listed with the number of peptide spectral matches (PSM) in each method applied. PSM = spectral counts.

Protein Accession	Protein Description	Σ# Unique Peptides	# PSM (A)	# PSM (B)	# PSM (C)	# PSM (D)
C9QUF4	CsbD family protein	9	11	17	15	11
C9QX85	D-ribose transporter subunit RbsB	43	221	319	249	245
C9R039	DNA protection during starvation protein	21	55	93	91	45
C9R140	Autonomous glycyl radical cofactor	11	10	18	23	14
C9QQ78	DNA-binding protein HU-beta	7	11	17	4	11
C9QTB5	Cold shock-like protein cspC	5	8	12	14	8
C9QZ73	Putative uncharacterized protein yccJ	5	4	2	2	4
C9QRS1	Galactose/methyl galactoside ABC transport system	32	45	73	53	59
C9QRL8	Elongation factor Ts	19	25	28	18	18
C9QXH9	30S ribosomal protein S5	11	23	42	34	21
C9QTM2	50S ribosomal protein L9	12	12	31	28	15
C9QXC8	Tryptophanase	40	153	157	133	155
C9QXN7	Malate dehydrogenase	18	37	66	39	41
C9QX67	Thioredoxin	6	10	23	26	11
C9R197	Cold shock protein CspE	5	7	6	8	7
C9QSU5	Periplasmic protein	21	37	65	54	42
C9QUL2	DNA-directed RNA polymerase subunit omega	3	2	3		2
C9QRL6	Ribosome-recycling factor	13	12	14	7	9
C9QXH3	50S ribosomal protein L24	12	16	27	24	20
C9QV92	50S ribosomal protein L10	10	11	14	14	9
C9QX44	Phage shock operon rhodanese PspE	6	5	3	3	5
C9QV44	Extracellular solute-binding protein family 1	21	26	33	32	27
C9R116	30S ribosomal protein S16	6	8	13	7	10
C9QXH4	50S ribosomal protein L5	14	23	14	19	22
C9QZJ1	Phosphoglycerate kinase	24	27	35	34	28
C9QU57	60 kDa chaperonin	39	95	103	90	96
C9R040	Cationic amino acid ABC transporter, periplasmic binding protein	15	19	34	24	27
C9QXE1	30S ribosomal protein S7	11	17	25	21	15
C9R1B4	Alkyl hydroperoxide reductase subunit C	14	24	38	32	19

Protein Accession	Protein Description	Σ# Unique Peptides	# PSM (A)	# PSM (B)	# PSM (C)	# PSM (D)
C9QVJ0	Cold shock protein cspA	3	2		4	2
C9QZ06	Aldo-keto reductase	16	21	17	20	17
C9QZ72	Flavoprotein WrbA	10	21	25	22	19
C9QTS9	Glyceraldehyde-3-phosphate dehydrogenase A	19	30	50	41	34
C9R0A2	Enolase	22	53	45	45	50
C9QTY9	Translation initiation factor IF-3	12	16	20	19	9
C9QX80	YifE protein	6	4	9	7	3
C9QQ45	Adenylate kinase	12	11	9	14	14
C9QTM3	30S ribosomal protein S18	6	7	8	8	8
C9QQP3	Putative uncharacterized protein yaiA	2	2			2
C9QQM4	Cationic amino acid ABC transporter, periplasmic binding protein	13	15	16	10	13
C9QXW3	DNA-binding protein H-NS	9	19	42	13	17
C9QPQ5	Nucleoside diphosphate kinase	6	5	14	13	5
C9QU58	10 kDa chaperonin	5	12	25	10	10
C9QXG7	50S ribosomal protein L22	10	8	18	11	10
C9QXH7	50S ribosomal protein L6	13	32	51	48	30
C9QXI4	30S ribosomal protein S13	7	9	14	9	8
C9QV76	DNA-binding protein HU-alpha	6	9	21	17	9
C9QS40	Dihydrolipoyl dehydrogenase	23	36	38	34	37
C9QUP2	ADP-L-glycero-D-manno-heptose-6-epimerase	15	9	12	14	17
C9QQ82	Trigger factor	26	38	44	35	39
C9QVY6	OsmC family protein	9	7	14	12	4
C9QXA0	ATP synthase subunit b	11	8	10	5	6
C9R0T1	Negative modulator of initiation of replication	8	3	4	5	5
C9QRL9	30S ribosomal protein S2	15	20	24	15	20
C9QZU1	30S ribosomal protein S1	29	40	45	42	40
C9QYL9	3-oxoacyl-(Acyl-carrier-protein) reductase	8	11	16	16	12
C9QZF7	Probable Fe(2+)-trafficking protein	5	4	6	4	5
C9QUS9	Glutaredoxin	5	6	7	8	6
C9QSQ5	Chaperone protein DnaK	34	47	75	48	47
C9QXE2	Elongation factor G	30	37	48	36	38
C9QZJ2	Fructose-bisphosphate aldolase	13	23	33	18	19
C9QXR0	Enoyl-[acyl-carrier-protein] reductase [NADH]	10	13	15	15	13
C9QZG2	L-asparaginase II	18	13	22	25	18
C9QXA4	ATP synthase subunit beta	19	35	30	30	34

Protein Accession	Protein Description	Σ# Unique Peptides	# PSM (A)	# PSM (B)	# PSM (C)	# PSM (D)
C9QXI1	50S ribosomal protein L15	7	9	13	11	10
C9QXI7	DNA-directed RNA polymerase subunit alpha	14	14	10	15	16
C9QW25	Extracellular solute-binding protein family 1	13	15	18	14	14
C9QQ92	UPF0234 protein yajQ	10	11	9	9	8
C9R0P3	Succinyl-CoA ligase [ADP-forming] subunit beta	19	22	26	18	25
C9QPM2	Serine hydroxymethyltransferase	17	23	23	24	23
C9QSR0	Transaldolase 2	19	24	33		22
C9R167	Extracellular solute-binding protein family 3	11	11	15	13	13
C9QSC8	30S ribosomal protein S20	7	11	9	12	11
C9QRM4	UPF0325 protein yaeH	7	3	8	3	4
C9QTZ7	Glutathione peroxidase	6	5	6	6	8
C9QTP8	Adenylosuccinate synthetase	19	27	30	22	28
C9QQC4	Glucose-specific phosphotransferase enzyme IIA component	7	9	17	18	10
C9QR70	Glycerophosphodiester phosphodiesterase	13	13	16	10	15
C9QZX1	Cold shock protein	3			4	
C9QXA8	Phosphate ABC transporter periplasmic substrate-binding protein PstS	14	9	10	11	9
C9QQC7	Cysteine synthase	11	8	12	9	12
C9QXH8	50S ribosomal protein L18	5	6	12	4	6
C9QTL1	Putative transcriptional regulator	6	4	3	3	3
C9QXE6	Bacterioferritin	7	9	13	12	5
C9QT90	Protein yebF	4	5	3	3	5
C9QRM2	2,3,4,5-tetrahydropyridine-2,6-dicarboxylate N-succinyltransferase	11	9	16	9	15
C9QSG0	6-phosphogluconate dehydrogenase, decarboxylating	17	17	17	18	16
C9QX29	Probable thiol peroxidase	8	10	13	21	13
C9QQ46	Chaperone protein htpG	24	22	33	23	22
C9QXG8	30S ribosomal protein S3	10	24	25	26	18
C9QU31	Pyruvate kinase	18	28	30	22	28
C9QQC6	Phosphocarrier protein ptsH	2	6			6
C9QWC1	Uridine phosphorylase	8	12	18	8	10
C9QZS0	4-deoxy-L-threo-5-hexosulose-uronate ketol-isomerase	9	26	24	23	22
C9QWK8	FAD dependent oxidoreductase	16	10	8	15	10
C9R1B2	Universal stress protein UP12	5	3		3	

Protein Accession	Protein Description	Σ# Unique Peptides	# PSM (A)	# PSM (B)	# PSM (C)	# PSM (D)
C9R0M2	2,3-bisphosphoglycerate-dependent phosphoglycerate mutase	14	17	24	25	21
C9QXY9	Ribose-phosphate pyrophosphokinase	12	20	26	17	16
C9R0L4	Molybdate transporter periplasmic protein	7	4	6	6	7
C9QRJ4	Proline--tRNA ligase	20	17	22	14	17
C9QXI6	30S ribosomal protein S4	10	14	23	21	18
C9QZW3	Leucine-responsive transcriptional regulator	7	5	4		5
C9QWN0	Phosphoenolpyruvate carboxykinase [ATP]	18	19	22	12	19
C9QUR0	YibT protein	2				2
C9QXA2	ATP synthase subunit alpha	22	51	60	36	51
C9QTZ3	Phenylalanine--tRNA ligase alpha subunit	11	8	12	9	10
C9QV93	50S ribosomal protein L1	9	16	22	22	19
C9R0P2	Succinyl-CoA ligase [ADP-forming] subunit alpha	11	17	19	13	15
C9QZE8	Aspartate aminotransferase	14	12	11	10	13
C9QYY7	YgiW	6	6	7	3	4
C9QWU1	Aldehyde Dehydrogenase	15	24	31	26	26
C9QXH0	50S ribosomal protein L29	2	3	5		3
C9QXI5	30S ribosomal protein S11	5	11	7	11	10
C9QTA2	Putative uncharacterized protein yebV	3	4		3	4
C9QRL0	Chaperone protein skp	6	4	7	7	5
C9QZ74	Glucose-1-phosphatase	13	19	17	16	21
C9QUS7	Superoxide dismutase	6	6	10	5	6
C9QVR9	GnsAGnsB family protein	2	2			2
C9QV69	Bifunctional purine biosynthesis protein PurH	19	12	19	16	12
C9QYP7	Glutaredoxin, GrxB family	8	7	9	7	9
C9R0J5	Molybdenum cofactor biosynthesis protein B	5	3	2	5	3
C9QXG1	30S ribosomal protein S10	6	9	12	9	9
C9QXG5	50S ribosomal protein L2	10	19	21	19	22
C9QSR8	Aerobic respiration control protein arcA	7	6	7	3	10
C9QS41	Dihydrolipoamide acetyltransferase	24	26	42	27	27
C9QUY2	Putative uncharacterized protein ydgH	9	8	11	7	9
C9QXI0	50S ribosomal protein L30	2		3		
C9QZS1	2-deoxy-D-gluconate 3-dehydrogenase	10	14	29	22	17

Protein Accession	Protein Description	Σ# Unique Peptides	# PSM (A)	# PSM (B)	# PSM (C)	# PSM (D)
C9QQT3	Lac repressor	15	29	45	29	31
C9QPZ7	Peptidyl-prolyl cis-trans isomerase	4	10	10		7
C9QTZ5	Integration host factor subunit alpha	5	7	9	5	6
C9R131	ATP-dependent chaperone ClpB	28	37	34	31	38
C9QY66	Transcription elongation factor GreA 2	5	4	3	6	4
C9QZY8	Arginine transporter subunit	8	17	22	14	10
C9QYK4	UPF0227 protein ycfP	5	6	10	5	2
C9QWI8	Putative uncharacterized protein yhhA	4	5	5	4	7
C9QU61	Aspartate ammonia-lyase	17	21	37	32	21
C9QVI6	Glycine--tRNA ligase beta subunit	22	22	29	20	22
C9QQC5	Phosphoenolpyruvate-protein phosphotransferase	18	18	20	13	18
C9QVM1	2-dehydro-3-deoxygluconokinase	13	25	37	41	26
C9R0N0	Protein TolB	12	9	9	14	9
C9QX88	D-ribose pyranase	4	7	9	9	7
C9QV64	Isocitrate lyase	15	33	47	21	37
C9QZB9	OmpA domain protein transmembrane region-containing protein	10	19	18	12	14
C9QRK0	Rof protein	3	2	3	2	3
C9QZA1	Hydrogenase-1 expression HyaE	3	3	3	2	2
C9QR98	Ecotin	6	8	7	5	4
C9QX65	Transcription termination factor Rho	17	15	16	16	15
C9QZT5	UPF0434 protein YcaR	2	2	3		2
C9QUA9	D-allose transporter subunit	8	7	9	5	7
C9QY55	Putative ABC-type organic solvent transporter	6	4	12	10	7
C9QPW1	Transaldolase 1	11	10	16		12
C9QRY4	Putative uncharacterized protein yegP	3	7	8	7	8
C9QWR9	Peptidyl-prolyl cis-trans isomerase	4	11	4	6	4
C9R127	Ribosome-associated inhibitor A	3	4	6	4	4
C9QRC1	50S ribosomal protein L25	3	8	11	8	8
C9QX87	ABC transporter related protein	13	15	14	10	15
C9QR68	Anaerobic glycerol-3-phosphate dehydrogenase subunit A	17	18	18	10	18
C9QZL8	tRNA-modifying protein ygfZ	10	7	6	6	9
C9QXM1	Putative oxidoreductase, Zn-dependent and NAD(P)-binding	9	6	9	10	5
C9QXV7	Extracellular solute-binding protein family 5	13	7	14	9	7

Protein Accession	Protein Description	Σ# Unique Peptides	# PSM (A)	# PSM (B)	# PSM (C)	# PSM (D)
C9QXG9	50S ribosomal protein L16	5	12	14	17	11
C9QQ38	Putative uncharacterized protein ybaK	5	4	7	3	3
C9QQJ3	UPF0381 protein yfcZ	5	7	8	6	7
C9QXD5	Peptidyl-prolyl cis-trans isomerase	10	7	7	11	9
C9QWS5	Catabolite gene activator	7	7	11	7	6
C9QS42	Pyruvate dehydrogenase E1 component	28	32	39	34	33
C9R0T4	Flavodoxin	4	4	4	2	3
C9QYZ7	2,5-didehydrogluconate reductase	7	6	7	5	7
C9QYU4	G/U mismatch-specific DNA glycosylase	6	2	4	3	6
C9QZ29	Putative uncharacterized protein glcG	3	3		2	3
C9QPQ2	Sulfurtransferase	7	5	7	4	5
C9QXI8	50S ribosomal protein L17	5	11	15	10	6
C9QV94	50S ribosomal protein L11	4	9	12	17	6
C9QW99	Thiol:disulfide interchange protein DsbA	4	4		2	5
C9QTK2	Inorganic pyrophosphatase	6	6	5	6	9
C9QU30	LPP repeat-containing protein	2	3		2	3
C9QYL8	Acyl carrier protein	3		9	10	7
C9QUP4	2-amino-3-ketobutyrate CoA ligase	11	16	9	5	16
C9QV91	50S ribosomal protein L7/L12	6	8	17	14	9
C9QTK1	Periplasmic binding protein/LacI transcriptional regulator	9	3	6	5	9
C9QTU3	Nitroreductase	5	4	5	5	4
C9QV70	Phosphoribosylamine--glycine ligase	9	11	10	14	11
C9QXP2	50S ribosomal protein L13	5	3	6	4	5
C9QZC2	Beta-hydroxyacyl-(Acyl-carrier-protein) dehydratase FabA	6	12	11	13	9
C9QYI9	Extracellular solute-binding protein family 1	9	6	10	7	6
C9QXG2	50S ribosomal protein L3	6	7	8	9	7
C9QTM5	30S ribosomal protein S6	4	2			5
C9QPU4	Peroxiredoxin	4	3	7	5	2
C9QRX1	Fructose-bisphosphate aldolase	13	13	14	17	16
C9QQL4	Erythronate-4-phosphate dehydrogenase	7	5	4	3	5
C9QZB1	CoA-binding domain protein	3	3	5	6	4
C9QSY8	Isoaspartyl dipeptidase	7	9	4	4	9
C9QUE8	Alcohol dehydrogenase zinc-binding domain protein	5	3	4	4	2
C9R0L0	6-phosphogluconolactonase	6	5	2	7	5

Protein Accession	Protein Description	Σ# Unique Peptides	# PSM (A)	# PSM (B)	# PSM (C)	# PSM (D)
C9QSE9	dTDP-glucose 4,6-dehydratase	9	5	6	5	5
C9QUM5	50S ribosomal protein L33	2	2			2
C9QXG3	50S ribosomal protein L4	4	5	5	6	5
C9QXW1	Aldehyde-alcohol dehydrogenase	25	25	31	21	25
C9QYE2	Putative uncharacterized protein yqjD	4	3	6	5	2
C9QXH5	30S ribosomal protein S14	5	8	7	8	7
C9QRJ1	Lipoprotein	5	5	7	5	7
C9QU29	ErfK/YbiS/YcfS/YnhG family protein	5	4	7	4	2
C9R0Q1	Citrate synthase	9	19	10	12	19
C9QVQ0	Oligopeptidase A	17	13	14	11	13
C9QT70	Aspartate--tRNA ligase	15	10	14	12	10
C9QXH2	50S ribosomal protein L14	2	5	7	5	6
C9QY78	Ribosome-binding factor A	3	2	2		2
C9QY43	PTS IIA-like nitrogen-regulatory protein PtsN	3	5		2	3
C9QXU0	Tryptophan synthase alpha chain	5	4		5	2
C9QPS6	Uracil phosphoribosyltransferase	4	9	11	9	10
C9QSF4	UDP-galactopyranose mutase	7	6		4	6
C9R0U9	CinA domain protein	3			3	
C9QV54	Glucose-6-phosphate isomerase	16	13	17	12	13
C9QX93	DNA-binding transcriptional regulator AsnC	4	5	5	3	4
C9QXY1	2-dehydro-3-deoxyphosphooctonate aldolase	5	4	5	2	3
C9R0V2	Alanyl-tRNA synthetase	19	19	20	11	19
C9QY81	Polyribonucleotide nucleotidyltransferase	16	18	19	11	18
C9QR11	Acetate kinase	8	11	12	11	13
C9QV89	DNA-directed RNA polymerase	31	29	32	29	29
C9QT38	L-arabinose ABC transporter substrate binding component	6	6	3	5	3
C9QVD6	ATP-dependent protease ATPase subunit HslU	10	8	14	12	9
C9QVC5	Catalase-peroxidase	19	20	18	18	20
C9QST9	Deoxyribose-phosphate aldolase	5	6	3	5	7
C9QTI6	Endoribonuclease L-PSP	2	4	8	7	4
C9QXJ5	Methionyl-tRNA formyltransferase	5	4		3	4
C9QY76	NusA antitermination factor	10	6	13	6	6
C9QQM5	Cationic amino acid ABC transporter, periplasmic binding protein	9	8	5	4	3
C9QPU8	Phosphoribosylaminoimidazole-succinocarboxamide synthase	5	3	6	5	2

Protein Accession	Protein Description	Σ# Unique Peptides	# PSM (A)	# PSM (B)	# PSM (C)	# PSM (D)
C9QWG4	Putative uncharacterized protein dcrB	4	4	9	4	4
C9QZV9	Serine--tRNA ligase	11	10	10	7	10
C9QVF5	Aldehyde Dehydrogenase	11	8	17	14	8
C9QZA4	Hydrogenase 1 large subunit	13	8	15	11	8
C9QSU9	DNA polymerase III subunit psi	2			2	
C9QXG6	30S ribosomal protein S19	3	3	4	2	3
C9QXX6	DsrE family protein	2	2	3	6	2
C9QT87	2-dehydro-3-deoxyphosphogluconate aldolase/4-hydroxy-2-oxoglutarate aldolase	5	9	18	17	10
C9R0P6	Succinate dehydrogenase and fumarate reductase iron-sulfur protein	5	2			4
C9QTS5	Putative serine protein kinase, PrkA	15	9	13	11	9
C9QTQ7	Putative uncharacterized protein yjeE	3	2	3	2	2
C9QXS3	Aconitate hydratase	19	16	20	25	16
C9QST6	Purine nucleoside phosphorylase DeoD-type	6	6	9	7	7
C9QPR6	GMP synthase [glutamine-hydrolyzing]	11	7	11	9	7
C9QPR5	Inosine-5'-monophosphate dehydrogenase	10	11	14	8	11
C9QXL3	DNA-binding protein fis	2		3		
C9QST7	Phosphopentomutase	12	12	9	10	14
C9QT82	Pyruvate kinase	13	19	15	12	20
C9QY22	Septum site-determining protein MinD	6	6		4	12
C9QXM3	Cell shape determining protein, MreB/Mrl family	10	6	9	6	8
C9QRP9	Elongation factor P-like protein	4	2			4
C9QYL7	3-oxoacyl-[acyl-carrier-protein] synthase 2	6	4	2	5	4
C9R0T5	Ferric uptake regulation protein	3	4	4	4	3
C9QWA1	YihD	2			2	
C9QUR8	Putative mono-oxygenase ydhR	2	3	4	4	4
C9QR04	D-erythro-7,8-dihydroneopterin triphosphate epimerase	3	4		2	4
C9QTW8	NH(3)-dependent NAD(+) synthetase	6	4	6	4	6
C9QTQ3	Protein hfq	3	3	6	3	2
C9QQS1	Transcriptional repressor frmR	2	2			2
C9QWM8	Osmolarity response regulator	4	3		2	4
C9R0X9	4-aminobutyrate aminotransferase	8	7	9	11	7

Protein Accession	Protein Description	Σ# Unique Peptides	# PSM (A)	# PSM (B)	# PSM (C)	# PSM (D)
C9QR10	Phosphate acetyltransferase	14	22	25	18	21
C9QS38	Aconitate hydratase 2	19	23	32	28	25
C9QT34	Ferritin-1	3	2	5	9	2
C9QZJ5	Putative uncharacterized protein yggE	5	4	2	3	5
C9QWV0	Aldo/keto reductase	4	2			4
C9R1E6	6,7-dihydropteridine reductase	6	7	8	8	6
C9QR42	Regulatory protein AmpE	3	8	8	4	3
C9QZK6	Cell division protein ZapA	2	2		2	2
C9QTU4	Selenide, water dikinase	6	5	5	3	4
C9QUM4	50S ribosomal protein L28	2		7		
C9QTX6	Catalase	20	15	23	18	14
C9R0P7	Succinate dehydrogenase flavoprotein subunit	11	7	6	3	7
C9QUU6	Tyrosine--tRNA ligase	8	5	8	9	5
C9QV90	DNA-directed RNA polymerase subunit beta	33	31	37	33	33
C9QUU8	Glutathione S-transferase	5	5	9	4	4
C9QUS1	Riboflavin synthase subunit alpha	4	6	4	2	4
C9QRX4	Galactitol-specific enzyme IIA component of PTS	3	3	10	4	3
C9QXK0	tRNA threonylcarbamoyladenosine biosynthesis protein RimN	3	2		2	2
C9QYK9	Histidine triad (HIT) protein	2		4	7	
C9QVH8	D-xylose ABC transporter, periplasmic substrate-binding protein	6	5	2	3	5
C9QVJ3	Glyoxylate/hydroxypyruvate reductase B	5	3	6		3
C9QQ84	Putative uncharacterized protein yajG	4	2		2	2
C9QT88	Phosphoribosylglycinamide formyltransferase 2	8	5	6	6	5
C9QZY0	Pyruvate dehydrogenase	9	7	6	6	7
C9QYR2	Glucans biosynthesis protein G	9	8	7	8	9
C9QYM0	Malonyl CoA-acyl carrier protein transacylase	4	5		4	5
C9QS99	Chaperone SurA	8	8	6	6	9
C9QX72	Peptidyl-prolyl cis-trans isomerase C	2	2			2
C9R0R1	NIF3 family protein	4		4	3	3
C9QPV4	Arsenate reductase	2	3		3	3
C9QV65	Malate synthase	10	5	17	11	5
C9R0L8	UDP-galactose-4-epimerase	5			3	5
C9QSA4	Dihydrofolate reductase	4	3	3	2	

Protein Accession	Protein Description	Σ# Unique Peptides	# PSM (A)	# PSM (B)	# PSM (C)	# PSM (D)
C9QW88	GTP-binding protein TypA	15	16	11	10	16
C9R112	Protein grpE	4	3	6	6	3
C9QUU1	Transcriptional regulator slyA	3		3		2
C9QXS8	Putative uncharacterized protein yciN	2	2			2
C9QZG0	Putative uncharacterized protein yggL	2	4	3	4	4
C9QW42	6-phosphofructokinase	6	4	4	5	3
C9QTZ4	Phenylalanine--tRNA ligase beta subunit	13	10	11	11	10
C9R0P5	2-oxoglutarate dehydrogenase E1 component	17	17	26	19	17
C9R0X2	DNA-binding protein H-NS	2	2	3	2	2
C9QY23	Cell division topological specificity factor	2	2			2
C9QZE6	Asparagine--tRNA ligase	8	6	8	9	6
C9QPQ9	Histidine--tRNA ligase	7	5	6	6	5
C9QQ99	2-carboxybenzaldehyde reductase	6	5	6	4	4
C9QR77	3-demethylubiquinone-9 3-methyltransferase	3	2			2
C9QYQ5	Protein yceI	4	3			2
C9QX23	Extracellular solute-binding protein family 5	8	6	10	6	6
C9QRM6	Protease Do	9	12	10	7	13
C9QQP1	UPF0345 protein YaiE	2	4	4		4
C9R0A1	CTP synthase	9	4	10	6	4
C9QPU6	Dihydrodipicolinate synthase	5	5	5	2	5
C9QWA7	Xaa-Pro dipeptidase	7	5	8	4	5
C9R0W9	Putative uncharacterized protein ygaM	2	3	3	3	3
C9R159	Asparagine synthetase	8	6	6	7	7
C9QRK4	Acetyl-coenzyme A carboxylase carboxyl transferase subunit alpha	5	3	4	4	2
C9QXK3	Conserved protein	4	4		2	
C9QZW4	Thioredoxin reductase	5	5	2	3	3
C9QRG0	Aminoacyl-histidine dipeptidase	7	2	5	4	2
C9QZU5	Phosphoserine aminotransferase	7	6	2	6	6
C9QS23	Pantothenate synthetase	6	5		3	3
C9QTC1	PTS system, mannose/fructose/sorbose family, IIA subunit	6	2	3	7	4
C9QRX2	D-tagatose-1,6-bisphosphate aldolase subunit GatY	4	15	13	8	12
C9QUD9	Single-stranded DNA-binding protein	6	6	8	5	5

Protein Accession	Protein Description	Σ# Unique Peptides	# PSM (A)	# PSM (B)	# PSM (C)	# PSM (D)
C9QQ94	DJ-1 family protein	3		3		2
C9QXD3	Peptidyl-prolyl cis-trans isomerase	3	2	2	3	3
C9QYI2	DNA-binding transcriptional regulator PhoP	6	6	6	5	5
C9QRH4	Phosphoheptose isomerase	4	6	11	10	6
C9QUE3	Class B acid phosphatase	3	4	3	4	2
C9QTL9	Peptidyl-prolyl cis-trans isomerase	4	6	4	6	4
C9QW47	MOSC domain containing protein	4		2	2	3
C9QTV1	Sulfurtransferase	9	5	5	5	5
C9QU45	Fumarate reductase iron-sulfur subunit	5	4	7	3	
C9QTK5	AIG2 family protein	2		3		
C9QTS8	Aldose 1-epimerase	5	3	5	5	3
C9QYM1	3-oxoacyl-[acyl-carrier-protein] synthase 3	5	4	4	3	3
C9R117	Ribosome maturation factor RimM	3		2	2	2
C9QPP1	RNA methyltransferase	5	3	5	5	5
C9QR13	UPF0304 protein yfbU	3	2	6		
C9QZL1	Aminomethyltransferase	5	7	11	11	8
C9QVA6	Soluble pyridine nucleotide transhydrogenase	6	6	4	4	6
C9QSI0	DNA gyrase inhibitor	3		5		
C9QXH6	30S ribosomal protein S8	2			6	
C9QXA7	Glucosamine--fructose-6-phosphateaminotransferase	8	9	14	7	9
C9QWB9	Ubiquinone/menaquinone biosynthesis methyltransferase ubiE	4	2	5	3	
C9R0P4	2-oxoglutarate dehydrogenase, E2 subunit, dihydrolipoamide succinyltransferase	10	17	26	17	17
C9QXA1	ATP synthase subunit delta	2			2	
C9QPM0	Nitrogen regulatory protein P-II	3	2	4		2
C9QVT0	3-hydroxy acid dehydrogenase	3		4	5	4
C9QR78	DNA gyrase subunit A	16	14	10	11	14
C9QY61	50S ribosomal protein L21	2		4		
C9QTD8	Putative dehydrogenase	6	6	11	9	6
C9QXJ6	Peptide deformylase	4	3	3	3	4
C9QZE7	Outer membrane protein F	6	6		3	5
C9QVD8	Regulator of ribonuclease activity A	4	2	5	2	
C9QQ39	5'-Nucleotidase domain protein	8	6	12	7	5
C9QSF2	dTDP-4-dehydrorhamnose 3,5-epimerase	3	2			2

Protein Accession	Protein Description	Σ# Unique Peptides	# PSM (A)	# PSM (B)	# PSM (C)	# PSM (D)
C9QWK1	Aspartate-semialdehyde dehydrogenase	5	2	8	6	4
C9QPP0	Inositol-1-monophosphatase	5	4		4	2
C9QS59	Cell division protein ftsZ	7	9	11	4	10
C9R180	Leucine--tRNA ligase	13	11	10	4	11
C9QTJ7	Fructose-1,6-bisphosphatase class 1	4	2	3	3	4
C9QT72	Probable transcriptional regulatory protein YebC	4	2			3
C9QS62	D-alanine--D-alanine ligase 2	4	3			2
C9QTY8	Threonine--tRNA ligase	10	10	7	5	10
C9QRS5	FAD-dependent pyridine nucleotide-disulphide oxidoreductase	5	6			6
C9QY77	Translation initiation factor IF-2	16	13	9	9	14
C9QXM6	Maf-like protein yceF 1	2				2
C9R032	ErfK/YbiS/YcfS/YnhG family protein	4		5	3	
C9R0M1	Aldose 1-epimerase	5	3	2	4	3
C9QVE5	Putative uncharacterized protein yiiS	2	2	3	3	2
C9QS22	3-methyl-2-oxobutanoate hydroxymethyltransferase	4	2	4	4	4
C9QZ62	Delta-1-pyrroline-5-carboxylate dehydrogenase	21	22	25	19	22
C9QTY5	1-phosphofructokinase	4	2	3	4	3
C9QTR7	Putative uncharacterized protein yeaO	2		2		
C9QQB1	Preprotein translocase subunit YajC	2		3	2	
C9QXU2	Putative uncharacterized protein yciF	3	2		2	5
C9QS11	DnaK transcriptional regulator DksA	2		3		3
C9R0M8	Tol-pal system protein YbgF	5	3	4	5	4
C9QT60	Arginine--tRNA ligase	9	4	7	7	4
C9QSS2	CreA family protein	2			3	
C9QUM1	Deoxyuridine 5'-triphosphate nucleotidohydrolase	2		4	3	
C9QPQ0	Peptidase B	6	5	4	4	5
C9QTW9	Osmotically-inducible lipoprotein E	2	2		2	
C9QR92	Outer membrane porin protein C	7	12	15	15	
C9QZK4	D-3-phosphoglycerate dehydrogenase	5	3	5	2	3
C9QPW2	Malate dehydrogenase (	10	10	18	11	10
C9QWP9	Tryptophanyl-tRNA synthetase	5	4	3	6	7

Protein Accession	Protein Description	Σ# Unique Peptides	# PSM (A)	# PSM (B)	# PSM (C)	# PSM (D)
C9R0X6	LysM domain/BON superfamily protein	3	2			3
C9QZL6	UPF0267 protein yqfB	2	2			2
C9QZ30	Malate synthase G	11	7	10	8	8
C9QTP5	23S rRNA (guanosine-2'-O-)-methyltransferase RlmB	3		5		
C9QQ81	ATP-dependent Clp protease proteolytic subunit	2	2	4		3
C9QZI3	Transketolase	11	9	14		9
C9QSS8	ABC transporter related protein	11	8	15	9	8
C9QUQ1	Glutaredoxin 3	2	3			3
C9QSG5	1-(5-phosphoribosyl)-5-[(5-phosphoribosylamino)methylidene amino] imidazole-4-carboxamide isomerase	3	2		2	3
C9QWI3	Extracellular solute-binding protein family 1	5	3	2	2	3
C9QTP7	HTH-type transcriptional repressor NsrR	2				2
C9QY54	Mammalian cell entry related domain protein	2	2			
C9QU44	Fumarate reductase flavoprotein subunit	8	7	9	8	7
C9QQP5	UPF0178 protein yaiI	2	2			
C9QW95	Probable GTP-binding protein EngB	4	4			2
C9QV40	Maltose operon periplasmic	2				4
C9QRR8	GTP cyclohydrolase 1	3	3	3	3	
C9QQL1	3-oxoacyl-(Acyl carrier protein) synthase I	9	14	9	11	14
C9QTI0	Putative uncharacterized protein yjgK	2	2	2		
C9QQ80	ATP-dependent Clp protease ATP-binding subunit ClpX	6	7	6	5	7
C9QQA3	6,7-dimethyl-8-ribityllumazine synthase	2			4	
C9QTY3	Fructosamine kinase	4	2	4	3	3
C9QVI5	Glycine--tRNA ligase alpha subunit	4	4	4	7	4
C9QSQ0	Flagellin	5	7	8	6	7
C9QW49	Superoxide dismutase	5	3	3		4
C9QR67	Anaerobic glycerol-3-phosphate dehydrogenase subunit B	5	5		4	5
C9QUC0	Putative uncharacterized protein yjcO	3	2			3
C9QYU7	30S ribosomal protein S21	2			2	
C9QZL3	Glycine dehydrogenase [decarboxylating]	13	14	15	13	14

Protein Accession	Protein Description	Σ# Unique Peptides	# PSM (A)	# PSM (B)	# PSM (C)	# PSM (D)
C9QRC3	Pseudouridine synthase	3	3	3	2	4
C9QUX3	Mannose-6-phosphate isomerase	5	3	4	6	2
C9QWY0	Stress-induced protein, ATP-binding protein	2		5	9	
C9R000	Nitroreductase	3			3	
C9QRF9	Xanthine phosphoribosyltransferase	2		2		
C9QZ48	Glyoxylate/hydroxypyruvate reductase A	4	2	5	3	3
C9QVD5	ATP-dependent protease subunit HslV	2				2
C9QYR5	O-acetyl-ADP-ribose deacetylase	2	2		2	
C9R179	Putative uncharacterized protein ybeL	3	5	8	4	4
C9QSC6	Isoleucine--tRNA ligase	13	10	18	13	11
C9QUQ0	Putative uncharacterized protein yibN	2		2	2	
C9QQ75	Putative uncharacterized protein ybaW	2	2			2
C9QQ34	Glutaminase 2	2			2	
C9QUL3	Guanylate kinase	3	3		2	2
C9QPL6	Phosphoribosylformylglycinamidine synthase	15	14	14	12	14
C9QZ16	Glutathione S-transferase domain protein	3	2		2	3
C9QVF1	Glutathione S-transferase	3	3			
C9QWL9	Fe/S biogenesis protein NfuA	3	4	4	4	
C9QXA5	ATP synthase epsilon chain	2	2			2
C9QRB5	Transcriptional regulator NarP	3		2	3	2
C9QY00	Periplasmic trehalase	7	4	4	4	4
C9QQB5	Short chain dehydrogenase	3		4	2	3
C9QZG8	Alanine racemase domain protein	3	3	3		4
C9QYS6	NAD(P)-binding dehydrogenase	4	3	3	2	2
C9QYC9	Endoribonuclease L-PSP	1	2			2
C9QU53	Elongation factor P	2	3	4		2
C9QT69	Isochorismatase hydrolase	2		3	3	2
C9QXC3	NADPH-dependent FMN reductase	2	3			
C9QZM5	Peptide chain release factor 2	4	2		3	2
C9QXP3	30S ribosomal protein S9	2	5	14		
C9QRT8	Putative transporter subunit:periplasmic-binding component of ABC superfamily	4	6	5	2	4
C9QUC9	Acetyl-coenzyme A synthetase	9	4	6	6	5
C9R0M4	Putative homeobox protein	2	4		4	5

Protein Accession	Protein Description	Σ# Unique Peptides	# PSM (A)	# PSM (B)	# PSM (C)	# PSM (D)
C9QVQ3	Universal stress protein A	2				3
C9QZH0	Putative Holliday junction resolvase	2			2	
C9R0Y0	Succinate-semialdehyde dehydrogenase I	5	5	5		6
C9QVJ2	Putative uncharacterized protein yiaF	3	2		3	
C9QTG3	Alcohol dehydrogenase GroES domain protein	6	4	5	4	3
C9QZK3	Ribose-5-phosphate isomerase A	4	6	6	7	8
C9QZ11	Hydrogenase 2 large subunit	5	3	6	3	3
C9QSJ7	ErfK/YbiS/YcfS/YnhG family protein	4		2	4	
C9QQ50	Adenine phosphoribosyltransferase	3		4	3	3
C9QPW0	Transketolase	10	8	10		8
C9QRS8	Cytidine deaminase	4	4	4		3
C9R0H7	Glycosyl transferase family protein	4		2	3	3
C9R082	Lactaldehyde reductase	5	3	4	4	3
C9QQ56	Efflux transporter, RND family, MFP subunit	3	3	2	3	3
C9R024	Molybdenum cofactor synthesis domain protein	4	7	11	4	7
C9QQ79	Lon protease	10	5		6	5
C9QYM5	Maf-like protein yceF 2	3	2	4	2	3
C9R0T0	Phosphoglucomutase	5	4	5	4	4
C9QQD9	Glutamate--tRNA ligase	6	5	4	3	5
C9QVK2	4-phytase	7	10		4	10
C9QT01	Chaperone, periplasmic	3			2	2
C9R077	L-fucose mutarotase	2		2		
C9QXZ3	GTP-binding protein YchF	4		6	3	
C9QSU6	Peptide chain release factor 3	6	5		3	5
C9R155	Pyridoxine 5'-phosphate synthase	4	4	6		3
C9R126	Bifunctional chorismate mutase/prephenatede hydratase	5	3	6	3	3
C9QXT4	Putative uncharacterized protein yciO	3	3	3	2	3
C9QWX5	D-isomer specific 2-hydroxyacid dehydrogenase NAD-binding protein	5	3	3	3	3
C9QSG4	Imidazole glycerol phosphate synthase subunit HisF	3			2	2
C9R091	Flavodoxin	2		3		
C9R1B5	Disulfide isomerase/thiol-disulfide oxidase	3			3	
C9R0V0	Protein RecA	5	5	3	4	6
C9QZ46	Cytoplasmic chaperone TorD	2		6	4	2

Protein Accession	Protein Description	Σ# Unique Peptides	# PSM (A)	# PSM (B)	# PSM (C)	# PSM (D)
	family protein					
C9QY95	Putative uncharacterized protein yraP	2	2		2	3
C9QW89	Glutamine synthetase	6	7	8	9	7
C9QTH4	Valine--tRNA ligase	11	8	10	5	8
C9QQA2	N utilization substance protein B homolog	2	2			2
C9QRN3	Glutamate-1-semialdehyde 2,1-aminomutase	4	3	3	5	3
C9QXA3	ATP synthase gamma chain	4	6	4	8	4
C9QRL7	UMP kinase	4	5	5	5	4
C9QR14	HAD-superfamily hydrolase, subfamily IA, variant 3	2	2			
C9QXX4	Nitrate/nitrite sensor protein NarX	3		3	2	
C9R0V9	Transcriptional regulator, MarR family	2	2	2	3	2
C9QUL7	Putative uncharacterized protein yicC	3			2	2
C9QY15	Hemolysin E	3		2	2	2
C9QYS1	Uronate isomerase	5			5	
C9QYI5	Peptidase T	5	4	5	4	4
C9QZV5	Isochorismatase hydrolase	3	2	7	4	5
C9QVV4	AI2 transporter	3	2		2	2
C9QR66	Glycerol-3-phosphate dehydrogenase, anaerobic, C subunit	5	6	5	3	6
C9R0U0	Glucosamine-6-phosphate deaminase	4	4	5	2	3
C9QW16	Alcohol dehydrogenase zinc-binding domain protein	3	3		5	
C9QUE5	Aromatic amino acid aminotransferase	4	4	5	4	4
C9QW71	Putative acetyltransferase	3	2		2	
C9QTJ1	Anaerobic ribonucleoside triphosphate reductase	6	5	6	4	5
C9QQQ1	D-alanine--D-alanine ligase 1	5	3		4	3
C9QQS4	Nucleoprotein/polynucleotide-associated enzyme	2	2			2
C9R161	(Dimethylallyl)adenosine tRNA methylthiotransferase MiaB	5	4	4	3	4
C9QXZ2	Peptidyl-tRNA hydrolase	2	2	4		3
C9R119	50S ribosomal protein L19	2	7	6	7	5
C9QWS2	Glutamine amidotransferase of anthranilate synthase	2				2
C9QYX7	ADP-ribose diphosphatase	2	2			
C9QWL7	4-alpha-glucanotransferase	5	2	3	2	2
C9QPS4	Phosphoribosylglycinamide	2	2			

Protein Accession	Protein Description	Σ# Unique Peptides	# PSM (A)	# PSM (B)	# PSM (C)	# PSM (D)
	formyltransferase					
C9QVM0	Peptidase M16 domain protein	4			4	
C9QUR2	Mannitol-1-phosphate 5-dehydrogenase	4		2	2	
C9QR75	Ribonucleoside-diphosphate reductase	8	6	6	6	6
C9QS84	Thiamine ABC transporter, periplasmic binding protein	3	2			2
C9QSL4	Molecular chaperone Hsp31 and glyoxalase 3	4	11	15	9	9
C9QTU7	Glutamate dehydrogenase	5			5	
C9QWN2	33 kDa chaperonin	3			2	3
C9QR46	Naphthoate synthase	2		3		
C9QS56	Protein translocase subunit SecA	8	8	6	4	9
C9QUQ3	Glycerol-3-phosphate dehydrogenase [NAD(P)+]	3	3	2	3	3
C9QRM0	Methionine aminopeptidase	3		2	2	
C9QUP5	L-threonine 3-dehydrogenase	4	3	3		4
C9QS46	N-acetyl-anhydromuranmyl-L-alanine amidase	2				2
C9R164	Magnesium and cobalt efflux protein corC	3	2			2
C9QZJ3	MscS Mechanosensitive ion channel	3			3	
C9QVE2	Fructose-1,6-bisphosphatase	3	3	2		3
C9QUF6	LexA repressor	2		4	3	
C9QT85	Glucose-6-phosphate 1-dehydrogenase	6	6	5	4	6
C9QTK8	Peptide methionine sulfoxide reductase MsrA	2	2	3	2	
C9QSZ5	Mannonate dehydratase	4	3	4		3
C9QPP3	Cysteine desulfurase	4	4			4
C9QX48	Phage shock protein	2	3			2
C9QXW4	UTP--glucose-1-phosphate uridylyltransferase	3	4	4	4	3
C9QS74	Fructose repressor	3			2	2
C9QTJ5	UPF0307 protein YjgA	2	2	3	2	
C9QZE9	Beta-lactamase domain protein	2				2
C9QUW6	7-alpha-hydroxysteroid dehydrogenase	1	2			
C9QPZ3	Bifunctional protein FolD	4	2			4
C9QTV9	Exodeoxyribonuclease III	4			2	2
C9QQE9	Glucokinase	3	2		3	2
C9R124	Phospho-2-dehydro-3-deoxyheptonate aldolase	2	2			2
C9QZM3	Thiol:disulfide interchange protein	2	2			

Protein Accession	Protein Description	Σ# Unique Peptides	# PSM (A)	# PSM (B)	# PSM (C)	# PSM (D)
C9QZW9	ATP-dependent Clp protease, ATP-binding subunit clpA	8	6	4	2	6
C9QXP4	Glutathione S-transferase domain protein	2	2			
C9QW21	Gamma-aminobutyraldehyde dehydrogenase	5	2	4	6	4
C9QV58	Peptidase E	2			2	2
C9QSV9	Putative uncharacterized protein yjjA	2	2		2	2
C9QWJ5	Oxidoreductase domain protein	3	3		3	3
C9QR22	NADH-quinone oxidoreductase subunit C/D	6		5	4	
C9QY74	Argininosuccinate synthase	3	3			3
C9QQB6	Sulfate ABC transporter, periplasmic sulfate-binding protein	3	3			2
C9QR21	NADH-quinone oxidoreductase subunit B	2	2			2
C9QSG8	Histidinol-phosphate aminotransferase	3	3		2	4
C9QXL8	Acetyl CoA carboxylase	4	4	3		4
C9QUQ4	Serine O-acetyltransferase	2		3		
C9QZY1	L-threonine aldolase	3	3			
C9R148	Sigma E regulatory protein, MucB/RseB	3	2	3		
C9QT23	D-cysteine desulfhydrase	3			3	
C9QXV0	Potassium channel protein	3	2			2
C9QZU2	Cytidylate kinase	2				2
C9QZK8	Peptidase M24	4	6	3	2	6
C9QRC0	Nucleoid-associated protein YejK	3	3			3
C9QYV9	Bifunctional protein HldE	4		3	3	
C9QSQ9	Molybdenum cofactor synthesis domain protein	3		3	2	
C9QYI1	Adenylosuccinate lyase	4	7	6	5	7
C9QYJ2	NAD-dependent deacetylase	2	2	2	3	3
C9QU05	Phosphoenolpyruvate synthase	6	4		3	6
C9QS47	Nicotinate-nucleotide pyrophosphorylase	2	2			2
C9QR25	NADH-quinone oxidoreductase, chain G	8	4	9	6	4
C9QY68	Ribosomal RNA large subunit methyltransferase E	2	2	3		2
C9QSK6	Protein MtfA	2	2			
C9QSA0	4-hydroxythreonine-4-phosphate dehydrogenase	2			2	
C9QQ27	Putative thioredoxin domain-containing protein	2				2
C9QWL6	Phosphorylase	7	6		3	6

Protein Accession	Protein Description	Σ# Unique Peptides	# PSM (A)	# PSM (B)	# PSM (C)	# PSM (D)
C9R0D6	tRNA pseudouridine synthase D	3	2	2	2	2
C9R0A5	Putative uncharacterized protein ygcF	2				3
C9QXA6	Bifunctional protein GlmU	3		2	2	
C9QTH2	Probable cytosol aminopeptidase	3		4	3	
C9QZS9	Aldo/keto reductase	3	4			3
C9QYV6	Putative signal transduction protein	2			2	
C9QSZ7	FimH mannose-binding domain protein	2				2
C9QYM7	Ribonuclease E	7	6	8	6	6
C9QZ04	Putative uncharacterized protein yghA	2				2
C9QZT4	3-deoxy-manno-octulosonate cytidylyltransferase	2		3	2	2
C9QXE0	30S ribosomal protein S12	2	2	4	4	
C9QY07	Alanine racemase 1	3	2	3	2	2
C9R087	NADPH-dependent 7-cyano-7-deazaguanine reductase	2	2		2	
C9QSR6	Aspartate kinase	6	3	4	3	3
C9QWM6	Putative transcriptional accessory protein	5	5			5
C9QUW2	Adenosine deaminase	4	2		2	3
C9QZ47	Probable phosphatase YcdX	2	2			
C9QVE8	Triosephosphate isomerase	2	2			
C9QZ96	Histidine acid phosphatase	3	5	4		5
C9QWE8	Uroporphyrinogen-III synthase	2	3			
C9QUU7	Pyridoxal kinase	2				2
C9QX19	Universal stress protein E	2	2		3	
C9QZE4	Aminopeptidase N	7	4	2	6	4
C9QXR2	Exoribonuclease 2	5	3	5	3	3
C9QUZ3	ATP-dependent dethiobiotin synthetase BioD 1	2			3	
C9QPQ8	4-hydroxy-3-methylbut-2-en-1-yl diphosphate synthase	3	3			3
C9QRM8	5'-methylthioadenosine/S-adenosylhomocysteine nucleosidase	2	3	2		
C9QQM2	Amidophosphoribosyltransferase	7	4	2	7	4
C9QWP5	Putative uncharacterized protein damX	2			2	
C9R0N8	Cytochrome bd ubiquinol oxidase subunit I	4	8	12	5	8
C9R0M3	Phospho-2-dehydro-3-deoxyheptonate aldolase	2				2
C9QW96	DNA polymerase I	6	6	2	2	6
C9R0M0	Galactokinase	2	2	2	2	2

Protein Accession	Protein Description	Σ# Unique Peptides	# PSM (A)	# PSM (B)	# PSM (C)	# PSM (D)
C9R0V6	Glutamate--cysteine ligase	3	2	3	3	3
C9QVA0	UDP-N-acetylenolpyruvoylglucosamine reductase	2	2			
C9QQN8	Fructokinase	2			2	2
C9QUT3	N-ethylmaleimide reductase	2	2			2
C9R0L6	Transcriptional regulator ModE	2	2			
C9QTB9	Mannose permease IID component	2		2		
C9QST4	Lipoate-protein ligase A	2				2
C9QXN9	Protease Do	3			3	
C9QR24	NADH dehydrogenase I subunit F	3	2		2	2
C9QWB0	FMN reductase	2			2	
C9QYZ1	Binding protein	3	2	5	4	2
C9QSR2	UPF0246 protein yaaA	2	2			
C9QVX0	Putative uncharacterized protein ydeN	3		2	2	
C9QT42	Alpha,alpha-trehalose-phosphate synthase (UDP-forming)	3		4	2	
C9QY71	Phosphoglucosamine mutase	4	2	5	4	2
C9QZH2	Glutathione synthetase	2				2
C9QQ77	Peptidyl-prolyl cis-trans isomerase	4	2	2	2	2
C9QUG1	DNA polymerase III subunit beta	2		2		
C9R0J7	Putative transferase	2	2			
C9QSQ4	Chaperone protein DnaJ	2	3			2
C9QRS4	Dihydroorotate dehydrogenase family protein	4	2	5	2	2
C9QSE8	Regulatory protein GalF	3			2	3
C9QX77	Branched-chain amino acid aminotransferase	2	2	2		2
C9R138	rRNA methylase	2	2			2
C9R031	ABC transporter related protein	3	3		3	
C9QWU2	Putative uncharacterized protein ydcF	2	4	3		
C9QRF4	Gamma-glutamyl phosphate reductase	3	3			3
C9QQN9	Nonspecific DNA binding protein	3	2			2
C9QWK5	Glycogen synthase	2			2	
C9QYZ2	DNA topoisomerase 4 subunit A	5	4	3	2	4
C9QUE0	Excinuclease ABC, A subunit	6	4	4	6	4
C9QYM6	Pseudouridine synthase	2				2
C9QPZ6	Cysteine--tRNA ligase	4	6	6	5	6
C9QUG3	DNA gyrase subunit B	6	6	2	6	6
C9QRV5	Mrp protein	2	3			

Protein Accession	Protein Description	Σ# Unique Peptides	# PSM (A)	# PSM (B)	# PSM (C)	# PSM (D)
C9QUM2	Dfp	2		2		
C9QWP4	3-dehydroquinate synthase	2	2	4	4	3
C9QPZ9	N5-carboxyaminoimidazole ribonucleotide mutase	2	2	4	3	2
C9QTV4	Extracellular solute-binding protein family 1	2	2			2
C9QST2	Phosphoserine phosphatase	2			2	2
C9QQD0	DNA ligase	4	2	3	3	2
C9R171	Pyrimidine-specific ribonucleoside hydrolase RihA	2				2
C9QRK8	Acyl-[acyl-carrier-protein]--UDP-N-acetylglucosamine O-acyltransferase	2				2
C9R129	Pseudouridine synthase	2			2	
C9QVT1	Dipeptidyl carboxypeptidase II	4	2	3	2	2
C9QYD8	Putative S-transferase	2				3
C9QWK4	Glucose-1-phosphate adenylyltransferase	3		6		2
C9QSV0	Ribosomal RNA small subunit methyltransferase C	2			2	
C9QTJ0	Alpha,alpha-phosphotrehalase	4	5	6	6	5
C9QV95	Transcription antitermination protein nusG	2	3	7		5
C9R0Y2	Protein CsiD	2			2	
C9QV60	B12-dependent methionine synthase	7	5	4	6	5
C9QW13	Putative receptor	2				2
C9R0U2	N-acetylglucosamine repressor	2			2	
C9QVC2	Glycerol dehydrogenase	2	2	3		2
C9R050	Malate/L-lactate dehydrogenase	2			2	
C9QWH2	Cell division protein FtsY	4	4	2	3	4
C9QPS2	Exopolyphosphatase	3	2		2	2
C9QY08	D-amino acid dehydrogenase small subunit	2			2	
C9QQA4	Bifunctional diaminohydroxyphosphoribosylaminopyrimidine deaminase / 5-amino-6-(5-phosphoribosylamino) uracil reductase	2		2		
C9QSS3	Right origin-binding protein	2		2		
C9QWT0	ABC transporter related protein	3			3	
C9QY34	Glutamate synthase subunit beta	2	2			2
C9QTH6	GCN5-related N-acetyltransferase	2			2	2
C9QU48	Beta-lactamase	2				2
C9QWF0	HemY protein	2	2			2

Protein Accession	Protein Description	Σ# Unique Peptides	# PSM (A)	# PSM (B)	# PSM (C)	# PSM (D)
C9R0T8	Glutamine--tRNA ligase	3		2	3	
C9QTP6	Ribonuclease R	4	2		4	2
C9R1E3	Carboxylate-amine ligase YbdK	2	2			
C9QS78	2-isopropylmalate synthase	2		3		
C9QTW5	Periplasmic protein	2		3		
C9QZU7	Putative uncharacterized protein ycaO	3			3	
C9R150	GTP-binding protein LepA	3	2		3	2
C9QTQ1	FtsH protease regulator HflK	3	2		2	2
C9QYP9	Dihydroorotase	2				3
C9QYU5	RNA polymerase sigma factor	3	3			3
C9QVB2	Phosphoenolpyruvate carboxylase	5	4	12	10	5
C9QSG9	Histidinol dehydrogenase	2			2	
C9QPT0	Peptidase M48 Ste24p	2			2	
C9QXM7	Ribonuclease G	2			2	
C9QRL1	Outer membrane protein assembly factor BamA	4	3		3	4
C9QWK6	Phosphorylase	4	2	2	2	2
C9QSG2	Lipopolysaccharide biosynthesis protein	2	2			
C9QZF2	Chromosome partition protein MukB	8	6	5	5	8
C9QWK2	1,4-alpha-glucan branching enzyme GlgB	3			2	2
C9QXS7	DNA topoisomerase	4	3	4	3	3
C9QTJ4	Peptidase U62 modulator of DNA gyrase	3			3	
C9QUR9	Putative uncharacterized protein ydhQ	2	2		2	2
C9QXC9	tRNA modification GTPase MnmE	2	2			2
C9QS93	RNA polymerase-associated protein RapA	4	2	2		2
C9QTG9	YjgR protein	2			2	
C9QZV8	Anaerobic dimethyl sulfoxide reductase, A subunit, DmsA/YnfE family	3	3			3
C9QY69	ATP-dependent zinc metalloprotease FtsH	2			3	
C9R021	Extracellular solute-binding protein family 5	2				2
C9QRT6	D-lactate dehydrogenase	2		2		
C9QUP9	2,3-bisphosphoglycerate-independent phosphoglycerate mutase	2	3		3	3
C9QTE2	Dehydratase, YjhG/YagF family	2	2			2
C9QVU9	Altronate oxidoreductase	2	2			2

Protein Accession	Protein Description	Σ# Unique Peptides	# PSM (A)	# PSM (B)	# PSM (C)	# PSM (D)
C9QVC7	Aspartate kinase	3	3			3
C9QSW9	DNA methylase M	2	2		2	2
C9QUX2	Putative uncharacterized protein ydgA	2			2	2
C9QVY9	NAD-dependent malic enzyme	2	2	2		2
C9QYT2	2,4-dienoyl-CoA reductase, NADH and FMN-linked	2	2			2
C9QUR3	Fused mannitol-specific PTS enzymes: IIA components/IIB components/IIC components	2	2			2
C9QPR2	GTPase Der	2	2		3	2
C9QXD0	Membrane protein insertase YidC	2		3		
C9QX76	Dihydroxy-acid dehydratase	2	2			2
C9QWD9	DNA helicase II	2			2	
C9QTN8	Acyl-CoA dehydrogenase domain protein	2			3	
C9QSB9	Carbamoyl-phosphate synthase large chain	3	3			3
C9R079	L-fucose isomerase	2			2	
C9R0U1	N-acetylglucosamine-6-phosphate deacetylase	2	2			2
C9QQ98	1-deoxy-D-xylulose-5-phosphate synthase	2	2			2
C9QWX8	Pyruvate-flavodoxin oxidoreductase	4	3	3	3	3
C9QRK3	Lysine decarboxylase	2	2			2
C9QVX6	Glutamate/g-aminobutyrate antiporter	2	5			6
C9QVF3	Selenocysteine-specific translation elongation factor	2	2			2
C9QVN3	Multidrug transporter, RpoS-dependent	3	2		3	2
C9QWU3	ATP-dependent RNA helicase HrpA	3	2		2	2
C9QQ57	Multidrug efflux system protein	2			4	
C9R063	Peptidase M16 domain protein	2	2			2
C9QW63	Formate dehydrogenase, alpha subunit	2	2			2

Table A2: All proteins identified in Chapter 5 (N = 3). Proteins are listed with total spectral counts (PSM), as well as the mean normalized spectral hit (NSpH) value ± standard deviation and the quasi-Poisson *p*-value associated with the protein following analysis. * Indicates the protein is significantly altered in abundance (*p*-value < 0.05).

Protein Accession	Protein Description	Σ# PSMs Total	Stretched NSpH ± SD	Control NSpH ± SD	p-value
D4A3S8 *	NOL1/NOP2/Sun domain family, member 2 (Predicted)	10	0 ± 0	2 ± 0	3.76E-54
D3ZKG3 *	Protein Sec14l1	6	0 ± 0	1 ± 0	1.20E-52
F1M0Z9 *	Protein Msi2 (Fragment)	6	0 ± 0	1 ± 0	1.20E-52
Q99J86 *	Attractin	5	0 ± 0	1 ± 0	1.20E-52
O35806 *	Latent-transforming growth factor beta-binding protein 2	5	0 ± 0	1 ± 0	1.20E-52
P61515 *	Putative 60S ribosomal protein L37a	5	0 ± 0	1 ± 0	1.20E-52
B1H257 *	Loss of heterozygosity, 12, chromosomal region 1 homolog (Human)	6	0 ± 0	1 ± 0	1.20E-52
Q5U204 *	Ragulator complex protein LAMTOR3	7	1 ± 0	0 ± 0	1.20E-52
D4A9I3 *	Calcium channel flower homolog	6	1 ± 0	0 ± 0	1.20E-52
D3ZDF0 *	Neuroplastin	6	1 ± 0	0 ± 0	1.20E-52
D3ZBP3 *	Exosome component 2 (Predicted)	6	1 ± 0	0 ± 0	1.20E-52
Q811S9 *	Guanine nucleotide-binding protein-like 3	22	3.5 ± 1	0 ± 0	8.86E-08
B5DFC3 *	Protein Sec23a	12	0 ± 0	2 ± 0.5	1.22E-07
G3V939 *	Protein Krt82	13	2.2 ± 0.8	0 ± 0	3.59E-07
Q641W4 *	Replication factor C subunit 2	8	0 ± 0	1 ± 0.5	9.87E-07
B2RYP3 *	Fam91a1 protein	10	0 ± 0	1 ± 0.5	9.87E-07
Q63377 *	Sodium/potassium-transporting ATPase subunit beta-3	98	12.2 ± 1.5	5 ± 1.2	3.44E-06
Q562C7 *	Pumilio domain-containing protein KIAA0020 homolog	10	1.7 ± 0.8	0 ± 0	8.29E-06
Q5U2S1 *	NEDD4 family-interacting protein 1	10	1.7 ± 0.8	0 ± 0	8.29E-06
A0JPQ9 *	Chitinase domain-containing protein 1	13	0 ± 0	2 ± 1	1.83E-05
G3V878 *	Sec11-like 3 (S. cerevisiae), isoform CRA_c	9	1.5 ± 0.8	0 ± 0	2.56E-05
Q5FVH2 *	Phospholipase D3	45	5.5 ± 1.4	2 ± 0.5	2.57E-05

G3V9U0 *	Acyl-CoA synthetase short-chain family member 2 (Predicted)	31	1 ± 0.6	4 ± 0.8	4.55E-05
Q794F9 *	4F2 cell-surface antigen heavy chain	239	30.5 ± 7.1	11 ± 3	4.65E-05
M0RCJ8 *	Protein Krt78	42	6.8 ± 2.8	1 ± 0.5	5.30E-05
D4A1N9 *	Peptidyl-glycine alpha-amidating monooxygenase	91	10.7 ± 2.1	5 ± 0.9	5.34E-05
Q62920 *	PDZ and LIM domain protein 5	10	0 ± 0	1 ± 0.8	5.64E-05
Q6AYE2 *	Endophilin-B1	6	0 ± 0	1 ± 0.6	7.36E-05
Q78P75 *	Dynein light chain 2, cytoplasmic	7	1 ± 0.6	0 ± 0	7.36E-05
F6Q5K7 *	Mitochondrial ribosomal protein S18B, isoform CRA_a	6	1 ± 0.6	0 ± 0	7.36E-05
Q6P9V7 *	Proteasome (Prosome, macropain) activator subunit 1	8	0 ± 0	1 ± 0.8	8.67E-05
Q5M9I5 *	Cytochrome b-c1 complex subunit 6, mitochondrial	8	0 ± 0	1 ± 0.8	8.67E-05
F1M9A7 *	Acyl-coenzyme A oxidase	9	1.2 ± 0.8	0 ± 0	8.67E-05
D3ZUY8 *	Adaptor protein complex AP-2, alpha 1 subunit (Predicted)	36	0.2 ± 0.4	5 ± 2.2	9.34E-05
G3V8Y8 *	Huntingtin interacting protein 1, isoform CRA_a	52	1.7 ± 1.2	7 ± 1.3	1.04E-04
Q68FQ0 *	T-complex protein 1 subunit epsilon	60	7.5 ± 0.5	3 ± 1.3	1.27E-04
D3ZZL3 *	Protein Naglu	23	0.5 ± 0.5	3 ± 0.8	1.45E-04
F1M5K3 *	Uncharacterized protein	9	1.5 ± 1	0 ± 0	1.65E-04
P31232 *	Transgelin	13	0 ± 0	2 ± 1.4	1.81E-04
P67779 *	Prohibitin	156	16.5 ± 2.4	10 ± 1.4	2.14E-04
B2GUZ5 *	F-actin-capping protein subunit alpha-1	38	1 ± 0	5 ± 2.5	2.38E-04
P62982 *	Ubiquitin-40S ribosomal protein S27a	469	45.2 ± 5.1	34 ± 0.8	2.44E-04
Q9JHE5 *	Sodium-coupled neutral amino acid transporter 2	68	8.3 ± 2	3 ± 1.2	2.93E-04
P24268 *	Cathepsin D	55	2 ± 1.1	7 ± 2.2	3.21E-04
Q63707 *	Dihydroorotate dehydrogenase (quinone), mitochondrial	32	1.3 ± 0.5	4 ± 1.3	3.56E-04
E9PSX3 *	Protein RT1-A2	9	0 ± 0	1 ± 1	3.65E-04
G3V9S9 *	Protein Sec24d	8	0 ± 0	1 ± 1	3.65E-04
G3V616 *	Divalent cation tolerant protein CUTA, isoform CRA_b	9	1.3 ± 1	0 ± 0	3.65E-04

P15650 *	Long-chain specific acyl-CoA dehydrogenase, mitochondrial	45	1.5 ± 0.8	6 ± 2.2	3.82E-04
Q66HD0 *	Endoplasmin	1056	69 ± 10.3	111 ± 17.7	4.00E-04
P62907 *	60S ribosomal protein L10a	167	19.8 ± 4.4	9 ± 2.9	4.04E-04
P04762 *	Catalase	87	3.7 ± 1	10 ± 3.3	4.69E-04
G3V6S2 *	Cytoplasmic aconitate hydratase	12	0 ± 0	2 ± 1.5	4.78E-04
B0BNB9 *	HtrA serine peptidase 2	11	0 ± 0	2 ± 1.4	5.57E-04
F7FL00 *	Carbonic anhydrase 9 (Predicted), isoform CRA_a	20	0.3 ± 0.5	3 ± 1.1	5.76E-04
D4A031 *	DEAD (Asp-Glu-Ala-Asp) box polypeptide 42 (Predicted)	8	0 ± 0	1 ± 1	6.82E-04
D3ZYI0 *	Grancalcin (Predicted)	8	1.2 ± 1	0 ± 0	6.82E-04
Q3KR86 *	Mitochondrial inner membrane protein (Fragment)	190	21.5 ± 5.2	11 ± 2.5	8.17E-04
M0R911 *	Protein Gm10108	15	0 ± 0	1 ± 0.9	1.04E-03
Q5U3Y8 *	Basic transcription factor 3	7	0 ± 0	1 ± 0.9	1.04E-03
P04904 *	Glutathione S-transferase alpha-3	7	1 ± 0.9	0 ± 0	1.04E-03
G3V9T7 *	ATPase Asna1	7	1 ± 0.9	0 ± 0	1.04E-03
Q5BK32 *	FAS-associated factor 2	7	1 ± 0.9	0 ± 0	1.04E-03
Q62848 *	ADP-ribosylation factor GTPase-activating protein 1	6	0 ± 0	1 ± 0.9	1.04E-03
P63322 *	Ras-related protein Ral-A	7	0 ± 0	1 ± 0.9	1.04E-03
P52631 *	Signal transducer and activator of transcription 3	6	0 ± 0	1 ± 0.9	1.04E-03
Q7M0E7 *	39S ribosomal protein L14, mitochondrial	8	0 ± 0	1 ± 0.9	1.04E-03
G3V6P8 *	Guanine nucleotide-binding protein subunit gamma	7	0 ± 0	1 ± 0.9	1.04E-03
P31044 *	Phosphatidylethanolamine-binding protein 1	55	6.2 ± 1.6	3 ± 0.5	1.05E-03
P06685 *	Sodium/potassium-transporting ATPase subunit alpha-1	686	67.8 ± 7.3	53 ± 4.1	1.10E-03
M0RBF0 *	Scaffold attachment factor B1	9	0 ± 0	1 ± 1.2	1.16E-03
P51639 *	3-hydroxy-3-methylglutaryl-coenzyme A reductase	9	0 ± 0	2 ± 1.4	1.26E-03
D3ZZZ9 *	Catenin (Cadherin associated protein), delta 1 (Predicted), isoform CRA_a	94	4.2 ± 1.5	11 ± 3.6	1.28E-03

Q9QZ86 *	Nucleolar protein 58	113	13.5 ± 3.2	6 ± 2.5	1.32E-03
O70509 *	CD44 antigen	24	3.3 ± 0.8	1 ± 0.8	1.32E-03
P62282 *	40S ribosomal protein S11	27	0.8 ± 1	4 ± 0.5	1.49E-03
G3V8L3 *	Lamin A, isoform CRA_b	920	93.5 ± 7.3	65 ± 13.9	1.80E-03
P18484 *	AP-2 complex subunit alpha-2	45	1.8 ± 0.8	6 ± 2.5	1.90E-03
G3V9I0 *	Procollagen-lysine,2-oxoglutarate 5-dioxygenase 2	203	12.8 ± 2.8	22 ± 4.6	1.91E-03
P18421 *	Proteasome subunit beta type-1	43	2.7 ± 1.2	5 ± 0.4	2.18E-03
Q6P9V1 *	CD81 antigen	109	7.3 ± 1.5	11 ± 1.7	2.19E-03
P29117 *	Peptidyl-prolyl cis-trans isomerase F, mitochondrial	7	0 ± 0	1 ± 1.2	2.25E-03
F1M0X7 *	Protein Ckap5	8	0 ± 0	1 ± 1.2	2.25E-03
P70584 *	Short/branched chain specific acyl-CoA dehydrogenase, mitochondrial	8	0 ± 0	1 ± 1.2	2.25E-03
D3ZAN3 *	Alpha glucosidase 2 alpha neutral subunit (Predicted)	109	7.2 ± 1.3	12 ± 2.4	2.50E-03
P35565 *	Calnexin	173	10.5 ± 1.9	19 ± 5.3	2.55E-03
D3ZFP4 *	Protein Mcm3	19	0.3 ± 0.5	3 ± 1.6	2.58E-03
B2RYJ7 *	ARP1 actin-related protein 1 homolog B (Yeast)	20	0.5 ± 0.5	3 ± 1.5	2.59E-03
A4KWA5 *	C-type lectin domain family 2 member D2	9	0 ± 0	1 ± 1.4	2.60E-03
F1LTU4 *	Protein Mrto4	10	1.3 ± 1.4	0 ± 0	2.60E-03
Q05962 *	ADP/ATP translocase 1	17	0 ± 0	3 ± 2.9	2.74E-03
Q5XIE8 *	Integral membrane protein 2B	37	4.7 ± 2.4	1 ± 0.8	2.80E-03
F1LTX4 *	Protein Lrrn4	148	7 ± 3.2	18 ± 6.7	2.83E-03
G3V679 *	Transferrin receptor protein 1	240	24.3 ± 3.3	17 ± 3.1	3.15E-03
D4A3I4 *	Protein Btf3l4	12	0 ± 0	2 ± 1.9	3.20E-03
Q6IFV6 *	Protein Krt35	15	2.5 ± 2.7	0 ± 0	3.34E-03
E2RUH2 *	Protein LOC100360501	76	4.2 ± 1.6	9 ± 2.6	3.34E-03
D3ZJX5 *	Protein Timm50	67	2.7 ± 1.5	7 ± 2.7	3.41E-03
P85515 *	Alpha-centractin	40	1.7 ± 1	5 ± 2	3.42E-03
Q6RJR6 *	Reticulon-3	51	5.3 ± 1.9	3 ± 0.5	3.44E-03
Q6IRJ7 *	Annexin	88	10.2 ± 2.9	5 ± 1.9	3.56E-03

P10888 *	Cytochrome c oxidase subunit 4 isoform 1, mitochondrial	35	1.3 ± 0.8	5 ± 2.2	3.75E-03
Q5XI77 *	Annexin	123	13.7 ± 3.5	7 ± 2.5	3.77E-03
B5DFM8 *	Breast carcinoma amplified sequence 2	39	4.8 ± 1.5	2 ± 1.2	3.78E-03
Q641Z4 *	Cyclin-dependent kinase 9	16	0.7 ± 0.5	2 ± 0.6	3.88E-03
D4A554 *	Eukaryotic translation initiation factor 4 gamma, 3 (Predicted), isoform CRA_a	7	0 ± 0	1 ± 1.1	3.95E-03
M0R3Z8 *	Protein Rbm15	7	0 ± 0	1 ± 1.1	3.95E-03
P70582 *	Nuclear pore complex protein Nup54	8	1 ± 1.1	0 ± 0	3.95E-03
M0RB67 *	Protein Ppidl1	7	1 ± 1.1	0 ± 0	3.95E-03
P17164 *	Tissue alpha-L-fucosidase	7	0 ± 0	1 ± 1.1	3.95E-03
Q920D2 *	Dihydrofolate reductase	7	0 ± 0	1 ± 1.1	3.95E-03
P08461 *	Dihydrolipoyllysine-residue acetyltransferase component of pyruvate dehydrogenase complex, mitochondrial	87	9.8 ± 1.7	5 ± 2.4	4.25E-03
P07153 *	Dolichyl-diphosphooligosaccharide--protein glycosyltransferase subunit 1	228	24.3 ± 3.8	15 ± 4.6	4.30E-03
G3V9V9 *	Cysteine and glycine-rich protein 2	33	1.7 ± 1	4 ± 0.8	4.42E-03
Q5XIF0 *	Protein Tex264	26	3.3 ± 1.6	1 ± 0.6	4.53E-03
D4A436 *	Integrin beta	48	2.2 ± 1.7	6 ± 1.2	4.74E-03
F1LMV6 *	Protein Dsp	8	1.3 ± 1.5	0 ± 0	4.75E-03
Q5FVL6 *	Tetraspanin-13	7	0 ± 0	1 ± 1.3	5.01E-03
M0RA08 *	Protein Plin3	7	0 ± 0	1 ± 1.3	5.01E-03
Q6IG02 *	Keratin, type II cytoskeletal 2 epidermal	24	0.3 ± 0.5	4 ± 2.9	5.07E-03
P13803 *	Electron transfer flavoprotein subunit alpha, mitochondrial	69	4.3 ± 0.8	7 ± 2.1	5.12E-03
P00787 *	Cathepsin B	77	3.3 ± 1	10 ± 5.1	5.12E-03
D3ZMS1 *	Protein Sf3b2	18	2.3 ± 1.4	0 ± 0.5	5.20E-03
P80254 *	D-dopachrome decarboxylase	15	1 ± 0	2 ± 0.5	5.23E-03
D4A7I8 *	Protein Sumf1	15	1.7 ± 0.5	1 ± 0	5.23E-03
Q5RKI0 *	WD repeat-containing protein 1	36	3.5 ± 0.8	2 ± 0.6	5.49E-03

M0RAR9 *	Uncharacterized protein (Fragment)	49	6 ± 2	2 ± 1.5	5.75E-03
D4A133 *	Protein Atp6v1a	110	12.7 ± 3.8	6 ± 2.6	5.82E-03
Q6IMF3 *	Keratin, type II cytoskeletal 1	1171	117.3 ± 15.3	85 ± 16.7	5.86E-03
F1LN70 *	Uncharacterized protein	14	0.3 ± 0.5	2 ± 0.5	5.89E-03
M0R4Z0 *	Protein Cbx1	10	0 ± 0	2 ± 1.8	5.97E-03
M0RCH8 *	Uncharacterized protein	101	11.7 ± 3.8	6 ± 2.3	6.02E-03
Q5U362 *	Annexin	171	18 ± 3	11 ± 3.4	6.02E-03
Q4QQV0 *	Protein Tubb6	116	4.2 ± 4.4	15 ± 6	6.51E-03
Q02769 *	Squalene synthase	81	5.2 ± 1	8 ± 1.7	6.57E-03
Q4QRB4 *	Tubulin beta-3 chain	62	0 ± 0	11 ± 12.6	6.83E-03
D3ZZV1 *	Mitochondrial import inner membrane translocase subunit TIM16	21	2.3 ± 1.2	1 ± 0.5	6.97E-03
F1M013 *	Protein LOC100910109 (Fragment)	217	23.7 ± 5.7	14 ± 4.7	7.18E-03
Q6AYS3 *	Protective protein for beta-galactosidase	16	0.3 ± 0.5	2 ± 1.1	7.19E-03
Q5XIN6 *	LETM1 and EF-hand domain-containing protein 1, mitochondrial	50	5.7 ± 1.8	3 ± 1.2	7.25E-03
F1M953 *	Stress-70 protein, mitochondrial	599	66 ± 5.4	38 ± 17.3	7.26E-03
P05964 *	Protein S100-A6	198	20.3 ± 7.2	11 ± 1.9	7.32E-03
D3ZKW6 *	Protein Upk3b	36	1.3 ± 1.5	5 ± 1.4	7.39E-03
P35280 *	Ras-related protein Rab-8A	24	2.7 ± 1.5	1 ± 0	7.60E-03
P39951 *	Cyclin-dependent kinase 1	20	0.7 ± 0.5	3 ± 1.6	7.76E-03
F1LQC1 *	Acyl-coenzyme A oxidase	260	30.7 ± 8.8	15 ± 7.5	7.94E-03
P07943 *	Aldose reductase	223	22.8 ± 2.6	16 ± 4.4	8.12E-03
G3V8I4 *	Syntaxin 4A (Placental), isoform CRA_a	17	0.5 ± 0.5	2 ± 0.8	8.43E-03
Q5XIV1 *	Phosphoglycerate kinase	15	2.7 ± 3.3	0 ± 0	8.44E-03
P07824 *	Arginase-1	22	1.3 ± 0.5	2 ± 0.5	8.76E-03
P00507 *	Aspartate aminotransferase, mitochondrial	485	46.7 ± 2.1	37 ± 6.9	8.87E-03
Q66HA7 *	Core-binding factor, beta subunit	16	0.7 ± 0.5	2 ± 0.9	8.95E-03
G3V640 *	Mitochondrial import inner membrane translocase subunit TIM44	10	0 ± 0	1 ± 1.5	8.98E-03
P39052 *	Dynamin-2	9	0 ± 0	1 ± 1.5	8.98E-03

P63004 *	Platelet-activating factor acetylhydrolase IB subunit alpha	8	0 ± 0	1 ± 1.5	8.98E-03
D3ZGM1 *	Protein Ptcd3	29	3.2 ± 1.5	1 ± 0.5	9.01E-03
F1LXV0 *	Ribosomal protein S6 kinase	7	0 ± 0	1 ± 1.3	9.11E-03
D4A2F1 *	Agrin	6	0 ± 0	1 ± 1.3	9.11E-03
G3V7L8 *	ATPase, H+ transporting, V1 subunit E isoform 1, isoform CRA_a	63	8.2 ± 4.9	3 ± 1.4	9.18E-03
Q5PQJ6 *	Pyrroline-5-carboxylate reductase 3	13	0.3 ± 0.5	2 ± 1	9.25E-03
B0BN82 *	Brix domain containing 1	23	2 ± 0.9	1 ± 0	9.61E-03
Q99MZ8 *	LIM and SH3 domain protein 1	37	2 ± 0.9	4 ± 1.5	9.74E-03
M0RDM4 *	Histone H2A	505	54.3 ± 13.8	32 ± 10.2	9.86E-03
M0R6K0 *	Laminin subunit beta-2	58	2.2 ± 1.8	8 ± 4	1.01E-02
D3ZLL8 *	Protein LOC100909878	51	6.3 ± 2.9	2 ± 1.5	1.06E-02
Q6AXM8 *	Serum paraoxonase/arylesterase 2	23	1.2 ± 0.8	3 ± 0.8	1.06E-02
Q62967 *	Diphosphomevalonate decarboxylase	58	3.5 ± 1.2	6 ± 1.7	1.06E-02
D3ZQI1 *	Glutathione peroxidase	44	1.7 ± 1.5	6 ± 2.9	1.06E-02
D3ZM57 *	Golgi integral membrane protein 4	21	0.7 ± 0.5	2 ± 1.4	1.07E-02
O88775 *	Embigin	27	3.5 ± 1.9	1 ± 0.9	1.07E-02
Q9Z270 *	Vesicle-associated membrane protein-associated protein A	113	12.5 ± 2.9	7 ± 2.9	1.08E-02
Q7TP15 *	S-methyl-5'-thioadenosine phosphorylase	19	1 ± 0	2 ± 0.8	1.11E-02
Q32PX2 *	Aminoacyl tRNA synthase complex-interacting multifunctional protein 2	15	0.5 ± 0.5	2 ± 1.1	1.12E-02
F1LML0 *	Protein Nars	25	3 ± 2.2	1 ± 0.5	1.12E-02
Q62812 *	Myosin-9	297	8.2 ± 9	34 ± 19.8	1.19E-02
P61589 *	Transforming protein RhoA	165	10.7 ± 3.8	17 ± 3.5	1.25E-02
Q5XI01 *	La-related protein 7	22	3 ± 1.3	1 ± 1	1.26E-02
P17220 *	Proteasome subunit alpha type-2	19	2.3 ± 0.8	1 ± 0.8	1.26E-02
Q4V898 *	RNA-binding motif protein, X chromosome	115	14 ± 2.9	6 ± 4.8	1.27E-02
D3ZRM5 *	Protein Rab23	26	1.3 ± 0.5	3 ± 1	1.31E-02
Q62733 *	Lamina-associated polypeptide 2, isoform beta	39	2 ± 1.3	5 ± 1.5	1.32E-02

Q08163 *	Adenylyl cyclase-associated protein 1	69	7.8 ± 2.1	4 ± 2.1	1.33E-02
D4AD70 *	Protein RGD1561636	51	6.5 ± 2.4	2 ± 2.1	1.35E-02
F1MA98 *	Nucleoprotein TPR	31	1.5 ± 0.5	4 ± 2	1.35E-02
D3Z9F2 *	Protein Ccdc96	7	0 ± 0	1 ± 1.6	1.40E-02
I6L9G6 *	Protein Tardbp	8	0 ± 0	1 ± 1.6	1.40E-02
M0R660 *	Protein RGD1565368	824	36.3 ± 28.9	104 ± 49.9	1.42E-02
P63036 *	DnaJ homolog subfamily A member 1	50	5.5 ± 1.6	3 ± 1.3	1.44E-02
Q9QXQ0 *	Alpha-actinin-4	542	40.7 ± 4.7	52 ± 8.2	1.51E-02
Q5M7W5 *	Microtubule-associated protein 4	24	0.3 ± 0.5	3 ± 3.3	1.52E-02
G3V9U2 *	3-ketoacyl-CoA thiolase, mitochondrial	31	1.7 ± 0.8	4 ± 1.4	1.56E-02
Q5U317 *	Pre-mRNA 3'-end-processing factor FIP1	18	2 ± 0	1 ± 0.8	1.60E-02
P00388 *	NADPH--cytochrome P450 reductase	98	11 ± 1.9	6 ± 3.5	1.60E-02
F1LN92 *	Protein Afg3l2	20	2.7 ± 0.8	1 ± 1	1.62E-02
D4AE41 *	RNA binding motif protein, X-linked-like-1	125	14 ± 2.9	8 ± 4.1	1.63E-02
P26453 *	Basigin	90	5.7 ± 2.3	10 ± 2.1	1.64E-02
D4A0C3 *	Protein Hid1	14	0.5 ± 0.8	2 ± 0	1.66E-02
Q3KRD8 *	Eukaryotic translation initiation factor 6	34	3.5 ± 0.8	2 ± 0.8	1.67E-02
B0BMT9 *	Protein Sqrdl	167	11 ± 3.9	18 ± 3.7	1.69E-02
P14668 *	Annexin A5	232	26.7 ± 10.9	13 ± 5.9	1.72E-02
D3ZIE9 *	Protein Aldh18a1	58	6.5 ± 2.8	3 ± 1	1.73E-02
F1M5V2 *	Protein Glipr2	44	5.2 ± 2.2	3 ± 1	1.73E-02
F1M4A0 *	Protein Tjp1	71	4.2 ± 1.9	8 ± 2.5	1.75E-02
G3V681 *	Protein Mcm4	25	0.7 ± 0.8	4 ± 2.7	1.76E-02
Q2I6B2 *	V-H+ATPase subunit a1-III	17	0.7 ± 0.8	2 ± 0.8	1.82E-02
Q64119 *	Myosin light polypeptide 6	283	20.5 ± 2.7	28 ± 6.1	1.88E-02
Q641Z8 *	Peflin	23	2.8 ± 0.8	1 ± 1.1	1.88E-02
F1M4T3 *	Protein Erh (Fragment)	10	0.3 ± 0.5	1 ± 0.5	1.96E-02
F1LT78 *	Protein Antxr2	10	1.3 ± 0.5	0 ± 0.5	1.96E-02

Q66HF1 *	NADH-ubiquinone oxidoreductase 75 kDa subunit, mitochondrial	56	6.5 ± 2.4	3 ± 1.7	2.00E-02
P45592 *	Cofilin-1	204	14.2 ± 2.3	21 ± 5.5	2.02E-02
G3V6E4 *	Acyl-Coenzyme A binding domain containing 3	27	0.8 ± 1.3	4 ± 1.9	2.06E-02
P63018 *	Heat shock cognate 71 kDa protein	1205	116.8 ± 13.4	91 ± 18.4	2.14E-02
Q9EQR2 *	Alkyldihydroxyacetonephosphate synthase, peroxisomal	26	3 ± 0.9	1 ± 1	2.15E-02
Q6MG60 *	N(G),N(G)-dimethylarginine dimethylaminohydrolase 2	15	0.7 ± 0.5	2 ± 1	2.21E-02
Q6B345 *	Protein S100-A11	40	5.5 ± 4.3	1 ± 1.2	2.24E-02
D3ZGE6 *	Protein Cttn	87	9 ± 2.4	7 ± 0.5	2.24E-02
B5DEK0 *	Protein Rprd1b	15	0.5 ± 0.8	2 ± 0.6	2.28E-02
D4A4D5 *	Protein LOC100362751	233	23.5 ± 5	17 ± 3.6	2.28E-02
F1LQ82 *	E3 ubiquitin-protein ligase NEDD4 (Fragment)	18	2.3 ± 1.2	1 ± 0.8	2.28E-02
D4A8P9 *	Protein Iars2	14	0.3 ± 0.5	2 ± 1.7	2.29E-02
G3V6L8 *	RCG61894, isoform CRA_a	16	0.3 ± 0.5	2 ± 1.7	2.29E-02
M0R3R6 *	Protein LOC100911677	89	9.8 ± 3.9	5 ± 2.1	2.45E-02
P04961 *	Proliferating cell nuclear antigen	98	6.2 ± 2	11 ± 3.9	2.45E-02
Q6AY21 *	GTPase activating protein (SH3 domain) binding protein 2	19	2.3 ± 0.5	1 ± 1	2.48E-02
D4A9U4 *	Elastin	8	0 ± 0	1 ± 2.1	2.50E-02
B2GV72 *	Carbonyl reductase 3	6	1 ± 1.5	0 ± 0	2.50E-02
D3ZHA7 *	Protein LOC100359980	12	0 ± 0	2 ± 3.1	2.50E-02
F1LLW7 *	Dehydrogenase/reductase SDR family member 9	12	1.7 ± 1.2	0 ± 0.5	2.50E-02
P14669 *	Annexin A3	353	38.8 ± 17.9	21 ± 4.3	2.52E-02
D3ZH41 *	Cytoskeleton-associated protein 4 (Predicted)	370	36 ± 5.4	27 ± 5.9	2.57E-02
Q9ER24 *	Ataxin-10	12	0 ± 0	2 ± 2.9	2.57E-02
M0R7A4 *	Uncharacterized protein (Fragment)	9	1.5 ± 2.3	0 ± 0	2.61E-02
D4A0W7 *	Protein Fndc3b	9	0 ± 0	2 ± 2.3	2.61E-02
Q6IG03 *	Keratin, type II cytoskeletal 73	40	7.5 ± 11.7	0 ± 0	2.61E-02
Q642B0 *	Glypican 4	69	3.8 ± 1	8 ± 4.2	2.61E-02

Q63151 *	Long-chain-fatty-acid--CoA ligase 3	36	4 ± 1.5	2 ± 1.1	2.62E-02
D3ZSY5 *	Protein Krt84	7	1.2 ± 1.8	0 ± 0	2.68E-02
Q6P7P5 *	Basic leucine zipper and W2 domain-containing protein 1	7	0 ± 0	1 ± 1.8	2.68E-02
E9PTK8 *	Protein Lmo7	155	10.8 ± 2.9	16 ± 3.8	2.69E-02
B0BMV6 *	Receptor-interacting serine-threonine kinase 3	40	1.8 ± 1.6	5 ± 2.3	2.71E-02
P27008 *	Poly [ADP-ribose] polymerase 1	79	4.5 ± 2.1	9 ± 3.6	2.74E-02
D3ZPR0 *	Chromosome segregation 1-like (S. cerevisiae) (Predicted)	64	3.2 ± 1.5	6 ± 1.9	2.75E-02
G3V7L9 *	Leucine zipper protein 1	14	0.7 ± 0.5	2 ± 0.8	2.76E-02
P63245 *	Guanine nucleotide-binding protein subunit beta-2-like 1	130	7.8 ± 0.8	13 ± 5	2.77E-02
Q66HA6 *	ADP-ribosylation factor-like protein 8B	33	3.5 ± 1	2 ± 0.8	2.79E-02
Q4QR81 *	Protein Rbms2	13	0.7 ± 0.5	2 ± 0.5	2.81E-02
P54921 *	Alpha-soluble NSF attachment protein	52	5.3 ± 1.6	4 ± 0.8	2.82E-02
Q91Y81 *	Septin-2	112	7 ± 3.2	12 ± 3.5	2.90E-02
D4A465 *	Protein Lamtor2	16	0.2 ± 0.4	2 ± 2.2	2.93E-02
D3ZQ74 *	Procollagen-lysine, 2-oxoglutarate 5-dioxygenase 1	132	9.2 ± 1.5	12 ± 2.8	2.96E-02
Q6AY30 *	Saccharopine dehydrogenase-like oxidoreductase	15	2 ± 0.9	1 ± 0.8	2.96E-02
D4A3J1 *	Protein RGD1309079	13	0.5 ± 0.5	2 ± 1	2.97E-02
G3V9D0 *	Protein Poglut1	11	0.3 ± 0.5	2 ± 1	3.11E-02
Q4FZU6 *	Annexin A8	11	1.5 ± 1	0 ± 0.5	3.11E-02
P11348 *	Dihydropteridine reductase	22	1.2 ± 1	3 ± 0.5	3.12E-02
Q5XI86 *	Peptidyl-tRNA hydrolase 2	68	7.7 ± 3.4	4 ± 1.7	3.14E-02
M0R7Q6 *	Uncharacterized protein	19	1 ± 0.6	2 ± 1	3.15E-02
D3ZD11 *	Protein Spcs2	14	1.8 ± 1.3	1 ± 0.5	3.18E-02
Q4KLK7 *	Nucleolar protein 5A	143	15 ± 5.5	9 ± 2.3	3.22E-02
O35821 *	Myb-binding protein 1A	243	24 ± 5.9	18 ± 2.4	3.29E-02
F7ELI0 *	Protein Drg1	39	2.3 ± 1.4	4 ± 1	3.32E-02
Q5XI78 *	2-oxoglutarate dehydrogenase, mitochondrial	24	1.3 ± 0.8	3 ± 1	3.38E-02

B2RYC9 *	Gba protein	72	7.2 ± 1.2	5 ± 1.4	3.44E-02
Q4AEF8 *	Coatomer subunit gamma-1	62	3.2 ± 1.8	7 ± 3.9	3.49E-02
F1LPI5 *	Laminin, beta 3, isoform CRA_a	6	0 ± 0	1 ± 1.7	3.50E-02
Q1EG89 *	Myocardial ischemic preconditioning associated protein 7	6	0 ± 0	1 ± 1.7	3.50E-02
Q5HZV9 *	Protein phosphatase 1 regulatory subunit 7	6	0 ± 0	1 ± 1.7	3.50E-02
G3V9G4 *	ATP citrate lyase, isoform CRA_b	625	43.3 ± 16.2	63 ± 9.8	3.60E-02
A0JPJ7 *	Obg-like ATPase 1	16	0.3 ± 0.5	2 ± 2.5	3.67E-02
B2GV01 *	Metastasis-associated gene family, member 2	28	3 ± 1.1	2 ± 0.8	3.69E-02
D4ACA5 *	Protein LOC100911130	15	0.5 ± 0.8	2 ± 1.1	3.70E-02
F7ENH8 *	Histone deacetylase	26	3 ± 0.9	1 ± 1.2	3.71E-02
Q6IFW6 *	Keratin, type I cytoskeletal 10	124	14 ± 5.1	7 ± 4.3	3.71E-02
P68370 *	Tubulin alpha-1A chain	687	49.2 ± 14.4	68 ± 11.7	3.76E-02
P69897 *	Tubulin beta-5 chain	465	29.7 ± 13	49 ± 14.6	3.80E-02
P02262 *	Histone H2A type 1	403	37.2 ± 3.9	29 ± 7.3	3.83E-02
D3ZTW9 *	Endonuclease G-like 1 (Predicted), isoform CRA_d	22	0.8 ± 1.3	3 ± 1	3.92E-02
D4A1G4 *	Cytochrome b5	23	2.8 ± 1.7	1 ± 0.8	3.94E-02
P46462 *	Transitional endoplasmic reticulum ATPase	258	17.8 ± 3.8	26 ± 7.8	3.96E-02
G3V7K5 *	Protein Npc1	23	2.5 ± 0.8	1 ± 0.8	4.02E-02
D4A9D6 *	DEAH (Asp-Glu-Ala-His) box polypeptide 9 (Predicted)	50	2.8 ± 2.1	6 ± 1.6	4.03E-02
G3V7P1 *	Syntaxin-12	51	3.3 ± 1.5	5 ± 1	4.07E-02
B2RZD5 *	Protein LOC688712	19	0.8 ± 1	2 ± 1	4.11E-02
F1LMP7 *	Granulins	112	12.8 ± 3.2	7 ± 5	4.17E-02
Q63355 *	Unconventional myosin-Ic	581	42.5 ± 3.7	57 ± 15.4	4.20E-02
M0R6L8 *	Protein RGD1560220	23	1.3 ± 0.5	3 ± 1.2	4.23E-02
B5DEN5 *	Eukaryotic translation elongation factor 1 beta 2	79	8.3 ± 2.4	5 ± 2.2	4.25E-02
Q5U302 *	Catenin (Cadherin associated protein), alpha 1	310	20 ± 9.6	33 ± 8.8	4.25E-02

P10860 *	Glutamate dehydrogenase 1, mitochondrial	213	15.2 ± 4.8	21 ± 3.5	4.27E-02
D4A914 *	5'-3' exoribonuclease 2 (Predicted), isoform CRA_c	61	4 ± 1.7	6 ± 1.8	4.27E-02
D3ZD97 *	DEAH (Asp-Glu-Ala-His) box polypeptide 15 (Predicted), isoform CRA_b	34	2 ± 1.1	4 ± 1.4	4.28E-02
G3V9E3 *	Caldesmon 1, isoform CRA_b	79	4.3 ± 2.7	9 ± 4.6	4.31E-02
P54313 *	Guanine nucleotide-binding protein G(I)/G(S)/G(T) subunit beta-2	38	2.2 ± 1.2	4 ± 1.8	4.31E-02
P60123 *	RuvB-like 1	50	5.3 ± 2.3	3 ± 1.3	4.32E-02
P16086 *	Spectrin alpha chain, non-erythrocytic 1	96	5.5 ± 3.4	11 ± 4.4	4.35E-02
O54975 *	Xaa-Pro aminopeptidase 1	26	2.8 ± 1.2	2 ± 0.8	4.45E-02
P00406 *	Cytochrome c oxidase subunit 2	45	3 ± 1.3	5 ± 0.8	4.47E-02
D4A9Z6 *	Mitochondrial ribosomal protein S35 (Predicted)	8	0.3 ± 0.5	1 ± 0	4.52E-02
Q6MG14 *	Nurim	7	0.3 ± 0.5	1 ± 0	4.52E-02
F1LYZ8 *	Protein RGD1565310	7	0.3 ± 0.5	1 ± 0	4.52E-02
P60522 *	Gamma-aminobutyric acid receptor-associated protein-like 2	7	1 ± 0	0 ± 0.5	4.52E-02
D4A5F1 *	Protein Pkd2	9	1 ± 0	0 ± 0.5	4.52E-02
B0BNJ1 *	LOC683667 protein	7	1 ± 0	0 ± 0.5	4.52E-02
Q5RK24 *	Phosphomevalonate kinase	8	1 ± 0	0 ± 0.5	4.52E-02
P61972 *	Nuclear transport factor 2	10	1 ± 0	0 ± 0.5	4.52E-02
F1LPV8 *	Protein Suclg2	21	1.3 ± 0.5	2 ± 0.8	4.56E-02
G3V7C6 *	RCG45400	390	24.3 ± 11.5	42 ± 14.5	4.62E-02
Q99068 *	Alpha-2-macroglobulin receptor-associated protein	25	0.8 ± 0.8	3 ± 3.2	4.70E-02
B0BN93 *	26S proteasome non-ATPase regulatory subunit 13	68	4 ± 2.6	7 ± 2.2	4.73E-02
D4ACB3 *	Protein RGD1559672	13	0.5 ± 0.8	2 ± 0.5	4.75E-02
P27615 *	Lysosome membrane protein 2	73	7.5 ± 2.9	5 ± 0.6	4.77E-02
D3ZL85 *	Protein Hccs	17	1 ± 0	2 ± 0.8	4.83E-02
Q9JIL3 *	Interleukin enhancer-binding factor 3	53	6.5 ± 4.9	2 ± 1.9	4.89E-02
P09117 *	Fructose-bisphosphate aldolase C	116	11.5 ± 3.4	8 ± 1.7	4.94E-02

Q4G079 *	Protein Aimp1	34	1.8 ± 1.3	4 ± 1.7	4.97E-02
P70500 *	CDP-diacylglycerol--inositol 3-phosphatidyltransferase	22	2.7 ± 1.4	1 ± 1.1	5.00E-02
Q4KM65	Cleavage and polyadenylation specificity factor subunit 5	27	2.8 ± 1	2 ± 0.8	5.02E-02
Q6AYG5	Ethylmalonyl-CoA decarboxylase	27	1.7 ± 0.8	3 ± 1	5.02E-02
Q641Z6	EH domain-containing protein 1	14	0.3 ± 0.5	2 ± 2.2	5.02E-02
Q5U334	Poliovirus receptor	44	5 ± 3.9	2 ± 0.6	5.09E-02
R9PXZ2	Heterogeneous nuclear ribonucleoprotein Q (Fragment)	69	7.5 ± 1.2	4 ± 2.9	5.16E-02
Q80U96	Exportin-1	33	2 ± 1.1	4 ± 1.2	5.26E-02
Q7TQ16	Cytochrome b-c1 complex subunit 8	26	3 ± 1.3	1 ± 1.2	5.26E-02
P97576	GrpE protein homolog 1, mitochondrial	10	0.3 ± 0.5	1 ± 1	5.29E-02
G3V913	Heat shock 27kDa protein 1	130	13.5 ± 3.9	9 ± 3.2	5.30E-02
B0BN52	Mitochondrial carrier homolog 2 (C. elegans)	40	4.5 ± 1.9	2 ± 1.5	5.34E-02
Q3T1J1	Eukaryotic translation initiation factor 5A-1	45	2.2 ± 1.2	4 ± 2	5.48E-02
D3ZJ08	Histone H3	16	1.5 ± 1	1 ± 0.5	5.52E-02
Q5FVI6	V-type proton ATPase subunit C 1	12	1.5 ± 1	1 ± 0.5	5.52E-02
F1M024	Uncharacterized protein (Fragment)	12	0.5 ± 0.5	2 ± 1	5.52E-02
P70490	Lactadherin	289	20.5 ± 6.2	29 ± 6.8	5.54E-02
P11980	Pyruvate kinase PKM	1468	140.2 ± 17.8	112 ± 25.7	5.55E-02
P35465	Serine/threonine-protein kinase PAK 1	11	0.3 ± 0.5	2 ± 1.4	5.62E-02
Q7TT49	Serine/threonine-protein kinase MRCK beta	10	0.2 ± 0.4	1 ± 1.2	5.62E-02
Q5I0K8	28S ribosomal protein S7, mitochondrial	23	1.3 ± 0.8	3 ± 1	5.74E-02
Q5VLR5	BWK4	71	4.7 ± 2.3	8 ± 2.1	5.80E-02
P43138	DNA-(apurinic or apyrimidinic site) lyase	18	0.7 ± 0.5	2 ± 2.3	5.81E-02
P45479	Palmitoyl-protein thioesterase 1	9	1.2 ± 0.8	0 ± 0.5	5.81E-02
D4A567	Protein Bub3	12	0.3 ± 0.5	1 ± 0.8	5.81E-02
P36201	Cysteine-rich protein 2	92	5.8 ± 2.9	9 ± 1.2	5.83E-02

M0R9D5	Protein Ahnak	687	50.5 ± 11.9	68 ± 15.8	5.90E-02
Q68FR9	Elongation factor 1-delta	142	9.5 ± 3.3	15 ± 5.2	5.90E-02
B2RZB7	Protein Snrpd1	14	0.5 ± 0.8	2 ± 1.2	5.92E-02
G3V7W1	Programmed cell death 6 (Predicted), isoform CRA_a	30	3.2 ± 0.4	2 ± 0.8	6.00E-02
F1LN88	Aldehyde dehydrogenase, mitochondrial	540	42 ± 4.2	51 ± 9.2	6.00E-02
P35571	Glycerol-3-phosphate dehydrogenase, mitochondrial	231	25.2 ± 8.2	15 ± 8.4	6.03E-02
M0R5U6	Torsin-1A-interacting protein 2	15	1.8 ± 1	1 ± 0.8	6.11E-02
P84100	60S ribosomal protein L19	37	2.2 ± 1.5	4 ± 1.4	6.17E-02
Q6P4Z9	COP9 signalosome complex subunit 8	31	1.2 ± 1.2	4 ± 3.6	6.21E-02
Q4V8H8	EH domain-containing protein 2	21	0.5 ± 0.8	3 ± 3.5	6.23E-02
P29457	Serpin H1	860	54.7 ± 45.2	101 ± 9.7	6.25E-02
P13832	Myosin regulatory light chain RLC-A	72	7.7 ± 3.6	5 ± 1.2	6.28E-02
Q6P0K8	Junction plakoglobin	53	6 ± 3.2	3 ± 1.8	6.31E-02
P81795	Eukaryotic translation initiation factor 2 subunit 3	15	0.3 ± 0.5	2 ± 2.7	6.51E-02
Q6IG05	Keratin, type II cytoskeletal 75	63	7.8 ± 12.2	1 ± 1.2	6.61E-02
Q6AYA5	Transmembrane protein 106B	34	3.8 ± 1.8	2 ± 1	6.62E-02
D3ZTP3	Protein RGD1310313	45	5 ± 2.4	3 ± 1.5	6.69E-02
D3ZZK1	Protein LOC100359563	90	6.5 ± 1.9	9 ± 2.6	6.72E-02
P50503	Hsc70-interacting protein	41	4.3 ± 2.1	3 ± 1	6.77E-02
Q63610	Tropomyosin alpha-3 chain	215	23.8 ± 12.4	14 ± 4.7	6.85E-02
R9PXU4	Thioredoxin reductase 1, isoform CRA_b	39	4.7 ± 2.7	2 ± 1.6	6.86E-02
Q5I0G4	Glycine--tRNA ligase (Fragment)	36	3.8 ± 1.2	2 ± 1.5	6.90E-02
Q5XIM7	Lysine--tRNA ligase	11	1.5 ± 1.5	0 ± 0.5	6.95E-02
Q9Z1P2	Alpha-actinin-1	275	19 ± 7.6	28 ± 7.8	6.99E-02
Q6P799	Serine--tRNA ligase, cytoplasmic	18	2.2 ± 1.2	1 ± 1	7.00E-02
F1MAA5	Protein Rangap1	74	7.8 ± 3.2	5 ± 1.7	7.12E-02
F1M3E5	Uncharacterized protein (Fragment)	10	1.3 ± 1.2	0 ± 0.5	7.16E-02

D4A777	Protein Fam114a1	10	0.3 ± 0.5	1 ± 1.2	7.16E-02
D3ZBS9	Protein Smarcd1	13	1.7 ± 1.5	1 ± 0.5	7.17E-02
Q6IFV3	Keratin, type I cytoskeletal 15	20	2.7 ± 3.8	0 ± 0.5	7.24E-02
Q5M7V8	Thyroid hormone receptor-associated protein 3	23	2.7 ± 1.2	1 ± 1	7.26E-02
G3V6T1	Protein Copa	42	2.8 ± 1	4 ± 1.3	7.32E-02
Q6P503	ATPase, H+ transporting, V1 subunit D, isoform CRA_c	16	1.8 ± 1.2	1 ± 0	7.33E-02
P62944	AP-2 complex subunit beta	63	3.8 ± 2	7 ± 2.9	7.36E-02
D4A9L2	Protein Srsf1	28	3.2 ± 1.3	2 ± 1.2	7.49E-02
F6T071	Golgi reassembly-stacking protein 2 (Fragment)	34	1.8 ± 1.8	4 ± 1.2	7.50E-02
B5DEY0	Pls1 protein	33	4.2 ± 3.2	2 ± 1.5	7.51E-02
D3ZHV2	Microtubule-actin cross-linking factor 1	13	0.3 ± 0.5	2 ± 2.2	7.62E-02
Q6AYQ1	Golgin subfamily A member 7	15	1.8 ± 1.2	1 ± 0.8	7.68E-02
P04692	Tropomyosin alpha-1 chain	121	7.7 ± 3.7	13 ± 5.7	7.70E-02
F1LP43	Tyrosine-protein kinase HCK (Fragment)	28	2 ± 2.2	1 ± 0.5	7.80E-02
Q63357	Unconventional myosin-Id	15	0.5 ± 0.8	2 ± 1.8	7.80E-02
F1LX07	Protein Slc25a12 (Fragment)	77	8.2 ± 3.4	5 ± 2.3	8.00E-02
G3V7Q6	Proteasome subunit beta type	14	1.7 ± 0.8	1 ± 0.8	8.00E-02
D4A0F5	Protein LOC100910706	30	1.5 ± 0.8	4 ± 2.7	8.04E-02
P35704	Peroxiredoxin-2	41	4.5 ± 2.1	3 ± 1.2	8.05E-02
Q6AY48	Poly(RC) binding protein 3	21	2.7 ± 2.3	1 ± 1	8.07E-02
Q5M920	EBNA1 binding protein 2	23	2.3 ± 0.5	2 ± 0.8	8.08E-02
P62853	40S ribosomal protein S25	59	5.8 ± 1.5	4 ± 1.5	8.13E-02
D4ACB8	Chaperonin subunit 8 (Theta) (Predicted), isoform CRA_a	220	22 ± 3.7	16 ± 6.4	8.16E-02
Q32KJ5	Glucosamine (N-acetyl)-6-sulfatase	23	1.2 ± 0.8	3 ± 2	8.20E-02
D3ZUJ8	Protein Tmtc3	12	1.7 ± 2	0 ± 0.5	8.22E-02
P30121	Metalloproteinase inhibitor 2	21	1.3 ± 0.5	2 ± 1	8.26E-02
Q4FZT9	26S proteasome non-ATPase regulatory subunit 2	75	8.3 ± 5.3	5 ± 1.4	8.32E-02

E9PTJ8	Rho guanine nucleotide exchange factor 1	19	2.2 ± 1.2	1 ± 0.9	8.36E-02
Q5RK17	Diablo homolog (Drosophila)	79	5.3 ± 2.6	8 ± 2.4	8.42E-02
D3ZGT6	Procollagen-proline, 2-oxoglutarate 4-dioxygenase (Proline 4-hydroxylase), alpha II polypeptide (Predicted), isoform CRA_a	61	4 ± 1.4	6 ± 2.8	8.47E-02
P07895	Superoxide dismutase [Mn], mitochondrial	39	4.3 ± 2.4	3 ± 0.8	8.49E-02
F1LMZ9	Prolyl 3-hydroxylase 1	30	2 ± 0.9	3 ± 0.9	8.61E-02
P68035	Actin, alpha cardiac muscle 1	472	53.7 ± 21.6	28 ± 22.6	8.61E-02
Q5PPJ6	Leucyl-tRNA synthetase	17	2.3 ± 2	1 ± 1	8.65E-02
D3ZHV0	Protein Nupl2	9	0.3 ± 0.5	1 ± 1	8.65E-02
P08699	Galectin-3	31	2.8 ± 1.2	2 ± 0	8.73E-02
D3ZIP8	Protein Endod1	27	2.8 ± 1.3	2 ± 0.8	8.75E-02
Q811A3	Procollagen-lysine,2-oxoglutarate 5-dioxygenase 2	135	8 ± 5.5	15 ± 7.9	8.87E-02
Q8R4A1	ERO1-like protein alpha	129	13.5 ± 5.1	9 ± 3.8	8.90E-02
P09456	cAMP-dependent protein kinase type I-alpha regulatory subunit	17	0.8 ± 0.8	2 ± 1.4	8.95E-02
P49134	Integrin beta-1	352	37 ± 16.5	24 ± 8.3	8.98E-02
P35213	14-3-3 protein beta/alpha	59	2.3 ± 3.7	8 ± 5.9	9.04E-02
Q68FU3	Electron transfer flavoprotein subunit beta	42	1.8 ± 0.8	3 ± 1.4	9.10E-02
Q496Z8	Low-density lipoprotein receptor-related protein 10	8	1 ± 0.6	0 ± 0.5	9.14E-02
Q5M862	Coiled-coil domain-containing protein 134	8	0.3 ± 0.5	1 ± 0.6	9.14E-02
G3V7J0	Aldehyde dehydrogenase family 6, subfamily A1, isoform CRA_b	8	0.3 ± 0.5	1 ± 0.6	9.14E-02
Q5RJM0	MKI67 FHA domain-interacting nucleolar phosphoprotein	8	1 ± 0.6	0 ± 0.5	9.14E-02
F1M265	Protein LOC100360205 (Fragment)	13	0.5 ± 0.8	2 ± 1.2	9.14E-02
G3V662	Nuclear pore complex protein Nup153	13	0.7 ± 0.5	2 ± 1	9.16E-02
G3V6N2	Protein Tmed4	16	1.5 ± 1	1 ± 0.5	9.16E-02
F1LM33	Leucine-rich PPR motif-containing protein, mitochondrial	255	25 ± 6.1	19 ± 4.8	9.17E-02

P62142	Serine/threonine-protein phosphatase PP1-beta catalytic subunit	41	2.3 ± 1.9	5 ± 2.1	9.35E-02
P23358	60S ribosomal protein L12	290	22 ± 2.1	29 ± 9.1	9.40E-02
Q5U2U4	Protein Scamp2	18	0.8 ± 1	2 ± 1.5	9.46E-02
Q64428	Trifunctional enzyme subunit alpha, mitochondrial	111	11.8 ± 1.5	7 ± 5.1	9.50E-02
Q7TQ85	Ac1164	14	0.5 ± 0.5	1 ± 0	9.51E-02
F1M2K3	Uncharacterized protein (Fragment)	8	0.5 ± 0.5	1 ± 0	9.51E-02
D3ZPL1	Cleavage and polyadenylation specific factor 6, 68kDa (Predicted), isoform CRA_b	10	1 ± 0	1 ± 0.5	9.51E-02
Q5U2V8	ER membrane protein complex subunit 3	35	4 ± 1.3	2 ± 2	9.51E-02
F1LZW6	Protein Slc25a13 (Fragment)	100	9.7 ± 3.1	7 ± 1.5	9.58E-02
M0R9G7	DNA topoisomerase 2 (Fragment)	11	0.5 ± 0.5	1 ± 1	9.63E-02
F8WFY1	Protein LOC100910212 (Fragment)	15	0.7 ± 0.5	2 ± 1.7	9.64E-02
D3ZTR4	Protein Sumf2	12	0.5 ± 0.5	2 ± 1.4	9.65E-02
Q4QQW4	Histone deacetylase 1	15	1.5 ± 1.4	1 ± 0.5	9.65E-02
P07150	Annexin A1	1577	161.3 ± 74.8	107 ± 24	9.68E-02
G3V7T6	Protein Sf3b1	60	6.7 ± 3.6	4 ± 2.4	9.68E-02
Q5PPJ4	Deoxyhypusine hydroxylase	20	2.2 ± 0.8	1 ± 1	9.70E-02
M0R6J9	Heterogeneous nuclear ribonucleoproteins A2/B1	198	12.2 ± 9.9	21 ± 4.4	9.85E-02
Q5EB77	Ras-related protein Rab-18	43	2.8 ± 1.3	4 ± 1.5	9.89E-02
D3ZLC1	Protein Lmnb2	24	2.7 ± 1.2	1 ± 1.2	9.96E-02
Q76GL9	Neutral amino acid transporter ASCT1	13	1.5 ± 0.5	1 ± 0.8	9.98E-02
B2GUZ3	Mthfd1l protein	78	5.5 ± 2.2	8 ± 1.9	9.98E-02
M0R7I0	Importin subunit alpha	44	2.3 ± 2.3	5 ± 2.5	9.99E-02
B2GV54	Neutral cholesterol ester hydrolase 1	24	2.8 ± 1.3	1 ± 1.4	1.00E-01
Q9Z269	Vesicle-associated membrane protein-associated protein B	95	9.5 ± 3.3	7 ± 1.7	1.00E-01
Q8K5A9	Death domain-containing membrane protein NRADD	20	1.2 ± 0.8	2 ± 1.2	1.00E-01
B1WBW4	Armadillo repeat-containing protein 10	19	2.2 ± 1.3	1 ± 0.9	1.01E-01

D4ACJ1	40S ribosomal protein S24	110	7.7 ± 1.9	11 ± 4.7	1.01E-01
O70257	Syntaxin-7	32	1.8 ± 1.5	4 ± 1.6	1.01E-01
D4AE56	Prostaglandin E synthase 2 (Predicted), isoform CRA_b	14	1.7 ± 1	1 ± 0.8	1.02E-01
G3V6T7	Protein disulfide isomerase associated 4	372	25 ± 4.8	39 ± 19.7	1.02E-01
Q6AY23	Pyrroline-5-carboxylate reductase 2	98	9.8 ± 1.3	7 ± 3.3	1.02E-01
Q9WVB1	Ras-related protein Rab-6A	56	6.2 ± 3.3	4 ± 1.9	1.03E-01
P0C5H9	Mesencephalic astrocyte-derived neurotrophic factor	74	4.8 ± 2.6	8 ± 2.7	1.03E-01
P22062	Protein-L-isoaspartate(D-aspartate) O-methyltransferase	18	1.2 ± 1	2 ± 0	1.03E-01
P34058	Heat shock protein HSP 90-beta	1129	91.7 ± 11.8	102 ± 7.9	1.04E-01
Q00238	Intercellular adhesion molecule 1	45	2.8 ± 0.8	5 ± 2.7	1.05E-01
D3ZCG9	Integrin alpha 3 variant A	138	13.7 ± 2.6	10 ± 4.1	1.06E-01
G3V667	Integrin, alpha 6, isoform CRA_a	21	1.3 ± 0.8	2 ± 0.8	1.06E-01
P15865	Histone H1.4	299	33.5 ± 17.5	18 ± 13.4	1.06E-01
Q07009	Calpain-2 catalytic subunit	21	2.5 ± 1.6	1 ± 1	1.08E-01
Q6TUG0	DnaJ homolog subfamily B member 11	57	4 ± 1.4	6 ± 1.9	1.08E-01
Q6URK4	Heterogeneous nuclear ribonucleoprotein A3	284	19.2 ± 8.2	26 ± 2.1	1.11E-01
G3V624	Coronin	69	7.5 ± 2.7	4 ± 3.2	1.11E-01
F1LMI3	Protein Cdh3	14	0.3 ± 0.5	2 ± 2.3	1.12E-01
M0R6J0	Protein Mrpl39	10	0.5 ± 0.5	1 ± 0.8	1.12E-01
Q56R18	Importin subunit alpha	12	0.7 ± 0.5	1 ± 0.8	1.13E-01
P52020	Squalene monooxygenase	12	0.7 ± 0.5	1 ± 0.8	1.13E-01
Q5U216	ATP-dependent RNA helicase DDX39A	14	0.7 ± 0.5	2 ± 1.5	1.13E-01
Q8VHV8	Selenoprotein S	34	2.2 ± 0.8	4 ± 1.9	1.13E-01
M0RBX8	Uncharacterized protein (Fragment)	23	2.5 ± 1.8	1 ± 0.5	1.14E-01
F1LTJ5	Protein Hspg2	9	0.3 ± 0.5	1 ± 1.2	1.15E-01
P52873	Pyruvate carboxylase, mitochondrial	17	1 ± 0	2 ± 1.7	1.19E-01
F1LS86	Isoleucine-tRNA synthetase (Predicted)	22	2.2 ± 1.7	1 ± 1	1.19E-01

G3V734	2,4-dienoyl CoA reductase 1, mitochondrial, isoform CRA_a	38	2.3 ± 1.6	4 ± 1.7	1.20E-01
B0BNG3	Lman2 protein	86	5.3 ± 3.9	9 ± 3.7	1.21E-01
B5DFI3	Adaptor protein complex AP-1, sigma 1 (Predicted), isoform CRA_b	15	1.3 ± 0.5	1 ± 0	1.21E-01
Q9Z1Z9	PDZ and LIM domain protein 7	17	0.8 ± 0.8	2 ± 1.7	1.22E-01
Q5HZY0	UBX domain-containing protein 4	28	3 ± 0.9	2 ± 1.5	1.22E-01
D4A9T3	Protein Hmg1l1	123	11 ± 3	9 ± 1.3	1.22E-01
F1LPC6	Carboxypeptidase D	13	0.7 ± 0.5	2 ± 1.2	1.24E-01
O55215	Ribosomal protein S2	56	6 ± 3.7	3 ± 1.9	1.25E-01
P30349	Leukotriene A-4 hydrolase	24	2.8 ± 2.3	1 ± 1.2	1.25E-01
Q6IMY8	Heterogeneous nuclear ribonucleoprotein U	276	21 ± 4.9	26 ± 5.5	1.26E-01
Q6AYS2	RCG24191	27	2.8 ± 0.8	2 ± 1.4	1.26E-01
D3ZEN5	Peroxiredoxin-5, mitochondrial (Fragment)	79	5.5 ± 2.5	8 ± 1.8	1.26E-01
G3V6S3	Calumenin	11	0.5 ± 0.5	1 ± 1.2	1.27E-01
Q5RKH0	Putative oxidoreductase GLYR1	11	0.5 ± 0.5	1 ± 1.2	1.27E-01
D3ZRN3	Protein Actbl2	35	0 ± 0	1 ± 2.4	1.27E-01
D3ZKR3	Glyceraldehyde-3-phosphate dehydrogenase	35	1.2 ± 2.9	0 ± 0	1.27E-01
D3Z941	Protein Mars	61	3.8 ± 1.5	6 ± 3.7	1.27E-01
P62198	26S protease regulatory subunit 8	55	6 ± 3.1	4 ± 2.2	1.30E-01
Q4V8H5	Aspartyl aminopeptidase	86	8.5 ± 2.9	6 ± 2	1.31E-01
P15651	Short-chain specific acyl-CoA dehydrogenase, mitochondrial	17	1.8 ± 0.8	1 ± 0.9	1.32E-01
Q6AYZ1	Tubulin alpha-1C chain	570	40.2 ± 21.3	56 ± 5.7	1.32E-01
Q6AYN8	Minichromosome maintenance deficient 7 (S. cerevisiae)	57	3.7 ± 2.3	6 ± 2.5	1.33E-01
D3ZN21	Protein RGD1309586	189	17.8 ± 2.9	15 ± 3.9	1.34E-01
M0RAE7	Uncharacterized protein	35	5.3 ± 8.5	1 ± 1.1	1.34E-01
D3ZSA9	Protein Nomo1	21	2.5 ± 1.6	1 ± 1.2	1.35E-01
D4A4T0	Protein Stub1	18	2.2 ± 2.1	1 ± 0.8	1.35E-01
B2GV24	E3 UFM1-protein ligase 1	14	1.5 ± 0.5	1 ± 0.8	1.36E-01

P70580	Membrane-associated progesterone receptor component 1	320	30 ± 6.3	25 ± 4.8	1.36E-01
P06762	Heme oxygenase 1	34	4.5 ± 6.2	1 ± 1.2	1.37E-01
M0R3V4	Protein D17Wsu104e	8	0.3 ± 0.5	1 ± 0.9	1.37E-01
B0BN02	Mtx1 protein	8	0.3 ± 0.5	1 ± 0.9	1.37E-01
Q9QYU2	Elongation factor Ts, mitochondrial	8	1 ± 0.9	0 ± 0.5	1.37E-01
P21775	3-ketoacyl-CoA thiolase A, peroxisomal	124	8.7 ± 2.8	13 ± 5.4	1.37E-01
P08430	UDP-glucuronosyltransferase 1-6	17	1 ± 0.6	2 ± 1.2	1.38E-01
G3V9K0	Cysteinyl-tRNA synthetase (Predicted), isoform CRA_b	15	1 ± 0	2 ± 0.8	1.39E-01
A2RUW1	Toll-interacting protein	24	2.5 ± 1	2 ± 1	1.39E-01
Q5XIE0	Acidic leucine-rich nuclear phosphoprotein 32 family member E	15	0.8 ± 0.8	2 ± 1	1.40E-01
P62912	60S ribosomal protein L32	101	7 ± 3.2	10 ± 3.2	1.40E-01
Q9EPH8	Polyadenylate-binding protein 1	207	19.2 ± 3	16 ± 3.4	1.41E-01
Q78EG7	Protein tyrosine phosphatase type IVA 1	18	2 ± 0.9	1 ± 1.1	1.41E-01
P05065	Fructose-bisphosphate aldolase A	667	62.8 ± 15	51 ± 9.8	1.42E-01
O88767	Protein DJ-1	51	5.7 ± 2.7	3 ± 2.3	1.42E-01
G3V983	Glutathione S-transferase Mu 1	9	0.3 ± 0.5	1 ± 1.3	1.42E-01
Q9ERA7	Mesothelin	26	1.7 ± 0.8	3 ± 1.4	1.42E-01
D4A3E8	Mitochondrial ribosomal protein S27 (Predicted), isoform CRA_b	16	1 ± 0.6	2 ± 0.8	1.43E-01
F1LNC4	Protein LOC100359512	16	1.7 ± 0.8	1 ± 0.6	1.43E-01
F1LT36	Protein RGD1564698	86	6.2 ± 0.8	9 ± 3.8	1.43E-01
M0R440	Zinc finger protein 326 (Fragment)	48	3.5 ± 0.5	5 ± 1.5	1.44E-01
D4A4B4	Protein U2surp	17	2 ± 1.5	1 ± 1	1.44E-01
G3V9H0	RAS p21 protein activator 1, isoform CRA_c	13	0.5 ± 0.5	2 ± 2.1	1.44E-01
Q5XIG4	OCIA domain-containing protein 1	39	2.3 ± 2.3	4 ± 1.2	1.44E-01
G3V6S0	Protein Sptbn1	32	3.3 ± 1.4	2 ± 1.2	1.44E-01
M0R402	Protein Tmx3	20	1.2 ± 1	2 ± 1.2	1.45E-01
F1LQ55	Synaptonemal complex protein 2	20	1 ± 0.9	2 ± 2.1	1.45E-01

G3V8C4	Chloride intracellular channel 4, isoform CRA_b	96	7.2 ± 2.3	10 ± 2.8	1.46E-01
M0R3L6	Protein LOC683007	10	0.3 ± 0.5	1 ± 1.8	1.46E-01
F1M980	Glutaminase kidney isoform, mitochondrial	10	0.3 ± 0.5	1 ± 1.8	1.46E-01
Q6P2A5	Adenylate kinase 3	71	3.8 ± 3.7	8 ± 6.3	1.47E-01
F1LQQ1	Malic enzyme (Fragment)	50	4.8 ± 1.2	4 ± 1.4	1.50E-01
Q5U2N2	Ubiquitin carboxyl-terminal hydrolase	24	2.7 ± 2	2 ± 0.5	1.52E-01
Q6AYU5	Poly(RC) binding protein 2	68	4.2 ± 2.1	7 ± 4.6	1.53E-01
P83732	60S ribosomal protein L24	171	11.8 ± 7.1	17 ± 2.4	1.53E-01
O08651	D-3-phosphoglycerate dehydrogenase	93	9.7 ± 4.5	6 ± 2.9	1.53E-01
G3V6P7	Myosin, heavy polypeptide 9, non-muscle	582	57.8 ± 23.5	42 ± 11.5	1.53E-01
P11507	Sarcoplasmic/endoplasmic reticulum calcium ATPase 2	58	4 ± 1.3	6 ± 2.8	1.54E-01
Q9JHL4	Drebrin-like protein	28	3.2 ± 2.6	2 ± 1.2	1.54E-01
F1M1W4	Protein Ndfip2	13	1.5 ± 1.4	1 ± 0.5	1.55E-01
B2GV96	Coiled-coil domain containing 115	16	0.8 ± 1.2	2 ± 0.8	1.55E-01
D4A5Y6	Mak3 homolog (S. cerevisiae) (Predicted)	11	0.5 ± 0.5	1 ± 1.4	1.56E-01
G3V8G2	Proteasome (Prosome, macropain) 26S subunit, non-ATPase, 5 (Predicted), isoform CRA_a	31	2.7 ± 1.4	2 ± 0.4	1.56E-01
Q56B11	Proline-, glutamic acid- and leucine-rich protein 1	12	1.5 ± 1.4	1 ± 0.8	1.56E-01
D3ZG43	NADH dehydrogenase (Ubiquinone) Fe-S protein 3 (Predicted), isoform CRA_c	40	4.3 ± 2.4	3 ± 1.4	1.57E-01
F1M9X4	Chloride intracellular channel protein 6 (Fragment)	9	1 ± 1.5	0 ± 0.4	1.58E-01
F1LR13	Atlastin-3	10	0.5 ± 0.5	1 ± 1	1.60E-01
D3ZUX7	Protein Acsf3	10	1.2 ± 1	1 ± 0.5	1.60E-01
E9PTW1	Protein Scamp3	56	5.5 ± 1.9	4 ± 1.2	1.61E-01
Q5FVQ4	Malectin	136	10.5 ± 2.4	12 ± 1	1.61E-01
B1WC34	Protein Prkcsh	54	3.3 ± 2.3	6 ± 3.9	1.61E-01

P41498	Low molecular weight phosphotyrosine protein phosphatase	37	2.5 ± 1	4 ± 1.6	1.62E-01
D3ZPP2	Protein Arl8a	29	1.8 ± 1.3	3 ± 1.3	1.62E-01
Q8VHK0	Acyl-coenzyme A thioesterase 8	13	1.5 ± 1	1 ± 0.8	1.62E-01
P20417	Tyrosine-protein phosphatase non-receptor type 1	13	1.5 ± 1	1 ± 0.8	1.62E-01
Q6AYK6	Calcyclin-binding protein	12	1.3 ± 1	1 ± 0.5	1.63E-01
D3ZVD8	Protein Hdac6	12	0.7 ± 0.8	1 ± 0.5	1.63E-01
Q9QX80	CArG-binding factor A	145	13.7 ± 2.3	11 ± 3.6	1.64E-01
Q498T9	Leucine-rich repeat-containing protein 8C	18	1.2 ± 0.8	2 ± 0.8	1.64E-01
P61983	14-3-3 protein gamma	186	15.5 ± 3.9	18 ± 1.7	1.66E-01
Q6IN37	GM2 ganglioside activator	104	6.2 ± 6.1	12 ± 5.7	1.67E-01
P62271	40S ribosomal protein S18	122	8.8 ± 2.8	12 ± 4.6	1.67E-01
O35567	Bifunctional purine biosynthesis protein PURH	92	6.8 ± 2.6	9 ± 1.9	1.68E-01
D4ABT8	Protein Hnrnpul2	88	6.7 ± 2.4	8 ± 1	1.68E-01
Q5RJR9	Serine (Or cysteine) proteinase inhibitor, clade H, member 1, isoform CRA_b	1187	93.3 ± 23.9	110 ± 12	1.68E-01
D3ZX87	Protein LOC100910017	100	9.3 ± 1.2	7 ± 3.7	1.68E-01
G3V7Z8	Poly(A) binding protein, nuclear 1, isoform CRA_a	17	1.8 ± 1.3	1 ± 0.6	1.70E-01
F1LX68	Protein Spats2	13	0.5 ± 0.5	2 ± 2.3	1.70E-01
Q9Z2Q7	Syntaxin-8	26	2.7 ± 1	2 ± 1.2	1.70E-01
Q9ET50	Protein Stau1	16	0.8 ± 1	2 ± 1.3	1.71E-01
P37397	Calponin-3	77	4.3 ± 1.4	6 ± 1.4	1.74E-01
O88321	Antisecretory factor	14	1.7 ± 1.2	1 ± 1	1.74E-01
F1LML7	Protein Hip1r	51	3.7 ± 1.5	5 ± 1.2	1.74E-01
P06761	78 kDa glucose-regulated protein	1896	178.3 ± 23.8	148 ± 43.6	1.77E-01
A2VD12	Pre-B-cell leukemia transcription factor-interacting protein 1	8	0.3 ± 0.5	1 ± 1.1	1.79E-01
E9PT53	Protein Wfs1	8	0.3 ± 0.5	1 ± 1.1	1.79E-01
Q8CGX0	Insulin-like growth factor 2 mRNA-binding protein 1	12	1 ± 1.1	0 ± 0.5	1.79E-01
P24368	Peptidyl-prolyl cis-trans isomerase B	336	26.3 ± 4.9	31 ± 6.7	1.79E-01

P16617	Phosphoglycerate kinase 1	260	19.5 ± 4.6	25 ± 8.1	1.80E-01
P38983	40S ribosomal protein SA	434	35.5 ± 3.5	39 ± 4.5	1.83E-01
P41565	Isocitrate dehydrogenase [NAD] subunit gamma 1, mitochondrial	36	3.5 ± 1.4	3 ± 1	1.83E-01
F1LP21	Protein Timm8a1	9	0.5 ± 0.5	1 ± 0.6	1.84E-01
Q5RKH2	Galactokinase 1	9	0.5 ± 0.5	1 ± 0.6	1.84E-01
Q9R0T3	DnaJ homolog subfamily C member 3	9	0.5 ± 0.5	1 ± 0.6	1.84E-01
D3ZYX8	Cytochrome c oxidase subunit VIIa polypeptide 2 like (Predicted), isoform CRA_e	9	0.5 ± 0.5	1 ± 0.6	1.84E-01
B2GV06	Succinyl-CoA:3-ketoacid coenzyme A transferase 1, mitochondrial	18	1 ± 1.1	2 ± 1.3	1.84E-01
G3V940	Coronin	20	1.2 ± 1.2	2 ± 1.2	1.85E-01
Q6PEC4	S-phase kinase-associated protein 1	20	1.3 ± 0.5	2 ± 1.1	1.86E-01
Q4KM74	Vesicle-trafficking protein SEC22b	159	11.7 ± 5.2	15 ± 3.3	1.89E-01
M0R4B8	Pyruvate kinase	602	64 ± 63.6	32 ± 9.1	1.89E-01
F1LST1	Fibronectin	83	8.5 ± 3.7	6 ± 2.5	1.92E-01
Q4FZU2	Keratin, type II cytoskeletal 6A	463	42.2 ± 6.8	37 ± 5.6	1.94E-01
A1A5R3	KRR1 small subunit processome component	13	1.7 ± 2.4	1 ± 0.5	1.95E-01
F1LNF7	Isocitrate dehydrogenase [NAD] subunit alpha, mitochondrial	81	8 ± 3.3	6 ± 2.1	1.96E-01
Q920J4	Thioredoxin-like protein 1	46	4.5 ± 1.9	3 ± 1.5	1.97E-01
D3ZD09	Cytochrome c oxidase subunit 6B1	26	2.8 ± 2.3	2 ± 1	1.98E-01
P05943	Protein S100-A10	52	5.7 ± 3.7	4 ± 1.8	1.98E-01
D4A6X4	Acylphosphatase	15	0.8 ± 0.8	2 ± 1.4	1.99E-01
B2RYW9	Fumarylacetoacetate hydrolase domain-containing protein 2	15	0.8 ± 0.8	2 ± 1.4	1.99E-01
Q5PPN7	Coiled-coil domain-containing protein 51	15	0.8 ± 0.8	2 ± 1.4	1.99E-01
O35142	Coatomer subunit beta'	11	0.5 ± 0.8	1 ± 1.2	2.00E-01
Q5RJR8	Leucine-rich repeat-containing protein 59	123	11.7 ± 3.7	9 ± 2.6	2.00E-01
F8WFI0	Delta-1-pyrroline-5-carboxylate dehydrogenase, mitochondrial	32	3.7 ± 3.2	2 ± 1.5	2.01E-01

Q68FX0	Isocitrate dehydrogenase [NAD] subunit beta, mitochondrial	36	3.8 ± 1.2	2 ± 2.2	2.01E-01
Q66HD3	Nuclear autoantigenic sperm protein	11	0.7 ± 0.5	1 ± 0.8	2.01E-01
B2RYS9	Protein Trmt112	23	2.3 ± 1.5	2 ± 0.5	2.01E-01
G3V8L9	Polymerase I and transcript release factor	293	22.7 ± 4.8	27 ± 6.6	2.02E-01
Q3B7D0	Coproporphyrinogen-III oxidase, mitochondrial	37	2.5 ± 1.5	4 ± 1.4	2.02E-01
D3ZPP9	Protein RGD1306058	23	1.7 ± 0.5	2 ± 0.8	2.02E-01
D4A601	Translational activator of cytochrome c oxidase 1	10	0.5 ± 0.5	1 ± 1.2	2.03E-01
P62864	40S ribosomal protein S30	10	0.5 ± 0.5	1 ± 1.2	2.03E-01
F1LRI5	Protein Gcn1l1	10	1.2 ± 1.2	1 ± 0.5	2.03E-01
Q5U3Z7	Serine hydroxymethyltransferase	98	9.7 ± 3.4	7 ± 2.9	2.04E-01
Q6P7A9	Lysosomal alpha-glucosidase	165	12.8 ± 2.5	16 ± 4.2	2.04E-01
F1M9V7	Protein Npepps	118	8.8 ± 3.1	11 ± 3.3	2.06E-01
D4AB03	Protein Fam120a	22	2.5 ± 1.6	1 ± 1.6	2.08E-01
Q66H98	Serum deprivation-response protein	27	1.7 ± 1.4	3 ± 1.6	2.08E-01
Q5EGY4	Synaptobrevin homolog YKT6	12	1.3 ± 0.8	1 ± 0.8	2.08E-01
P21531	60S ribosomal protein L3	15	1 ± 0	2 ± 1.4	2.09E-01
D4A2G9	Protein RGD1565297	17	1.7 ± 1.4	1 ± 0	2.09E-01
D3ZLT1	NADH dehydrogenase (Ubiquinone) 1 beta subcomplex, 7 (Predicted)	7	0.3 ± 0.5	1 ± 0.8	2.10E-01
D4ADM8	Protein Rhod	7	0.3 ± 0.5	1 ± 0.8	2.10E-01
D3ZAZ0	Eukaryotic translation initiation factor 3 subunit M	11	0.3 ± 0.5	1 ± 0.8	2.10E-01
Q4KM98	Mitochondrial fission factor	7	0.8 ± 0.8	0 ± 0.5	2.10E-01
D4AB01	Histidine triad nucleotide binding protein 2 (Predicted), isoform CRA_a	7	0.8 ± 0.8	0 ± 0.5	2.10E-01
P05370	Glucose-6-phosphate 1-dehydrogenase	7	0.8 ± 0.8	0 ± 0.5	2.10E-01
Q9Z1B2	Glutathione S-transferase Mu 5	7	0.8 ± 0.8	0 ± 0.5	2.10E-01
M0RCH0	Eukaryotic translation initiation factor 3 subunit I (Fragment)	7	0.3 ± 0.5	1 ± 0.8	2.10E-01
Q5U2U8	Bcl2-associated athanogene 3	7	0.3 ± 0.5	1 ± 0.8	2.10E-01

F7ESM5	Nitrilase 1, isoform CRA_a	7	0.3 ± 0.5	1 ± 0.8	2.10E-01
D4A4T9	Cysteine and histidine-rich domain-containing protein 1	7	0.8 ± 0.8	0 ± 0.5	2.10E-01
M0R8D7	Protein LOC679565 (Fragment)	7	0.8 ± 0.8	0 ± 0.5	2.10E-01
B0BNE5	S-formylglutathione hydrolase	13	0.7 ± 0.5	2 ± 1.6	2.10E-01
Q6P762	Mannosidase 2, alpha B1	13	0.5 ± 0.8	2 ± 2.3	2.10E-01
Q75WE7	von Willebrand factor A domain-containing protein 5A	21	1.2 ± 1	2 ± 2.1	2.11E-01
E9PT29	Uncharacterized protein	81	7.7 ± 2	6 ± 2.3	2.11E-01
M0R907	Protein Snrpd3	34	3.5 ± 2.4	2 ± 1	2.11E-01
P20070	NADH-cytochrome b5 reductase 3	142	10 ± 4.4	14 ± 6.5	2.12E-01
D4A2D7	Importin 4 (Predicted), isoform CRA_b	24	2.5 ± 1	2 ± 1.4	2.12E-01
D3ZSP1	Protein LOC100361838	30	2.8 ± 1	2 ± 0.8	2.12E-01
P24051	40S ribosomal protein S27-like	28	2 ± 0.9	3 ± 0.8	2.14E-01
B1WC26	N-acetylneuraminic acid synthase	50	4.3 ± 0.5	4 ± 0.8	2.15E-01
Q3MIB4	Lon protease homolog 2, peroxisomal	10	0.5 ± 0.8	1 ± 0.8	2.16E-01
D4A9H0	Protein Rab22a	10	1.2 ± 0.8	1 ± 0.8	2.16E-01
F1M335	Protein Pxdn	8	0.3 ± 0.5	1 ± 1.3	2.16E-01
D3ZI68	PRP31 pre-mRNA processing factor 31 homolog (Yeast) (Predicted)	8	1 ± 1.3	0 ± 0.5	2.16E-01
Q6AXN3	Transmembrane emp24 domain-containing protein 5	8	1 ± 1.3	0 ± 0.5	2.16E-01
Q5U1W6	Apolipoprotein O-like	57	5.7 ± 3.4	4 ± 1.2	2.16E-01
P14841	Cystatin-C	77	5.7 ± 1	7 ± 3.1	2.17E-01
Q5FVC4	DnaJ (Hsp40) homolog, subfamily B, member 12	36	3.7 ± 1.5	3 ± 1.5	2.17E-01
P62832	60S ribosomal protein L23	220	17 ± 3	21 ± 6	2.18E-01
Q792I0	Protein lin-7 homolog C	32	2.2 ± 1.2	3 ± 1.5	2.19E-01
F1LQW3	Protein Sfpq (Fragment)	241	16.7 ± 6.4	24 ± 13.6	2.20E-01
Q5XI34	Protein Ppp2r1a	28	2.8 ± 1	2 ± 1.5	2.21E-01
D4A1Q0	Protein LOC100361644	32	3.8 ± 5.3	1 ± 1.5	2.22E-01

F1M8K0	Protein Dag1	23	1.3 ± 0.5	3 ± 2.4	2.23E-01
P04166	Cytochrome b5 type B	42	2.5 ± 2.8	5 ± 2.1	2.23E-01
Q6P9V9	Tubulin alpha-1B chain	583	41.8 ± 15.5	57 ± 25.3	2.23E-01
Q5U367	Procollagen-lysine,2-oxoglutarate 5-dioxygenase 3	126	9 ± 5.2	12 ± 2.9	2.23E-01
G3V9Y1	Myosin, heavy polypeptide 10, non-muscle, isoform CRA_b	23	2.7 ± 2	1 ± 1.8	2.25E-01
P82995	Heat shock protein HSP 90-alpha	918	75.7 ± 9.5	82 ± 6.6	2.26E-01
Q5BJP4	Protein LOC100363776	33	3.7 ± 2.3	2 ± 2.1	2.26E-01
P17077	60S ribosomal protein L9	62	4 ± 3.1	6 ± 3	2.26E-01
P62260	14-3-3 protein epsilon	148	11.5 ± 1	15 ± 6.3	2.27E-01
B0BN81	Ribosomal protein S5, isoform CRA_b	84	5.8 ± 1.8	9 ± 5.1	2.28E-01
P41542	General vesicular transport factor p115	44	2.8 ± 1.5	5 ± 3	2.29E-01
P17425	Hydroxymethylglutaryl-CoA synthase, cytoplasmic	68	4.3 ± 3.9	7 ± 4	2.29E-01
Q5RKI1	Eukaryotic initiation factor 4A-II	113	11.3 ± 5.1	8 ± 4.4	2.29E-01
D4A8F2	Protein Rsu1	23	2.3 ± 1.6	2 ± 0.5	2.30E-01
Q04970	GTPase NRas	45	4.3 ± 1.5	3 ± 1.2	2.31E-01
D4A269	Uncharacterized protein	50	3.7 ± 1.2	5 ± 1.5	2.31E-01
F7FEZ6	Heterogeneous nuclear ribonucleoprotein A1	154	11.5 ± 4.6	15 ± 4.4	2.33E-01
P24049	60S ribosomal protein L17	46	3.5 ± 0.8	4 ± 1	2.33E-01
P68255	14-3-3 protein theta	86	5.7 ± 2.9	8 ± 2.3	2.33E-01
P35427	60S ribosomal protein L13a	56	5.5 ± 2.4	4 ± 1.7	2.33E-01
B2RYX0	Naca protein	146	14 ± 1.3	11 ± 5	2.34E-01
D3ZXJ5	Protein Eftud1	13	0.8 ± 0.8	1 ± 0.5	2.36E-01
P10688	1-phosphatidylinositol 4,5-bisphosphate phosphodiesterase delta-1	13	0.8 ± 0.8	1 ± 0.5	2.36E-01
Q4V8F9	Hydroxysteroid dehydrogenase-like protein 2	23	2.3 ± 0.5	2 ± 1.4	2.36E-01
F1LND7	Farnesyl pyrophosphate synthase	69	4.7 ± 2.8	7 ± 4.2	2.41E-01
D4ABM5	Mitochondrial ribosomal protein S34 (Predicted), isoform CRA_a	27	1.7 ± 1.6	3 ± 1.5	2.41E-01

F1LPK7	Phospholipid scramblase 3	39	4 ± 2.3	3 ± 1.9	2.41E-01
P48037	Annexin A6	151	14.3 ± 1.4	11 ± 5.4	2.42E-01
Q6AXX5	Protein Rdh11	17	1 ± 1.1	2 ± 1.2	2.44E-01
F1LRT9	Cytoplasmic dynein 1 heavy chain 1	46	3.3 ± 1	5 ± 2.2	2.44E-01
P38656	Lupus La protein homolog	74	7 ± 1.4	6 ± 2.2	2.46E-01
B5DES0	Protein Snrpd2	45	4.5 ± 1.4	3 ± 2.1	2.49E-01
F1LQ81	Vesicle-fusing ATPase (Fragment)	62	6 ± 1.9	5 ± 1.9	2.50E-01
F1MAA7	Protein Lamc1	144	10.2 ± 3.6	15 ± 8.4	2.50E-01
Q4QQV3	Protein FAM162A	15	1.7 ± 0.5	1 ± 1.3	2.50E-01
Q6AY55	Dephospho-CoA kinase domain-containing protein	15	0.8 ± 1	2 ± 1.4	2.50E-01
D4AB17	Protein Pfas	21	2.2 ± 1.3	1 ± 1	2.50E-01
Q9QZA2	Programmed cell death 6-interacting protein	87	5.7 ± 2.9	9 ± 6	2.51E-01
Q76K24	Ankyrin repeat domain-containing protein 46	15	1.7 ± 1.5	1 ± 0	2.51E-01
O55171	Acyl-coenzyme A thioesterase 2, mitochondrial	16	1.8 ± 1.7	1 ± 0.6	2.52E-01
Q9Z2L0	Voltage-dependent anion-selective channel protein 1	143	14.5 ± 10.4	10 ± 2	2.53E-01
P27881	Hexokinase-2	137	13.7 ± 3.8	10 ± 6.6	2.53E-01
Q4V7C7	Actin-related protein 3	61	6 ± 1.3	5 ± 2.6	2.53E-01
Q6MG08	ATP-binding cassette sub-family F member 1	9	0.5 ± 0.5	1 ± 0.9	2.55E-01
P20788	Cytochrome b-c1 complex subunit Rieske, mitochondrial	9	0.5 ± 0.5	1 ± 0.9	2.55E-01
D4AAV9	Protein Tspan9	9	0.5 ± 0.5	1 ± 0.9	2.55E-01
P19944	60S acidic ribosomal protein P1	27	2.8 ± 1.2	2 ± 1.9	2.59E-01
P32089	Tricarboxylate transport protein, mitochondrial	26	2.3 ± 2.1	1 ± 0.8	2.60E-01
G3V6H5	Mitochondrial 2-oxoglutarate/malate carrier protein	44	4.3 ± 2.1	3 ± 1.3	2.61E-01
O35394	Prenylated Rab acceptor protein 1	19	1.2 ± 0.8	2 ± 1.7	2.62E-01
Q66HR2	Microtubule-associated protein RP/EB family member 1	17	1 ± 1.3	2 ± 1	2.64E-01

G3V886	Protein LOC100910779	57	5.7 ± 2	4 ± 2.3	2.64E-01
G3V8G5	Golgi apparatus protein 1	48	3.3 ± 1.8	5 ± 2.2	2.65E-01
P43278	Histone H1.0	24	2.7 ± 1.6	1 ± 2	2.65E-01
B2RYP4	Protein Snx2	15	1.5 ± 0.8	1 ± 0.6	2.65E-01
Q7TNK0	Serine incorporator 1	15	1 ± 0.6	2 ± 0.8	2.65E-01
F1LPS8	Transcriptional activator protein Pur-alpha	21	1.3 ± 1.2	2 ± 1.2	2.66E-01
P08010	Glutathione S-transferase Mu 2	108	8.2 ± 3.3	10 ± 2.5	2.67E-01
Q924S5	Lon protease homolog, mitochondrial	65	6.5 ± 2.6	5 ± 2.7	2.67E-01
F1LN18	Hypoxia up-regulated protein 1	175	17.2 ± 5.1	13 ± 7.1	2.68E-01
Q9JJ19	Na(+)/H(+) exchange regulatory cofactor NHE-RF1	16	0.8 ± 0.8	2 ± 2.2	2.70E-01
Q5U2Q7	Eukaryotic peptide chain release factor subunit 1	25	1.7 ± 0.8	3 ± 1.6	2.71E-01
G3V6S5	C-1-tetrahydrofolate synthase, cytoplasmic	52	3.8 ± 1.5	5 ± 2	2.71E-01
F1LMM8	[Pyruvate dehydrogenase [lipoamide]] kinase isozyme 2, mitochondrial	7	0.3 ± 0.5	1 ± 1	2.71E-01
Q5U2X8	Acyl-CoA thioesterase 9	7	0.3 ± 0.5	1 ± 1	2.71E-01
Q6P5P3	Tetratricopeptide repeat protein 9C	7	0.8 ± 1	0 ± 0.5	2.71E-01
Q498R3	DnaJ homolog subfamily C member 10	7	0.8 ± 1	0 ± 0.5	2.71E-01
F1LPG5	Protein LOC691675	11	1.2 ± 1	1 ± 0.5	2.72E-01
F8WG91	ADP-ribosylation factor-like protein 3 (Fragment)	11	1.2 ± 1	1 ± 0.5	2.72E-01
D3ZTW8	Mitochondrial ribosomal protein L27 (Predicted), isoform CRA_a	15	0.8 ± 1.3	2 ± 0.8	2.73E-01
Q62636	Ras-related protein Rap-1b	32	2.2 ± 1.5	3 ± 1.5	2.73E-01
Q02874	Core histone macro-H2A.1	47	4.8 ± 2.6	3 ± 2	2.77E-01
M0R785	Protein Chchd2	12	0.7 ± 0.8	1 ± 1.2	2.82E-01
Q5XI32	F-actin-capping protein subunit beta	51	2.8 ± 3.8	6 ± 4.6	2.82E-01
P48500	Triosephosphate isomerase	312	25 ± 5.9	28 ± 4	2.82E-01
P62755	40S ribosomal protein S6	34	3.8 ± 3.7	2 ± 2.4	2.83E-01
Q62940	E3 ubiquitin-protein ligase NEDD4	27	1.7 ± 0.8	3 ± 2.6	2.84E-01

Q6QD51	Coiled-coil domain-containing protein 80	10	0.5 ± 0.8	1 ± 1.2	2.84E-01
D3ZDG0	Protein 1110038F14Rik	10	0.5 ± 0.8	1 ± 1.2	2.84E-01
Q6AXV4	Sorting and assembly machinery component 50 homolog	19	2 ± 1.8	1 ± 0.8	2.85E-01
Q562A2	Zinc finger RNA-binding protein	18	2 ± 1.3	1 ± 1.5	2.85E-01
P13221	Aspartate aminotransferase, cytoplasmic	56	4 ± 1.3	5 ± 2.7	2.85E-01
D4AC20	Cytidine deaminase (Predicted)	17	1 ± 1.3	2 ± 1.2	2.86E-01
P85972	Vinculin	440	40.3 ± 7.6	35 ± 8.2	2.87E-01
Q6TXE9	LRRGT00050	44	4.7 ± 2.2	3 ± 3.1	2.88E-01
Q6P685	Eukaryotic translation initiation factor 2, subunit 2 (Beta)	13	0.7 ± 1	2 ± 1.5	2.88E-01
P63025	Vesicle-associated membrane protein 3	119	8.7 ± 4.3	11 ± 3.8	2.88E-01
A0JN30	Canopy 2 homolog (Zebrafish)	46	4.2 ± 1	4 ± 0.5	2.88E-01
P39069	Adenylate kinase isoenzyme 1	66	6.3 ± 2.3	5 ± 1.8	2.89E-01
Q09073	ADP/ATP translocase 2	50	5 ± 1.8	4 ± 2.6	2.90E-01
F1M3B4	Protein unc-13 homolog A (Fragment)	20	1.3 ± 0.5	2 ± 0.5	2.92E-01
P49242	40S ribosomal protein S3a	90	9 ± 5.9	6 ± 3.5	2.94E-01
F2Z3T9	Protein U2af2	17	1.2 ± 0.8	2 ± 0.8	2.99E-01
P04642	L-lactate dehydrogenase A chain	236	13.2 ± 4.8	20 ± 15.4	3.00E-01
P13264	Glutaminase kidney isoform, mitochondrial	34	3.7 ± 1.9	2 ± 2.6	3.03E-01
Q6QI16	LRRGT00192	19	1.3 ± 0.8	2 ± 0.8	3.04E-01
Q62991	Sec1 family domain-containing protein 1	75	7.2 ± 1.7	6 ± 2.4	3.04E-01
Q63413	Spliceosome RNA helicase Ddx39b	25	1.7 ± 1	3 ± 1.6	3.05E-01
D3ZDR2	Chromatin modifying protein 6 (Predicted)	17	1 ± 1.3	2 ± 1.3	3.06E-01
P26772	10 kDa heat shock protein, mitochondrial	277	26.7 ± 7.8	21 ± 9	3.07E-01
Q63081	Protein disulfide-isomerase A6	692	59.2 ± 6.1	56 ± 5.2	3.07E-01
Q62904	3-keto-steroid reductase	74	5.7 ± 2.2	7 ± 1.5	3.09E-01
Q642E6	Tripeptidyl peptidase I	16	1 ± 0	1 ± 0.8	3.09E-01

Q9EPJ3	28S ribosomal protein S26, mitochondrial	13	1.3 ± 0.8	1 ± 0	3.09E-01
M0R535	Protein RGD1565829 (Fragment)	13	1.3 ± 0.8	1 ± 0	3.09E-01
D3ZHB3	40S ribosomal protein S12	55	5.5 ± 2.9	4 ± 2	3.11E-01
Q6P6V0	Glucose-6-phosphate isomerase	140	10.8 ± 2.2	13 ± 4.6	3.12E-01
D3Z8Q7	Protein Fam96b	9	0.5 ± 0.8	1 ± 0.6	3.12E-01
Q5RJQ4	NAD-dependent protein deacetylase sirtuin-2	9	1 ± 0.6	1 ± 0.8	3.12E-01
Q63524	Transmembrane emp24 domain-containing protein 2	9	1 ± 1.1	1 ± 0.5	3.12E-01
Q641X9	39S ribosomal protein L9, mitochondrial	9	0.5 ± 0.5	1 ± 1.1	3.12E-01
Q5U3Y2	Protein Smarcd3	6	0.3 ± 0.5	1 ± 0.5	3.12E-01
D3ZPY2	3 beta-hydroxysteroid dehydrogenase type 7	6	0.3 ± 0.5	1 ± 0.5	3.12E-01
D3ZDL0	Protein RGD1559903	6	0.3 ± 0.5	1 ± 0.5	3.12E-01
F1LMB5	Protein kintoun (Fragment)	6	0.3 ± 0.5	1 ± 0.5	3.12E-01
D4AAE2	Epithelial V-like antigen 1 (Predicted)	6	0.3 ± 0.5	1 ± 0.5	3.12E-01
Q64232	Very-long-chain enoyl-CoA reductase	6	0.3 ± 0.5	1 ± 0.5	3.12E-01
G3V774	F-box only protein 2	6	0.3 ± 0.5	1 ± 0.5	3.12E-01
F1LLX8	Lysosome-associated membrane glycoprotein 2	6	0.7 ± 0.5	0 ± 0.5	3.12E-01
G3V985	Protein Sco1	6	0.7 ± 0.5	0 ± 0.5	3.12E-01
F1LQ62	Ras-related protein Ral-B (Fragment)	6	0.7 ± 0.5	0 ± 0.5	3.12E-01
Q63768	Adapter molecule crk	6	0.7 ± 0.5	0 ± 0.5	3.12E-01
Q5M7T5	Protein Serpinc1	6	0.7 ± 0.5	0 ± 0.5	3.12E-01
F1LQC3	Collagen alpha-1(XII) chain (Fragment)	6	0.3 ± 0.5	1 ± 0.5	3.12E-01
P62628	Dynein light chain roadblock-type 1	6	0.3 ± 0.5	1 ± 0.5	3.12E-01
D3ZZT9	Protein Col14a1	8	0.7 ± 0.5	0 ± 0.5	3.12E-01
Q5RKH1	Serine/threonine-protein kinase PRP4 homolog	6	0.7 ± 0.5	0 ± 0.5	3.12E-01
P36972	Adenine phosphoribosyltransferase	6	0.7 ± 0.5	0 ± 0.5	3.12E-01

Q6XFR6	Glycophorin-C	6	0.3 ± 0.5	1 ± 0.5	3.12E-01
G3V6P2	Dihydrolipoamide S-succinyltransferase (E2 component of 2-oxo-glutarate complex), isoform CRA_a	8	0.3 ± 0.5	1 ± 0.5	3.12E-01
Q4KM38	FUS interacting protein (Serine-arginine rich) 1	6	0.7 ± 0.5	0 ± 0.5	3.12E-01
Q641X3	Beta-hexosaminidase subunit alpha	30	2 ± 0.9	3 ± 2.3	3.12E-01
B4F7C2	Protein Tubb4a	37	0.2 ± 0.4	1 ± 2.4	3.12E-01
Q8CHN5	Epididymal secretory protein 1	47	4.5 ± 1.8	4 ± 1.5	3.15E-01
Q27W02	Protein mago nashi homolog	11	0.7 ± 0.8	1 ± 0.8	3.16E-01
Q7TP48	Adipocyte plasma membrane-associated protein	11	1.2 ± 0.8	1 ± 0.8	3.16E-01
F1M978	Inositol monophosphatase 1	63	4.7 ± 2.7	6 ± 2.1	3.17E-01
A1L134	Ancient ubiquitous protein 1	44	3.3 ± 1.5	4 ± 1.2	3.18E-01
D3ZHB5	Protein Serpinb8	14	1.5 ± 0.8	1 ± 1.2	3.19E-01
Q3B8Q1	Nucleolar RNA helicase 2	70	6.8 ± 3.8	5 ± 2.3	3.19E-01
D3ZPU3	Estradiol 17-beta-dehydrogenase 12	99	7.7 ± 2.4	10 ± 3.6	3.19E-01
P62804	Histone H4	455	41.8 ± 9.5	35 ± 11.6	3.20E-01
M0R5S0	Uncharacterized protein	105	7.8 ± 4	10 ± 3	3.20E-01
D4A781	Protein Ipo5	70	7.2 ± 3.5	5 ± 3.6	3.20E-01
G3V912	Protein Tmx4	7	0.3 ± 0.5	1 ± 1.2	3.21E-01
F1LPP0	Amphiphysin (Fragment)	7	0.3 ± 0.5	1 ± 1.2	3.21E-01
Q642E2	Protein LOC100362069	7	0.8 ± 1.2	0 ± 0.5	3.21E-01
D3ZGF8	DNA-directed RNA polymerase	7	0.8 ± 1.2	0 ± 0.5	3.21E-01
P62870	Transcription elongation factor B polypeptide 2	9	0.8 ± 1.2	0 ± 0.5	3.21E-01
D4A450	Protein Bclaf1	7	0.8 ± 1.2	0 ± 0.5	3.21E-01
P22734	Catechol O-methyltransferase	7	0.3 ± 0.5	1 ± 1.2	3.21E-01
P05708	Hexokinase-1	126	12.3 ± 3.8	9 ± 6.4	3.21E-01
G3V7U4	Lamin-B1	187	18.5 ± 6	13 ± 9.9	3.21E-01
P62898	Cytochrome c, somatic	76	5.2 ± 2.1	8 ± 6.4	3.23E-01
Q9JHY1	Junctional adhesion molecule A	40	2.8 ± 1.2	4 ± 2.1	3.23E-01
B0BN20	Protein Tspan6	41	4.3 ± 2.2	3 ± 2.6	3.25E-01

G3V936	Citrate synthase	34	2.3 ± 1.8	3 ± 1.5	3.26E-01
Q66X93	Staphylococcal nuclease domain-containing protein 1	304	22.5 ± 11.6	29 ± 11.1	3.27E-01
P85834	Elongation factor Tu, mitochondrial	47	4.8 ± 1.9	3 ± 2.8	3.28E-01
P07340	Sodium/potassium-transporting ATPase subunit beta-1	40	3.8 ± 2	3 ± 1.3	3.28E-01
Q9EPB1	Dipeptidyl peptidase 2	14	0.7 ± 0.5	1 ± 1.2	3.29E-01
D3ZH23	Protein RGD1560917	11	0.7 ± 0.5	1 ± 1.2	3.29E-01
Q6AYC4	Macrophage-capping protein	40	3 ± 0	3 ± 0.8	3.29E-01
Q6PDV7	60S ribosomal protein L10	56	4.2 ± 1.8	5 ± 1.5	3.30E-01
P40329	Arginine--tRNA ligase, cytoplasmic	81	7.3 ± 1.9	7 ± 0.8	3.32E-01
P60711	Actin, cytoplasmic 1	1570	129.2 ± 19.8	141 ± 18.7	3.34E-01
P41562	Isocitrate dehydrogenase [NADP] cytoplasmic	23	1.5 ± 0.8	2 ± 2	3.34E-01
D4A4J0	Protein Supt16h	39	2.8 ± 1.8	4 ± 1.5	3.34E-01
P18886	Carnitine O-palmitoyltransferase 2, mitochondrial	13	0.7 ± 0.8	2 ± 2.1	3.36E-01
Q64361	Latexin	22	1.7 ± 0.5	2 ± 0.6	3.38E-01
B4F7B2	Protein Taf10	10	0.7 ± 0.5	1 ± 0.6	3.39E-01
D3ZYM4	Protein Mst1r	10	0.7 ± 0.5	1 ± 0.6	3.39E-01
Q99PK0	Pre-mRNA-splicing factor SYF1	10	0.7 ± 0.5	1 ± 0.6	3.39E-01
B2RZB3	Fam176b protein	19	1.3 ± 0.5	2 ± 1.2	3.39E-01
Q6AZ33	Biliverdin reductase A	30	2.2 ± 1	3 ± 1.3	3.41E-01
D3ZXS8	Huntingtin interacting protein 2 (Predicted), isoform CRA_a	38	2.7 ± 1.5	4 ± 2	3.41E-01
F7EZZ0	Disks large-associated protein 3	33	2.3 ± 1.5	3 ± 1.3	3.42E-01
F1LT49	Protein Lrrc47	21	2 ± 0.9	2 ± 0.8	3.43E-01
P62243	40S ribosomal protein S8	214	19.8 ± 5.3	17 ± 5.6	3.43E-01
Q63584	Transmembrane emp24 domain-containing protein 10	140	11.2 ± 2.5	13 ± 3.3	3.44E-01
Q5XIE3	39S ribosomal protein L11, mitochondrial	43	3.2 ± 1.5	4 ± 1.4	3.45E-01
G3V7Q7	IQ motif containing GTPase activating protein 1 (Predicted), isoform CRA_b	93	9.2 ± 4.6	7 ± 3.5	3.45E-01

Q5XIH7	Prohibitin-2	78	7.8 ± 4.5	6 ± 3.7	3.48E-01
P62775	Myotrophin	43	3.2 ± 1.6	4 ± 1.3	3.50E-01
Q5I0H4	Transmembrane and coiled-coil domains protein 1	78	8 ± 7.3	5 ± 2.3	3.51E-01
Q04679	Sodium/potassium-transporting ATPase subunit gamma	15	1.5 ± 0.8	1 ± 0.9	3.52E-01
P97887	Presenilin-1	20	1.3 ± 0.8	2 ± 1.5	3.53E-01
D3ZXK4	Protein Abhd11	13	1.3 ± 1	1 ± 0.8	3.54E-01
Q63965	Sideroflexin-1	32	2.3 ± 1.4	3 ± 0.9	3.55E-01
P18422	Proteasome subunit alpha type-3	28	1.8 ± 0.8	3 ± 2.6	3.56E-01
B0BMZ1	Protein RGD1305587	31	2.3 ± 0.8	3 ± 1	3.58E-01
F1M124	Protein Cobll1 (Fragment)	9	1 ± 1.3	1 ± 0.5	3.58E-01
O35244	Peroxiredoxin-6	9	0.5 ± 0.5	1 ± 1.3	3.58E-01
Q5PPM8	Transmembrane protein 55B	9	0.5 ± 0.8	1 ± 0.9	3.58E-01
P19139	Casein kinase II subunit alpha	9	0.5 ± 0.8	1 ± 0.9	3.58E-01
D3ZBN0	Histone H1.5	113	7.7 ± 5.6	11 ± 7	3.59E-01
F1M9N5	Ubiquitin conjugation factor E4 A	21	2 ± 0.6	2 ± 1	3.60E-01
F1LQJ7	Protein Pck2	54	5.7 ± 4.2	4 ± 3	3.60E-01
G3V8U8	Branched-chain-amino-acid aminotransferase	49	3.5 ± 2	5 ± 2.9	3.61E-01
B5DF91	ELAV (Embryonic lethal, abnormal vision, Drosophila)-like 1 (Hu antigen R)	96	7 ± 4.4	9 ± 3.1	3.61E-01
P08644	GTPase KRas	10	1.2 ± 1.6	1 ± 0.8	3.62E-01
M0R735	Uncharacterized protein (Fragment)	15	1.7 ± 2.1	1 ± 1	3.62E-01
M0R544	Glucosidase, alpha, acid, isoform CRA_a	91	9.3 ± 5.6	6 ± 5.2	3.63E-01
Q9ES21	Phosphatidylinositide phosphatase SAC1	65	4.8 ± 1.6	6 ± 2.6	3.63E-01
P07314	Gamma-glutamyltranspeptidase 1	171	16 ± 5.3	13 ± 5	3.63E-01
F1LMM9	Elongation factor G, mitochondrial	11	1.2 ± 1	1 ± 0.8	3.64E-01
F7F744	Plectin	646	58.2 ± 10.9	52 ± 10.4	3.65E-01
P27605	Hypoxanthine-guanine phosphoribosyltransferase	64	5.2 ± 0.4	6 ± 1.7	3.66E-01
P08592	Amyloid beta A4 protein	14	0.8 ± 1.3	2 ± 0.8	3.66E-01

D4A9Q3	Protein RGD1563570	37	3.2 ± 1.3	2 ± 1.6	3.67E-01
Q6AY09	Heterogeneous nuclear ribonucleoprotein H2	95	9.8 ± 7.1	6 ± 6.2	3.67E-01
D3ZGQ1	Torsin-1A-interacting protein 1	102	9.7 ± 3.3	8 ± 3.9	3.67E-01
P04897	Guanine nucleotide-binding protein G(i) subunit alpha-2	101	7.5 ± 3.3	10 ± 4.7	3.70E-01
P62716	Serine/threonine-protein phosphatase 2A catalytic subunit beta isoform	28	2 ± 1.5	3 ± 1.5	3.70E-01
D3ZF34	Uncharacterized protein (Fragment)	44	4.3 ± 2.3	3 ± 2	3.70E-01
Q5U3Z5	Bri3 binding protein	27	2.5 ± 1.4	2 ± 0	3.71E-01
P62250	40S ribosomal protein S16	57	5.3 ± 2.2	4 ± 2.1	3.72E-01
P13383	Nucleolin	333	30.2 ± 7.8	27 ± 5.1	3.72E-01
Q2PQA9	Kinesin-1 heavy chain	154	14.7 ± 6.3	12 ± 3.4	3.73E-01
Q63569	26S protease regulatory subunit 6A	72	5.7 ± 2	7 ± 0.8	3.74E-01
Q9EQS0	Transaldolase	44	3 ± 2.1	4 ± 2.9	3.74E-01
P53534	Glycogen phosphorylase, brain form (Fragment)	11	0.7 ± 0.5	1 ± 1.3	3.74E-01
F1LRS8	Protein Cd2ap (Fragment)	40	2.8 ± 1.2	4 ± 2.5	3.74E-01
D3ZQ77	Protein RGD1310352	22	1.3 ± 1.5	2 ± 2.3	3.77E-01
Q794E4	Heterogeneous nuclear ribonucleoprotein F	90	7.2 ± 2.3	8 ± 1.2	3.77E-01
G3V8A5	Protein Vps35	115	10.2 ± 0.8	9 ± 2.5	3.78E-01
Q6AYD3	Proliferation-associated 2G4	13	0.7 ± 0.8	2 ± 2.3	3.79E-01
Q5XIA1	Nicalin	13	0.8 ± 1	1 ± 0.8	3.81E-01
Q8R3Z7	EH-domain containing 4	18	1.2 ± 1.2	2 ± 1.3	3.81E-01
F2Z3Q8	Importin subunit beta-1	201	16 ± 4.2	18 ± 4	3.84E-01
M0R7I3	Protein Larp4 (Fragment)	39	4 ± 3.2	3 ± 1.9	3.85E-01
Q6AYQ4	Transmembrane protein 109	56	5.3 ± 2.1	4 ± 2.3	3.85E-01
R9PXR7	Prostaglandin E synthase 3 (Fragment)	29	2 ± 1.3	3 ± 1.9	3.88E-01
P97690	Structural maintenance of chromosomes protein 3	19	1.2 ± 0.8	2 ± 2.4	3.89E-01
D4AC23	Protein Cct7	36	2.5 ± 2.1	4 ± 1.6	3.90E-01
F1M790	Prostaglandin F2 receptor negative regulator (Fragment)	10	0.7 ± 0.8	1 ± 0	3.91E-01

P10760	Adenosylhomocysteinase	24	1.5 ± 0.8	3 ± 2.9	3.92E-01
P14408	Fumarate hydratase, mitochondrial	134	12.2 ± 2.1	11 ± 2.4	3.93E-01
Q66HC5	Nuclear pore complex protein Nup93	50	3 ± 2.3	6 ± 7.2	3.93E-01
D3ZWZ6	Protein Igf2bp2 (Fragment)	11	1.2 ± 0.8	1 ± 1	3.94E-01
Q7TPB1	T-complex protein 1 subunit delta	172	16 ± 3.5	13 ± 6.2	3.94E-01
E9PSJ4	Protein Spag9	8	0.5 ± 0.5	1 ± 0.8	3.95E-01
P85007	Immediate early response 3-interacting protein 1	8	0.5 ± 0.5	1 ± 0.8	3.95E-01
B5DFF4	Protein LOC100910929	8	0.5 ± 0.5	1 ± 0.8	3.95E-01
Q5FWY5	AH receptor-interacting protein	8	0.5 ± 0.5	1 ± 0.8	3.95E-01
Q5XI64	Monoacylglycerol lipase ABHD6	8	0.8 ± 0.8	1 ± 0.5	3.95E-01
Q5PQP2	Receptor-binding cancer antigen expressed on SiSo cells	8	0.5 ± 0.5	1 ± 0.8	3.95E-01
Q6P6Q2	Keratin, type II cytoskeletal 5	199	20.3 ± 16	13 ± 11.3	3.95E-01
F1LM66	Protein Eftud2	13	0.8 ± 0.8	1 ± 1.2	3.96E-01
O35165	Golgi SNAP receptor complex member 2	9	1 ± 1.1	1 ± 0.8	3.97E-01
D3ZUX5	Coiled-coil-helix-coiled-coil-helix domain containing 3 (Predicted), isoform CRA_a	81	8 ± 3.9	6 ± 4.4	4.00E-01
D4ADF5	Protein LOC100912106	18	1.8 ± 1.8	1 ± 0.8	4.00E-01
P62909	40S ribosomal protein S3	198	15.8 ± 3.4	18 ± 4.4	4.01E-01
Q8CGU6	Nicastrin	178	16.2 ± 4.4	14 ± 2.7	4.01E-01
Q9EST6	Acidic leucine-rich nuclear phosphoprotein 32 family member B	44	3.2 ± 2	4 ± 2.6	4.02E-01
Q3KRF2	High density lipoprotein binding protein (Vigilin)	139	10.7 ± 3.6	13 ± 5.6	4.03E-01
Q63798	Proteasome activator complex subunit 2	11	0.7 ± 0.8	1 ± 1.2	4.03E-01
D3ZC87	Protein Maff	11	0.7 ± 0.8	1 ± 1.2	4.03E-01
Q03346	Mitochondrial-processing peptidase subunit beta	11	0.7 ± 0.8	1 ± 1.2	4.03E-01
R9PXR4	Mitochondrial import receptor subunit TOM70	13	1.3 ± 0.5	1 ± 1.2	4.04E-01
Q04462	Valine--tRNA ligase	42	4.3 ± 2.9	3 ± 2.4	4.05E-01

P32198	Carnitine O-palmitoyltransferase 1, liver isoform	6	0.3 ± 0.5	1 ± 0.8	4.05E-01
P15205	Microtubule-associated protein 1B	6	0.3 ± 0.5	1 ± 0.8	4.05E-01
Q4KLH4	Paraspeckle component 1	6	0.3 ± 0.5	1 ± 0.8	4.05E-01
D4A0Y4	Oxidoreductase NAD-binding domain containing 1 (Predicted), isoform CRA_b	6	0.3 ± 0.5	1 ± 0.8	4.05E-01
F1MAA1	Ubiquitin carboxyl-terminal hydrolase	6	0.3 ± 0.5	1 ± 0.8	4.05E-01
F1M7V4	Protein piccolo (Fragment)	6	0.7 ± 0.8	0 ± 0.5	4.05E-01
D4A2I3	Protein Tmem63a	6	0.7 ± 0.8	0 ± 0.5	4.05E-01
D3ZAA0	PRA1 domain family 2 (Predicted)	8	0.3 ± 0.5	1 ± 0.8	4.05E-01
D3ZJ67	Protein Sun2	6	0.7 ± 0.8	0 ± 0.5	4.05E-01
Q4FZT8	SPRY domain-containing protein 4	6	0.7 ± 0.8	0 ± 0.5	4.05E-01
G3V9X6	DNA repair protein RAD50	6	0.3 ± 0.5	1 ± 0.8	4.05E-01
F1MAH8	Protein Clip1	6	0.3 ± 0.5	1 ± 0.8	4.05E-01
Q71UE8	NEDD8	6	0.7 ± 0.8	0 ± 0.5	4.05E-01
M0R913	Protein Phactr4 (Fragment)	6	0.7 ± 0.8	0 ± 0.5	4.05E-01
F1LR38	ATP-binding cassette sub-family D member 3 (Fragment)	8	0.3 ± 0.5	1 ± 0.8	4.05E-01
Q01986	Dual specificity mitogen-activated protein kinase kinase 1	6	0.3 ± 0.5	1 ± 0.8	4.05E-01
F1LQ05	Endophilin-A1 (Fragment)	6	0.3 ± 0.5	1 ± 0.8	4.05E-01
Q2LAP6	Testin	6	0.3 ± 0.5	1 ± 0.8	4.05E-01
D4ACI3	Myc box-dependent-interacting protein 1	6	0.3 ± 0.5	1 ± 0.8	4.05E-01
D4A181	Protein Mettl13	6	0.7 ± 0.8	0 ± 0.5	4.05E-01
Q6AYA1	H/ACA ribonucleoprotein complex subunit 1	6	0.7 ± 0.8	0 ± 0.5	4.05E-01
G3V8T4	DNA damage-binding protein 1	6	0.7 ± 0.8	0 ± 0.5	4.05E-01
D3ZUF9	Pitrilysin metallepetidase 1 (Predicted)	83	5.5 ± 1	8 ± 6	4.06E-01
P18418	Calreticulin	261	20.3 ± 4.3	24 ± 10.9	4.07E-01
P19511	ATP synthase subunit b, mitochondrial	94	7.5 ± 2.6	6 ± 2.7	4.07E-01

Q5XHZ0	Heat shock protein 75 kDa, mitochondrial	437	40.2 ± 11.3	36 ± 7.1	4.07E-01
Q5XIC6	Proteasome (Prosome, macropain) 26S subunit, non-ATPase, 12	43	3.3 ± 1.5	4 ± 1.1	4.09E-01
B0BNK1	Protein Rab5c	96	9 ± 4.7	7 ± 1.5	4.09E-01
F1LNT8	Vesicle-associated membrane protein 8 (Fragment)	77	7.3 ± 4.5	6 ± 2.9	4.10E-01
G3V9N7	Protein Pacsin3	18	1.2 ± 1	2 ± 1.7	4.12E-01
Q32PX6	Protein Rhog	57	5.5 ± 4	4 ± 0.8	4.12E-01
P70550	Ras-related protein Rab-8B	16	1.2 ± 0.8	2 ± 0.5	4.13E-01
H7C5Y5	60S ribosomal protein L6	105	9.8 ± 5.8	8 ± 2.8	4.13E-01
P61980	Heterogeneous nuclear ribonucleoprotein K	232	21.3 ± 6.7	19 ± 4.7	4.14E-01
P52555	Endoplasmic reticulum resident protein 29	330	31 ± 13.2	26 ± 6.6	4.15E-01
P04182	Ornithine aminotransferase, mitochondrial	115	9.3 ± 2.9	11 ± 1.6	4.16E-01
F1LM69	Dolichyl-diphosphooligosaccharide--protein glycosyltransferase 48 kDa subunit	53	5 ± 2.6	4 ± 1.4	4.17E-01
O35547	Long-chain-fatty-acid--CoA ligase 4	19	1.3 ± 1	2 ± 1	4.17E-01
Q63692	Hsp90 co-chaperone Cdc37	19	1.8 ± 1	1 ± 1	4.17E-01
P48508	Glutamate--cysteine ligase regulatory subunit	13	1 ± 0	1 ± 1	4.17E-01
Q66H80	Coatomer subunit delta	21	1.5 ± 1.2	2 ± 0.6	4.17E-01
P13086	Succinyl-CoA ligase [ADP/GDP-forming] subunit alpha, mitochondrial	49	4.8 ± 3.8	4 ± 1.5	4.17E-01
D4ACU9	Protein Itga5 (Fragment)	18	1.8 ± 0.8	1 ± 1.6	4.18E-01
P30919	N(4)-(Beta-N-acetylglucosaminyl)-L-asparaginase	54	5.2 ± 2.8	4 ± 2	4.18E-01
Q642E3	CDK5 regulatory subunit associated protein 3, isoform CRA_b	13	1.3 ± 1	1 ± 1	4.18E-01
Q6AYK8	Eukaryotic translation initiation factor 3 subunit D	38	3.5 ± 1.2	3 ± 1.5	4.20E-01
B1WC02	Ctps protein	14	1.5 ± 2	1 ± 0.8	4.20E-01
P70470	Acyl-protein thioesterase 1	86	7.7 ± 6.6	6 ± 1.5	4.20E-01

G3V9R8	Heterogeneous nuclear ribonucleoprotein C	228	20.7 ± 5.7	18 ± 3.8	4.21E-01
P10960	Sulfated glycoprotein 1	26	2.5 ± 1.8	2 ± 1	4.23E-01
P13471	40S ribosomal protein S14	158	12.3 ± 3.3	15 ± 5.6	4.23E-01
G3V7A5	Low density lipoprotein receptor, isoform CRA_a	241	19.5 ± 3.7	22 ± 5.2	4.25E-01
P63088	Serine/threonine-protein phosphatase PP1-gamma catalytic subunit	37	2.7 ± 1.5	4 ± 2	4.26E-01
Q5RJK5	Chromobox homolog 3 (HP1 gamma homolog, Drosophila)	57	4.3 ± 2.4	6 ± 2.4	4.27E-01
P43244	Matrin-3	124	10 ± 2.8	11 ± 2.7	4.27E-01
M0R3M8	Protein Rrp12	9	0.5 ± 0.8	1 ± 1.3	4.29E-01
Q6AYQ8	Acylpyruvase FAHD1, mitochondrial	29	2.8 ± 1.5	2 ± 1.3	4.30E-01
Q498U4	SAP domain-containing ribonucleoprotein	28	2.7 ± 1.9	2 ± 0.9	4.31E-01
Q566E5	KDEL motif-containing protein 2	13	0.8 ± 0.8	1 ± 1.4	4.32E-01
Q71UF4	Histone-binding protein RBBP7	13	1.3 ± 1.4	1 ± 0.8	4.32E-01
Q7TQ86	Ac1158	38	3.8 ± 3.2	3 ± 1.8	4.34E-01
Q4QQV8	Charged multivesicular body protein 5	20	1.7 ± 1.4	1 ± 0.8	4.35E-01
P68101	Eukaryotic translation initiation factor 2 subunit 1	47	3.5 ± 1.9	4 ± 1.6	4.36E-01
G3V7G9	Eukaryotic translation initiation factor 3 subunit L	30	2.2 ± 1.5	3 ± 1.3	4.36E-01
P31399	ATP synthase subunit d, mitochondrial	51	3.8 ± 2.4	5 ± 1.7	4.37E-01
P83871	PHD finger-like domain-containing protein 5A	53	4 ± 1.7	5 ± 3.3	4.39E-01
M0R7B4	Protein Hist1h1d	300	30.2 ± 23.7	22 ± 13.6	4.42E-01
F1M7T6	Translocon-associated protein subunit gamma	30	2.2 ± 1.6	3 ± 1.2	4.42E-01
D3ZF07	Protein RGD1562402	14	1.3 ± 0.8	1 ± 0.6	4.43E-01
Q68FY0	Cytochrome b-c1 complex subunit 1, mitochondrial	16	0.8 ± 0.4	1 ± 1.6	4.44E-01
F7FLF2	Protein LOC100360057 (Fragment)	108	8.5 ± 2.4	10 ± 3.4	4.46E-01
O35303	Dynamin-1-like protein	27	1.8 ± 0.8	3 ± 2.7	4.46E-01
D3ZUR9	Uncharacterized protein (Fragment)	85	7.8 ± 2.8	7 ± 1.5	4.47E-01

F1MAN8	Laminin, alpha 5, isoform CRA_a	23	1.2 ± 1	2 ± 1.2	4.48E-01
P61023	Calcineurin B homologous protein 1	42	3.5 ± 1	3 ± 1.7	4.49E-01
Q9JHY2	Sideroflexin-3	24	1.5 ± 2.1	3 ± 2.3	4.50E-01
G3V9N0	Pabpc4 protein	36	1.2 ± 1.3	2 ± 1.6	4.51E-01
Q4V8E1	GATA zinc finger domain containing 2B	18	1.8 ± 1.6	1 ± 1.3	4.51E-01
D3ZW08	Adenylosuccinate lyase (Predicted)	21	2 ± 0.9	2 ± 1.2	4.51E-01
G3V8B6	26S proteasome non-ATPase regulatory subunit 1	36	2.5 ± 1.5	4 ± 2.9	4.53E-01
P28023	Dynactin subunit 1	26	1.8 ± 0.8	3 ± 2.1	4.53E-01
G3V8T9	Apoptosis regulator BAX	34	2.5 ± 1.4	3 ± 1.6	4.56E-01
Q9Z1W6	Protein LYRIC	46	3.3 ± 1.6	4 ± 2.8	4.56E-01
B0K031	60S ribosomal protein L7	80	6.2 ± 2.9	7 ± 2.2	4.57E-01
D3Z9I1	Protein Coa3	11	0.7 ± 1	1 ± 1.2	4.57E-01
P05197	Elongation factor 2	337	27.3 ± 5.9	30 ± 6.9	4.60E-01
P29147	D-beta-hydroxybutyrate dehydrogenase, mitochondrial	59	5.5 ± 2.3	5 ± 2.2	4.61E-01
M0RDD7	RCG29880	24	2.2 ± 0.8	2 ± 0.8	4.62E-01
B1WC67	Protein Slc25a24	85	8.2 ± 6.1	6 ± 2.6	4.62E-01
D3ZTH8	Protein LOC689899	58	5.5 ± 3	5 ± 1.4	4.64E-01
P04764	Alpha-enolase	750	58.7 ± 18.5	69 ± 27.6	4.65E-01
G3V6P6	Putative RNA-binding protein 3	10	0.7 ± 0.8	1 ± 0.6	4.66E-01
D4A8G0	Protein Lsm12	10	1 ± 0.6	1 ± 0.8	4.66E-01
Q9R066	Coxsackievirus and adenovirus receptor homolog	8	0.8 ± 1	1 ± 0.5	4.66E-01
O08769	Cyclin dependent kinase inhibitor	8	0.5 ± 0.5	1 ± 1	4.66E-01
D3ZTL3	Protein Phldb2	8	0.5 ± 0.5	1 ± 1	4.66E-01
D4AE96	Importin 7 (Predicted), isoform CRA_c	8	0.8 ± 1	1 ± 0.5	4.66E-01
Q68FS2	COP9 signalosome complex subunit 4	8	0.8 ± 1	1 ± 0.5	4.66E-01
Q07266	Drebrin	8	0.8 ± 1	1 ± 0.5	4.66E-01
Q4G009	Malignant T-cell-amplified sequence 1	14	1 ± 0.9	1 ± 0.5	4.66E-01
Q6AYS8	Estradiol 17-beta-dehydrogenase 11	14	1.3 ± 0.5	1 ± 0.9	4.66E-01

B1H269	Ddx27 protein	14	1.3 ± 0.5	1 ± 0.9	4.66E-01
P14562	Lysosome-associated membrane glycoprotein 1	92	8.5 ± 3.1	7 ± 2.2	4.66E-01
M0R961	Far upstream element-binding protein 2	141	11.3 ± 3.7	13 ± 3.1	4.67E-01
Q64057	Alpha-aminoadipic semialdehyde dehydrogenase	67	5.2 ± 1.7	6 ± 2.1	4.67E-01
D3ZGL5	PRP38 pre-mRNA processing factor 38 (Yeast) domain containing A (Predicted), isoform CRA_b	6	0.3 ± 0.5	1 ± 1	4.69E-01
Q4V8E2	Proteasome (Prosome, macropain) 26S subunit, non-ATPase, 14	6	0.7 ± 1	0 ± 0.5	4.69E-01
B2RYG6	Ubiquitin thioesterase OTUB1	6	0.3 ± 0.5	1 ± 1	4.69E-01
P62828	GTP-binding nuclear protein Ran	61	4.8 ± 2	6 ± 1.8	4.69E-01
P09895	60S ribosomal protein L5	105	8.5 ± 3.1	10 ± 2.2	4.71E-01
Q5PQV5	Trophoblast glycoprotein	23	1.7 ± 0.8	2 ± 1.5	4.71E-01
D4AAE9	Protein Cisd2	79	7.2 ± 1.5	6 ± 2.3	4.71E-01
Q66H50	Fatty acyl-CoA reductase 1	98	7.8 ± 1.7	9 ± 4.2	4.74E-01
P50475	Alanine--tRNA ligase, cytoplasmic	44	4 ± 2	3 ± 1	4.75E-01
P25235	Dolichyl-diphosphooligosaccharide--protein glycosyltransferase subunit 2	40	3 ± 1.1	4 ± 2	4.75E-01
D4A401	Protein Tex10	33	3 ± 1.1	3 ± 1.2	4.77E-01
Q07936	Annexin A2	1790	146.3 ± 27.2	160 ± 35.3	4.78E-01
P09495	Tropomyosin alpha-4 chain	104	10.3 ± 7.2	8 ± 4.5	4.79E-01
O55096	Dipeptidyl peptidase 3	19	1.8 ± 1.3	1 ± 1	4.80E-01
E9PT66	Protein Sf3b3	50	3.8 ± 1.5	5 ± 2.4	4.80E-01
Q1RP77	Nucleolar protein 16	27	2.5 ± 1	2 ± 1.3	4.80E-01
Q8CFN2	Cell division control protein 42 homolog	30	3.2 ± 3.7	2 ± 1.8	4.81E-01
Q5XHY5	Threonine--tRNA ligase, cytoplasmic	55	5.3 ± 3.7	4 ± 1.6	4.81E-01
P40307	Proteasome subunit beta type-2	29	2.8 ± 1.8	2 ± 1.3	4.82E-01
F1LM55	Protein RGD1309922	63	5.8 ± 2.5	5 ± 1.4	4.84E-01
Q9JLJ3	4-trimethylaminobutyraldehyde dehydrogenase	93	8.7 ± 4.5	7 ± 3.4	4.84E-01

O70593	Small glutamine-rich tetratricopeptide repeat-containing protein alpha	16	1.5 ± 0.8	1 ± 0.8	4.85E-01
Q66HA8	Heat shock protein 105 kDa	180	14.2 ± 7.6	17 ± 3.1	4.86E-01
G3V8P4	RCG50226, isoform CRA_a	31	2.8 ± 1.2	2 ± 1.2	4.86E-01
Q7M0E3	Destrin	106	7.8 ± 4.3	10 ± 6.1	4.86E-01
P17764	Acetyl-CoA acetyltransferase, mitochondrial	125	10 ± 3.6	12 ± 4.4	4.86E-01
D3ZHZ3	Oxysterol-binding protein	13	1 ± 0	1 ± 1.2	4.87E-01
P97852	Peroxisomal multifunctional enzyme type 2	20	2 ± 0.6	1 ± 2	4.88E-01
O35987	NSFL1 cofactor p47	20	1.5 ± 0.8	2 ± 0.8	4.89E-01
G3V918	Phosphoribosylglycinamide formyltransferase, isoform CRA_a	16	1.7 ± 2	1 ± 1.3	4.89E-01
B0BN18	Prefoldin subunit 2	41	3.7 ± 1	3 ± 0.5	4.90E-01
P26284	Pyruvate dehydrogenase E1 component subunit alpha, somatic form, mitochondrial	31	2.5 ± 1.6	3 ± 0	4.93E-01
P16975	SPARC	35	2.5 ± 2.3	3 ± 1.6	4.94E-01
D3ZYW2	Heterogeneous nuclear ribonucleoprotein H	203	16.7 ± 3.3	18 ± 3.2	4.94E-01
Q5M9G3	Caprin-1	43	4.2 ± 2.7	3 ± 1.2	4.94E-01
B5DF65	Biliverdin reductase B (Flavin reductase (NADPH))	10	0.7 ± 0.5	1 ± 1.1	4.94E-01
Q7TP77	Aa2-277	10	0.7 ± 0.5	1 ± 1.1	4.94E-01
D3ZW55	Inosine triphosphate pyrophosphatase	58	5.3 ± 1.6	5 ± 1.6	4.96E-01
P35435	ATP synthase subunit gamma, mitochondrial	74	7 ± 2.8	6 ± 2.9	5.01E-01
A1L1J9	Lipase maturation factor 2	8	0.5 ± 0.8	1 ± 0.8	5.02E-01
D4A0E2	Protein Napg	8	0.8 ± 0.8	1 ± 0.8	5.02E-01
Q9EQX9	Ubiquitin-conjugating enzyme E2 N	8	0.5 ± 0.8	1 ± 0.8	5.02E-01
D3ZM03	Protein LOC100912478	8	0.5 ± 0.8	1 ± 0.8	5.02E-01
F1LZ00	Protein BC005561 (Fragment)	8	0.8 ± 0.8	1 ± 0.8	5.02E-01
D4A7D7	Hexose-6-phosphate dehydrogenase (Glucose 1-dehydrogenase) (Predicted), isoform CRA_b	8	0.5 ± 0.8	1 ± 0.8	5.02E-01
F7FJR8	Protein Las1l	8	0.8 ± 0.8	1 ± 0.8	5.02E-01

Q6VEU8	DEAD (Asp-Glu-Ala-Asp) box polypeptide 24	8	0.8 ± 0.8	1 ± 0.8	5.02E-01
P62718	60S ribosomal protein L18a	87	6.7 ± 4.1	8 ± 1.9	5.03E-01
P14604	Enoyl-CoA hydratase, mitochondrial	57	4.3 ± 1.2	5 ± 3.5	5.08E-01
D3ZQN7	Protein Lamb1	24	1.7 ± 1.9	3 ± 2.3	5.08E-01
P62083	40S ribosomal protein S7	61	6 ± 4.2	5 ± 3.4	5.09E-01
Q6AXX6	Redox-regulatory protein FAM213A	51	3.8 ± 1.2	5 ± 3.5	5.09E-01
Q5M884	Protein Eci3	26	2.3 ± 1	2 ± 0.6	5.09E-01
P47727	Carbonyl reductase [NADPH] 1	57	4.3 ± 1.8	5 ± 2.5	5.12E-01
F7EM24	Protein Tsn	32	3 ± 1.8	3 ± 0.5	5.13E-01
P28480	T-complex protein 1 subunit alpha	52	4.7 ± 1.2	4 ± 1.3	5.13E-01
P55770	NHP2-like protein 1	113	10.5 ± 4.1	9 ± 4.4	5.14E-01
P62914	60S ribosomal protein L11	187	15.3 ± 2.5	17 ± 3.4	5.16E-01
F7EWC1	Protein Vasp	8	0.5 ± 0.5	1 ± 1.2	5.17E-01
A9CMB8	DNA replication licensing factor MCM6	36	2.7 ± 2.3	4 ± 2	5.18E-01
Q4G061	Eukaryotic translation initiation factor 3 subunit B	23	1.7 ± 1.4	2 ± 1.2	5.18E-01
M0RC99	Protein LOC100361891	18	1.2 ± 1.3	2 ± 2.1	5.19E-01
B5DF46	Phosphomannomutase 2	10	0.7 ± 0.8	1 ± 0.9	5.19E-01
Q63750	39S ribosomal protein L23, mitochondrial	10	1 ± 0.9	1 ± 0.8	5.19E-01
G3V998	Lanosterol synthase	10	0.7 ± 0.8	1 ± 0.9	5.19E-01
B5DEP7	Protein LOC100911683	10	1 ± 0.9	1 ± 0.8	5.19E-01
D3ZB30	Polypyrimidine tract binding protein 1, isoform CRA_c	179	13.8 ± 8.5	17 ± 4.2	5.20E-01
E9PU01	Protein Chd4	22	1.5 ± 1.2	2 ± 2.2	5.20E-01
P69736	Endothelial differentiation-related factor 1	12	0.8 ± 0.8	1 ± 1	5.20E-01
Q6GQP4	Ras-related protein Rab-31	12	1.2 ± 1	1 ± 0.8	5.20E-01
D4A0T0	Protein Ndufb10	45	3.5 ± 1.6	4 ± 1.8	5.22E-01
G3V7I3	ATPase type 13A1 (Predicted), isoform CRA_a	17	1.7 ± 1.6	1 ± 1	5.23E-01

F1LV13	Heterogeneous nuclear ribonucleoprotein M	164	13.2 ± 2.3	15 ± 6.6	5.24E-01
F1LQ48	Protein Hnrnpl	44	3.7 ± 1.8	3 ± 0.8	5.25E-01
B4F7A5	Cd99 protein	91	8.3 ± 2.3	7 ± 2.9	5.28E-01
Q63570	26S protease regulatory subunit 6B	27	2 ± 1.3	3 ± 1.4	5.28E-01
Q6P747	Heterochromatin protein 1-binding protein 3	32	3 ± 1.3	2 ± 2.1	5.29E-01
P19945	60S acidic ribosomal protein P0	164	12.8 ± 6.9	15 ± 4.2	5.32E-01
P50399	Rab GDP dissociation inhibitor beta	94	7 ± 2.8	9 ± 6.6	5.32E-01
P50137	Transketolase	147	13.3 ± 5.4	12 ± 2.1	5.32E-01
Q6MG61	Chloride intracellular channel protein 1	92	7.5 ± 1.4	9 ± 3.6	5.32E-01
D3Z8D7	Protein LOC100361854	76	7.2 ± 2.1	6 ± 3.7	5.32E-01
P54001	Prolyl 4-hydroxylase subunit alpha-1	79	6.3 ± 1.4	7 ± 2.9	5.34E-01
Q5BJZ3	Nicotinamide nucleotide transhydrogenase	33	3.2 ± 2.3	2 ± 2.2	5.36E-01
Q5M819	Phosphoserine phosphatase	16	1.5 ± 1	1 ± 0.8	5.36E-01
Q6AYQ9	Peptidyl-prolyl cis-trans isomerase	42	3.8 ± 1.3	3 ± 1.4	5.36E-01
D3ZFY8	Protein LOC100912618	21	1.2 ± 0.8	1 ± 1	5.38E-01
P04636	Malate dehydrogenase, mitochondrial	878	79.3 ± 12.8	71 ± 30	5.38E-01
F1LQT3	Rho-associated protein kinase 2 (Fragment)	21	1.5 ± 1.5	2 ± 1.1	5.40E-01
P56571	ES1 protein homolog, mitochondrial	20	1.5 ± 0.8	2 ± 1	5.40E-01
Q5U2R7	LDLR chaperone MESD	21	2.2 ± 2.1	2 ± 1.5	5.40E-01
Q5XIU9	Membrane-associated progesterone receptor component 2	234	18.2 ± 3.2	20 ± 4.1	5.41E-01
Q6EV70	GDP-fucose protein O-fucosyltransferase 1	29	2.2 ± 0.8	3 ± 1.9	5.42E-01
B0BNB0	Golt1b protein	8	0.5 ± 0.8	1 ± 1	5.44E-01
B0BNL2	PDZ domain-containing protein 2	8	0.5 ± 0.8	1 ± 1	5.44E-01
D3ZI15	Uncharacterized protein	8	0.8 ± 1	1 ± 0.8	5.44E-01
F1LNL2	Protein Smarca5	8	0.5 ± 0.8	1 ± 1	5.44E-01
P85970	Actin-related protein 2/3 complex subunit 2	12	0.5 ± 0.8	1 ± 1	5.44E-01

D3ZVQ0	Ubiquitin carboxyl-terminal hydrolase	38	2.8 ± 1.7	4 ± 2	5.46E-01
Q99P75	Ras-related protein Rab-9A	45	4.2 ± 1.9	4 ± 1.8	5.47E-01
P85968	6-phosphogluconate dehydrogenase, decarboxylating	185	14.8 ± 6.2	17 ± 4.8	5.49E-01
P25113	Phosphoglycerate mutase 1	215	17.5 ± 6.3	19 ± 3.4	5.49E-01
Q4KM73	UMP-CMP kinase	21	1.5 ± 1.4	2 ± 1.4	5.52E-01
P05982	NAD(P)H dehydrogenase [quinone] 1	101	9.3 ± 4.8	8 ± 2.4	5.53E-01
D3ZRM9	60S ribosomal protein L13	70	6.3 ± 3.2	6 ± 1.2	5.55E-01
D3ZN05	Protein Lama3	8	0.5 ± 0.5	1 ± 1.3	5.56E-01
D3ZYM7	Protein Lyrm4	8	0.5 ± 0.5	1 ± 1.3	5.56E-01
P12007	Isovaleryl-CoA dehydrogenase, mitochondrial	12	0.8 ± 0.8	1 ± 1.2	5.61E-01
P62703	40S ribosomal protein S4, X isoform	116	10.7 ± 3.3	9 ± 4.2	5.61E-01
D3ZWM5	Histone H2B	1083	93.2 ± 8.1	88 ± 19.3	5.63E-01
F1LR77	Protein Ttc13	15	1 ± 0.9	2 ± 2	5.64E-01
M0R757	Elongation factor 1-alpha	428	38.8 ± 9.8	35 ± 13.2	5.68E-01
P12785	Fatty acid synthase	237	21.3 ± 6.2	19 ± 5.6	5.69E-01
Q3KRD5	Mitochondrial import receptor subunit TOM34	23	1.7 ± 0.5	2 ± 2.1	5.69E-01
G3V828	Protein Cnpy3	25	1.8 ± 1.8	2 ± 0.8	5.73E-01
F7DLY1	EPS8-like 2 (Predicted), isoform CRA_d	100	8.3 ± 1.4	9 ± 1.6	5.73E-01
Q499N5	Acyl-CoA synthetase family member 2, mitochondrial	33	3 ± 1.3	3 ± 1.6	5.74E-01
Q63691	Monocyte differentiation antigen CD14	36	3.3 ± 2.3	3 ± 1.6	5.74E-01
D4A1Z2	Uncharacterized protein	14	1 ± 1.1	1 ± 0.8	5.74E-01
P84903	Stromal interaction molecule 1	12	0.8 ± 1	1 ± 1	5.75E-01
O08837	Cell division cycle 5-like protein	19	1.3 ± 1	2 ± 1.9	5.77E-01
Q920L2	Succinate dehydrogenase [ubiquinone] flavoprotein subunit, mitochondrial	8	0.5 ± 0.8	1 ± 1.2	5.77E-01
Q925G0	Putative RNA-binding protein 3	8	0.5 ± 0.8	1 ± 1.2	5.77E-01

Q5M7T6	ATPase, H+ transporting, lysosomal 38kDa, V0 subunit d1	30	2.2 ± 2.3	3 ± 1.5	5.78E-01
P51635	Alcohol dehydrogenase [NADP(+)]	36	3.3 ± 2.6	3 ± 1.4	5.78E-01
Q06647	ATP synthase subunit O, mitochondrial	191	15.7 ± 5	17 ± 3.9	5.79E-01
D4A412	Protein LOC688684	87	6.5 ± 4.1	8 ± 4.9	5.79E-01
P85971	6-phosphogluconolactonase	49	4.5 ± 2.4	4 ± 1.6	5.82E-01
Q4KLI7	Protein Sf3a3	18	1.7 ± 1.2	1 ± 0.8	5.83E-01
B0BMW2	3-hydroxyacyl-CoA dehydrogenase type-2	383	31 ± 9.4	35 ± 15.7	5.83E-01
G3V741	Phosphate carrier protein, mitochondrial	96	7.3 ± 3.3	8 ± 1.2	5.84E-01
Q6NYB7	Ras-related protein Rab-1A	94	7.3 ± 4.1	9 ± 4	5.86E-01
D3ZS58	NADH dehydrogenase [ubiquinone] 1 alpha subcomplex subunit 2	14	1 ± 0	1 ± 0.8	5.86E-01
B2RZ37	Receptor expression-enhancing protein 5	112	7.8 ± 2.3	9 ± 6.3	5.87E-01
G3V796	Acetyl-Coenzyme A dehydrogenase, medium chain	28	2.5 ± 0.8	2 ± 1.2	5.88E-01
Q5FVL2	ER membrane protein complex subunit 8	10	0.7 ± 0.8	1 ± 1.3	5.90E-01
M0R875	Protein LOC100366044 (Fragment)	10	0.7 ± 0.8	1 ± 1.3	5.90E-01
Q6AYH6	ER membrane protein complex subunit 10	10	0.7 ± 0.8	1 ± 1.3	5.90E-01
G3V8M5	Serine/threonine-protein phosphatase	10	0.7 ± 0.8	1 ± 1.3	5.90E-01
Q6P742	Proteolipid protein 2	36	2.7 ± 1.6	3 ± 2.5	5.90E-01
B0K020	CDGSH iron-sulfur domain-containing protein 1	36	2.7 ± 2.1	3 ± 2.1	5.90E-01
P04785	Protein disulfide-isomerase	699	58.2 ± 5.3	62 ± 13.8	5.90E-01
Q5XI22	Acetyl-CoA acetyltransferase, cytosolic	106	9.8 ± 5.3	8 ± 5.1	5.92E-01
P68511	14-3-3 protein eta	206	17 ± 5.9	19 ± 2.9	5.93E-01
P07632	Superoxide dismutase [Cu-Zn]	92	7 ± 3.5	8 ± 4.8	5.94E-01
D4AEH3	Proteasome (Prosome, macropain) 26S subunit, non-ATPase, 7 (Predicted)	109	9.8 ± 5.1	9 ± 1.5	5.95E-01
Q4FZT0	Stomatin-like protein 2, mitochondrial	65	5.2 ± 2.3	6 ± 3	5.97E-01

P62494	Ras-related protein Rab-11A	68	6.3 ± 3.9	5 ± 2.3	5.98E-01
D4AD67	Protein Ktn1	31	2.8 ± 1.2	2 ± 1.9	5.99E-01
D3ZUB0	Protein Rcn1	17	1.3 ± 0.5	2 ± 0.5	5.99E-01
F1MAB9	Protein Tpd52	19	1.7 ± 0.5	2 ± 0.5	6.00E-01
D3ZXF9	Protein Mrpl12	59	5.5 ± 4.1	5 ± 2.3	6.03E-01
Q498R7	UPF0587 protein C1orf123 homolog	7	0.5 ± 0.5	1 ± 0.5	6.04E-01
G3V928	Protein Lrp1	7	0.7 ± 0.5	1 ± 0.5	6.04E-01
P42667	Signal peptidase complex catalytic subunit SEC11A	7	0.5 ± 0.5	1 ± 0.5	6.04E-01
P07151	Beta-2-microglobulin	7	0.7 ± 0.5	1 ± 0.5	6.04E-01
P21670	Proteasome subunit alpha type-4	7	0.7 ± 0.5	1 ± 0.5	6.04E-01
B0BN68	Mitochondrial ribosomal protein S9	7	0.5 ± 0.5	1 ± 0.5	6.04E-01
Q5M823	NudC domain-containing protein 2	7	0.5 ± 0.5	1 ± 0.5	6.04E-01
D3ZF12	Signal peptidase complex subunit 3	7	0.7 ± 0.5	1 ± 0.5	6.04E-01
Q09325	Alpha-1,3-mannosyl-glycoprotein 2-beta-N-acetylglucosaminyltransferase	7	0.7 ± 0.5	1 ± 0.5	6.04E-01
P17074	40S ribosomal protein S19	79	7.3 ± 2.7	6 ± 3.7	6.05E-01
D3ZXB7	Protein Krt71	26	1.8 ± 2.1	3 ± 2.2	6.07E-01
Q3T1K5	F-actin-capping protein subunit alpha-2	33	3 ± 2	3 ± 1.2	6.07E-01
P49432	Pyruvate dehydrogenase E1 component subunit beta, mitochondrial	98	7.7 ± 4	9 ± 2.2	6.07E-01
G3V6A4	Heterogeneous nuclear ribonucleoprotein D, isoform CRA_b	78	6.5 ± 1.2	7 ± 2	6.10E-01
Q5PQK2	Fusion, derived from t(1216) malignant liposarcoma (Human)	40	3.5 ± 1.2	3 ± 1	6.13E-01
B5DEI0	Pcyox1l protein	12	1 ± 0	1 ± 0.8	6.16E-01
B5DF51	Membrane magnesium transporter 1	10	1 ± 0	1 ± 0.8	6.16E-01
Q5FVM4	Non-POU domain-containing octamer-binding protein	13	0.8 ± 0.8	1 ± 0	6.16E-01
M0RC14	Protein Hcr (Fragment)	10	0.8 ± 0.8	1 ± 0	6.16E-01
Q6P6R2	Dihydrolipoyl dehydrogenase, mitochondrial	99	8.8 ± 1.6	8 ± 2.7	6.19E-01

Q5RJT2	pre-rRNA processing protein FTSJ3	20	1.8 ± 0.8	2 ± 1.4	6.25E-01
Q4KLF8	Actin-related protein 2/3 complex subunit 5	22	2 ± 1.3	2 ± 1	6.26E-01
F1LMZ8	26S proteasome non-ATPase regulatory subunit 11	120	10.7 ± 2.6	10 ± 2	6.27E-01
Q5M7U6	Actin-related protein 2	22	2 ± 1.1	2 ± 1.2	6.31E-01
B0BNG0	ER membrane protein complex subunit 2	42	3.8 ± 1.6	3 ± 1.9	6.31E-01
Q9JM53	Apoptosis-inducing factor 1, mitochondrial	26	2.3 ± 1	2 ± 1.3	6.31E-01
Q5XI73	Rho GDP-dissociation inhibitor 1	146	12.2 ± 2	13 ± 3.6	6.32E-01
F1LSS0	Golgin subfamily A member 2	16	1.5 ± 0.5	1 ± 1.5	6.32E-01
D4AEI5	Protein Myef2	24	2.2 ± 1.2	2 ± 1.2	6.33E-01
B1WBY7	ER lipid raft associated 1	12	1.2 ± 1.2	1 ± 1.2	6.36E-01
D4AEP0	Adenylosuccinate synthetase isozyme 2	23	2.2 ± 2.4	2 ± 1	6.36E-01
D3Z8M2	Vacuolar protein-sorting-associated protein 25	10	1 ± 1.5	1 ± 0.8	6.37E-01
Q5U300	Ubiquitin-like modifier-activating enzyme 1	361	29.5 ± 13.2	32 ± 5.2	6.40E-01
D4AEC0	Histone H2A	27	2 ± 1.4	3 ± 2.2	6.40E-01
G3V6L9	Peptidyl-prolyl cis-trans isomerase	14	1 ± 0.9	1 ± 1.5	6.42E-01
Q6AYH5	Dynactin subunit 2	62	5 ± 1.3	6 ± 2.3	6.42E-01
P29314	40S ribosomal protein S9	41	3.7 ± 1.5	3 ± 2	6.44E-01
P60901	Proteasome subunit alpha type-6	34	3.2 ± 2.1	3 ± 1.5	6.46E-01
F1LP60	Moesin (Fragment)	234	20.7 ± 4.2	19 ± 6.4	6.46E-01
G3V8Z9	COP9 (Constitutive photomorphogenic) homolog, subunit 7a (Arabidopsis thaliana) (Predicted)	22	2 ± 1.4	2 ± 1	6.48E-01
P08753	Guanine nucleotide-binding protein G(k) subunit alpha	29	2.2 ± 2.1	3 ± 1.4	6.48E-01
P58775	Tropomyosin beta chain	82	6.3 ± 4.8	8 ± 6.2	6.48E-01
F7EP67	Endothelin-converting enzyme 1	16	1.2 ± 0.8	2 ± 1.6	6.50E-01
Q9Z142	Transmembrane protein 33	24	1.8 ± 1.2	2 ± 1.3	6.54E-01

Q9R1Z0	Voltage-dependent anion-selective channel protein 3	14	1 ± 1.3	1 ± 1.2	6.55E-01
F1LWZ8	Protein Lemd3	49	4.3 ± 2.3	4 ± 1.5	6.55E-01
F2Z3T7	Isochorismatase domain-containing protein 1	29	2.2 ± 1.7	3 ± 2.1	6.57E-01
F1LP82	Ras-related protein Rab-2A (Fragment)	140	11.3 ± 4.5	12 ± 2.9	6.57E-01
Q497B0	Omega-amidase NIT2	38	3.5 ± 2.4	3 ± 1.3	6.58E-01
O70377	Synaptosomal-associated protein 23	36	2.8 ± 1.5	3 ± 1	6.58E-01
G3V9W6	Aldehyde dehydrogenase	91	8.2 ± 3.4	8 ± 1.4	6.59E-01
F1LZX9	Protein Itgav	88	8 ± 3	7 ± 2.1	6.59E-01
D4A4B1	Mitochondrial ribosomal protein L15 (Predicted), isoform CRA_c	9	0.7 ± 0.5	1 ± 0.8	6.59E-01
P41350	Caveolin-1	9	0.8 ± 0.8	1 ± 0.5	6.59E-01
D3ZRA3	Acetyl-CoA carboxylase 1	9	0.8 ± 0.8	1 ± 0.5	6.59E-01
Q8CHN6	Sphingosine-1-phosphate lyase 1	18	1.3 ± 1	2 ± 1.5	6.59E-01
P47942	Dihydropyrimidinase-related protein 2	156	12.8 ± 5	14 ± 1.8	6.60E-01
Q9EPC6	Profilin-2	39	3.5 ± 1.4	3 ± 1.2	6.60E-01
P21807	Peripherin	134	10.8 ± 6.1	12 ± 3.7	6.61E-01
Q64560	Tripeptidyl-peptidase 2	12	0.8 ± 1.3	1 ± 1.2	6.62E-01
D4A5T1	Protein Sf3b5	12	0.8 ± 1.3	1 ± 1.2	6.62E-01
Q63716	Peroxiredoxin-1	215	19 ± 4.6	18 ± 4.4	6.65E-01
Q07984	Translocon-associated protein subunit delta	120	10.5 ± 3.9	10 ± 2.5	6.66E-01
P62859	40S ribosomal protein S28	43	3.5 ± 0.5	3 ± 1.7	6.68E-01
D3ZF26	Protein Tnks1bp1	18	1.3 ± 1.4	2 ± 1.2	6.68E-01
D3ZGY2	OTU domain containing 6B (Predicted), isoform CRA_b	15	1.3 ± 0.5	1 ± 0.8	6.69E-01
D3ZKX1	Protein Ccdc53	15	1.3 ± 0.5	1 ± 0.8	6.69E-01
P11598	Protein disulfide-isomerase A3	909	76.3 ± 8.4	79 ± 14.8	6.74E-01
Q5XI31	GPI transamidase component PIG-S	46	4 ± 0.9	4 ± 1.6	6.74E-01

Q6PDU7	ATP synthase subunit g, mitochondrial	101	9.2 ± 2.1	8 ± 4.1	6.75E-01
D4A7D9	Uncharacterized protein	16	1.2 ± 1.2	2 ± 1.5	6.76E-01
G3V6H0	Protein LOC100363782	39	2.8 ± 2.6	3 ± 0.8	6.78E-01
D3ZYX5	Protein Myo6	26	2.3 ± 0.8	2 ± 1.7	6.78E-01
Q75Q41	Mitochondrial import receptor subunit TOM22 homolog	18	1.3 ± 1.2	2 ± 1.5	6.79E-01
D3ZQB6	Cat eye syndrome chromosome region, candidate 5 homolog (Human) (Predicted)	7	0.7 ± 0.8	1 ± 0.5	6.81E-01
Q5RJR2	Twinfilin-1	7	0.7 ± 0.8	1 ± 0.5	6.81E-01
F1M110	Glycylpeptide N-tetradecanoyltransferase (Fragment)	7	0.7 ± 0.8	1 ± 0.5	6.81E-01
P24155	Thimet oligopeptidase	7	0.7 ± 0.8	1 ± 0.5	6.81E-01
D3ZXH7	Protein Thoc4	7	0.7 ± 0.8	1 ± 0.5	6.81E-01
Q5XII6	Protein Zcchc9	7	0.7 ± 0.8	1 ± 0.5	6.81E-01
F1LPQ7	Golgin subfamily A member 4	7	0.5 ± 0.5	1 ± 0.8	6.81E-01
D4A4H5	Protein Sdf2	7	0.5 ± 0.5	1 ± 0.8	6.81E-01
F1M7V1	Kin of IRRE-like protein 1	7	0.5 ± 0.5	1 ± 0.8	6.81E-01
Q62651	Delta(3,5)-Delta(2,4)-dienoyl-CoA isomerase, mitochondrial	16	1.2 ± 0.8	2 ± 1.9	6.82E-01
P51583	Multifunctional protein ADE2	19	1.5 ± 0.8	1 ± 0.5	6.83E-01
F1LR10	Epithelial protein lost in neoplasm	85	6.5 ± 4.6	8 ± 3.5	6.84E-01
Q66H06	Protein Tspan3	13	1 ± 0.6	1 ± 0.8	6.86E-01
Q68FP1	Gelsolin	71	5.7 ± 2.7	7 ± 4.1	6.86E-01
M0R4M3	Protein 1190003K10Rik	278	24.2 ± 4.3	23 ± 2.5	6.87E-01
Q9Z1X1	Extended synaptotagmin-1	51	4.7 ± 2.8	4 ± 2.8	6.87E-01
D3ZJH9	Malic enzyme	155	13 ± 1.9	14 ± 3.5	6.89E-01
O35796	Complement component 1 Q subcomponent-binding protein, mitochondrial	29	2.3 ± 0.8	3 ± 0.5	6.89E-01
B4F772	Heat shock 70 kDa protein 4L	77	6 ± 5.4	7 ± 2	6.89E-01
D4A6W6	Protein RGD1561333	45	4 ± 1.9	4 ± 2.3	6.89E-01
Q9ER34	Aconitate hydratase, mitochondrial	310	25.5 ± 8.1	28 ± 10.1	6.90E-01
F1LM47	Protein Sucla2	16	0.8 ± 0.8	1 ± 0.6	6.90E-01

M0R9Q9	Cytosol aminopeptidase (Fragment)	11	0.8 ± 0.8	1 ± 0.6	6.90E-01
P54311	Guanine nucleotide-binding protein G(I)/G(S)/G(T) subunit beta-1	78	7 ± 2.8	6 ± 2.9	6.91E-01
Q68FR6	Elongation factor 1-gamma	176	15.5 ± 2.4	15 ± 4.3	6.91E-01
Q6AY18	Protein Sar1a	39	3.5 ± 1.6	3 ± 1.2	6.92E-01
P09527	Ras-related protein Rab-7a	454	40.3 ± 11.9	38 ± 9.6	6.97E-01
P63039	60 kDa heat shock protein, mitochondrial	956	84.7 ± 13	80 ± 25.2	6.98E-01
F1LS02	Nuclear pore complex protein Nup155	7	0.7 ± 0.5	1 ± 0.8	6.98E-01
O55156	CAP-Gly domain-containing linker protein 2	7	0.5 ± 0.8	1 ± 0.5	6.98E-01
P11608	ATP synthase protein 8	7	0.5 ± 0.8	1 ± 0.5	6.98E-01
Q6IFW7	Protein Krt28	7	0.7 ± 0.5	1 ± 0.8	6.98E-01
Q5RKJ9	RAB10, member RAS oncogene family	10	0.7 ± 0.5	1 ± 0.8	6.98E-01
Q68FY1	Nucleoporin NUP53	39	3.5 ± 2.9	3 ± 1.3	6.98E-01
D3ZBL3	Protein Ngdn	12	1 ± 0	1 ± 1	7.00E-01
F1LRB8	S-adenosylmethionine synthase	38	3 ± 1.5	3 ± 1.4	7.02E-01
D4A0W5	Leucine-rich repeat and fibronectin type-III domain-containing protein 5	17	1.7 ± 1.9	1 ± 1	7.02E-01
E9PTI6	Protein Raly	46	3.7 ± 1.8	4 ± 2.6	7.04E-01
Q64654	Lanosterol 14-alpha demethylase	71	6.3 ± 1.6	6 ± 2.6	7.04E-01
Q99ML5	Prenylcysteine oxidase	132	11.7 ± 1	11 ± 4	7.05E-01
P31000	Vimentin	2453	217 ± 59.2	206 ± 37	7.06E-01
E9PTN6	Glyceraldehyde-3-phosphate dehydrogenase	194	13.2 ± 20.5	19 ± 29	7.08E-01
M0R3M3	Uncharacterized protein (Fragment)	25	2.3 ± 2.4	2 ± 2.1	7.12E-01
Q09167	Serine/arginine-rich splicing factor 5	9	0.8 ± 1	1 ± 0.5	7.13E-01
Q5BJZ4	Protein Surf6	15	0.8 ± 1	1 ± 0.5	7.13E-01
Q5BJS0	Putative ATP-dependent RNA helicase DHX30	9	0.7 ± 0.5	1 ± 1	7.13E-01
O35760	Isopentenyl-diphosphate Delta-isomerase 1	25	2 ± 1.5	2 ± 1.5	7.14E-01
M0RAU4	Uncharacterized protein (Fragment)	323	29.7 ± 20.5	25 ± 19.4	7.15E-01

P50398	Rab GDP dissociation inhibitor alpha	18	1.8 ± 2.9	1 ± 1.8	7.15E-01
D4A510	Protein LOC685179	31	2.3 ± 1.8	3 ± 2.9	7.17E-01
D4A9Y0	Protein Sdf2l1	30	2.7 ± 1.9	2 ± 1.2	7.18E-01
D4A0W1	Protein Emc4	44	3.5 ± 1.5	4 ± 1.6	7.19E-01
P63281	SUMO-conjugating enzyme UBC9	15	1.2 ± 0.8	1 ± 0.8	7.21E-01
Q5XIP9	Transmembrane protein 43	28	2.2 ± 0.8	3 ± 2.2	7.22E-01
G3V7L6	26S protease regulatory subunit 7	61	5.5 ± 4.2	5 ± 1.7	7.22E-01
F1LRE1	Glutathione reductase	9	0.8 ± 0.8	1 ± 0.8	7.23E-01
D4ACS0	Protein phosphatase 1 regulatory subunit 12A	9	0.7 ± 0.8	1 ± 0.8	7.23E-01
Q5RKI6	Probable RNA-binding protein EIF1AD	9	0.7 ± 0.8	1 ± 0.8	7.23E-01
F1M0W9	Uncharacterized protein (Fragment)	9	0.8 ± 0.8	1 ± 0.8	7.23E-01
B0BN63	LOC681996 protein	9	0.8 ± 0.8	1 ± 0.8	7.23E-01
D3ZZY2	Protein Utp14a	9	0.7 ± 0.8	1 ± 0.8	7.23E-01
Q923V8	15 kDa selenoprotein	18	1.3 ± 1	2 ± 2.1	7.23E-01
Q9JLA3	UDP-glucose:glycoprotein glucosyltransferase 1	162	14.7 ± 6.4	13 ± 6.3	7.24E-01
D4ADD7	Glutaredoxin 5 homolog (S. cerevisiae) (Predicted), isoform CRA_b	12	1 ± 0	1 ± 1.2	7.24E-01
F1LSW7	60S ribosomal protein L14	124	10.8 ± 4	10 ± 2.1	7.25E-01
Q3SWU3	Heterogeneous nuclear ribonucleoprotein D-like	46	3.7 ± 3.2	4 ± 0.8	7.25E-01
G3V8Q1	Protein Cope	7	0.7 ± 1	1 ± 0.5	7.26E-01
Q5BK63	NADH dehydrogenase [ubiquinone] 1 alpha subcomplex subunit 9, mitochondrial	7	0.7 ± 1	1 ± 0.5	7.26E-01
Q5FVG4	Protein LOC100911440	7	0.7 ± 1	1 ± 0.5	7.26E-01
Q9Z2S9	Flotillin-2	7	0.7 ± 1	1 ± 0.5	7.26E-01
D4AD15	Protein Eif4g1	41	3.2 ± 2.2	4 ± 2.6	7.26E-01
P02793	Ferritin light chain 1	61	5.5 ± 2.2	5 ± 2.6	7.27E-01
E9PTD2	Phosphatidylinositol-binding clathrin assembly protein	27	2.2 ± 1.2	2 ± 0	7.29E-01
P22509	rRNA 2'-O-methyltransferase fibrillarin	27	2.2 ± 1.2	2 ± 0	7.29E-01

Q5PQL7	Integral membrane protein 2C	43	3.8 ± 1.6	4 ± 1.6	7.30E-01
P52759	Ribonuclease UK114	17	1.3 ± 0.5	2 ± 1	7.30E-01
Q3KRE2	Methyltransferase like 7A	19	1.5 ± 1	1 ± 0.5	7.30E-01
Q9WUL0	DNA topoisomerase 1	17	1.5 ± 1	1 ± 0.5	7.30E-01
Q5U2U0	ATP-dependent Clp protease ATP-binding subunit clpX-like, mitochondrial	13	1 ± 0.6	1 ± 1	7.31E-01
D3Z8L7	Ras-related protein R-Ras	28	2.2 ± 1.7	3 ± 1.5	7.31E-01
B5DFI9	Pdk3 protein	49	4.3 ± 1.9	4 ± 1.4	7.33E-01
Q641X8	Eukaryotic translation initiation factor 3 subunit E	22	1.7 ± 1.5	2 ± 1.8	7.33E-01
B5DEL3	Protein Ttc17	11	1 ± 0.9	1 ± 0.8	7.33E-01
M0R959	Protein Mmab	11	0.8 ± 0.8	1 ± 0.9	7.33E-01
D3ZA85	Histone cell cycle regulation defective interacting protein 5 (Predicted), isoform CRA_a	11	1 ± 0.9	1 ± 0.8	7.33E-01
D4A7X1	Protein Mrps16	11	0.8 ± 0.8	1 ± 0.9	7.33E-01
D3ZAS8	Protein Sart3	11	1 ± 0.9	1 ± 0.8	7.33E-01
P81155	Voltage-dependent anion-selective channel protein 2	63	5.5 ± 2.7	5 ± 2.3	7.33E-01
Q6AXW2	Protein Tmod3	13	1 ± 0.9	1 ± 0.8	7.36E-01
G3V7R1	Nuclear pore complex protein Nup50	13	1.2 ± 0.8	1 ± 0.9	7.36E-01
Q4V8I7	Leucine-rich repeat-containing protein 8A	13	1 ± 0.9	1 ± 0.8	7.36E-01
G3V6Q6	Guanine nucleotide binding protein, alpha 11	13	1.2 ± 0.8	1 ± 0.9	7.36E-01
F1M964	Mitochondrial-processing peptidase subunit alpha	7	0.5 ± 0.8	1 ± 0.8	7.37E-01
F1LT30	Uncharacterized protein	7	0.7 ± 0.8	1 ± 0.8	7.37E-01
F1LNV5	Calcium uptake protein 1, mitochondrial	7	0.7 ± 0.8	1 ± 0.8	7.37E-01
F1LM16	Plasminogen activator inhibitor 1	7	0.7 ± 0.8	1 ± 0.8	7.37E-01
P83860	Orexigenic neuropeptide QRFP	7	0.7 ± 0.8	1 ± 0.8	7.37E-01
Q6IFU7	Keratin, type I cytoskeletal 42	14	0.7 ± 0.8	1 ± 0.8	7.37E-01
Q63083	Nucleobindin-1	7	0.5 ± 0.8	1 ± 0.8	7.37E-01

Q9ES53	Ubiquitin fusion degradation protein 1 homolog	7	0.7 ± 0.8	1 ± 0.8	7.37E-01
Q9WVJ4	Synaptojanin-2-binding protein	7	0.7 ± 0.8	1 ± 0.8	7.37E-01
Q4V8C2	Centromere/kinetochore protein zw10 homolog	7	0.5 ± 0.8	1 ± 0.8	7.37E-01
G3V699	Protein transport protein Sec31A	54	5 ± 0.6	5 ± 2.3	7.38E-01
P62076	Mitochondrial import inner membrane translocase subunit Tim13	19	1.7 ± 0.5	2 ± 1	7.38E-01
P63095	Guanine nucleotide-binding protein G(s) subunit alpha isoforms short	95	7.8 ± 2.1	9 ± 4.3	7.39E-01
P61805	Dolichyl-diphosphooligosaccharide--protein glycosyltransferase subunit DAD1	22	2 ± 0	2 ± 1.2	7.40E-01
B3GNI6	Septin-11	66	6 ± 2.9	6 ± 2.2	7.41E-01
P10111	Peptidyl-prolyl cis-trans isomerase A	225	18 ± 9.1	17 ± 3.7	7.44E-01
G3V9N8	AP-1 complex subunit beta-1	20	1.5 ± 1.6	2 ± 1.8	7.47E-01
Q4KMA8	Endoplasmic reticulum aminopeptidase 1	59	5.2 ± 1	5 ± 2.2	7.47E-01
F1M8V2	Protein Ube4b	47	4.3 ± 3.1	4 ± 2	7.48E-01
B0BNJ4	Ethylmalonic encephalopathy 1	53	4.3 ± 2.3	5 ± 2.9	7.49E-01
Q0ZFS8	Protein LOC100910660	28	2.2 ± 3.1	3 ± 2	7.50E-01
Q4V7D9	Protein Smpdl3b	21	1.8 ± 1.2	2 ± 0.5	7.52E-01
P32551	Cytochrome b-c1 complex subunit 2, mitochondrial	178	15.7 ± 4.5	15 ± 4.4	7.52E-01
D3ZPW7	Glutathione peroxidase	84	7.5 ± 2.1	7 ± 4.5	7.54E-01
P11240	Cytochrome c oxidase subunit 5A, mitochondrial	89	7.8 ± 2	8 ± 1.5	7.54E-01
O08984	Lamin-B receptor	9	0.7 ± 0.8	1 ± 1	7.55E-01
M0R7V3	Protein Apoo	9	0.8 ± 1	1 ± 0.8	7.55E-01
B2RZD6	Ndufa4 protein	9	0.7 ± 0.8	1 ± 1	7.55E-01
P49793	Nuclear pore complex protein Nup98-Nup96	15	1.2 ± 1	1 ± 0.8	7.58E-01
Q32PZ3	Protein unc-45 homolog A	21	1.7 ± 1	2 ± 0.8	7.58E-01
M0R7Z0	Uncharacterized protein	44	3.5 ± 2.3	4 ± 1	7.59E-01
D3ZN59	Protein LOC100911856	111	8.5 ± 5.3	8 ± 3.8	7.59E-01
O35814	Stress-induced-phosphoprotein 1	13	1.2 ± 1.2	1 ± 0.6	7.61E-01

G3V8R7	GATA zinc finger domain containing 2A	9	0.8 ± 0.8	1 ± 1	7.61E-01
Q8CG45	Aflatoxin B1 aldehyde reductase member 2	15	1.2 ± 1.2	1 ± 0.5	7.62E-01
Q5XIC0	Enoyl-CoA delta isomerase 2, mitochondrial	11	1 ± 1.1	1 ± 0.8	7.62E-01
Q9WV25	Poly(U)-binding-splicing factor PUF60	11	1 ± 1.1	1 ± 0.8	7.62E-01
Q5U1W8	High-mobility group nucleosome binding domain 1	7	0.5 ± 0.8	1 ± 1	7.64E-01
D4A6V3	Uncharacterized protein	17	1.3 ± 0.8	2 ± 1	7.64E-01
B2RZ78	Vacuolar protein sorting-associated protein 29	13	1 ± 0.9	1 ± 1	7.65E-01
Q62902	Protein ERGIC-53	13	1 ± 0.9	1 ± 1	7.65E-01
Q1JU68	Eukaryotic translation initiation factor 3 subunit A	51	4.8 ± 2.6	4 ± 4.5	7.65E-01
D3ZA93	Protein Acot13	17	1.3 ± 1	2 ± 0.8	7.67E-01
Q6MG49	Large proline-rich protein BAG6	19	1.5 ± 1	2 ± 0.8	7.67E-01
Q6TUD4	Protein YIPF3	15	0.8 ± 1	1 ± 0.9	7.67E-01
B1H2A6	Fxr2 protein	11	1 ± 0.9	1 ± 1	7.67E-01
P52944	PDZ and LIM domain protein 1	45	4 ± 2.4	4 ± 3.2	7.68E-01
D4A054	Protein LOC100911178	27	2.5 ± 2.5	2 ± 1.2	7.69E-01
Q06C60	BolA-like 1 (E. coli) (Predicted)	11	0.8 ± 1.2	1 ± 0.6	7.71E-01
F1LSK6	Cytochrome P450 20A1	50	4.3 ± 1.9	4 ± 2	7.72E-01
D4ADL2	Uncharacterized protein	13	0.8 ± 1.3	1 ± 0.5	7.72E-01
Q6P502	T-complex protein 1 subunit gamma	165	13.5 ± 3.7	14 ± 5.9	7.72E-01
Q5EAJ6	Inhibitor of nuclear factor kappa-B kinase-interacting protein	88	6.8 ± 2.2	7 ± 1.6	7.73E-01
P23965	Enoyl-CoA delta isomerase 1, mitochondrial	53	4.8 ± 2.1	4 ± 3.5	7.74E-01
F1M3H8	Protein Hnrnpa0	30	2.7 ± 2	2 ± 2	7.75E-01
P21708	Mitogen-activated protein kinase 3	9	0.7 ± 0.8	1 ± 1.2	7.77E-01
D3ZW38	Protein Exosc6	62	3.7 ± 2.3	3 ± 1.6	7.79E-01
G3V6W6	Protein Psmc6	126	11 ± 4.7	10 ± 3.3	7.82E-01
Q8K1Q0	Glycylpeptide N-tetradecanoyltransferase 1	13	1.2 ± 1.3	1 ± 0.6	7.82E-01

D3ZUL8	Protein Zcchc8	11	0.8 ± 0.8	1 ± 1.3	7.83E-01
Q6AYP7	7-methylguanosine phosphate-specific 5'-nucleotidase	15	1.2 ± 1.2	1 ± 0.8	7.83E-01
M0R5N9	Protein 4933426M11Rik	42	3.8 ± 2.3	4 ± 1.8	7.84E-01
P97536	Cullin-associated NEDD8-dissociated protein 1	148	13.2 ± 2.4	12 ± 6.8	7.85E-01
F1LMJ8	Calcium uptake protein 2, mitochondrial	17	1.3 ± 0.8	2 ± 1.2	7.85E-01
M0R5N4	Protein LOC100366237	17	1.5 ± 1.2	1 ± 0.8	7.85E-01
Q5U2V1	FK506 binding protein 10	47	3.8 ± 1.5	4 ± 2.6	7.86E-01
Q6AYF8	Protein Serpinb9	15	1.3 ± 0.5	1 ± 1.3	7.86E-01
Q5XIM9	T-complex protein 1 subunit beta	140	12.2 ± 4.9	12 ± 3.3	7.87E-01
F1M6W2	Endoplasmic reticulum metallopeptidase 1	17	1.3 ± 1	2 ± 1	7.87E-01
P61765	Syntaxin-binding protein 1	17	1.5 ± 1	1 ± 1	7.87E-01
Q6MGC4	H2-K region expressed gene 2, rat orthologue	13	1 ± 1.1	1 ± 1	7.89E-01
G3V8T5	Protein Ruvbl2	13	1 ± 1.1	1 ± 1	7.89E-01
F1LSL2	Nuclear pore complex protein Nup107	19	1.5 ± 1.2	2 ± 0.8	7.89E-01
Q5XFX0	Transgelin-2	186	15.2 ± 9.4	16 ± 4.6	7.93E-01
Q5U2S7	Proteasome (Prosome, macropain) 26S subunit, non-ATPase, 3	78	6.3 ± 1.4	6 ± 0.8	7.98E-01
P62963	Profilin-1	354	29.2 ± 8.4	28 ± 4.3	7.99E-01
O55158	D6.1A protein	312	26.3 ± 6	27 ± 5	7.99E-01
P19234	NADH dehydrogenase [ubiquinone] flavoprotein 2, mitochondrial	25	1.7 ± 1.2	2 ± 1	8.00E-01
D4A8N1	Protein Dpm1	22	1.5 ± 0.5	2 ± 1.5	8.00E-01
B2RYP0	Protein Rhoc	42	3.3 ± 4.4	4 ± 4.5	8.01E-01
O88989	Malate dehydrogenase, cytoplasmic	61	5.3 ± 1.5	5 ± 2.8	8.02E-01
F1LPB6	Protein Triobp	11	0.8 ± 1	1 ± 1.3	8.03E-01
Q5I0D1	Glyoxalase domain-containing protein 4	30	2.7 ± 1.2	3 ± 1	8.04E-01
M0RCH6	Protein LOC100359642	31	2.5 ± 1	3 ± 1.2	8.04E-01
Q52KJ9	Protein Tmx1	203	17 ± 5.8	18 ± 5.5	8.04E-01
D4A442	40S ribosomal protein S21	29	2.5 ± 1	2 ± 1.2	8.05E-01

M0R7E6	Protein Srrt	40	3.5 ± 1.4	3 ± 2.9	8.05E-01
D4A8H8	Cytoplasmic FMR1 interacting protein 1 (Predicted)	11	0.8 ± 1.3	1 ± 0.9	8.08E-01
Q2M2S1	Protein Tor1b	15	1.2 ± 0.8	1 ± 1.5	8.10E-01
F1LQN3	Reticulon-4	256	22.5 ± 2.3	22 ± 7.9	8.11E-01
Q6P3V8	Eukaryotic translation initiation factor 4A1	168	13.7 ± 3.8	15 ± 11.3	8.13E-01
D4A4W6	Protein Slirp	15	1.3 ± 1.2	1 ± 1.2	8.13E-01
P62815	V-type proton ATPase subunit B, brain isoform	63	5.5 ± 4.3	5 ± 2.8	8.16E-01
F7EKL8	UDP-glucose 4-epimerase	17	1.3 ± 1	2 ± 1.4	8.16E-01
M0R8Q2	Protein LOC100360791	23	2 ± 1.4	2 ± 1	8.16E-01
Q6P791	Ragulator complex protein LAMTOR1	95	8 ± 2.2	8 ± 2.7	8.17E-01
F1LR87	Beta-hexosaminidase	47	3.8 ± 1.2	4 ± 1.3	8.17E-01
O08629	Transcription intermediary factor 1-beta	175	14.8 ± 3.2	15 ± 1.3	8.19E-01
D3ZNQ6	Protein Ube2m	20	1.8 ± 1.7	2 ± 0.5	8.22E-01
Q64303	Serine/threonine-protein kinase PAK 2	13	1.2 ± 0.8	1 ± 1.5	8.22E-01
B5DFC8	Eukaryotic translation initiation factor 3 subunit C	30	2.8 ± 1.7	3 ± 0.5	8.23E-01
P17078	60S ribosomal protein L35	50	4 ± 1.4	4 ± 3.3	8.24E-01
B2RZ72	Actin related protein 2/3 complex, subunit 4 (Predicted), isoform CRA_a	11	1 ± 1.7	1 ± 0.8	8.24E-01
D3ZJF9	Protein Gla	39	3.3 ± 1.4	3 ± 1.2	8.25E-01
F1LW91	Protein Numa1 (Fragment)	34	3.2 ± 3.4	3 ± 1.3	8.25E-01
Q6AXS4	Renin receptor	31	2.7 ± 1.5	3 ± 1	8.28E-01
G3V7Y3	ATP synthase subunit delta, mitochondrial	17	1.5 ± 1.4	1 ± 1.2	8.28E-01
M0R9D0	Acidic leucine-rich nuclear phosphoprotein 32 family member A	13	1 ± 1.3	1 ± 1.3	8.29E-01
B1WC84	Canopy 4 homolog (Zebrafish)	76	6.7 ± 2.7	6 ± 2.6	8.30E-01
G3V6D3	ATP synthase subunit beta	938	78.7 ± 21.8	81 ± 15.4	8.35E-01
D4A3W2	Protein Crb2	17	1.3 ± 1	2 ± 1.6	8.36E-01

P12001	60S ribosomal protein L18	378	32 ± 5.4	33 ± 7.9	8.36E-01
R9PXZ3	Ankycorbin (Fragment)	26	2.2 ± 1.6	2 ± 1	8.36E-01
Q3MHS9	Chaperonin containing Tcp1, subunit 6A (Zeta 1)	151	12.8 ± 3	13 ± 2.5	8.38E-01
Q3KRE0	ATPase family AAA domain-containing protein 3	21	1.7 ± 1	2 ± 1.7	8.41E-01
Q08851	Syntaxin-5	15	1.2 ± 1.2	1 ± 1.6	8.42E-01
Q6AZ61	Probable lysosomal cobalamin transporter	27	2.3 ± 1.5	2 ± 1.3	8.43E-01
B1WC61	Acad9 protein	45	3.8 ± 1.2	4 ± 1.6	8.44E-01
P15999	ATP synthase subunit alpha, mitochondrial	481	40.8 ± 6.9	42 ± 10.4	8.48E-01
Q66H12	Alpha-N-acetylgalactosaminidase	44	3.8 ± 1.6	4 ± 1.4	8.50E-01
B0BMW0	RAB14, member RAS oncogene family	187	15.8 ± 6.4	17 ± 5.5	8.51E-01
G3V743	Glucosidase 1	29	2.3 ± 1	3 ± 1.9	8.51E-01
Q6AXS5	Plasminogen activator inhibitor 1 RNA-binding protein	29	2.3 ± 1	3 ± 1.9	8.51E-01
Q5U2X6	Coiled-coil domain-containing protein 47	33	2.8 ± 1	3 ± 1.9	8.51E-01
P07154	Cathepsin L1	47	3.8 ± 1.3	4 ± 1.7	8.52E-01
Q9Z1H9	Protein kinase C delta-binding protein	111	9.7 ± 1.4	9 ± 4	8.53E-01
P11762	Galectin-1	128	10.5 ± 7.1	11 ± 4.8	8.53E-01
D3ZME3	Glyceraldehyde-3-phosphate dehydrogenase	170	12.8 ± 20	15 ± 25.6	8.53E-01
P29266	3-hydroxyisobutyrate dehydrogenase, mitochondrial	56	5 ± 2.6	5 ± 3.4	8.55E-01
D3ZXK9	Purine nucleoside phosphorylase (Fragment)	71	6.3 ± 2.8	6 ± 3.3	8.56E-01
A1L1J8	Protein Rab5b	73	6 ± 3.2	6 ± 3	8.57E-01
G3V7I0	Peroxiredoxin 3	31	2.5 ± 1.5	3 ± 1.6	8.58E-01
D3ZFA8	Protein LOC100362366	45	4 ± 3	4 ± 3.3	8.59E-01
D3ZRF6	Protein Pnpla6	35	3 ± 1.8	3 ± 1.5	8.63E-01
D4A1Q9	Protein Ttll12	28	2.5 ± 1.5	2 ± 1.8	8.64E-01
O88600	Heat shock 70 kDa protein 4	209	18.3 ± 8.5	18 ± 4.2	8.65E-01

B2GUV5	ATPase, H transporting, lysosomal V1 subunit G1	33	2.7 ± 1.4	3 ± 1.9	8.66E-01
Q642A4	UPF0598 protein C8orf82 homolog	32	2.8 ± 1.7	3 ± 1.6	8.67E-01
F1LQP9	Protein Tnpo1 (Fragment)	29	2.3 ± 1.8	3 ± 1.6	8.69E-01
M0RC65	Cofilin 2, muscle (Predicted), isoform CRA_b	27	2.2 ± 1.5	2 ± 2	8.71E-01
Q5PQZ8	RCG49978	27	2.2 ± 1.5	2 ± 2	8.71E-01
P53987	Monocarboxylate transporter 1	69	5.7 ± 4	6 ± 3	8.74E-01
P61206	ADP-ribosylation factor 3	49	4 ± 0.9	4 ± 2.4	8.76E-01
D3ZJ32	Protein Esyt2	23	1.8 ± 1.5	2 ± 2.1	8.76E-01
M0RDC5	Acyl-CoA-binding protein (Fragment)	31	2.5 ± 1.5	3 ± 2.1	8.76E-01
P15429	Beta-enolase	218	18.8 ± 6.9	18 ± 8.1	8.81E-01
E9PT82	Striatin-3	33	2.7 ± 2.2	3 ± 1.6	8.83E-01
P23928	Alpha-crystallin B chain	106	8.8 ± 3.4	9 ± 4.3	8.84E-01
D4ACW1	Protein Nop2	54	3.7 ± 2.4	4 ± 1.4	8.86E-01
F1M0E9	Uncharacterized protein (Fragment)	43	3.7 ± 2.7	4 ± 0.8	8.87E-01
D4ACN7	Protein Myof	209	18 ± 4.7	18 ± 3.1	8.87E-01
P29419	ATP synthase subunit e, mitochondrial	59	5 ± 2.4	5 ± 1.6	8.89E-01
P62749	Hippocalcin-like protein 1	66	5.5 ± 2.6	6 ± 1.4	8.92E-01
G3V852	Protein Tln1	779	66 ± 34.4	68 ± 8.8	8.94E-01
P13084	Nucleophosmin	46	4 ± 1.9	4 ± 2.3	8.95E-01
Q3MIE4	Synaptic vesicle membrane protein VAT-1 homolog	102	8.8 ± 4.3	9 ± 4.3	8.96E-01
Q6RUV5	Ras-related C3 botulinum toxin substrate 1	87	7.5 ± 2.9	7 ± 5.6	9.01E-01
Q5PPL3	Sterol-4-alpha-carboxylate 3-dehydrogenase, decarboxylating	137	11.5 ± 5	12 ± 3.9	9.01E-01
R9PY00	Vesicle-associated membrane protein 2 (Fragment)	31	2.7 ± 2.3	3 ± 2.5	9.08E-01
P62747	Rho-related GTP-binding protein RhoB	31	2.5 ± 3.1	3 ± 1.6	9.10E-01
Q5I0E7	Transmembrane emp24 domain-containing protein 9	148	12.7 ± 2.4	13 ± 2.6	9.11E-01
B0BNM1	NAD(P)H-hydrate epimerase	107	9.3 ± 2.6	9 ± 6.7	9.12E-01

D3ZYS7	Protein G3bp1	80	6.8 ± 3.5	7 ± 1	9.12E-01
Q9Z0V5	Peroxiredoxin-4	71	6 ± 2.3	6 ± 2.9	9.13E-01
Q6AYI1	DEAD (Asp-Glu-Ala-Asp) box polypeptide 5	178	14.7 ± 2.1	15 ± 3	9.13E-01
P26376	Interferon-induced transmembrane protein 3	130	9.3 ± 2.7	10 ± 3	9.22E-01
P45953	Very long-chain specific acyl-CoA dehydrogenase, mitochondrial	51	4.3 ± 2.8	5 ± 3.3	9.26E-01
P47875	Cysteine and glycine-rich protein 1	127	10.8 ± 2.3	11 ± 3.7	9.27E-01
A1A5S1	Pre-mRNA-processing factor 6	39	3.2 ± 1.9	3 ± 4	9.28E-01
C0JPT7	Filamin alpha	1327	115.2 ± 49.1	113 ± 25.3	9.31E-01
P19804	Nucleoside diphosphate kinase B	65	5.7 ± 2.3	6 ± 4.3	9.36E-01
P62193	26S protease regulatory subunit 4	79	6.7 ± 3.1	7 ± 4	9.37E-01
P04797	Glyceraldehyde-3-phosphate dehydrogenase	1489	128 ± 33.4	126 ± 46.7	9.39E-01
P63102	14-3-3 protein zeta/delta	265	22.8 ± 14.9	23 ± 6.5	9.41E-01
O70196	Prolyl endopeptidase	91	7.7 ± 4.1	8 ± 3.7	9.43E-01
P29410	Adenylate kinase 2, mitochondrial	75	6.5 ± 3.7	6 ± 4.3	9.44E-01
D3ZQ57	Plexin B2	174	15 ± 2.5	15 ± 5.4	9.47E-01
D3ZHA0	Protein Flnc	943	81.5 ± 22.8	81 ± 11	9.50E-01
Q6P3V9	60S ribosomal protein L4	353	30 ± 9.7	30 ± 8.4	9.51E-01
P84817	Mitochondrial fission 1 protein	138	6.8 ± 5.7	7 ± 4.6	9.57E-01
F1M779	Clathrin heavy chain 1	403	34.5 ± 7.8	35 ± 13	9.58E-01
Q6IFU8	Keratin, type I cytoskeletal 17	111	9.3 ± 4.8	10 ± 6.4	9.60E-01
D4A8D5	Filamin, beta (Predicted)	458	39.5 ± 8.2	39 ± 4.6	9.66E-01
P31977	Ezrin	264	22.5 ± 3.3	23 ± 4.3	1.00E+00
B2RZ12	IMP3, U3 small nucleolar ribonucleoprotein, homolog (Yeast)	31	2.7 ± 1.9	3 ± 0.5	1.00E+00
P62634	Cellular nucleic acid-binding protein	38	3.2 ± 1.7	3 ± 1	1.00E+00
B5DFN4	Prefoldin 5 (Predicted), isoform CRA_a	11	1 ± 0	1 ± 0.6	1.00E+00
P62890	60S ribosomal protein L30	146	12.3 ± 2.7	12 ± 6.2	1.00E+00

Q5U2R0	Methionine adenosyltransferase 2 subunit beta	14	1.2 ± 1	1 ± 0.8	1.00E+00
F1LP67	Prostacyclin synthase (Fragment)	21	1.5 ± 0.8	2 ± 0.5	1.00E+00
D3ZZC1	Protein Txndc5	111	9.5 ± 4.6	10 ± 3.9	1.00E+00
Q498E0	Thioredoxin domain-containing protein 12	35	3 ± 2.1	3 ± 1.3	1.00E+00
P11232	Thioredoxin	57	4.8 ± 2.5	5 ± 2.2	1.00E+00
B2GUZ9	Fam49b protein	14	1.2 ± 0.8	1 ± 1	1.00E+00
P06214	Delta-aminolevulinic acid dehydratase	14	1.2 ± 1.2	1 ± 1.3	1.00E+00
Q6P501	Lysosomal-associated transmembrane protein 4A	22	1.8 ± 1.5	2 ± 1.8	1.00E+00
G3V9L3	MAGUK p55 subfamily member 3	24	2 ± 0.9	2 ± 0.9	1.00E+00
P20673	Argininosuccinate lyase	14	1.2 ± 1.2	1 ± 0.8	1.00E+00
Q9R175	Interferon induced transmembrane protein 2	110	9 ± 2.4	9 ± 1.4	1.00E+00
D3ZY39	Protein Rrp1b	10	0.8 ± 0.8	1 ± 1	1.00E+00
A1L108	Actin-related protein 2/3 complex subunit 5-like protein	24	2 ± 1.3	2 ± 0.6	1.00E+00
P0C5W1	Microtubule-associated protein 1S	8	0.7 ± 0.5	1 ± 1	1.00E+00
Q3B7U9	Peptidyl-prolyl cis-trans isomerase FKBP8	14	1.2 ± 1	1 ± 1.2	1.00E+00
D4A7J8	PRP4 pre-mRNA processing factor 4 homolog (Yeast)	14	1.2 ± 1.2	1 ± 1	1.00E+00
M0R9Y3	Protein Nup43	12	1 ± 1.1	1 ± 0.9	1.00E+00
M3ZCQ2	U5 small nuclear ribonucleoprotein 200 kDa helicase	14	1.2 ± 1.3	1 ± 0.8	1.00E+00
P63086	Mitogen-activated protein kinase 1	15	1 ± 0.6	1 ± 1.3	1.00E+00
Q6MG66	LSM2 homolog, U6 small nuclear RNA associated [S. cerevisiae]	26	2.2 ± 0.8	2 ± 2	1.00E+00
P04906	Glutathione S-transferase P	297	24.8 ± 2.9	25 ± 5.4	1.00E+00
B1H282	Glycosyltransferase 25 domain containing 1	102	8.8 ± 3.9	9 ± 3.2	1.00E+00
Q4FZX7	Signal recognition particle receptor subunit beta	129	10.2 ± 1.8	10 ± 1.7	1.00E+00
Q568Z8	Ddx17 protein	58	5 ± 2.8	5 ± 2.8	1.00E+00

Q32PX7	Far upstream element-binding protein 1	48	4 ± 0.9	4 ± 1.9	1.00E+00
F1LNN1	Proteasome subunit beta type	41	3.5 ± 1	4 ± 2.1	1.00E+00
D4A720	Protein Srsf7	24	2 ± 1.8	2 ± 2.8	1.00E+00
G3V786	Protein Akr1b8	95	8.2 ± 1.8	8 ± 2.7	1.00E+00
M0R979	Protein Thbs1 (Fragment)	28	2.3 ± 1.2	2 ± 1.8	1.00E+00
D4A7U1	Protein Zyx	28	2.3 ± 1.9	2 ± 1.6	1.00E+00
Q5FVM2	Glucose-6-phosphatase	20	1.7 ± 1.2	2 ± 1.4	1.00E+00
P62278	40S ribosomal protein S13	79	6.8 ± 1	7 ± 4.2	1.00E+00
D3ZQM0	Protein Sf3a1	50	4.3 ± 2.2	4 ± 2.1	1.00E+00
Q5M860	Protein Arhgdib	37	3.2 ± 2.1	3 ± 1	1.00E+00
D4A2B0	Polymerase (DNA-directed), delta interacting protein 3 (Predicted), isoform CRA_a	17	1.5 ± 2	2 ± 1.2	1.00E+00
F1M5X1	Protein Rrbp1	44	3.7 ± 3.3	4 ± 3.2	1.00E+00
B5DF60	Eukaryotic translation initiation factor 1A, Y-linked	20	1.7 ± 0.8	2 ± 1.2	1.00E+00
Q7TP98	Interleukin enhancer-binding factor 2	20	1.7 ± 1.4	2 ± 1	1.00E+00
Q561S0	NADH dehydrogenase [ubiquinone] 1 alpha subcomplex subunit 10, mitochondrial	24	2 ± 1.8	2 ± 1.4	1.00E+00
Q920A6	Retinoid-inducible serine carboxypeptidase	30	2.5 ± 0.8	3 ± 1.5	1.00E+00
Q63518	Myosin-binding protein C, slow-type (Fragment)	10	0.8 ± 0.8	1 ± 1	1.00E+00
Q9R1E9	Connective tissue growth factor	20	1.7 ± 1.9	2 ± 1.6	1.00E+00
Q5PQZ9	NADH dehydrogenase [ubiquinone] 1 subunit C2	12	1 ± 0.9	1 ± 0.6	1.00E+00
Q6AXT0	39S ribosomal protein L37, mitochondrial	10	0.8 ± 0.8	1 ± 0.8	1.00E+00
Q5U1Z9	Metaxin 2	16	1.3 ± 1	1 ± 0.5	1.00E+00
Q4QQW8	Putative phospholipase B-like 2	12	1 ± 0.9	1 ± 0.6	1.00E+00
D3ZZR9	Peptidyl-prolyl cis-trans isomerase	8	0.7 ± 0.5	1 ± 0.8	1.00E+00
B0BNF6	Membrane-associated ring finger (C3HC4) 5	10	0.8 ± 1.2	1 ± 1	1.00E+00
G3V7G0	Cytoplasmic dynein 1 light intermediate chain 1	32	2.7 ± 1.9	3 ± 1.5	1.00E+00

D4ABI6	Ubiquitin carboxyl-terminal hydrolase isozyme L3	11	1 ± 0	1 ± 1.1	1.00E+00
F1LQS6	RCG61833	14	1.2 ± 1.6	1 ± 0.8	1.00E+00
Q66H15	Regulator of microtubule dynamics protein 3	12	1 ± 1.3	1 ± 0.6	1.00E+00
Q99N27	Sorting nexin-1	10	1 ± 0	1 ± 0	1.00E+00
Q8CF97	Deubiquitinating protein VCIP135	6	0.5 ± 0.8	1 ± 0.5	1.00E+00
F1LU71	AU RNA binding protein/enoyl-coenzyme A hydratase (Predicted), isoform CRA_a	6	0.5 ± 0.5	1 ± 0.5	1.00E+00
F1LRW6	Plasma membrane calcium-transporting ATPase 1	12	1 ± 0.9	1 ± 0.6	1.00E+00
Q5U2X0	CDKN2A-interacting protein	8	0.7 ± 1	1 ± 0.5	1.00E+00
P50408	V-type proton ATPase subunit F	8	0.7 ± 0.8	1 ± 0.5	1.00E+00
D3ZIX4	Protein H1fx	8	0.7 ± 0.5	1 ± 0.5	1.00E+00
Q56A27	Nuclear cap-binding protein subunit 1	6	0.5 ± 0.5	1 ± 0.5	1.00E+00
G3V6K6	Epidermal growth factor receptor, isoform CRA_b	10	0.8 ± 0.8	1 ± 0.8	1.00E+00
G3V8U3	D4, zinc and double PHD fingers family 2 (Predicted)	8	0.7 ± 0.5	1 ± 0.5	1.00E+00
Q5XHZ8	Component of oligomeric golgi complex 3	6	0.5 ± 0.8	1 ± 0.5	1.00E+00
B2GV94	Fam134c protein	6	0.5 ± 0.5	1 ± 0.5	1.00E+00
F7F1N8	Protein Usp39	6	0.5 ± 0.5	1 ± 0.5	1.00E+00
D4A7N1	Coiled-coil-helix-coiled-coil-helix domain-containing protein 6, mitochondrial	6	0.5 ± 0.5	1 ± 0.5	1.00E+00
B2GV38	Ubiquitin-like protein 4A	12	1 ± 0.6	1 ± 1.3	1.00E+00
D3ZR95	Protein Cystm1	12	1 ± 0	1 ± 0	1.00E+00
Q6AYK5	Cell growth-regulating nucleolar protein	11	1 ± 0.6	1 ± 0	1.00E+00
Q27W01	RNA-binding protein 8A	18	1.5 ± 1.2	2 ± 1	1.00E+00
D3ZW15	Protein Sec24b	11	1 ± 0	1 ± 0.9	1.00E+00
F1LSQ6	Proteasome subunit alpha type	16	1.3 ± 1	1 ± 1	1.00E+00
B5DFD8	SH3 domain-binding glutamic acid-rich-like protein	8	0.7 ± 0.5	1 ± 0.8	1.00E+00

D4A8G7	Protein Snw1	8	0.7 ± 0.5	1 ± 0.5	1.00E+00
P07633	Propionyl-CoA carboxylase beta chain, mitochondrial	8	0.7 ± 0.8	1 ± 0.5	1.00E+00
D3ZIT4	Anaphase promoting complex subunit 7 (Predicted)	6	0.5 ± 0.5	1 ± 0.5	1.00E+00
F1M5Q1	E3 ubiquitin-protein ligase parkin (Fragment)	6	0.5 ± 0.5	1 ± 0.5	1.00E+00
Q6AXT5	Ras-related protein Rab-21	6	0.5 ± 0.8	1 ± 0.5	1.00E+00
P04550	Parathymosin	10	0.5 ± 0.8	1 ± 0.5	1.00E+00
F1LUV9	Neural cell adhesion molecule 1 (Fragment)	6	0.5 ± 0.5	1 ± 0.5	1.00E+00
G3V6K3	Exosome component 7	6	0.5 ± 0.5	1 ± 0.5	1.00E+00
D3ZNK1	Protein Mtx3	6	0.5 ± 0.8	1 ± 0.5	1.00E+00
D4A9Y2	Protein 5730508B09Rik	6	0.5 ± 0.8	1 ± 0.5	1.00E+00
Q641Y8	ATP-dependent RNA helicase DDX1	10	0.8 ± 0.8	1 ± 0.8	1.00E+00
D4A5G2	Protein Nop14	13	1 ± 0	1 ± 0.6	1.00E+00
D3ZP96	Protein Mcm2	10	0.8 ± 0.8	1 ± 0.8	1.00E+00
F1LQH9	Protein Bag2 (Fragment)	13	1 ± 0	1 ± 0.6	1.00E+00
F1LYA4	AT-rich interactive domain-containing protein 4B (Fragment)	6	0.5 ± 0.5	1 ± 0.5	1.00E+00
P97519	Hydroxymethylglutaryl-CoA lyase, mitochondrial	10	0.8 ± 0.8	1 ± 0.8	1.00E+00
Q7TP78	Aa2-258	6	0.5 ± 0.5	1 ± 0.5	1.00E+00
O35274	Neurabin-2	8	0.7 ± 0.8	1 ± 0.8	1.00E+00
D3ZAK1	Protein 1110018J18Rik	6	0.5 ± 0.5	1 ± 0.5	1.00E+00
P61354	60S ribosomal protein L27	20	1.7 ± 0.8	2 ± 1.6	1.00E+00
P52925	High mobility group protein B2	24	2 ± 2.3	2 ± 2.3	1.00E+00
Q9JI92	Syntenin-1	12	0.5 ± 0.5	1 ± 0.8	1.00E+00
D4A786	Protein LOC100360002	10	0.8 ± 1	1 ± 0.8	1.00E+00
D3ZD24	Protein Syne3	6	0.5 ± 0.5	1 ± 0.5	1.00E+00
D4A746	GDP-mannose pyrophosphorylase B (Predicted), isoform CRA_a	6	0.5 ± 0.8	1 ± 0.5	1.00E+00
D4ABX9	Protein Emc6	11	0.5 ± 0.5	1 ± 0.5	1.00E+00
D3ZEM8	Protein Tsr1	6	0.5 ± 0.8	1 ± 0.5	1.00E+00

F8WFH8	Tryptophan--tRNA ligase, cytoplasmic	6	0.5 ± 0.5	1 ± 0.5	1.00E+00
D3ZBN3	Protein Epha2	10	0.8 ± 0.8	1 ± 1.3	1.00E+00
Q5RK00	39S ribosomal protein L46, mitochondrial	8	0.7 ± 0.8	1 ± 1	1.00E+00
D4A040	Protein Mrps11	6	0.5 ± 0.5	1 ± 0.8	1.00E+00

Table A3: All proteins identified in rat urine exosomes. Each protein is listed with the number of normalized spectral hits associated with it. Superscript letters indicates the protein is significantly altered in abundance as compared to [n] Control, [p] PUO, [t] CUO. Protein is significant with a quasi-poisson p-value < 0.05.

Protein Accession	Protein Description	Control NSpH	Partial NSpH	Complete NSpH
F8WG91	ADP-ribosylation factor-like protein 3 (Fragment)	9 [p, t]	0 [n, t]	2 [n, p]
P12346	Serotransferrin	61 [p, t]	10 [n, t]	156 [n, p]
P17475	Alpha-1-antiproteinase	42 [p, t]	8 [n, t]	74 [n, p]
G3V7W7	Alanyl (Membrane) aminopeptidase	332 [p, t]	444 [n, t]	216 [n, p]
G3V7K3	Ceruloplasmin	5 [p, t]	0 [n, t]	24 [n, p]
P15684	Aminopeptidase N	337 [p, t]	448 [n, t]	207 [n, p]
Q9WTW7	Solute carrier family 23 member 1	14 [p, t]	3 [n, t]	0 [n, p]
P02770	Serum albumin	404 [p, t]	289 [n, t]	851 [n, p]
P02091	Hemoglobin subunit beta-1	2 [p, t]	0 [n, t]	56 [n, p]
P14740	Dipeptidyl peptidase 4	187 [p, t]	247 [n, t]	121 [n, p]
F1LT69	Aldehyde dehydrogenase (Fragment)	16 [p, t]	27 [n, t]	52 [n, p]
P53790	Sodium/glucose cotransporter 1	37 [t]	15 [t]	3 [n, p]
D3ZFG3	Elastase 3B, pancreatic (Predicted), isoform CRA_b	8 [t]	2 [t]	0 [n, p]
P61983	14-3-3 protein gamma	1 [t]	0 [t]	8 [n, p]
Q00715	Histone H2B type 1	1 [t]	0 [t]	10 [n, p]
Q03626	Murinoglobulin-1	13 [t]	3 [t]	32 [n, p]
G3V8I1	Alkaline phosphatase	17 [t]	9 [t]	1 [n, p]
P14046	Alpha-1-inhibitor 3	12 [t]	3 [t]	41 [n, p]
G3V8X5	Protein Slc5a10	85 [t]	109 [t]	40 [n, p]
P07314	Gamma-glutamyltranspeptidase 1	315 [t]	348 [t]	258 [n, p]
P07861	Neprilysin	234 [t]	260 [t]	115 [n, p]
Q5RLM2	Solute carrier family 22 member 7	64 [t]	74 [t]	16 [n, p]
M0RAV0	Uncharacterized protein (Fragment)	20 [t]	15 [t]	32 [n, p]
F1LT79	Aldehyde dehydrogenase	19 [t]	25 [t]	51 [n, p]
F1M8L3	CUB and zona pellucida-like domain-containing protein 1	6 [t]	3 [t]	0 [n, p]
D3ZUQ1	Lipase	8 [t]	12 [t]	1 [n, p]
P19468	Glutamate--cysteine ligase catalytic subunit	30 [t]	35 [t]	3 [n, p]
P43427	Solute carrier family 2, facilitated glucose transporter member 5	15 [t]	17 [t]	0 [n, p]
F1M6C2	Elongation factor 1-alpha (Fragment)	10 [t]	13 [t]	1 [n, p]

Protein Accession	Protein Description	Control NSpH	Partial NSpH	Complete NSpH
Q6AYR5	Clarin-3	6 [t]	5 [t]	0 [n, p]
Q6MG61	Chloride intracellular channel protein 1	61 [t]	63 [t]	33 [n, p]
Q64230	Meprin A subunit alpha	290 [t]	282 [t]	193 [n, p]
D4A6I7	Protein Psca	12 [t]	12 [t]	30 [n, p]
Q99MA2	Membrane-bound aminopeptidase P	141 [t]	140 [t]	83 [n, p]
O70352	CD82 antigen	18 [t]	17 [t]	1 [n, p]
P11517	Hemoglobin subunit beta-2	0 [t]	0 [t]	26 [n, p]
P01946	Hemoglobin subunit alpha-1/2	0 [t]	0 [t]	11 [n, p]
P06866	Haptoglobin	0 [t]	0 [t]	19 [n, p]
F1LPR6	Uncharacterized protein (Fragment)	10 [t]	10 [t]	29 [n, p]
F1LMV6	Protein Dsp	8 [t]	8 [t]	0 [n, p]
Q9R175	Interferon induced transmembrane protein 2	8 [p]	0 [n, t]	7 [p]
D3ZF96	Lymphocyte antigen 6 complex, locus D (Predicted)	7 [p]	0 [n, t]	4 [p]
M0RBJ7	Complement C3	18 [p]	0 [n, t]	39 [p]
D4A111	Protein Col6a3	64 [p]	33 [n, t]	65 [p]
Q64319	Neutral and basic amino acid transport protein rBAT	433 [p]	787 [n, t]	407 [p]
Q6IRK9	Carboxypeptidase Q	22 [p]	2 [n, t]	15 [p]
Q3MIE4	Synaptic vesicle membrane protein VAT-1 homolog	6 [p]	0 [n, t]	7 [p]
Q5I0E1	Leucine-rich alpha-2-glycoprotein 1	7 [p]	0 [n, t]	21 [p]
P85971	6-phosphogluconolactonase	30 [p]	7 [n, t]	29 [p]
P20759	Ig gamma-1 chain C region	11 [p]	0 [n, t]	16 [p]
P20760	Ig gamma-2A chain C region	28 [p]	5 [n, t]	39 [p]
D4A9Q5	Carboxypeptidase M (Predicted)	7 [p]	0 [n, t]	2 [p]
F1M7X5	Dipeptidyl peptidase 4	219 [p]	303 [n, t]	170 [p]
Q5XI43	Matrix-remodeling-associated protein 8	7 [p]	0 [n, t]	14 [p]
Q9EPB1	Dipeptidyl peptidase 2	46 [p]	15 [n, t]	39 [p]
Q3KR86	Mitochondrial inner membrane protein (Fragment)	0 [p]	7 [n, t]	0 [p]
P62815	V-type proton ATPase subunit B, brain isoform	4 [p]	0 [n, t]	7 [p]
D3ZGK7	Carboxylesterase 1C	4 [p]	0 [n, t]	6 [p]
D3ZRG6	Protein Rnf6	3 [p]	0 [n, t]	9 [p]
F1M8B7	Protein Chmp2b	15 [p]	3 [n, t]	12 [p]

Protein Accession	Protein Description	Control NSpH	Partial NSpH	Complete NSpH
P0CG51	Polyubiquitin-B	66 p	37 n, t	82 p
D4A133	Protein Atp6v1a	25 p	7 n, t	26 p
P68255	14-3-3 protein theta	15 p	23 n, t	9 p
P23680	Serum amyloid P-component	18 p	4 n, t	18 p
Q4V8K5	BRO1 domain-containing protein BROX	27 p	9 n, t	28 p
D3Z9E5	Protein Slc5a8	8 p	28 n, t	3 p
B5DFC9	Nidogen-2	2 p	0 n, t	8 p
F1LM05	Protein LOC299282	223 p	168 n, t	220 p
F1LVL9	Uncharacterized protein (Fragment)	8 p	1 n, t	8 p
P20767	Ig lambda-2 chain C region	51 p	32 n, t	57 p
P27274	CD59 glycoprotein	20 p	7 n, t	24 p
B2GV31	Muc1 protein	13 p, t	0 n	2 n
O70244	Cubilin	34 p, t	2 n	10 n
Q9JI92	Syntenin-1	19 p, t	1 n	6 n
Q642B0	Glypican 4	10 p, t	0 n	0 n
Q9JJ40	Na(+)/H(+) exchange regulatory cofactor NHE-RF3	126 p, t	61 n	60 n
P98158	Low-density lipoprotein receptor-related protein 2	200 p, t	127 n	113 n
P07943	Aldose reductase	19 p, t	2 n	2 n
F1LST1	Fibronectin	7 p, t	0 n	0 n
D3ZHK4	Protein Rb1cc1	0 p, t	13 n	6 n
P04897	Guanine nucleotide-binding protein G(i) subunit alpha-2	35 p, t	7 n	10 n
P01835	Ig kappa chain C region, B allele	108 p, t	173 n	175 n
Q6IFU7	Keratin, type I cytoskeletal 42	126 p, t	187 n	185 n
B0BNK1	Protein Rab5c	30 p, t	6 n	13 n
D3ZH25	Protein Vps8	0 p, t	14 n	19 n
D3ZEV8	Protein Susd2	33 p, t	4 n	11 n
Q05BA4	Myadm protein	16 p, t	38 n	34 n
Q6AYZ1	Tubulin alpha-1C chain	7 p, t	0 n	0 n
P70490	Lactadherin	42 p, t	16 n	11 n
Q9R1Z0	Voltage-dependent anion-selective channel protein 3	49 p, t	10 n	14 n
D3Z851	Protein Fbxl21	1 p, t	19 n	13 n
P62963	Profilin-1	15 p, t	3 n	4 n
B0BND0	Ectonucleotide pyrophosphatase/phosphodiesterase	17 p, t	5 n	4 n

Protein Accession	Protein Description	Control NSpH	Partial NSpH	Complete NSpH
	family member 6			
Q6AXV4	Sorting and assembly machinery component 50 homolog	13 p, t	2 n	2 n
P09527	Ras-related protein Rab-7a	16 p, t	3 n	3 n
P10824	Guanine nucleotide-binding protein G(i) subunit alpha-1	21 p, t	5 n	7 n
Q62867	Gamma-glutamyl hydrolase	7 p, t	1 n	0 n
Q32KJ5	Glucosamine (N-acetyl)-6-sulfatase	20 p, t	7 n	2 n
P20171	GTPase HRas	8 p, t	1 n	0 n
P54313	Guanine nucleotide-binding protein G(I)/G(S)/G(T) subunit beta-2	20 p, t	8 n	5 n
P10111	Peptidyl-prolyl cis-trans isomerase A	10 p	0 n	5
Q9WUW9	Sulfotransferase 1C2A	15 p	0 n	3
Q9Z2L0	Voltage-dependent anion-selective channel protein 1	215 p	91 n	153
M0RAK7	Uncharacterized protein	352 p	160 n	232
M0R628	Uncharacterized protein (Fragment)	6 p	0 n	1
Q5RKI7	Solute carrier family 7 member 13	44 p	87 n	53
Q6IRJ7	Annexin	21 p	2 n	7
P81155	Voltage-dependent anion-selective channel protein 2	64 p	18 n	41
F1M5V2	Protein Glipr2	11 p	1 n	6
P51907	Excitatory amino acid transporter 3	0 p	11 n	3
O70513	Galectin-3-binding protein	21 p	3 n	12
D3Z9A9	Uncharacterized protein (Fragment)	110 p	58 n	79
D3ZJF8	Protein Fcgbp	31 p	7 n	19
Q63257	Interleukin-4 receptor subunit alpha	10 p	1 n	4
Q4KLZ0	Protein Vnn1	29 p	11 n	18
Q9JJ19	Na(+)/H(+) exchange regulatory cofactor NHE-RF1	60 p	27 n	47
P50399	Rab GDP dissociation inhibitor beta	10 p	1 n	6
Q5BJU0	Protein Rras2	20 p	6 n	14
A1L1J8	Protein Rab5b	13 p	1 n	3
Q4KM55	Protein Vta1	10 p	1 n	4
P06685	Sodium/potassium-transporting ATPase subunit alpha-1	50 p	88 n	55
M0R5J4	Uncharacterized protein	34 p	12 n	20

Protein Accession	Protein Description	Control NSpH	Partial NSpH	Complete NSpH
G3V741	Phosphate carrier protein, mitochondrial	26 p	11 n	31
F6PTN9	Uncharacterized protein	22 p	3 n	10
P08289	Alkaline phosphatase, tissue-nonspecific isozyme	22 p	5 n	17
P63095	Guanine nucleotide-binding protein G(s) subunit alpha isoforms short	24 p	7 n	11
O88989	Malate dehydrogenase, cytoplasmic	33 p	9 n	21
G3V8H1	Protein Klk1c7	20 p	5 n	11
P08753	Guanine nucleotide-binding protein G(k) subunit alpha	21 p	5 n	8
Q8R3Z7	EH-domain containing 4	2 p	0 n	6
P01048	T-kininogen 1	3 p	0 n	6
Q6P7B6	Ephrin B1	20 p	5 n	17
O70247	Sodium-dependent multivitamin transporter	17 p	5 n	8
M0RD98	Uncharacterized protein (Fragment)	30 p	16 n	29
Q5XI73	Rho GDP-dissociation inhibitor 1	14 p	3 n	10
Q3ZAV1	Solute carrier family 22 member 12	17 p	6 n	7
Q9Z0M0	Cd55 molecule	15 p	5 n	8
F1LZX9	Protein Itgav	7 p	1 n	6
Q6P777	Multivesicular body subunit 12A	7 p	1 n	2
P28570	Sodium- and chloride-dependent creatine transporter 1	7 p	1 n	2
E9PSI7	Uncharacterized protein	63 p	107 n	85
P50123	Glutamyl aminopeptidase	90 p	63 n	73
M0R544	Glucosidase, alpha, acid, isoform CRA_a	7 p	1 n	3
P54311	Guanine nucleotide-binding protein G(I)/G(S)/G(T) subunit beta-1	18 p	6 n	9
G3V7S0	Folate hydrolase	1 p	8 n	5
P97675	Ectonucleotide pyrophosphatase/phosphodiesterase family member 3	13 p	4 n	5
G3V7W1	Programmed cell death 6 (Predicted), isoform CRA_a	20 t	7	5 n
Q812E9	Neuronal membrane glycoprotein M6-a	6 t	1	0 n
M0R444	Lipase (Fragment)	9 t	2	0 n
G3V7L4	Protein Cdh16	11 t	6	2 n

Protein Accession	Protein Description	Control NSpH	Partial NSpH	Complete NSpH
P68370	Tubulin alpha-1A chain	16 t	8	6 n
Q641Z6	EH domain-containing protein 1	8 t	2	0 n
Q794F9	4F2 cell-surface antigen heavy chain	23 t	14	9 n
Q07936	Annexin A2	49 t	65	70 n
F7DN64	Protein Slc22a13	13 t	7	2 n
Q8CJD3	Zymogen granule membrane protein 16	8 t	3	0 n
P07150	Annexin A1	72 t	61	38 n
P62494	Ras-related protein Rab-11A	6 t	3	0 n
G3V8S9	Cathelicidin antimicrobial peptide	8 t	6	1 n
P04642	L-lactate dehydrogenase A chain	6 t	8	16 n
P42123	L-lactate dehydrogenase B chain	6 t	8	16 n
G3V9W9	Protein Fat1	9 t	7	1 n
Q5HZW7	Placenta-expressed transcript 1 protein	2	9 t	1 p
Q64240	Protein AMBP	16	5 t	26 p
Q5I0E9	Multidrug and toxin extrusion protein 1	48	72 t	33 p
D3ZYX5	Protein Myo6	1	7 t	0 p
P61589	Transforming protein RhoA	18	9 t	19 p
P81828	Urinary protein 2	53	37 t	54 p
F1M9X2	Pancreatic secretory granule membrane major glycoprotein GP2	23	10 t	36 p
D3ZBQ6	Carbonic anhydrase 15 (Predicted)	8	2 t	10 p
M0RA79	Uncharacterized protein (Fragment)	6	2 t	15 p
E9PSQ1	Protein Amy1a	95	109 t	83 p
Q9QX71	Napsin	40	51 t	21 p
D4A707	Ly6/Plaur domain containing 2 (Predicted), isoform CRA_b	6	1	2
Q64602	Kynurenine/alpha-aminoadipate aminotransferase, mitochondrial	7	1	2
D3ZD19	Extracellular link domain-containing 1 (Predicted)	11	4	8
D3ZUM4	Beta-galactosidase	15	3	10
G3V6U1	RCG26347, isoform CRA_d	7	1	5
Q63041	Alpha-1-macroglobulin	123	82	85
D4A269	Uncharacterized protein	11	3	6

Protein Accession	Protein Description	Control NSpH	Partial NSpH	Complete NSpH
Q7M0E3	Destrin	11	3	4
Q4KLL7	Protein Vps4b	19	8	9
Q62745	CD81 antigen	27	11	21
Q6RUV5	Ras-related C3 botulinum toxin substrate 1	18	5	9
O55158	D6.1A protein	20	9	12
P63081	V-type proton ATPase 16 kDa proteolipid subunit	25	10	13
Q64119	Myosin light polypeptide 6	11	5	10
M0R7K9	Protein LOC171161 (Fragment)	10	3	8
D3ZDI5	Protein Arhgap12	34	13	16
F1LUS1	Uncharacterized protein (Fragment)	10	3	11
P00762	Anionic trypsin-1	1	7	5
G3V7C6	RCG45400	1	6	4
Q68FP1	Gelsolin	18	7	17
F7FIH7	Protein LOC100909412	14	4	5
F7DLY1	EPS8-like 2 (Predicted), isoform CRA_d	7	1	2
Q9JJI3	Alpha-2u globulin	16	5	8
P01836	Ig kappa chain C region, A allele	61	87	98
P26453	Basigin	15	7	5
Q793F9	Vacuolar protein sorting-associated protein 4A	17	8	8
Q8CFN2	Cell division control protein 42 homolog	11	5	3
F1LSA5	Protein Scgb2b3	38	57	37
P07632	Superoxide dismutase [Cu-Zn]	12	5	6
Q9WTQ2	Podocalyxin	26	14	21
E9PT65	Protein Rdx	16	7	5
Q62797	Protein Ptpro	9	3	8
F1LRB7	Tumor susceptibility gene 101 protein	9	2	6
Q4QQV8	Charged multivesicular body protein 5	66	50	62
Q04679	Sodium/potassium-transporting ATPase subunit gamma	1	7	5
P48284	Carbonic anhydrase 4	15	7	6
P60711	Actin, cytoplasmic 1	162	135	142

Protein Accession	Protein Description	Control NSpH	Partial NSpH	Complete NSpH
D3ZQ45	Protein Dsg1b	6	2	6
Q9QX79	Fetuin-B	10	5	12
M0RC65	Cofilin 2, muscle (Predicted), isoform CRA_b	6	2	4
F1M9I3	Mucin-13 (Fragment)	17	9	16
F1M7H2	Polymeric immunoglobulin receptor	11	6	7
P63018	Heat shock cognate 71 kDa protein	62	39	46
Q3KRC4	G-protein coupled receptor family C group 5 member C	63	80	75
Q568Z6	IST1 homolog	31	19	17
D4A0E6	Protein Upk2	9	3	7
Q05175	Brain acid soluble protein 1	2	7	2
D3ZCG9	Integrin alpha 3 variant A	30	38	35
P06761	78 kDa glucose-regulated protein	5	10	5
F1LVP4	Uncharacterized protein (Fragment)	16	8	7
P07171	Calbindin	32	19	27
F1LTN6	Uncharacterized protein (Fragment)	11	7	9
F1LS97	Serine protease hepsin (Fragment)	9	3	6
Q9JHL7	Carcinoembryonic antigen-related cell adhesion molecule 1	7	4	2
D4A3W2	Protein Crb2	9	5	5
P00758	Kallikrein-1	33	28	27
D3ZDW5	Cytochrome c oxidase, subunit VIb (Predicted)	4	9	13
P02650	Apolipoprotein E	74	56	93
F1LP60	Moesin (Fragment)	62	73	56
Q8K4G9	Podocin	7	3	6
P21704	Deoxyribonuclease-1	12	7	8
B2RZB5	Chromatin modifying protein 2A	10	6	5
P07340	Sodium/potassium-transporting ATPase subunit beta-1	5	7	4
D3ZRN3	Protein Actbl2	62	54	66
G3V8M6	Folate receptor 1 (Adult), isoform CRA_b	12	7	7
Q6P0K8	Junction plakoglobin	11	16	18
P81827	Urinary protein 1	31	26	37

Protein Accession	Protein Description	Control NSpH	Partial NSpH	Complete NSpH
D3ZFP5	Protein 2210407C18Rik	11	7	13
P48508	Glutamate--cysteine ligase regulatory subunit	25	33	19
D2XZ41	Androgen-binding protein (Fragment)	8	5	13
Q9R0T4	Cadherin-1	14	9	6
F1M0B2	Uncharacterized protein (Fragment)	76	86	105
P49134	Integrin beta-1	13	17	16
P69897	Tubulin beta-5 chain	9	5	8
M0R5T8	Ferritin	6	3	1
F1M792	Sucrase-isomaltase, intestinal	1	3	6
D3ZEN5	Peroxiredoxin-5, mitochondrial (Fragment)	1	2	6
Q63424	Solute carrier family 15 member 2	24	29	13
F1LQQ8	Beta-glucuronidase	46	33	14
P52759	Ribonuclease UK114	9	7	5
P27615	Lysosome membrane protein 2	8	5	2
F1M927	Protein RGD1560997 (Fragment)	7	5	16
P48500	Triosephosphate isomerase	23	17	16
Q4V7D9	Protein Smpdl3b	11	13	12
P05545	Serine protease inhibitor A3K	228	213	284
P27590	Uromodulin	273	286	276
M0RD14	Pyruvate kinase	3	2	11
G3V8I8	Protein Akp3	6	9	1
F1M9Z5	Protein Cd300le-ps1	22	25	25
D4A7D9	Uncharacterized protein	33	30	53
G3V8G0	Solute carrier family 12 member 3	8	7	17
P00884	Fructose-bisphosphate aldolase B	29	25	37
P63102	14-3-3 protein zeta/delta	43	41	41
M0R4V3	Synaptosomal-associated protein	17	14	9
Q6MG71	Choline transporter-like protein 4	83	78	78
M0RA54	Protein LOC100366121	20	22	18
P34058	Heat shock protein HSP 90-beta	11	8	4
Q5U316	Ras-related protein Rab-35	3	4	7

Protein Accession	Protein Description	Control NSpH	Partial NSpH	Complete NSpH
F7FI74	Protein Prom1	21	20	12
M0R849	Uncharacterized protein (Fragment)	12	10	14
G3V6D9	Na(+)/H(+) exchange regulatory cofactor NHE-RF2	14	15	6
G3V812	Prolactin induced protein, isoform CRA_d	26	22	38
F1LZH0	Uncharacterized protein (Fragment)	13	14	11
M0RCH6	Protein LOC100359642	42	44	31
Q9QZA2	Programmed cell death 6-interacting protein	94	90	79
F1LMI6	Sodium/glucose cotransporter 2	26	24	15
M0R660	Protein RGD1565368	89	91	89
P29975	Aquaporin-1	8	8	8
M0RAZ1	Uncharacterized protein (Fragment)	7	8	10
P40241	CD9 antigen	29	30	34
D3ZP75	Protein Lypd8	9	10	14
Q07439	Heat shock 70 kDa protein 1A/1B	13	13	5
F1LRH8	Solute carrier organic anion transporter family member 4C1	9	10	2
Q5U362	Annexin	65	63	76
F1LZY6	Uncharacterized protein (Fragment)	27	25	34
D3ZIC6	Cadherin-related family member 5	35	34	26
P28826	Meprin A subunit beta	171	170	168
P31977	Ezrin	109	111	87
Q5XI77	Annexin	181	183	140
P14562	Lysosome-associated membrane glycoprotein 1	8	8	10
D3ZTX4	Protein Mgam	68	68	62
P83121	Urinary protein 3	15	15	18
P14841	Cystatin-C	14	14	13
P05065	Fructose-bisphosphate aldolase A	5	4	10
F1LM19	Alpha-2-HS-glycoprotein	12	13	12
F1LNI3	Protein F5	9	9	2
F1M547	Protein Zfhx3 (Fragment)	6	6	4

Appendix B: Copyright permission letters

This is a License Agreement between Dennis J Orton ("You") and Elsevier ("Elsevier"). The license consists of your order details, the terms and conditions provided by Elsevier, and the payment terms and conditions.

Get the printable license.

License Number	3307211107555
License date	Jan 13, 2014
Licensed content publisher	Elsevier
Licensed content publication	Journal of Chromatography B
Licensed content title	A universal, high recovery assay for protein quantitation through temperature programmed liquid chromatography (TPLC)
Licensed content author	Dennis J. Orton,Alan A. Doucette
Licensed content date	15 March 2013
Licensed content volume number	921–922
Number of pages	6
Type of Use	reuse in a thesis/dissertation
Portion	full article
Format	both print and electronic
Are you the author of this Elsevier article?	Yes
Will you be translating?	No
Title of your thesis/dissertation	Protein biomarker discovery of urinary tract obstruction by mass spectrometry
Expected completion date	Apr 2014
Estimated size (number of pages)	300
Elsevier VAT number	GB 494 6272 12
Permissions price	0.00 USD
VAT/Local Sales Tax	0.00 USD / 0.00 GBP
Total	**0.00 USD**

Back

This is a License Agreement between Dennis J Orton ("You") and Elsevier ("Elsevier"). The license consists of your order details, the terms and conditions provided by Elsevier, and the payment terms and conditions.

Get the printable license.

License Number	3307210937253
License date	Jan 13, 2014
Licensed content publisher	Elsevier
Licensed content publication	Journal of Proteomics
Licensed content title	Proteomic analysis of rat proximal tubule cells following stretch-induced apoptosis in an*in vitro*model of kidney obstruction
Licensed content author	Dennis J. Orton,Alan A. Doucette,Geoffrey N. Maksym,Dawn L. MacLellan
Licensed content date	4 December 2013
Number of pages	1
Type of Use	reuse in a thesis/dissertation
Portion	full article
Format	both print and electronic
Are you the author of this Elsevier article?	Yes
Will you be translating?	No
Title of your thesis/dissertation	Protein biomarker discovery of urinary tract obstruction by mass spectrometry
Expected completion date	Apr 2014
Estimated size (number of pages)	300
Elsevier VAT number	GB 494 6272 12
Permissions price	0.00 USD
VAT/Local Sales Tax	0.00 USD / 0.00 GBP
Total	**0.00 USD**

Back